β^{3R3}-Peptides -

Peptidomimetic Foldamers for Biomedical Applications:

Design, Structure and Activity

Inaugural-Dissertation

to obtain the academic degree

Doctor rerum naturalium (Dr. rer. nat.)

submitted to the Department of Biology, Chemistry and Pharmacy

of Freie Universität Berlin

by

Simone Mosca

from Monza, Italy

2013

This thesis is based on research conducted between November 2009 and June 2013 with the supervision of Dr. Laura Hartmann as Group Leader of the Polymeric Biomimetic group, in the Department of Biomolecular Systems under the direction of Prof. Dr. Peter H. Seeberger, at the Max Planck Institute of Colloids and Interfaces, and the Free University of Berlin, Institute of Chemistry and Biochemistry.

1st Reviewer: Dr. Laura Hartmann

2nd Reviewer: Prof. Dr. Nora Kulak

Date of defense: 04/10/2013

Acknowledgements

I am very grateful to my Group Leader Dr. Laura Hartmann for the support for this thesis and providing me with optimal conditions while granting me the freedom to develop my own ideas. I am also grateful to Prof. Dr. Peter H. Seeberger for giving me the opportunity to work in his group and his support.

Moreover, I would like to thank Prof. Dr. Nora Kulak for agreeing to review this thesis. I would like to thank all the collaboration partners, in particular Dr. Nahid Azzouz and Dr. Felicitas Lewrick. A special thank to Prof. Dr. Gerald Brezesinski for fruitful and stimulating discussions. I would particularly like to thank Daniela Ponader, Muriel Behra, Sinaida Lel, Felix Wojcik, Daniel Pussak and the other colleagues of the "Polymeric Biomimetics" group for their friendship and understanding. Besides all the colleagues from the department of Biomolecular Systems department, I would like to express my gratitude to valid colleagues and honest friends I have been honored to meet: Davide, Mattan, Anish, Claney, Yoshi, Paola, Bopanna, Sharu, Oliviana, Subru Hahm, Gianfranco, Daniele, Luca, Felipe. And of course, I thank the football allies and worthy enemies, especially Prof. Dr. Helmuth Möhwald. Finally I'm still sincerely grateful to Prof. Dr. Laura Cipolla and Prof. Dr. Francesco Nicotra, and the other Professors from the University of Milano Bicocca and University of Pavia that provided me with the bases in chemistry and biomedicine for this research.

Most importantly, I would like to thank all my family for all of this and everything else.

Table of Contents

Experimental Part

Summary

β-peptides are one of the most explored peptidomimetic structures and are based on the introduction of an additional CH_2-group within the peptidic backbone. In comparison to their natural counterparts, the α-peptides, they exhibit similar biological activity but overcome the limited stability and risk of cytotoxicity and immunogenicity and thus have a great potential for various biomedical applications. However, β-peptides are still limited in their structural space as so far they mainly form helical conformations. Thus, in order to fully explore the potential of β-peptides as peptidomimetics, an extension towards strand conformations and sheet structures as well as an optimization of their biological activity and reduction of their hemolytic effect is required.

Therefore this thesis presents a novel class of peptidomimetics, the β^{3R3}-peptides, with the goal to access strand and sheet conformations as well as to evaluate their potential as novel peptidomimetic agents for biomedical applications. More specifically, β^{3R3}-peptides are based on alternating directions of the amide bonds along β-peptide sequences and have been designed to combine intrinsic physicochemical properties of α- and β-peptides. On the one hand, as for β-peptides, Cβ homologation can promote the formation of secondary structures along with improved proteolytic stability. On the other hand, the novel qualities of the backbone with alternating direction of the amide bonds are expected to extensively modulate both the structural and biological properties of classical β-peptide.

The synthetic strategy towards this new class of peptidomimetics is based on solid phase synthesis using tailor-made building blocks. Initial focus of this work was devoted to the development of a versatile and efficient route for the synthesis of a set of chiral β-diamine building blocks with proteinaceous side chains. In addition, novel diacid building blocks were prepared either via asymmetric synthesis with chiral auxiliary or selected from the pool of commercially available chiral β-diacids with bioactive side chains (e.g. aspartic acid and malic acid). Moreover, diamine and diacid building blocks were coupled in solution to provide dimer building blocks suitable for conventional Fmoc solid phase peptide synthesis protocols. Conclusively, the synthetic protocols fulfill the requirements for the synthesis of building blocks suitable for solid phase synthesis, giving high yield and purity on multigram scale and relying exclusively on convenient purification methods. These building blocks were then applied to a standard peptide synthesizer for the fully automated synthesis of designed sets of oligomers with different physicochemical features and specific biomedical application - hydrophobic and amphiphilic cationic β^{3R3}-peptides.

Structural characterization showed that the β^{3R3}-peptides with hydrophobic proteinaceous side

chains are able to form strand conformations and sheet assemblies with different crystallinity at the air/water interface and thus extend the structural and functional space of β-peptides. Furthermore β^{3R3}-peptides exhibit a high proteolytic stability making them an interesting new class of peptidomimetics for biomedical applications such as modulators/inhibitors of hydrophobic β-sheet formation or recognition, which has been proposed as a viable therapeutic strategy e.g. against Alzheimer's disease.

As a second class of β^{3R3}-peptides, amphiphilic cationic β^{3R3}-peptides were investigated as antimicrobial peptidomimetics. Designed oligomers showed highly selective antibacterial activity and a striking correlation between building block features, primary sequences, overall physicochemical properties and biological activity. Thus these systems are highly suitable for the development of novel antibacterial agents with high therapeutic index, as defined by the ratio between amounts of a therapeutic agent resulting a therapeutic effect and those amounts resulting toxicity.

Lastly, rhodamine B conjugates of the amphiphilic cationic β^{3R3}-peptides were carachterized as cell-penetrating agents showing very high specific cellular uptake into HeLa, MDCKII and A10 cells. Furthermore they showed significantly increased and sequence-based tunable protease stability. Thus these systems are highly suitable for the development as a new class of cell penetrating peptidomimetics for drug delivery.

Overall, the synthesis of a novel class of peptidomimetics, the β^{3R3}-peptides, was developed based on the solid phase coupling of tailor-made building blocks. The obtained systems have shown specific structural and biological properties and thus a high potential for biomedical applications such as β-strand mimetics as well as antimicrobial and cell-penetrating agents. β^{3R3}-peptides provide a potential tool to address a variety of biomedical issues and overcome current limitations of both natural α-peptides as well as other peptidomimetics.

Zusammenfassung

β-Peptide sind eine der meist untersuchten peptidomimetischen Strukturen und basieren auf einer zusätzlichen CH_2-Gruppe innerhalb des peptidischen Rückgrats. Im Vergleich zu ihrem natürlichen Vorbild, den α-Peptiden, besitzen sie eine ähnliche biologische Aktivität, sind aber stabiler und haben eine geringere Zytotoxizität und Immunogenizität. Daher besitzen solche Peptidomimetika ein großes Potential für verschiedene biomedizinische Anwendungen. Allerdings sind β-Peptide bisher in ihrer strukturellen Vielfalt begrenzt, da sie zumeist helikale Strukturen ausbilden. Um das volle Potenzial von β-Peptiden als Peptidomimetika zu nutzen, ist es notwendig, auch andere Konformationen wie etwa Faltblattstrukturen zugänglich zu machen. Darüber hinaus ist eine Optimierung der biologischen Aktivität bei gleichzeitiger Reduzierung der hämolytischen Wirkung ein wichtiges Ziel zur Weiterentwicklung von Wirkstoffen auf Basis von Peptidomimetika.

Aus diesem Grund befasst sich diese Arbeitmit der Entwicklung einer neuen Klasse von Peptidomimetika, der sogenannten β^{3R3}-Peptide. Ziel ist es, zum einen Strang- und Faltblattkonformationen zu ermöglichen, und zum anderen das Potential dieser neuen Peptidomimetika für verschiedene biomedizinische Anwendungen zu erforschen. Die β^{3R3}-Peptide basieren auf der alternierenden Austrichtung der Amidbindungen in Kombination klassischen β-Peptidsequenz und kombinieren so die intrinsischen physikochemischen Eigenschaften von α- und β-Peptiden. Auf der einen Seite ermöglich dies, wie auch bei den klassischen ß-Peptiden, die Ausbildung von Sekundärstrukturen und gleichzeitig eine verbesserte proteolytische Stabilität. Auf der anderen Seite kann die Neuorientierung der Amidgruppen entlang des Rückgrats nun zu einer Erweiterung der möglichen Strukturbildung und somit auch zu neuen, verbesserten biologischen Eigenschaften führen.

Die Synthese der β^{3R3}-Peptide basiert auf der Festphasensynthese und Verwendung maßgeschneiderter Bausteine. Der erste Teil dieser Arbeit befasst sich daher mitder Entwicklung einer schnellen und effizienten Syntheseroute für ein erstes Alphabet von chiralen β Diaminbausteinen mit proteinogenen Seitenketten. Des Weiteren wurden neue Disäure Bausteine hergestellt, einerseits durch asymmetische Synthese mit chiralen Auxiliaren, andererseits durch die Verwendung von käuflich erhältlichen, chiralen β-Disäuren (z.B. Asparaginsäure und Maleinsäure). Zudem wurden Diamin- und Disäurebausteine in Lösung gekuppelt, um so Dimer-Bausteine zu erhalten, welche für die Standard-Fmoc-Peptidfestphasensynthese (SPPS) verwendet werden können. Die erhaltenen Bausteine wurden dann in vollautomatisierten Synthesen an einem Standard-Peptidsynthesizer eingesetzt und so verschiedene Oligomere mit unterschiedlichen

physikochemischen Eigenschaften erhalten. Im Speziellen wurden hierbei zwei Klassen von Oligomeren synthetisiert: hydrophobe und amphiphil-kationische β^{3R3}-Peptide.

Die strukturelle Charakterisierung zeigte, dass β^{3R3}-Peptide mit hydrophoben proteinogenen Seitenketten Strang- und Faltblatt-Konformationen ausbilden können, die unterschiedliche Kristalllinität an der Wasser/Luft Grenzfläche aufweisen und dadurch den funktionellen und strukturellen Rahmen von β-Peptiden erweitern. Außerdem weisen die β^{3R3}-Peptide hohe proteolytische Stabilität auf, was sie zu einer interessanten neuen Klasse von Peptidomimetika für biomedizinische Anwendungen macht, etwa als Modulatoren/Inhibitoren von hydrophoben β-Faltblatt Strukturen und somit möglicherweise als Therapie gegen Alzheimer.

Zweitens wurden amphiphile kationische β^{3R3}-Peptide als antimikrobielle Peptidomimetika untersucht. Speziell ausgewählte Oligomersequenzen zeigten hohe Selektivität gegen Bakterien und eine herausragende Übereinstimmung zwischen Wahl der Bausteine, Primärstruktur, physikochemischen Eigenschaften und biologischer Aktivität. Diese Systeme sind gut geeignet für die Entwicklung von neuen antibakteriellen Wirkstoffen mit hohem therapeutischem Index, also einer hohen biologischen Aktivität bei gleichzeitig geringer Toxizität.

Zusätzlich wurden Rhodamin-B Konjugate der amphiphilen kationischen β^{3R3}-Peptide hergestellt und als Zell-durchdringende Wirkstoffe charakterisiert. Alle untersuchten Oligomere zeigten eine hohe spezifische Aufnahme in HeLa, MDCKII und A10 Zellen und wiesen abhängig von ihrer Sequenz eine erhöhte Stabilität gegenüber Protease auf. Somit sind diese Strukturen gut geeignet für die Weiterentwicklung als neue Klasse Zell-durchdingender Peptidomimetika und besitzen ein großes Potential für Anwendungen im Bereich des Wirkstofftransports.

Zusammenfassend wurde in dieser Arbeit eine neue Klasse von Peptidomimetika entwickelt, die β^{3R3}-Peptide, basierend auf der Festphasenkupplung von maßgeschneiderten Bausteinen. Die erhaltenen Strukturen zeigten spezifische strukturelle und biologische Eigenschaften und besitzen somit ein großes Potential für verschiedene biomedizinische Anwendungen etwa als β-Faltblatt-Mimetika oder Zell-durchdingende und antimikrobielle Wirkstoffe. Insgesamt stellen die β^{3R3}-Peptide also eine neue Klasse der Peptidomimetika dar, die die Einschränkungen der bisher untersuchten α-Peptide und Peptidmimetika überwinden und somit breite Anwendung in der Biomedizin aber auch Biotechnologie und den Materialwissenschaften finden können.

1. Introduction

1.1. Peptidomimetics and Peptidomimetic Foldamers for Biomedical Applications

Complexity in nature stems from a hierarchical organization of biomolecular components and interactions between them.[1] Among biomacromolecules, peptides represent a unique and versatile toolbox for multi-level hierarchical structure design as the amino acid sequence itself dictates the folding into specific secondary structures which can further self-assemble to form higher-order complexes and exert the biological functions (Figure 1.1).

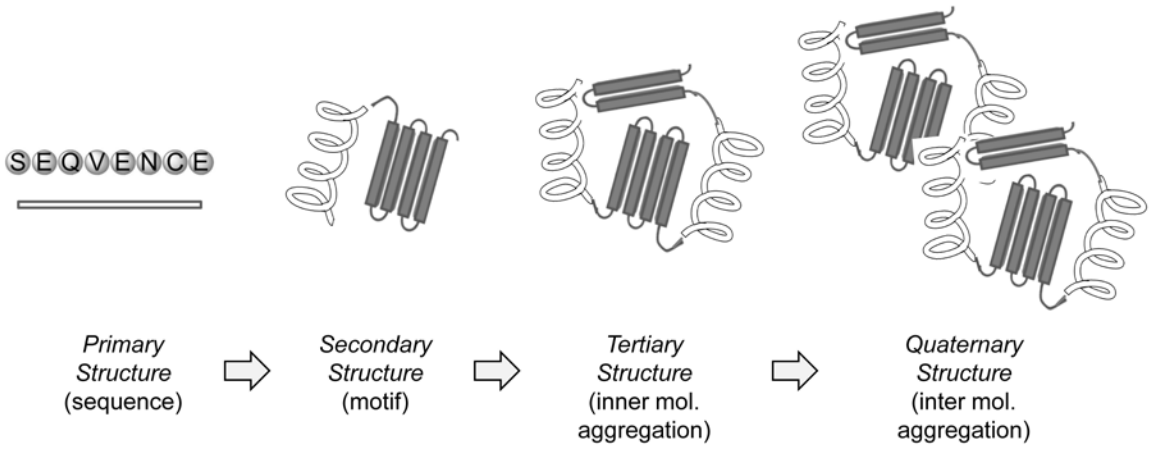

Figure 1.1. *Multi-level hierarchical structure organization of proteins.*

Indeed, secondary structure elements mediate peptide/protein-protein interactions that are crucial both in biological and pathological processes. For instance, mimicking β-strands to antagonize β-sheet formation or recognition has been proposed as a viable therapeutic strategy *e.g.* against Alzheimer's disease.[2] In addition, the large surface area and chemical flexibility of peptides allows for fine-tuned interactions with different biomacromolecules, such as biomembranes, oligonucleotides (DNA and RNA), and oligosaccharides. For examples, amphiphilic cationic peptides can interact with negative charged cell membranes in highly potent and selective way and thereby act as antimicrobial (AMP) and cell-penetrating (CPP) agents.[3]

However, use of peptides brings severe drawbacks which have historically meant they have not been actively pursued as therapeutics. These include e.g. low oral availability, poor tissue penetration, and more importantly high proteolytic susceptibility and short in vivo half-life. Indeed, there are very few

examples of unmodified peptides that have made good drug candidates.[4] Nevertheless, in the recent years yet fewer drugs are being brought to market the development of peptide-based therapeutics has gained attention due to their complementary potential with respect to traditional low molecular weight drugs. On the one hand, strategies are now arising to improve the pharmacokinetic properties of peptides comprising alternative delivery methods and post-synthetic structural modification of short natural peptides.[5] On the other hand, synthetic molecules with alternatives chemical structure have been proposed to mimic the overall topology and the biological activity of natural peptides while improving their pharmacological properties ("peptidomimetics").[4] Related to this, unnatural oligomers have been also designed as bioorthogonal systems with a strong tendency to adopt specific conformations in order to expand the structural and thereby functional space available to natural peptides ("foldamers").[2,6-10] β-peptides are one very prominent example of peptidomimetic foldamers and will be discussed in more detail in the next section.[11-13]

1.2 β-Peptidic Peptidomimetics

β-peptides are oligomers made up of homologated amino acids which differ from natural peptides/proteins by a single additional CH_2 groups per amino acid unit (Figure 1.2).

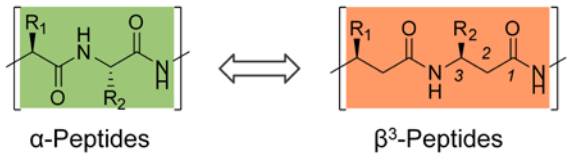

Figure 1.2. *Structural comparison of repeating units of the α- and the β-peptides backbone.*

Although, β-amino acids and convenient methods for their synthesis and condensation have been known for several decades, the currently acknowledged research path of β-peptide research was primarily a surprising step from organic synthesis methodology to supramolecular chemistry.[14] Indeed, despite the increased number of possible conformers that the CH_2 homologation implies with respect to natural α-peptides, surprisingly the presence of the additional C-C bonds in the backbones of β-peptides did not produce a chaotic increase in their folding tendencies. Indeed, seminal contributions reported the ability of short β-peptides to adopt stable helical conformations,[15,16] and

triggered a comprehensive conformational exploration of β-peptides. Thus β-peptides became prominent in the development of the foldamer field and extensive design efforts have been devoted to β-peptides having one, two or even more cyclic or non-cyclic side chains, placed on the C2 or the C3 carbon, with various absolute and relative stereochemical arrangements.[11,13,14,17] Hence, the most important structural properties of β-peptidic foldamers have been uncovered as:[12,17]

i. Each layer of a β-peptidic sheet is polar, with all C-O bonds pointing in the same direction and all N-H bonds in the opposite direction (Figure 1.2).
ii. In linear arrangement of homo-chiral β-peptides the side chains are all exposed on the same face (Figure 1.2).
iii. β-peptides can fold to helices in MeOH solution, with chain length of as few as four residues.
iv. The stability of the helices increases from α- to β-peptides, although the number of hydrogen bond donors and acceptors per chain atom decreases (one of each in 3 and 4 chain atoms, respectively).
v. More different secondary structures have been detected due to more constitutional (β^3, β^2, $\beta^{2,3}$) and configurational ((R), (S), like, unlike) variety of the β-peptide building blocks; five different helices (8-, 10-, 10/12-, 12- and 14-helices), for example, have so far been discovered being the 3_{14}-helix the most established conformation of β-peptides.
vi. The helicity, that is the screw sense of the helix, reverses with homologation, being (P) or right-handed for the α-peptide 3.6_{13}- and 3_{10}-helices, and (M) or left-handed for the β-peptide 3_{14}-helix (Figure 1.3).
vii. The direction of the helix macrodipole also reverses: it points from N- to C- in α-peptide, and from C- to N- in β-peptide helices (Figure 1.3).
viii. The helices of β^3- and β^2-peptides have opposite chirality, (M) versus (P), and the helix consisting of β^2-amino acids is less stable.
ix. β-peptidic chains of β^2/β^3-segments fold to helix consisting of alternating 10- and 12-membered hydrogen-bonded rings.
x. In the NMR-solution structures of β-peptide helices, the C-terminus is generally less structurally ordered and unwinding occurs.
xi. The folding/unfolding process of β-peptides is noncooperative.

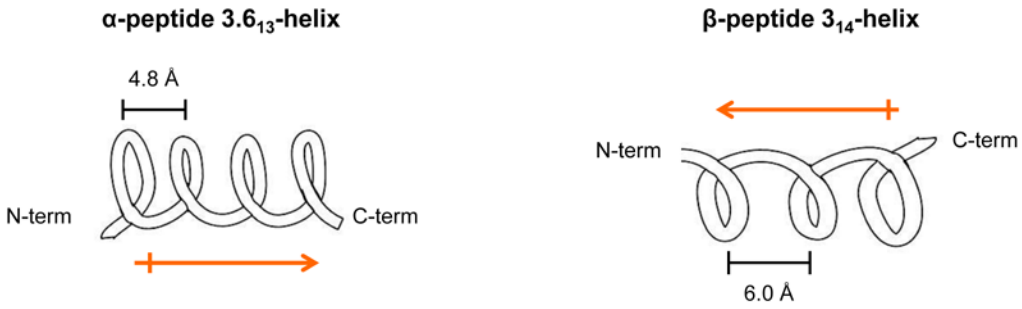

Figure 1.3. *Topological comparison of the α-peptide 3.6$_{13}$- helix and β-peptide 3$_{14}$-helix.*

The enthusiasm arisen from these unique structural properties has then prompted biochemical and biological tests on β-peptides. The different chemical and structural characteristics of the α- and the β-peptides resulted in fundamental bio-orthogonality between these systems as will be discussed for the following aspects: 1) biostability, 2) immunogenicity/toxicity.[14]

First, most α-peptides are degraded by luminal, pancreatic, cytosolic, or lysosomal proteases resulting in low bioavailability and relatively short half-life *in vivo*. Since there is an entire series of natural β-amino acids and most enzymes are highly substrate-specific, it would have not been extremely surprising if β-peptides with proteinogenic side chains were themselves metabolized.[14] Nevertheless, different recent studies *in vitro* have proven that β-peptides and mixed α,β-peptide sequences are extremely resistant towards enzymatic hydrolysis by many common proteases and peptidases of all kinds (endo- and exopeptidases, serine-, threonine-, cysteine-, aspartyl-, or metalloproteases, -peptidases, or amidases).[14,18] At the active centers of peptidases, the peptide chains to be cleaved are present in an extended conformation and, in addition, longer chains away from the active center settle on other regions of the enzyme in sheet formations,[2] which is not possible for β-peptides.[14] Exclusively pronase, a mixture of several endo- and exo-peptidase without sequence specificity, has so far displayed the capability for the digestion of α/β-peptides.[14] Additionally, as demonstrated with a β-peptidic tetrapeptide, the short-chain β-peptides may be orally bioavailable and excreted within a reasonably short half-life,[14] which is considered as an essential prerequisite for the clinical development of drug candidates. In contrast, longer-chain β-peptides so far investigated for their pharmacokinetic properties are neither orally bioavailable nor effectively excreted. Thus long-chain β-peptides may require intravenous administration but will have longer half-lives of clearance.[14] However, the extraordinary metabolic stability can concur with the high cell-penetrating potential of

β-peptides to produce accumulation phenomena which represent a major drawback for *in vivo* application of long-chain β-peptides.

Second, numerous investigations have been addressed the immunogenicity and toxicity of β-peptides.[12] Indeed, neither with conjugates (bovine serum albumin or thyroglobulin β-peptide as hapten), nor with pure β-peptides of high molecular weight (2500-5300 Da) has it yet been possible to produce a monoclonal antibody.[14] Thus β-peptides have so far shown to have neither immunogenic nor inflammatory properties. Furthermore, most of the β-peptides so far examined normally display no or only very weak cytotoxic, antiproliferative, antimicrobial and hemolytic activity been observed either in cell cultures or in vivo.[14] However, cationic amphiphilc β-peptides with helical conformation can display both high antimicrobial and hemolytic activity,[19,20,21,22,23] which indicates indiscriminant toxicity for prokaryotic and human eukaryotic cells. This substantially hampered the development of these systems for biomedical applications such as antimicrobial and cell-penetrating agents for drug delivery.

Nevertheless, with increasing knowledge and understanding of the secondary structures of β-peptides, it has been also possible to mimic the biological functions of α-peptidic secondary structures without having to cope with hydrolytic and metabolic instability of the α-peptide backbone.[12] In the next section the most promising biomedical applications of the β-peptides will be discussed.

1.3. Biomedical Applications of β-Peptides

The β-peptides are considered a prominent class of peptidomimetic foldamers as they are particularly suitable for biomedical applications where the ability of foldamers to adopt specific conformations intrinsically brings the possibility to reproduce the biological activity of natural peptides. In particular, β-peptide secondary structure elements and mainly helical β-peptides have found applications for their ability to modulate important peptide/protein-protein interactions as well as to promote strong interactions with biomembranes and act as mimetics of antimicrobial (AMPs) and cell-penetrating (CPPs) peptides. These indeed represent major current topics of the biomedical research and the related potential of β-peptides will be here discussed.

β-Peptides as Modulators/Inhibitors of Peptide/Protein-Protein Interactions

Although their primary and secondary structures have completely different geometries and chemical properties, the β- and α-peptide chains can organize themselves into complementary spatial arrangements and effectively act as mimetics.[12] In particular, short helical β-peptides carrying

proteinogenic side chains can efficiently mimic biofunctional helical sections of natural α-peptides and proteins.[12] Specifically, the topological coordination of individual proteinaceous side chains and secondary structure of β-peptides makes a decisive contribution to the affinity to α-peptide sequences and promote the activity as agonists or antagonists (inhibitors). Some important examples of so far studied systems are:[12] i) the major histocompatibility complex (MHC) proteins (immune response) ;[14] ii) the lipid transport protein SR-B1 (cholesterol uptake from the small intestine);[24] iii) the core (1-60) of interleukin-8 (inflammation);[14] iv) the oncoprotein RDM2;[25,26] v) the HIVgp41 fusion protein;[27,28] vi) the TNF immune response receptor CD40 (apoptosis).

From these data definitely show that β-peptides carrying proteinogenic side chains can mimic their progenitors, the α-peptides with helical mimics that can consist of as few as six β-amino acid residues.[12] In addition, turn- and hairpin-mimicking β-peptides have been reported e.g. for the somatostatin hsst receptors.[29-31] Therefore these β-peptides are expected to play an increasing role in biomedical research in the near future.[12]

In contrast, only few examples of β-peptidic strands and sheets have been reported. As a consequence, a large area with important biomedical potential cannot be covered by these β-peptidic peptidomimetics. Indeed, besides the α-helix, the β-sheet conformation is the most important of protein secondary structures and plays key biological roles.[32] For instance, β-strands aggregation ad sheet formation are crucial in the pathogenesis of several amyloidosis and mimicking β-strand mimetics have been proposed as a viable therapeutic strategy *e.g.* against Alzheimer's disease.[2] Therefore, extensive design efforts have been focused on the substitution of the C2 and the C3 atoms in order to extend the structural space of β-peptides towards strand conformations and sheet structures.[11-13] In particular, the use of heterochirally disubstituted β-amino acids has been presented as the only suitable strategy aiming at strand conformations.[11-13,33,34] However, strand conformations have been reported only for β-peptide sequences which are quite short (3 residues),[35] constrained in hairpin structures by turn-forming segments,[35,36,37,29,38,39] or conformationally stabilized through ring incorporation in the β-amino acid residues.[33,40] This limited outcome has further promoted the development of alternative strategies.[41-45] For instance, hybrid oligomers made of both α- and β-amino acids ("α/β-peptides") have been designed to form strands which can assemble through the formation of hydrogen-bonded sheets at the air/water interface.[41] This hints to the possibility of alternative design for the development of β-peptide derivatives with orthogonal folding behavior which can extend the potential of classical β-peptides as peptidomimetic foldamers for biomedical application.

β-Peptides as Membrane Active Agents

The unique structural properties and the set of proteinaceous side chains also provides to β-peptides with exclusive combinations of physicochemical properties that drive the interactions with different biomacromolecules. In particular, amphiphilic cationic β-peptides with helical conformation can strongly interact with biomembranes and act as mimetics of membrane active peptides (MAPs). Consequently, these β-peptides have attracted wide research interest for their potential as antimicrobial and cell-penetrating agents. Indeed, amphiphilic cationic helices of either cyclic or β-peptides with proteinaceous side chains can display high antimicrobial activity and penetrate eukaryotic cell membranes.[19,20,21,22,23,46] However, the hemolytic activity of these systems in general results not conclusively low,[19,21,22,23] which can substantially hampered their development as therapeutics. Nevertheless, based on these results β-peptides are in general attractive candidates for further research and design towards the development of novel antimicrobial and cell-penetrating agents for drug delivery. Alternative design approaches can allow for the development of β-peptide derivatives with improved therapeutic index compared to membrane active classical β-peptides. Therefore, the essential physicochemical properties required for the biological activity of natural AMPs and CPPs have to be taken in account and will be now detailed.

Membrane Active Peptides

MAPs represent a broad variety of molecules which exert their biological functions by directly interacting with the cell membrane. According to their distinct biological functions, membrane-active peptides are generally classified as AMPs, CPPs, or fusion peptides (FPs). AMPs can kill micro-organisms by destabilizing their membranes, while CPPs are used to transport functional cargos across cell membranes. FPs are generally part of viral envelope proteins,[47] yet they represent the minimally active agent that triggers fusion between lipid vesicles in vitro.[48] In particular, AMPs and CPPs are two major current topics of biomedical research for their acknowledged potential as novel therapeutic agents.

AMPs and CPPs share defined physicochemical and structural characteristics, which make them very attractive for design and rational optimization. Indeed, these classes of MAP are relatively small size (around 30 amino acids) peptides with cationic charges and globally amphiphilic conformations. Therefore, mimetics of AMPs and CPPs have to reproduce such highly cationic and globally amphiphilic three-dimensional character.

Moreover, linear α-helical MAPs are the most diffused and studied class which promoted the applications of helical β-peptides as particularly suitable antimicrobial and cell-penetrating agents. Nevertheless, the conformation of different MAPs varies to a great extent and a consistent correlation between the extent of conformational change and the respective membrane activities can be generally found. Specifically, it has been suggested that MAPs-lipid fusion can be triggered by any type of conformation acquired upon binding, whether α-helical, β-stranded, or other, and the process is energetically driven by membrane binding, peptide folding, and possibly further aggregation.[49] Although CPPs and AMPs are similar in physicochemical features and structural motif, they become functionally discriminated on the basis of the biological activities within the lipid membrane.[50] Nevertheless, it is not surprising that comparative studies of AMPs and CPPs could emphasize the multifunctional aspects of membrane-active peptides. Indeed, many AMPs and CPPs show overlapping activities, i.e., certain AMPs can penetrate membranes, and some CPPs are good antibiotics.[51,52] Thus, the traditional nomenclature of AMPs/CPPs is becoming blurred,[3] as the molecular mechanisms attributed to these ‘‘different’’ types of agents are not clearcut. Therefore, for the development of novel MAPs mimetics the structural or functional relationships between AMPs and CPPs in particular seem to be not so obvious and need to be explored.

Antimicrobial Peptides

Bacterial resistance to conventional antibiotics has been recognized as one of the greatest threat to public health in the 21st century.[53] Indeed, most of conventional antibiotics attach very specific bacteria targets. In addition, the timescale of action mechanism of the antibiotic could be significantly longer than the bacterial cell cycle, which allows for intensive mutation and the development of resistance. As a consequence, the number of newly introduced antibiotics has been declining steadily over the last decades,[54] and significant research efforts have been devoted to the development of alternative antibacterial agents with novel mode of action.[55] Since the first antimicrobial peptide (AMP) was discovered,[56] AMPs have been proposed as a potential source of future antibiotics because of their broad-spectrum and different mechanisms of action compared to conventional antibiotics.[57] AMPs are key components of the innate immune system of virtually all life forms, ranging from bacteria to plants and mammals,[58] where they constitute an important first line of defense against invading pathogens.[57] The fact that many organisms use such substances since ages testifies the potential of AMPs as a feasible solution to bacteria resistance.

Despite different mechanisms of action have been proposed, AMPs indisputably interact with negatively charged microbial surfaces leading to perturbation and disruption of the membrane.[59,60] Sequential steps are generally considered to occur: attraction, attachment, peptide insertion and

membrane permeabilization.[61] Initially, AMPs are attracted to bacterial surfaces by electrostatic binding between positively charged peptide and negatively charged structures of a cell surface. This first causes efficient concentration of the peptide and attachment to the target cell membrane. The surface-bound peptides lie parallel to the lipid bilayer in a functionally inactive state (referred to as the surface or S state) and efficient peptide aggregation occurs upon exceeding a critical threshold in local concentration. Finally, as the peptide concentration increases, the molecules tend to orient perpendicular to the membrane and insert into the bilayers. After the initial peptide-membrane interaction, several alternative models of AMPs mechanisms of action have been described (barrel-stave, toroidal pore, carpet, molecular electroporation, and sinking raft model).[62]

Based on this mechanism, the activity of AMP cannot depend on specific amino-acid pattern or motif; rather, it primarily originates from a combination of physicochemical properties which drive the interaction with hydrophobic anionic cellular membranes.[59,60]

Hydrophobicity is perhaps the most leading property for the membrane activity as it is required for the interaction with the fatty acyl tails of phospholipids. Nevertheless, high hydrophobicity is directly correlated with loss of antimicrobial selectivity and toxicity towards mammalian cells, inducing hemolysis at relatively low concentrations. Furthermore, excess hydrophobicity and consequent aggregation in aqueous media may result in enhanced hemolytic and cytotoxic effects along with decreasing the antimicrobial activity.[63] Therefore, most AMPs are moderately hydrophobic, such that they optimize activity against microbial cell membranes.

In contrast, besides triggering the attraction to bacterial surfaces by electrostatic binding, the cationic nature can explain the selectivity of AMPs. Cationic residues can interact with negatively charged components of bacterial membranes, such as teichoic and teichuronic acids in the cell wall of Gram-positive bacteria and lipopolysaccharides in Gram-negative bacteria.[57] Differently, the phospholipids of human eukaryotic cell membranes are mainly zwitterionic and therefore do not generate electrostatic interaction with cationic AMPs (Figure 1.4).

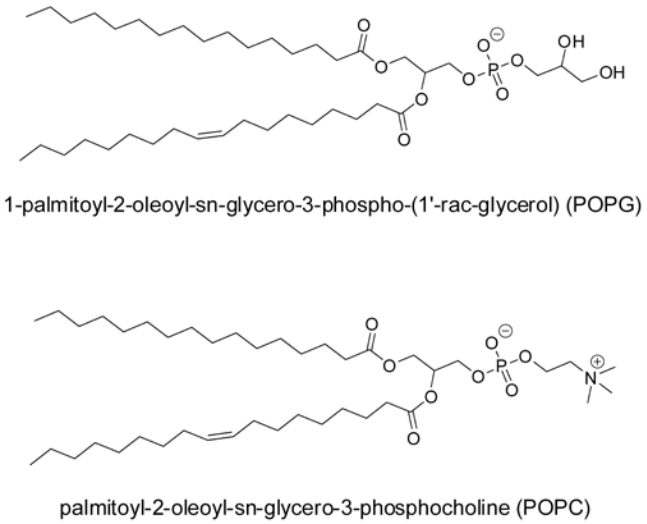

Figure 1.4. *Chemical structure of the anionic 1-palmitoyl-2-oleoyl-sn-glycero-3-phospho-(1'-rac-glycerol) (POPG) and the zwitterionic 1-palmitoyl-2-oleoyl-sn-glycero-3-phosphocholine (POPC) lipids employed as model membrane to mimic prokaryotic and eukaryotic membranes, respectively.*

In addition, the asymmetry between inner and outer membrane leaflets of microbial and host cells as well as different transmembrane potential (Δψ), which is stronger in bacterial cells (Δψ of approximately –120 mV), are believed to account for the electrostatically driven selectivity of AMPs (Figure 1.5).[64]

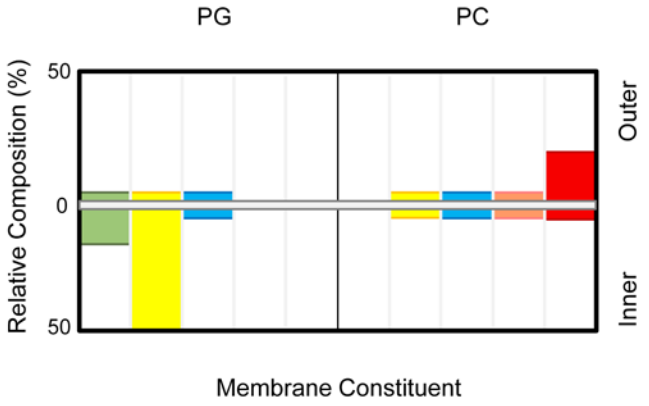

Figure 1.5. *Relative composition of anionic phosphatidylglycerol (PG) and zwitterionic phosphatidylcholine (PC) in microbial and human inner and outer cytoplasmic membrane leaflets. Key: green, E. coli; yellow, S. aureus; blu, B. subtilis; pink, C. albicans; red, human erythrocytes*

However, based on the available data, cationicity alone cannot explain the selectivity of AMPs. Instead, the preference for a certain membrane or classes of membranes likely requires nascent or induced (via peptide–membrane interaction) structural elements of AMPs or results from the change in the peptide primary sequence.[60]

In this perspective, the relevance of secondary structures still needs to be clarified. Indeed, AMPs can present a variety of conformational motifs and rather share globally amphipathic feature. For example, α-helical AMPs display conformation-dependent amphiphilicity which arranges on the same side of the helix normal all the hydrophobic residues that frequently appear in patterns of 1-2 for every 3-4 residues (Figure 1.6).[65] On the other side, β-sheet AMPs are also amphiphilic with a variable number of β-strands organized to create both polar and nonpolar surfaces (Figure 1.6).

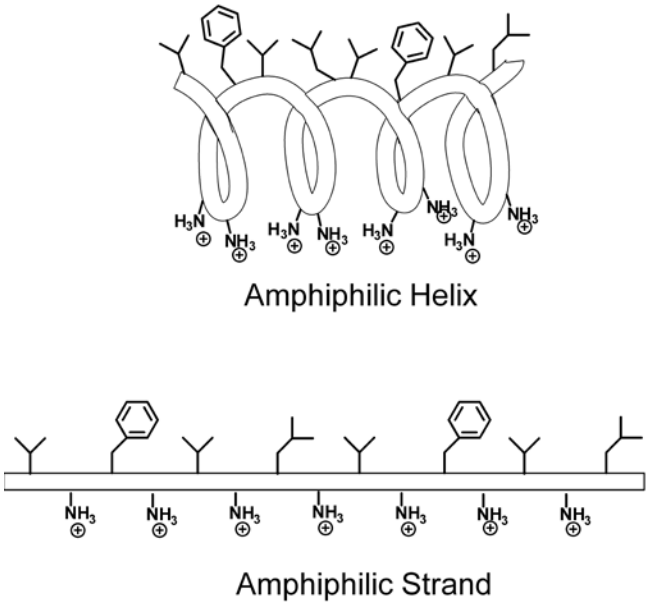

Figure 1.6. *Schematic representation of amphiphilic cationic helix and strand*

Nevertheless, reported effects of secondary-structure disruption or modification through D-aminoacid replacements in AMPs suggest that secondary-structure preference and biological activity are not directly coupled.[60] Therefore, it is widely accepted that pre-organized secondary structures are not necessary, and oligomers could be potent antimicrobial agents as long as can adopt globally amphiphilic structures upon binding to bacterial membranes.[66,67,68,22] Indeed, segregating the cationic and hydrophobic elements mirrors the anionic hydrophobic microbial cell membranes and produce complementary electrostatic and hydrophobic interactions.[57]

Lastly, the preference for a certain membrane or classes of membranes could also result from pattern of specific side chains.[60] In particular, aromatic moieties can also play a role producing π-π

interactions with e.g. unsaturated fatty acids which also differentiate microbial and human cytoplasmic membranes.[64] Indeed, several natural AMPs can be classified as particularly rich in aromatic Phe residues.[69] Additionally, classes of synthetic macromolecules with outstanding antimicrobial activity are based on aromatic polyamides backbones.[70] Furthermore, aromatic rings are known bioisosters of polyunsaturated fatty acids, which are involved in inflammatory processes and have antimicrobial activity being primarily effective against Gram-positive bacteria.[71,70,72,73]

Thus, optimal efficacy of AMPs lies in the relevant coordination of the interrelationship among structural determinants in AMPs.[64] However, AMPs display highly variable abilities to discriminate between microbial targets versus eukaryotic host cells and the rules underlying such selectivity still remain to be fully elucidated. Therefore understanding the structure-activity relationship (SAR) of AMPs is essential for the design and development of novel antimicrobial agents with improved properties.[74] Specifically, this can rely on rational variation of residue patterns in the primary sequence to directly tune essential physicochemical determinants, such as hydrophobicity and net charge. Additionally, the primary composition in terms of e.g. chiral configuration and amino acid sequence also encode for structural factors that can influence the membrane activity and selectivity of natural AMPs.[60]

Cell-Penetrating Peptides

Cellular delivery and internalization of bioactive agents attracts significant biomedical interest as a key step for the development of novel therapeutics.[75] Indeed, despite an urgent need for new drugs for the treatment of e.g. cancers or infectious diseases and the discovery of new potent agents, many of these therapeutics do not reach the clinic due to delivery issues and low bioavailability. In addition, the therapeutic potential of biomacromolecules such as nucleic acids still remains unexploited because of poor pharmacokinetics. Therefore, cell-penetrating peptides (CPPs) represent a particularly promising tool for non-invasive intracellular delivery of cargo varying from small chemical molecule, nucleic acids, proteins, peptides, liposomes and particles.[75]

Classification based on linkage with therapeutic agent divides CPPs into two major classes, one connected to bioactive agents through covalent bond (CPP conjugation) and the second one involving formation of stable, non-covalent complexes (CPP complexation).[75] Most CPPs described so far have been designed to be covalently conjugated to the cargo.[76] Indeed, the covalent conjugation offers several advantages for *in vivo* applications including rationalization, reproducibility, and control over the stoichiometry of the CPP-cargo. Nevertheless, CPP conjugation necessarily implies the risk of altering the biological activity of the cargo,[75] a major specific drawback primarily observed for the

delivery of DNA or other oligonucleotides, such as Decoy oligonucleotides and short interfering RNAs (siRNA).[77]

Numerous studies have investigated structure–activity relationships of CPPs with respect to their ability to bind to a lipid bilayer or to cross this barrier.[78] In general, the ability to interact with cell membrane and thereby the cellular uptake pathway is driven by several parameters including: (i) the physicochemical features of the CPP; (ii) the nature, type and active concentration of the cargo; and (iii) the cell type and membrane composition.[75] As a consequence, it appears quite problematic and simplistic to provide a general scheme for CPP uptake mechanism.[75] However, there is a consensus that the conformation of CPPs and their dynamics can be generally considered to be a major factor in determining the direct cellular uptake mechanism.[79-81] Specifically, transient trans-membrane helical or beta structures could temporarily affect membrane organization, thereby facilitating insertion into the membrane and initiation of the translocation process associated with membrane potential.[82,83] Nevertheless, depending on the nature of the peptide/cell interaction, CPPs can be also taken up by cells through receptor mediated endocytosis pathways which actually represent the preferential mode of uptake for most CPPs.[76,84-86] This has a factual impact on the efficacy of CPPs and the elucidation of cellular uptake mechanism is an essential step in the development of mimetics of CPPs for therapeutic applications.[75] For example, along endocytic pathway, the CPP conjugates can become entrapped in endosomes which could result in protease and acidic degradation of CPP and cargos.[87] The endocytic pathways can be grouped in two major categories, namely clathrin-mediated and clathrin-independent endocytosis such as caveolin-dependent endocytosis[88,8988,8988,89] and macropinocytosis.[88-91,100,115] In general, most CPPs can simultaneously undertake different mechanisms of membrane translocation and endocytosis so that a simple endocytic scheme rarely emerges.

Macropinocytosis has been reported as the major route of internalization of cationic arginine-rich CPPs and does not usually operate in cells but is rather activated by specific stimuli (e.g., growth factors or viruses).[92-94] It has been suggested that membrane-associated proteoglycans such as heparan or chondroitin sulfate proteoglycans serve as the primary receptor to induce macropinocytosis.[95,96,97] The diameters of these macropinosomes are much greater (>∼1 μm) than those for clathrin- or caveolae-mediated endocytosis (∼120 and 80 nm, respectively),[98] which may allow easier cellular uptake of nanoparticles.[99]

On the other side, clathrin- and caveolin-dependent endocytosis have been described as preferred endocytic mechanisms of different other CPPs.[100,101] In particular, the clathrin-mediated endocytosis

is the most established cell uptake pathway.[86] This engenders early endosome as earliest separated station from the plasma membrane which temporally can be loosely defined as an organelle containing material that has been internalised by endocytosis for between 2 and 5 min. The intravesicular pH drops along the endocytic pathway, from pH 6.0–6.5 in early endosomes to pH 4.5–5.5 in late endosomes and lysosomes. In contrast, caveolin-dependent endocytosis implies caveosomes, which are pre-existing intermediate cytosolic stations having neutral pH.[102] Thus, molecules internalised through this endocytic pathway may not be exposed to low pH with important consequences for drug delivery, in case of acid sensitive cargo.

Although should be always taken in consideration the risk that fluorescent dyes may alter the uptake mechanism or trigger an unusual cell entry pathway of the CPPs,[75] the use of labeled endocytic probes, especially in association with fluorescence microscopy and flow cytometry, as well as specific inhibition of endocytosis pathways can reveal considerable information regarding the cellular association, uptake and fate inside the cell of CPPs.[86,103]

Crucial limitation for the development of CPPs as therapeutics are related to: i) the lack of selectivity due to aspecific direct translocation across the plasma membrane; ii) difficulties in improving the translocation across the endosomal membrane without concurrently increasing the CPPs cytotoxicity; iii) pH degradation within the endosomial route.[76] Therefore, novel mimetics with different backbone has to be designed to overcome these specific issues and the intrinsic proteolytic susceptibility of the α-peptide backbone of CPPs.

1.4. Structural Characterization of Membrane Active Peptides and Peptidomimetics

Structural characterization is a critical step for in the development of peptides, peptidomimetics and foldamers in particular. Acquired for α-peptide/proteins, several analytical techniques are currently available for structural characterized of β-peptides and peptidomimetics in general. All these methods feature strengths, weaknesses, and limitations that must to be considered while selecting and employing them for structural determination. In addition, the specific qualities of peptidomimetic backbones have to be taken in account to avoid misinterpretation of the data and spectra acquired through techniques developed for parental α-peptide/proteins.

Circular Dichroism

Circular dichroism (CD) is a simple but sensitive tool for crude analysis of peptides and proteins.[104] The optical activity of peptides is determined by the relative spatial arrangement of the amide chromophores repeated periodically along the backbone.[105] The electronic transitions cause light absorption in the UV region and appearance of bands in the CD spectra. The different arrangement of these peptide bonds in different secondary structures, such as α-helix, β-sheets, and β-turns, produces distinct and particular patterns in CD spectra (Figure 1.5). The spectrum of an α-helix shows a negative band at about 222 nm and negative and positive bands near 208 and 190 nm, respectively. The β-sheet has a characteristic spectrum with a negative band near 215 nm and a positive band near 197 nm (± 5 nm). The degree of twisting of the β-sheet is related to the magnitude of the bands. Weakly twisted sheets have bands of equal magnitude whereas for highly twisted sheets the band near 197 nm is much stronger than the negative band. Peptides in unordered conformation generally show a strong negative band just below 200 nm and a very weak band at 217 nm, which can be either a positive band or a negative shoulder.

Thus, CD spectra also provide quantitative information as from the trace can be estimated that a protein might contain e.g. 50% helix, 30% pleated sheet, and 20% other structures.[106] The strengths of this method is that various aspects of protein structure can be measured (secondary structures, aggregation, aromatic side chain content), a minimal quantity of substance is sufficient, the influence of terminal protecting groups could rapidly be ascertained, and various solvents could be tested. Nevertheless, in case of homologated peptidomimetics, the different backbones and different intramolecular hydrogen bond patterns available of e.g. β-peptides and α-peptides lead to different conformational geometries which result in different CD spectra.[107] For example, the CD of 3_{14}-helix, that emerged as the best documented conformation of β^3-peptides, show a negative band band at ca. 215 nm,[108] whereas CD spectrum typical of the 10/12-helix of mixed β^2/β^3-peptides contains only one intense maximum between 200 and 205 nm, and sheetlike structures (apolar strands) of β-peptides give negative bands at ca 190 and 203 nm.[33] Thus, the interpretation of CD spectra of β-peptides is not always unambiguous.[14,109] For these reasons high resolution methods, such as NMR, are always required for definitive findings on secondary structures and to gain conclusive insight into the relationship between the preferred conformation of peptidomimetics and their CD spectra. Nevertheless, for peptidomimetic foldamers in general, CD spectra can be applied to draw first conclusions on the conformational and aggregation behavior. Additionally, strongly decreased CD signals can indicate aggregation, which leads to a shading of chromophores and absorption flattening.[110-112]

NMR Spectroscopy

NMR Spectroscopy has progressed to become the method for determination of protein structures in aqueous solution. This has been applied to ^{2}H-, ^{13}C-, ^{15}N-labeled proteins with molecular mass of up to 44 kD, ca. 380 amino acids.[113] Since the timescales of nuclear resonance spectroscopy are much longer than those of UV and IR spectroscopy,[104] 'average' structures are obtained; a structure present in small proportion will disappear to some extent; on the other hand, a conformation that gives rise to the (r^{-6})-dependent nuclear Overhauser effects (NOEs) will be massively overrepresented, even in relation to a present predominant conformation that gives no, or other, much weaker, NOEs. A major drawback of NMR is the complexity of the analysis which is only possible through collaboration with specialists in this field already for short (3-6 β-amino acids) sequences.[14] In addition, longer sequences generally require the incorporation of ^{13}C and/or ^{15}N labels in defined positions in order to make assignments, which is a basic prerequisite for the interpretation of the 2D NOESY/ROESY spectra demanded for conformational analysis. Lastly, NMR structural investigation in bulk of hydrophobic β-peptides are commonly performed using organic solvents.[12,11,13] However, the relationship between such structures and those that would be formed in a more physiological solution is questionable as β-peptides generally fold to the 3_{14}-helix in organic solvents but special design features are required to enable helical folding in water.[114] Indeed, the structures in H_2O are consistently more important, as the unanticipated physiological properties of β-peptides rapidly shifted interest in them in the direction of biochemistry, biology, pharmacology, and even medicine.

X-Ray Structure Analysis

X-Ray structure analysis of proteins has in recent times developed from an art into a technique,[115] which, every year, mainly in industrial pharmaceutical research, produces hundreds if not thousands of new structures.[116] Substrates of crystallized enzymes can be washed in and out without the disintegration of the single crystal, so that information relevant to the solution state is obtained. However, especially with smaller molecules, such as short-chain peptides, and also β-peptides, though, intermolecular interactions may stabilize a conformer that does not predominate either in the solution or in the gas phase.[14] More important, β-peptides made up of homologated proteinogenic β-amino acids are practically never obtainable in a crystalline state.[14]

Structure Analysis at the Air/Water Interface

In addition, the use of a confined space at the hydrophilic/hydrophobic interface in combination with sophisticated surface sensitive techniques represents an appropriate and convenient method for analysis of surface active biomacromolecules. On the one hand, the air/water interface has been established as a simplified model to mimic the physicochemical properties of the aqueous layer of a few nanometer thicknesses at the interface of biological membranes, thus allowing for the investigation of potential interaction of peptides and peptidomimetics with cell membranes and related biomedical targets.[117-120] On the other hand, Langmuir monolayer techniques provide a unique and accurate methodology to establish the relationship between chemical properties and assembly behavior at the air/water interface.[41,42,119,121-127]

There are several methods to study Langmuir monolayers in detail. The adsorption process of the peptide to the lipid monolayer can be monitored using Langmuir film balances detecting surface pressure changes and infrared reflection-absorption spectroscopy (IRRAS) detecting the appearance and changes of characteristic bands.

Langmuir Film Balances

Langmuir film balances characterize molecules that have an affinity to the air/water interface due to their amphipathic structure.

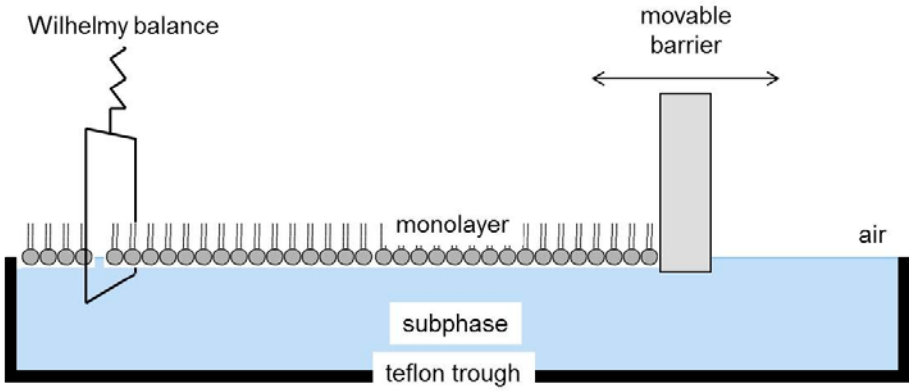

Figure 1.7. *Schematic device for Langmuir balance experiments*

Water soluble amphiphiles can adsorb to the air/water interface from a subphase forming a Gibbs monolayer which is characterized by an adsorption-desorption equilibrium. In contrast, unsoluble amphiphiles can be dissolved in an apolar solvent such chloroform and spread on the subphase and the Langmuir monolayer is formed after solvent evaporation. The structure of the monolayer can be

stabilized trough different interactions: 1) hydrophobic attraction between apolar groups which are oriented towards air; ii) electrostatic interactions bonds between polar groups which are oriented towards water; iii) polar group – subphase interactions; iv) hydrogen bonding between peptide amide groups laying parallel to the air/water surface. These interactions with and at the air/water interface lead to the reduction of the surface energy and therefore to the reduction of the surface tension γ, which can be expressed through the surface pressure π. Keeping the temperature constant, lipid monolayers can be described by the area per lipid molecule *A* and surface pressure as a twodimensional system using the isotherm $\pi = f(A)$ in analogy to a 3D isotherm $P = f(V)$. Using such an isotherm, the changes in Langmuir monolayer upon compression and phase transitions can be detected. In Gibbs monolayers, the adsorption process can be also followed by measuring the surface pressure *versus* time, but the area per molecule cannot be calculated due to desorption and uncertain number of molecules at the air-water interface.

Infrared Reflection-Absorption Spectroscopy

IRRAS provides a unique means of acquiring molecular structure information from lipid-protein Langmuir monolayer films *in situ* at the air-water interface.[128] Specifically, a shuttle system was developed to solve the problem of water vapor signal overlapping with important bands of peptides and lipids in the 1400 – 1800 cm^{-1} region (Figure 1.8).

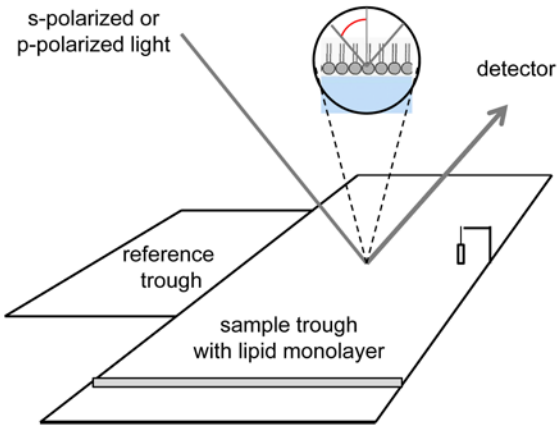

Figure 1.8. *Scheme of the IRRAS setup. A shuttle mechanism allows either the reference or the sample trough to move into the IR beam spot. Subtracting the reference from the sample spectrum yields the differential spectrum that displays the characteristic absorption bands of the monolayer.*

Infrared radiations produce motions among vibrational states of specific bonds. Vibrations fall into two main categories, stretching, producing a change in bond length, and bending, resulting in a

change in bond angle. Each of these two main types of vibrations can have variations, as a stretch can be symmetric or asymmetric and bending can occur in the plane of the molecule or out of plane. Thereby, two types of spectral information can be obtained from IRRAS measurements: frequencies and intensities. Frequencies are easier to interpret, and they provide information in the usual way about molecular structure and interactions. IRRAS peaks may be directly correlated with molecular structures or configurations. The most useful information about protein structure comes from amide I frequencies can be observed in the region of wavenumbers between 1700 – 1620 cm^{-1}. This is well correlated with protein secondary structures as basically arises from only one of the amide functional groups, the C=O stretch. Therefore, the Amide I band is exclusively determined by the length of the hydrogen bonds.[129,130] Therefore, this primarily allows for differentiating between secondary structures that are supported by weaker intramolecular hydrogen bonding pattern (higher vibrational frequencies), such helices, and stronger intermolecular hydrogen bonding networks (lower vibrational frequencies), such sheets. This has been confirmed by IRRA spectra of α-peptides as well as β-peptides.[33,124,120,126] Particular values are then assigned to specific conformations of α-peptide sequences (1657-1648 cm^{-1}, α-helix; 1657-1642 cm^{-1}, random coil; 1682-1662 cm^{-1}, turns; 1641-1623 cm^{-1}, β-sheet). The amide II band (1580 – 1520 cm^{-1}) has a more complex nature and results from C-N stretching and N-H in-plane bending vibrations. In addition, the amide A band is assigned to the amide stretching mode of the peptide backbone and appears near 3260 cm^{-1}. The broad band at 3600 cm^{-1} which corresponds to the OH stretching vibration of water molecules is important for monitoring of changes in monolayer thickness. For lipids the most important bands appear near 1735 cm^{-1} (C=O stretching vibration of lipid ester group), 1205 – 1240 cm^{-1} (phosphate vibrations), and three bands in the range between 2849 cm^{-1} and 2960 cm^{-1} corresponding to methylene stretching vibrations, which are sensitive to the conformational order of the hydrocarbon chains. The CH_2 symmetrical and asymmetrical stretching modes shift from 2854 cm^{-1} and 2924 cm^{-1} to approximately 2849 cm^{-1} and 2919 cm^{-1}, respectively, upon a transition from liquid to condensed state. The second, less widely used aspect of IRRAS involves the determination of chain and group orientation from quantitative evaluation of measured band intensities. Comparison of spectra using s- and p-polarized light can provide information about the orientation of peptide or lipid molecules.

Thus, IRRAS provides information not only about the functional groups of the molecules forming the monolayer at the air-water interface, but allows also to evaluate lipid phase transitions, tilt of the lipid hydrocarbon chain to the surface normal as well as to determine the secondary structure and orientation of peptide molecules during adsorption to the air-water interface or to lipid monolayers. Thus IRRAS is an established method to obtain structural information and show the precise influence

of MAPs, and especially AMPs, on membrane lipids, and eventually to obtain conformational and orientational information on peptides in mixed peptide-lipid monolayers in order to suggest the most possible mechanism of action.

X-Ray Structure Analysis at the Air/Water Interface

Structures of condensed phases within a monolayer can be characterized with Å-resolution using grazing incidence X-Ray diffraction (GIXD). GIXD provides information only about ordered domains within the monolayer, disordered regions contribute only to the background. Thereby, the two-dimensional structure of strand assemblies and sheet monolayers of e.g. peptides and peptidomimetics can be elucidated. In addition, the specular reflection of short wavelength radiations, i.e. X-Rays or neutrons, can yield information about the density variation across a Langmuir layer and thus elucidate the structure of such a layer on a microscopic or atomic length scale. Thus variation in electron density of a Langmuir film in the direction normal to the surface can be obtained from specular X-Ray reflectivity (XR) measurements. Thereby, XR provides an averaged electron density profile normal to the interface of all lipid and peptide components, which complements the in-plane information from GIXD.

2. Aims and Outline

Among biomacromolecules, peptides are unique systems for the hierarchical organization and fine-tuned coordination of primary sequence, physicochemical features, structural properties and biological activity. Indeed, the amino acid sequence itself encodes the physicochemical and structural qualities that result in the vast biological functions and wide potential of natural peptides. However, α-peptides generally suffer from intrinsic drawbacks such as high proteolytic susceptibility which have historically meant that very few unmodified peptides have made good drug candidates.[4] Thus wide research efforts have been devoted to the design of peptidomimetics as bioorthogonal systems with improved properties for specific biomedical applications.

One important class of such peptidomimetics are the β-peptides, which differ from natural α-peptides by having a one-carbon moiety inserted into every amino acid residue.[11-13] Besides extreme proteolytic stability, the β-peptides feature unique folding propensity for helical conformations. Therefore they are applied for two major areas of biomedical research: On the one hand, β-peptides with proteinaceous side chains are synthesized and show the possibility to efficiently mimic biofunctional helical sections of natural α-peptides and proteins and modulate important peptide/protein-protein interactions.[6,12,34,131] On the other hand, amphiphilic cationic β-peptides with helical conformation are obtained showing strong interactions with biomembranes and can act as mimetics of antimicrobial (AMPs) and cell-penetrating (CPPs) peptides.

Nevertheless, only few examples of β-peptide strands and sheets have been reported. Besides the α-helix, the β-sheet conformation is the most important of protein secondary structures and plays a key role in many biological processes.[32] For instance, β-strands aggregation and sheet formation are crucial in the pathogenesis of several amyloidosis. Thus mimicking β-strands has been proposed as a viable therapeutic strategy *e.g.* against Alzheimer's disease.[2] Therefore, extensive design efforts have been focused on the substitution of the C2 and the C3 atoms in order to extend the structural space of β-peptides towards strand conformations and sheet structures.[11-13] However, limited outcome has further prompted alternative strategies, such as hybrid oligomers of both α- and β-amino acids ("α/β-peptides") designed to form strands which can assemble through the formation of hydrogen-bonded sheets at the air–water interface.[41]

In addition, despite their potential as e.g. antimicrobial and cell-penetrating agents for drug delivery, cationic amphiphilc β-peptides with helical conformation tend to display significant hemolytic activity,[19,20,21,22,23] which essentially hampers the development of these systems as therapeutics. Therefore, to further realize the biomedical potential of classical β-peptides, novel design attempts are required to: 1) extend the structural space available to β-peptides towards non-

helical conformations, and 2) optimize the biocompatibility and increase the therapeutic index of β-peptides while keeping their high biological activity and enzymatic stability.

The aim of this work is to introduce a novel class of peptidomimetics, the β^{3R3}-peptides. This novel system is based on alternating directions of the amide bonds along β-peptide sequences and has been designed to combine intrinsic physicochemical properties of α- and β-peptides. On the one hand, as for β-peptides, Cβ homologation can promote the formation of secondary structures along with improved proteolytic stability. On the other hand, the novel qualities of the backbone with alternating direction of the amide bonds are expected to extensively modulate both the structural and biological properties of classical β-peptide.

The synthetic strategy towards this new class of peptidomimetics is based on solid phase synthesis (SPS) using tailor-made building blocks. Initial focus of this work is devoted to the synthesis of a set of chiral β-diamine building blocks starting from natural amino acids thus introducing a proper set of proteinaceous side chains with tunable physicochemical properties. In addition, novel diacid building blocks will be prepared via asymmetric synthesis with chiral auxiliary or selected from the pool of commercially available chiral β-diacids with bioactive side chains (e.g. aspartic acid and malic acid). Moreover, diamine and diacid building blocks will be coupled in solution to provide dimer building blocks suitable for conventional Fmoc SPPS protocols and allow for fully automated synthesis using a standard peptide synthesizer.

These building blocks will then be applied for the synthesis of designed sets of oligomers with different physicochemical features: hydrophobic and amphiphilic cationic β^{3R3}-peptides. Thus, specific structure-activity relationship studies comprising physicochemical and biological investigations will be detailed to evaluate the potential of these classes of β^{3R3}-peptides as peptidomimetics for designed biomedical applications. Specifically, β^{3R3}-peptides with hydrophobic proteinaceous side chains will be introduced with particular emphasis dedicated to their design and characterization of their folding and self-assembling properties at the air/water interface. As a second class of β^{3R3}-peptides, amphiphilic cationic β^{3R3}-peptides will be evaluated for their potential as antimicrobial as well as cell-penetrating agents.

Results and Discussion

3. Building Block Design and Synthesis

The aim of this work is to introduce a novel class of β-peptidic peptidomimetics for selected biomedical applications. β-peptides have been prominent in the development of the foldamer field displaying a distinct propensity for helical conformations.[11-13] Additionally, β-peptides have been further recognized for their proteolytic stability and potential self-assembling properties, which have strongly promoted their application as peptidomimetics in biomedical sciences.[6,12,33,34,131] However, the strong propensity for helical conformations and lack of strands and sheet structures still limits the wide potential of β-peptides. Therefore, the strategy of this work is based on a novel class of peptidomimetic foldamers using tailor-made building blocks and SPS to combine intrinsic physicochemical features of α- and β-peptides and display designed properties for a variety of biomedical applications.

The first chapter of the results and discussion section therefore will deal with the design principle and the synthesis of the required tailor-made building blocks. These building blocks will be applied in the following chapter for the SPS of oligomers. These oligomers will be evaluated in the last chapter for both, their structural and biological properties, and thus their potential for different biomedical applications.

3.1. Design Principle

β-peptides with proteinaceous side chains have recently attracted considerable biomedical interest for their potential such as inhibitors or modulators of peptide-protein interactions and antibacterial or cell-penetrating agents. However, to further develop the biomedical potential of classical β-peptides extensive research efforts are still devoted to extend their structural space towards non-helical conformations and to optimize their therapeutic index by reducing their cytotoxicity.

Indeed, only few examples of β-peptide strands and sheets have been reported. Besides the α-helix, the β-sheet conformation is the most important of protein secondary structures and plays key roles in biological and pathological processes.[32] For instance, mimicking β-strands have been proposed as a viable therapeutic strategy *e.g.* against Alzheimer's disease.[2] Therefore, extensive design efforts have been devoted to extend the structural space of β-peptides towards strand conformations and sheet structures.[11-13] In particular, extensive design has been focused on the substitution of the C2 and the C3 atoms in the β-peptide backbone, and the use of heterochirally disubstituted β-amino acids has been proposed as the only suitable strategy aiming at strand conformations.[11-13,33,34] However, strand conformations have been reported only for β-peptide sequences which are quite short (3 residues),[35] constrained in hairpin structures by turn-forming segments,[35,36,37,29,38,39] or conformationally stabilized through ring incorporation in the β-amino acid residues.[33,40] Thus, the limited outcome has further promoted the development of alternative strategies.[41-45] For instance, oligomers made of both α- and β-amino acids ("α/β-peptides") have been designed to form strands which can assemble through the formation of hydrogen-bonded sheets at the air–water interface.[41] Indeed, a major difference between linear strands of α- and β-peptides is the carbonyl orientation of sequentially alternated amide bonds (Figure 3.1),[14,132] which can promote intermolecular hydrogen bonds and sheet self-assembling of α-peptides strands.

Thus the idea is to install such alternating amide bond orientations and combine this novel peptidic backbone with the chiral side chains of the natural α--peptides, giving a new class of ß-peptide analogues (Figure 3.1). According to the nomenclature of β-peptide regioisomers,[133] these oligomers are termed β^{3R3}-peptides, where 3 and 3 indicate the position of the side chains on the diacid and diamine subunits, and 'R' stands for 'Retro' referring to the direction of the amide bond which reverses within each repeating unit (Figure 3.1. a). On the one hand, these novel β-peptides analogues have the potential to form α-peptide-like apolar strands in extended conformation (Figure 3.1. a).[14,132,134] On the other hand, the Cβ homologation can induce a folding propensity favoring specific conformations with dihedral angles about the C(2)-C(3) bonds that e.g. minimize steric repulsion of bulky substituents at the C(2) or C(3) positions (Figure 3.1. b).[14,15132] Finally, this backbone has the

potential to formally access intramolecular hydrogen bond patterns which differ from the ones observed for β-peptides (Figure 3.1. c). Thereby and due to the potential to form apolar strand in extended conformation, β^{3R3}-peptides are expected to display orthogonal folding behaviour with respect to β-peptides. In order to obtain such β^{3R3}-peptides tailor-made building blocks have to be synthesized. In the following chapter, the design and synthesis of such building blocks will be presented.

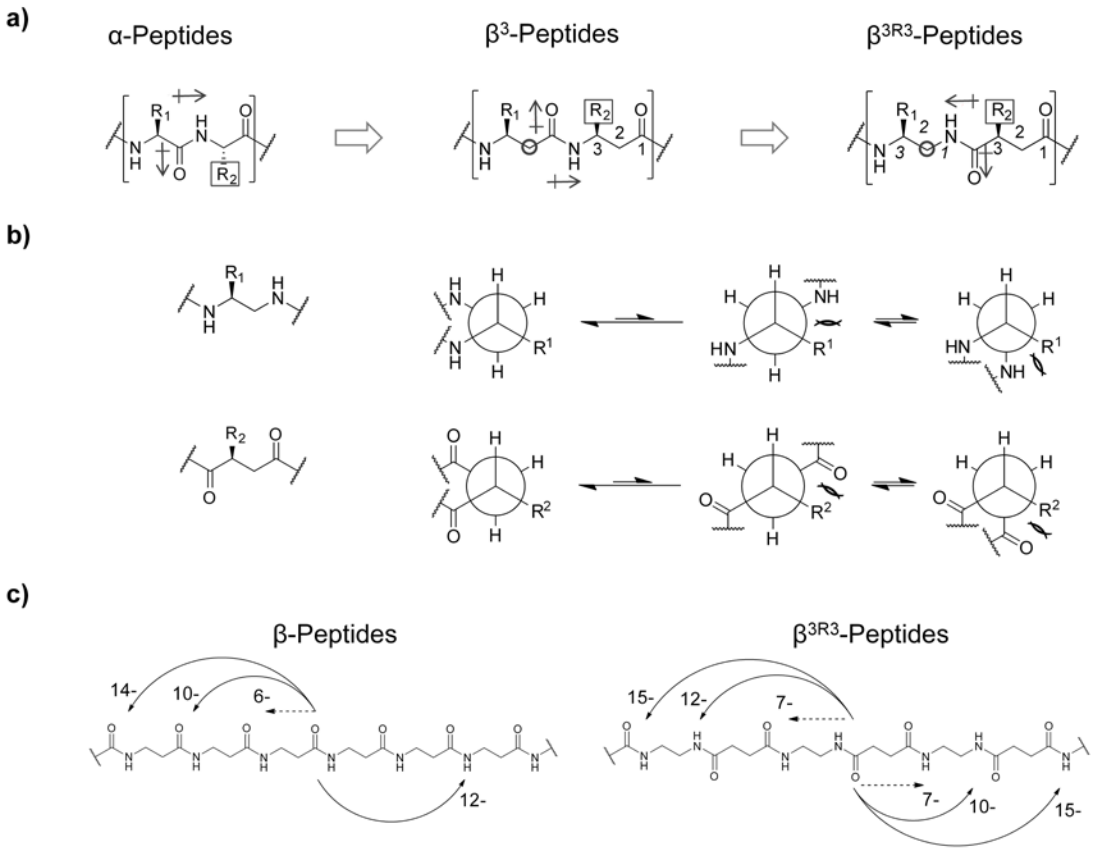

Figure 3.1. *Design criteria of the β^{3R3}-peptides backbone. a) Comparison of repeating units and linear strands of α-, β^3- and β^{3R3}-peptides. In β^{3R3}-peptides: i) monomers are homologated by CH_2 insertion; ii) the side chains are all exposed on the same face of a linear arrangement; iii) the direction of the amide bond reverses at each bond; iv) each layer of a linear strand is apolar with alternating orientation of carbonyl groups. Thus alternating the direction of the amide bonds β^{3R3}-peptides can combine structural features of α- and β-peptides. b) Effect of bulky alkyl substituents on the C1-C2 torsional angle of β^{3R3}-peptides. Similarly to other β-peptides, monosubstitution at C2 or C3 in both the diamine and diacid subunits favors a gauche conformation, which minimizes steric repulsion present in other conformers. c) Comparison of the tightest intramolecular hydrongen bond patterns observed in β-peptide oligomers and available to β^{3R3}-peptides. β-peptides show mainly C_{10}-, C_{12} and C_{14}-type intramolecular hydrogen bonds leading to helical conformations. In addition, homo-oligomers composed of heterochiral disubstituted cyclic β-amino acids can form self-stabilizing apolar strands with C_6-type hydrogen bonds (linear dotted arrows).[33] In contrast β^{3R3}-peptides can formally access C_7-, C_{10}-, C_{12}-, and C_{15}-type intramolecular hydrogen bonds.*

3.2 Building Block Synthesis

Our synthetic strategy takes advantage of SPS using novel synthetic building blocks to build up sequence-defined oligomers.[135-138] Such building blocks are conveniently based on the fundamental repeating unit of the β^{3R3}-peptide backbone, which is constituted by alternating condensation of β-diamines and β-diacids (Scheme 3.1). Thus, a basic retrosynthetic analysis suggests the use of building blocks of chiral monosubstituted β-diamines and β-diacids (Scheme 3.1).

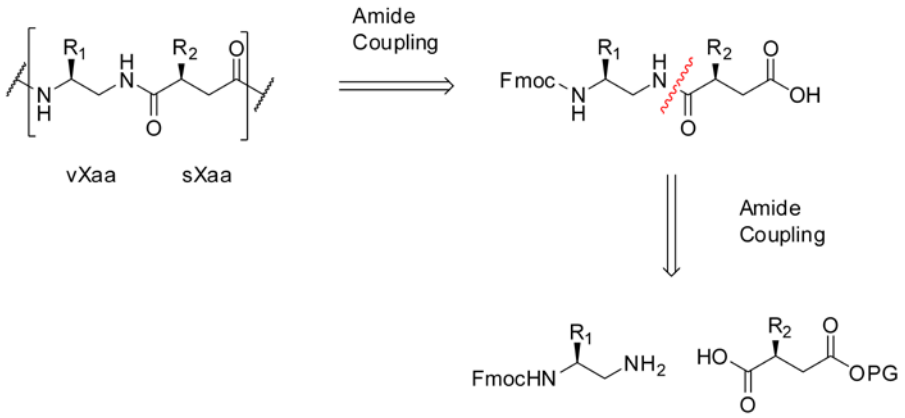

Scheme 3.1. *General synthetic strategy towards the synthesis of β^{3R3}-peptide oligomers.*

Referring to partially modified retro-inverso analogues of α-peptides,[139] for the nomenclature of the building block library was applied the *v*/*s* prefix system in which *v*Xaa symbolizes the vicinal diaminoalkyl analogue and *s*Xaa symbolizes the succinyl analogue of the indicated amino acid residue Xaa (Scheme 3.1). Thus, the first step was to synthesize a proper set of diamine (*v*Xaa) and diacid (*s*Xaa) building blocks suitable for SPS.

3.2.1 Diamine Building Blocks

Building blocks suitable for SPS need to fulfill specific requirements: building block synthesis generally should employ readily available starting materials and give high yields on a multigram scale while avoiding laborious purification procedures. Furthermore, building block coupling on solid phase should proceed according to conventional Fmoc SPPS protocols, which can be fully automated using a standard peptide synthesizer. Accordingly, the diamine units were equipped with an Fmoc-protective group on the primary amino group placed in the original Cα position. This allows for regioselective amide coupling reaction involving the amino group in β position and keeps a defined polarity of the diamine units along the β^{3R3}-peptide sequences.

Hydrophobic Proteinaceous Diamine Building Blocks

First, Fmoc-protected monosubstituted β-diamines with L configuration at the stereocenter and different hydrophobic proteinaceous side chains were targeted. L configuration was chosen as it allows employing natural and less expensive L-α-amino acids as starting material. On the other side, hydrophobicity is perhaps the most critical physicochemical parameter for the different β^{3R3}-peptide sequences that will be presented in the next chapters. All these classes of β^{3R3}-peptides have been designed and developed to target biomedical applications for which physicochemical factors rather than the specific primary sequence are essential, which will be detailed in chapter 5. In addition, specific patterns of proteinaceous side chains not only allow for the fine tuning of physicochemical properties of β^{3R3}-peptide sequences, but could also make a decisive contribution to their affinity to biomedical targets.

Several synthetic strategies have been presented for the synthesis of mono Fmoc-protected vicinal diamines derived from L-α-amino acids. The choice of Fmoc-protected α-amino acids as starting materials is common and apparently convenient. However, the relatively low solubility of Fmoc-protected α-amino acids critically hampers large scale synthesis and none synthetic route has been so far reported to produce more than a few grams of product. Additionally, not convenient reagents, such as the extremely explosive hydrazoic acid (HN_3), have been employed.[140] Moreover, laborious purification methods, such as column chromatography are required.[140,141]

The major chemical issue of using Fmoc-protected α-amino acids along the whole route is the sensitivity of the Fmoc group to common amine synthons, such as azide nucleophiles. Thereby,

neither reaction temperature above room temperature (rt) nor long reaction times can be applied. Thus, a novel synthetic route was attempted based on iodine as key reagent. Iodine is on the one hand a powerful nucleophile which can substitute at rt and within short reaction time the mesyl living group of easily accessible Fmoc-protected vicinal derivatives of α-amino acids. On the other hand the weakness of the carbon-iodine bond can allow for the nucleophile substitution of iodine by the convenient amine synthon sodium azide (NaN_3). However, starting from Fmoc-protected Ala as pilot model in 20g scale, severe solubility issue and not reproducible yield of the azido intermediate were encountered. Indeed, such problems have been already reported for different Fmoc-protected derivatives of natural amino acids.[141]

Therefore a novel versatile route was developed using Boc-protected L-α-amino acids as starting material for the synthesis of the Fmoc-protected enantiomerically pure vicinal diamines with proteinaceous side chains (Scheme 3.2). All that was most important in the process was to have the necessary building blocks available in quantities suitable for solid-phase synthesis which does not leave much space for synthetic elegance. Indeed, this route allowed for scale up to 30g without any solubility issue.

L-Ala was also here selected as pilot model for development of the synthetic protocols. Then, the route was extended to L-Val, L-Leu and L-Phe. This set of side chains primarily provides fine scale of hydrophobicity, which is perhaps the most critical physicochemical parameter for the different classes of β^{3R3}-peptides developed in this work. In addition, the aromatic side chain of Phe can play a peculiar role producing both hydrophobic and π-π interactions with biomedically relevant targets, which will be specifically investigated in chapter 5.

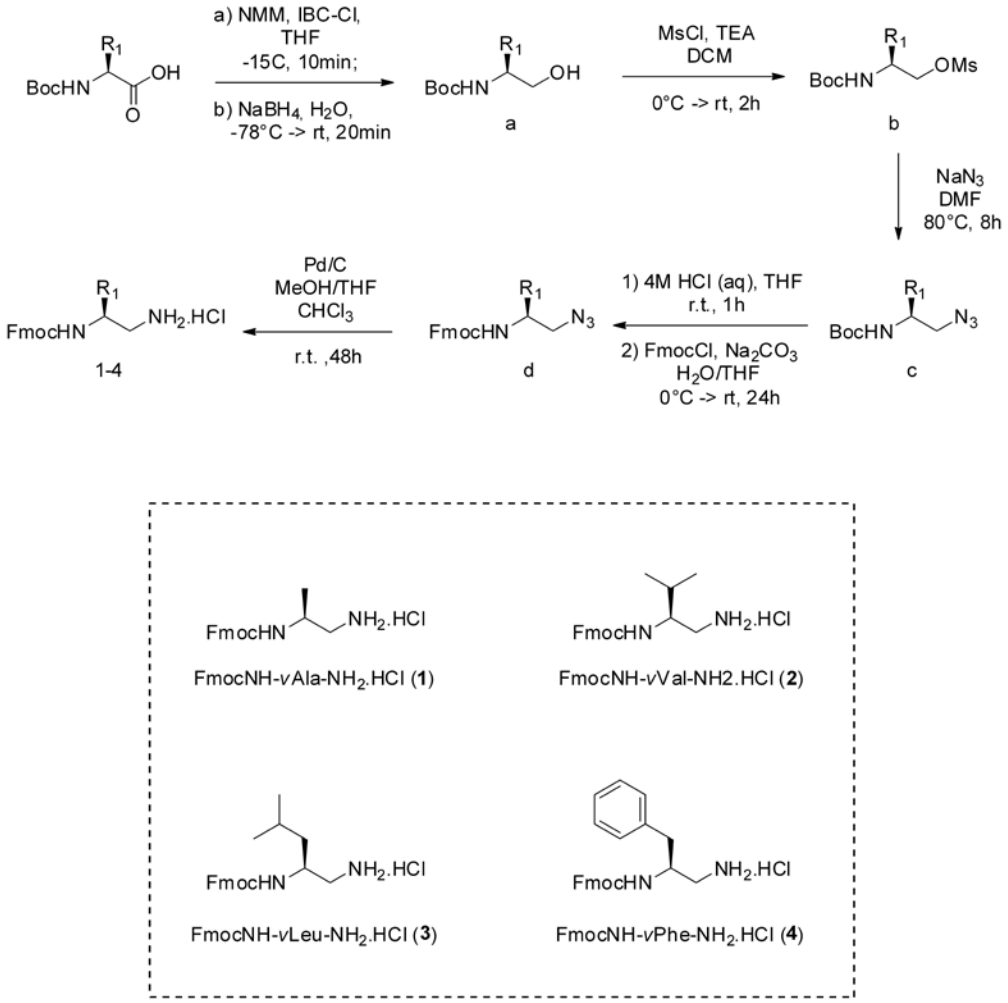

Scheme 3.2. *Synthetic scheme for the synthesis of the β^{3R3}-peptide diamine building blocks FmocNH-vAla-NH_2.HCl (**1**), FmocNH-vVal-NH_2.HCl (**2**), FmocNH-vLeu-NH_2.HCl (**3**), and FmocNH-vPhe-NH_2.HCl (**4**).*

Thus, commercially available Boc-protected natural α-amino acids were first reduced to the corresponding β-amino alcohols. The reduction of the carboxylic function was achieved through preactivation as isobutyl mixed anhydride and reduction with $NaBH_4/H_2O$.[140] The literature protocol was modified to allow for substantial scale up (30g scale), varying the concentration of the reagents as well as the reaction temperature and time. The hydroxyl group was then converted with Mesyl Chloride into the Mesyl derivative as a leaving group. Here, both THF and DCM provided good yield, but DCM resulted preferable allowing for more straightforward purification (direct washing of the organic phase with acidic water solution). Nucleophilic substitution of the mesyl moiety in DMF with sodium azide as nitrogen nucleophile afforded the Boc-protected azido derivative as diamine precursor. Then the protective group switch from Boc to Fmoc was performed. First, Boc was removed with HCl(aq) in H_2O/THF mixture and the free amino group was then protected with

Fmoc-Cl in H_2O/THF mixture and Na_2CO_3 as base. Finally the azide moiety was reduced to amine and yielded the Fmoc-protected enantiomerically pure vicinal diamines. The reduction was performed via catalytic hydrogenation with Pd/C in THF/$CHCl_3$, as the addition of $CHCl_3$ directly affords the hydrochloridric salt of the mono Fmoc-protected diamine which avoids the autocleavage of the Fmoc protective group.[142] Additionally, a Staudinger reduction using PPh_3 in aq. THF acidic conditions proved to be a suitable alternative for the azide reduction. However, this protocol also brings more considerable purification issues and therefore catalytic hydrogenation has been preferred and established as method of choice. Thereby, all the Fmoc-protected diamine monomers, FmocNH-*v*Ala-NH_2.HCl (**1**), FmocNH-vVal-NH_2.HCl (**2**), FmocNH-*v*Leu-NH_2.HCl (**3**), and FmocNH-*v*Phe-NH_2.HCl (**4**), were produced using natural amino acids as a pool of chiral starting materials, in 30 g scale with high yield (Table 3.1) and purity (Figure 3.2).

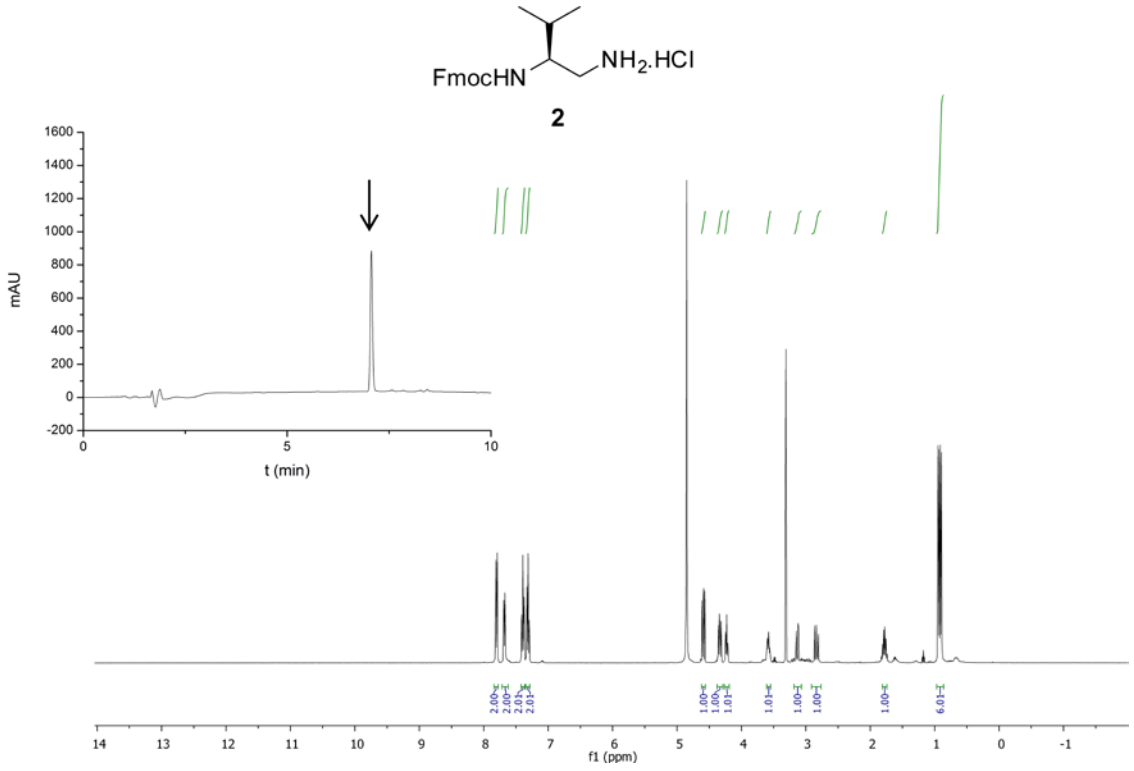

Figure 3.2. *HPLC trace (5 to 95% MeCN to H_2O in 10min) and NMR spectrum in MeOD of FmocNH-vVal-NH_2.HCl* ***(2)****, as representative example showing the efficiency of the purification protocols developed for the synthesis of β^{3R3}-peptide diamine building block with proteinaceous hydrophobic side chains.*

Conclusively, the developed route fulfills the requirements for the synthesis of building blocks suitable for SPS, employing readily available starting materials and giving high yields on a multigram scale. Most notably, these procedures were developed to rely exclusively on simple and convenient purification methods and no chromatographic purification was required, allowing for performing reactions in parallel and further scale up.

Hydrophilic Non Chiral Diamine Building Block

Afterwards, the non-chiral analogue of Gly (*v*Gly) was targeted. This represents a convenient less hydrophobic residue that further allows for fine tuning of physicochemical determinants of β^{3R3}-peptide sequences. Therefore, a novel convenient route was developed for the preparation of mono Fmoc-protected ethylenediamine (EDA) as trifluoroacetic acid (TFA) salt, FmocNH-vGly-NH_2.TFA (**5**) (Scheme 3.3).

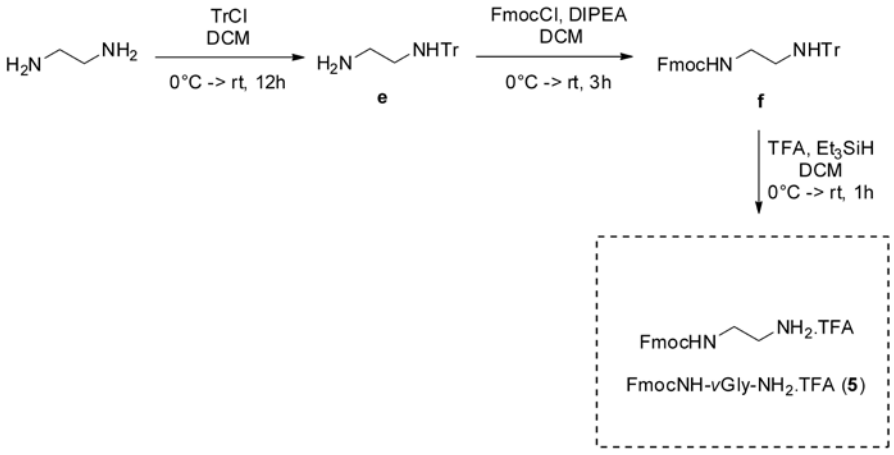

Scheme 3.3. *Synthetic scheme for the synthesis of the β^{3R3}-peptide diamine building block FmocNH-vGly-NH_2.TFA (**5**).*

First, the two primary amine groups of EDA were differentiated by quantitative protection of just one amine group. This was achieved dropping at 0°C the chloro derivative of the bulky triphenylmethyl group into an excess of EDA to give the corresponding monoprotected trityl (Tr) diamine. Then FmocCl in dry DCM and DIPEA as base were used to protect the remaining free amine group and gave the asymmetrical protected diamine on scale of up to 50 g (Table 3.1). Finally the Tr protecting group was removed using 5% TFA in DCM in presence of Triethylsilane as scavenger for the Tr cation. Thereby the TFA salt of the mono Fmoc-protected *v*Gly derivative, FmocNH-*v*Gly-NH_2.TFA (**5**) was obtained with an overall yield of 75%.

Functionalized Diamine Building Blocks

Lastly, diamine building blocks with functional side chains were synthesized to extend the range of functional β^{3R3}-peptide constructs and potential biomedical applications. In particular, functionalized diamine monomers were prepared to provide acidic and negative charged carboxyl functionality as side chain. This in combination with positively charged diacid building blocks can allow for making up e.g. zwitterionic β^{3R3}-peptide sequences as novel anti-fouling agents.

Specifically, diamine building blocks protected as allyl ester (*v*COO(Allyl)) were targeted due to compatibility of the protective group with Fmoc SPS protocols and a convenient synthetic route already reported in literature.[143]

In addition, two enantiomeric building blocks, FmocNH-(S)*v*COO(Allyl)-NH_2.HCl (**6**) and FmocNH-(R)*v*COO(Allyl)-NH_2.HCl (**7**), have been synthesized (Scheme 3.4). Indeed, structural factors can be prominent for the β^{3R3}-peptides not just as foldamer but eventually also for specific biomedical application (Chapter 5). Specifically, the configuration of the chiral center on *v*COOH diamine units is expect to dictate to a significant extent the conformation of β^{3R3}-peptide sequences. In particular, here the electrostatic interactions of the carboxy moiety in α position can produce a stronger influence on the backbone conformation than e.g. the carboxy functionality in β and γ position of Asp and Glu, where the flexible alkyl moiety can relieve the conformational drive.

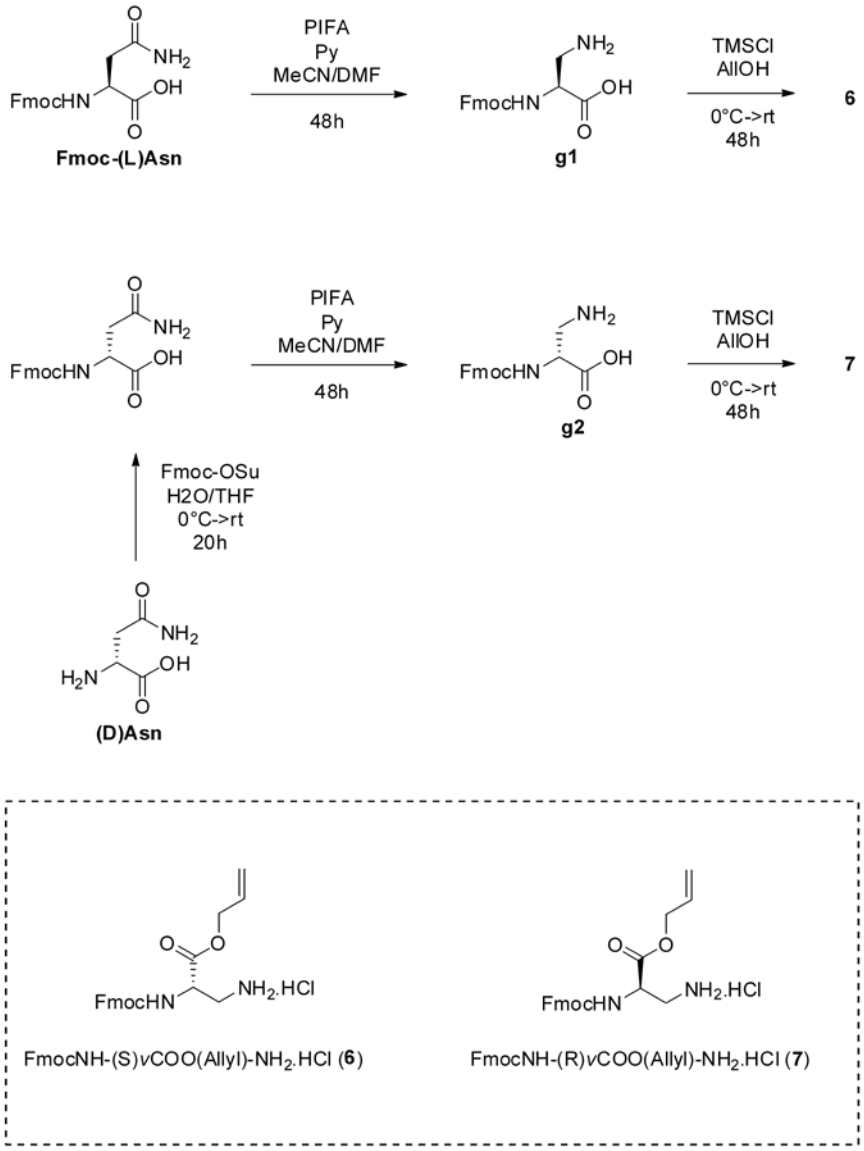

Scheme 3.4. *Synthetic scheme for the synthesis of the β^{3R3}-peptide diamine building blocks FmocNH-(S)vCOO(Allyl)-NH_2.HCl (**6**) and FmocNH-(R)vCOO(Allyl)-NH_2.HCl (**7**).*

A literature protocol was adapted using Fmoc-Asparagine (Asn) as starting material.[143] The two enantiomers FmocNH-(S)*v*COO(Allyl)-NH_2.HCl (**6**) and FmocNH-(R)*v*COO(Allyl)-NH_2.HCl (**7**) have been synthesized from (L)-Asn and (D)-Asn, respectively. Specifically, as commercially available Fmoc-(L)-Asn was employed as convenient starting material for the synthesis of FmocNH-(S)*v*COO(Allyl)-NH_2.HCl (**6**). Thus, the building blocks **6** and **7** were synthesized on 15g scale following a two and three step routes, respectively. In the first step towards building block **7,** the free amine was protected with Fmoc-OSu in in water/THF using $NaHCO_3$ as base. Then, primary amide in β position on the Asn side chain was transformed into a primary amine moiety via Hofmann

rearrangement. This reaction was performed in a mixture of DMF/water using Phenyliodine bis(trifluoroacetate) (PIFA) and pyridine (Py) as base. Finally, the α-carboxylic acid was esterified with allyl alcohol employing the Lewis acid chlorotrimethylsilane (TMSCl) as catalyst. This directly gave the desired HCl salts of the building blocks FmocNH-(S)*v*COO(Allyl)-NH_2.HCl (**6**) and FmocNH-(R)*v*COO(Allyl)-NH_2.HCl (**7**) in high purity with overall yields of 54% and 44%, respectively (Table 3.1).

Table 3.1. *Scale and yield for the synthesis of Fmoc-protected diamine monomers* ***1-7****.*

Diamine Building Block (**n_o**)	**Yield** [%]	**Scale** [g]
FmocNH-*v*Ala-NH_2.HCl (**1**)	39	30
FmocNH-*v*Val-NH_2.HCl (**2**)	42	30
FmocNH-*v*Leu-NH_2.HCl (**3**)	42	30
FmocNH-*v*Phe-NH_2.HCl (**4**)	44	30
FmocNH-*v*Gly-NH_2.TFA (**5**)	75	50
FmocNH-(S)*v*COO(Allyl)-NH_2.HCl (**6**)	54	15
FmocNH-(R)*v*COO(Allyl)-NH_2.HCl (**7**)	44	15

3.2.2. Diacid Building Blocks

The β^{3R3}-peptide backbone is constituted by alternating condensation of β-diamines and β-diacids (Scheme 3.1). Thus, in the previous section different β-diamine building blocks have been prepared. In this section, the synthesis of the β-diacid building blocks will be detailed.

A major synthetic advantage of using β-diamines and β-diacids as building blocks (Scheme 3.1), is the pool of commercially available chiral β-diacids with functionalized side chains, such as aspartic and malic acid. This indeed provides an attractive platform of β-diacid units suitable for the design of building blocks with different physicochemical properties and biological activities. Therefore, in combination with the set of Fmoc-protected β-diamines presented in the previous sections, distinct classes of β^{3R3}-peptides for different biomedical applications can be accessed.

For instance, Succinic anhydride (Suc) is an extremely convenient building block and can be directly used as synthon for the β^{3R3}-peptide diacid derivative *s*Gly (Scheme 3.5). Indeed, Suc is highly cheap and chemically efficient and has been already employed *e.g.* as building block for the assembly of diacids and diamines on solid-support to obtain monodisperse, sequence-defined PAA segments.[144]

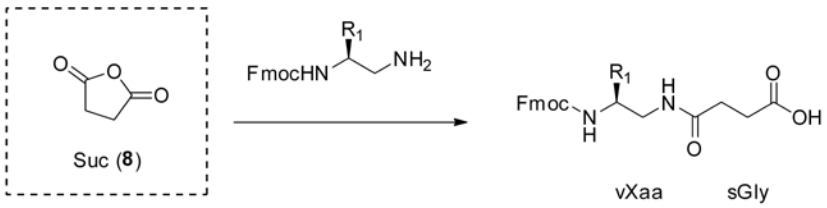

Scheme 3.5. *Commercially available Suc* ***(8)*** *was exploited as building block for the* β^{3R3}*-peptide diacid unit sGly.*

On the other hand, for substituted β^{3R3}-peptide diacid units, the building blocks have to be monoprotected in order to keep a defined polarity and allow for regioselective amide coupling reaction the diamine counterparts. This can be achieved using specific routes based on asymmetric synthesis protocols. In alternative, commercially available monoprotected β-diacid can be employed either as starting material or directly as β^{3R3}-peptide building blocks.

Hydrophobic Proteinaceous Diacid Building Blocks

Different synthetic route presented in literature for the synthesis of β-amino acids can be properly tailored for the preparation of β^{3R3}-peptides diacid (*s*Xaa) building blocks with hydrophobic proteinaceous side chains. Indeed, monoprotected enantiomerically pure vicinal diacids with proteinaceous side chains represent common intermediates of the most efficient routes developed for the synthesis of β^2-amino acids.[14] Compared to β^3-amino acids, β^2-amino acids are accessible only with difficulty. However, especially for β^2hAla, β^2hLeu, or β^2hPhe, convenient synthetic paths have been established based on Evans auxiliaries.[145-149] Here, the Evan's auxiliary (4R)-4-Benzyl-1,3-Oxazolidin-2-one was selected as it affords through A(1,3) allylic strain and steric interaction the β^{3R3}-peptide diacid building blocks OH-*s*Ala-O*t*Bu (**9**) and OH-*s*Phe-O*t*Bu (**10**) with S configuration (Scheme 3.6).[145] Such configuration is also featured by the diamine building blocks as well as most of classical β-peptides and therefore allows for direct comparison and exploiting the knowledge already established with classical β-peptides.

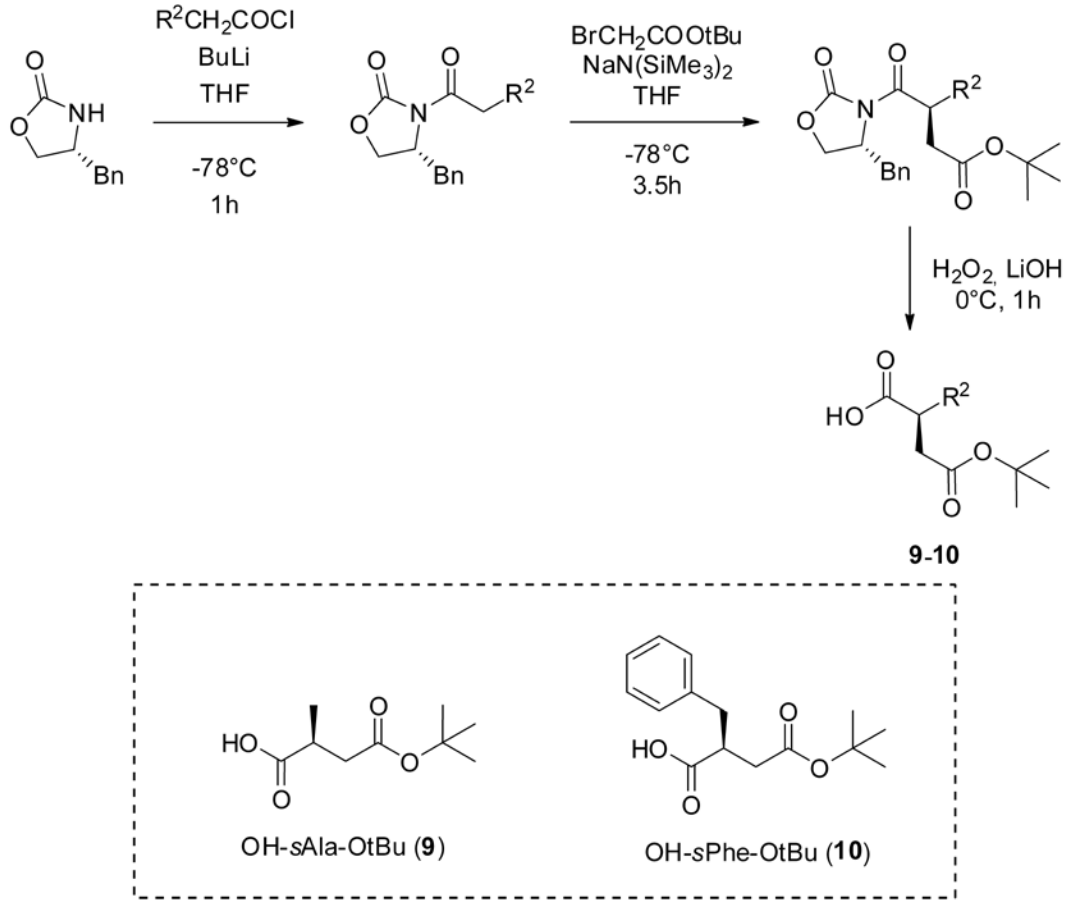

Scheme 3.6. *Synthetic scheme for the synthesis of the β^{3R3}-peptide diacid building blocks OH-sAla-OtBu (**9**) and OH-sPhe-OtBu (**10**).*

The Evan's auxiliary presents several attractive features: it is commercial available; it is easy to be synthesized in large scale; it provides intermediates which are prone to recrystallized and so do not generally requires column chromatography purifications; it gives high diastereoselectivity which allows to get the products in absolute enantiomeric purity after recrystallization. Due to the high commercial cost, the chiral auxiliary was synthesized in 100 scale starting from D-Phe (Scheme 3.7).

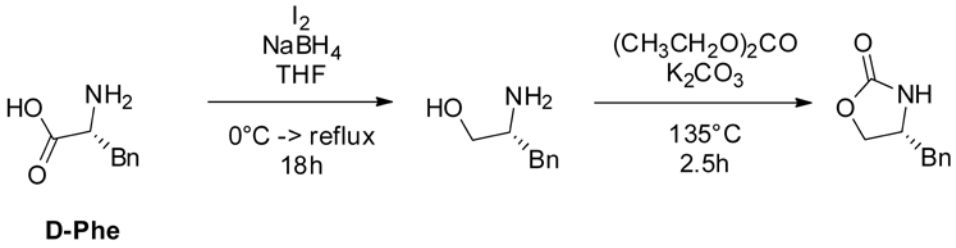

Scheme 3.7. *Synthetic scheme for the synthesis of the Evan's auxiliary (4R)-4-Benzyl-1,3-Oxazolidin-2-one.*

Thus, D-Phe was reduced by the combination of $NaBH_4/I_2$ and the Oxazolidin-2-one of the auxiliary finally formed using Diethylcarbonate and K_2CO_3. The auxiliary was then N-acylated with the appropriate acyl chloride in dry THF and BuLi as base giving the crystalline imides in good yield. This was then alkylated with *tert*-butyl bromoacetate were obtained via enolization with sodium hexamethyldisilazide (THF, 0.5 M, -78°C) and following addition of the electrophile. After isolation of alkylated imides, the oxazolidinone auxiliary was removed using lithium hydroperoxide,[150] giving the mono *tert*Butyl-ester protected carboxylic acids in high yields with reaction times about 3.5 h at 0 °C (table 3.2).

Such *tert*Butyl-ester could be then directly employed for the coupling with the Fmoc-protected diamine counterparts (*v*Xaa). Indeed, the *tert*Butyl-ester protecting group, on the one hand, introduce a define polarity in the asymmetric diacid units thereby allowing for regioselective coupling; on the other, the *tert*Butyl-ester is conveniently removed under acidic condition being orthogonal to the Fmoc-protecting group. Thus, the *tert*Butyl-ester protected β-diacids **9** and **10** will be coupled in solution with the previously presented Fmoc-protected β-diamine building blocks (Section 3.2.3).

Functionalized Cationic Diacid Building Blocks

Among natural chiral β-diacids with functionalized side chains, aspartic acid (Asp) is particularly attractive as building block for β^{3R3}-peptides. Indeed, as succinic acid analogue, Asp can display as side chain the primary amino group in α-position. This represents a potential bioisoster of lysine (Lys) providing biological activities suitable for targeting currently demanding biomedical applications. For example the cationic character is essential for the activity of MAPs such as AMPs and CPPs (Chapter 5). Additionally, a variety of differentially protected derivatives of Asp is commercially available. Specifically, Boc-S-Asp(Bn)-OH is a good candidate as β^{3R3}-peptide diacid monomer, being the Boc and Benzyl (Bn) ester orthogonal to the Fmoc-protecting group. Moreover, the R enantiomer Boc-R-Asp(Bn)-OH have been also employed. Here, in analogy to the *v*COOH diamine unit previously presented, the configuration of the chiral center is expected to produce a strong influence on the conformation of β^{3R3}-peptide sequences. Indeed, being the cationic NH_2 group in α position directly connected to the backbone without interposition of flexible alkyl chains, electrostatic interactions that drive the juxtaposition of the side chains can have a direct effect on the oligomer conformation.

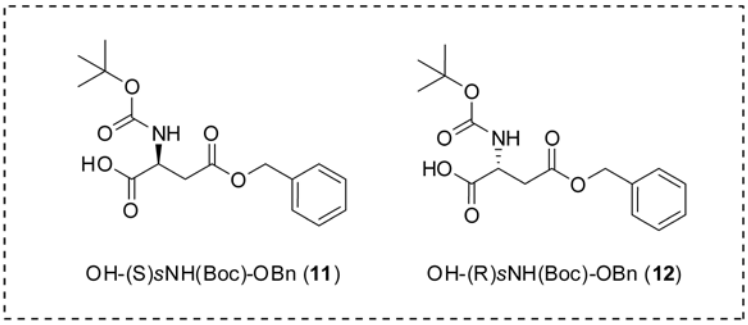

Scheme 3.8. *Commercially available Boc-L-Asp(Bn)-OH (**11**) and Boc-L-Asp(Bn)-OH (**12**) were employed as monomer building blocks OH-(S)sNH(Boc)-OBn (**11**) and OH-(R)sNH(Boc)-OBn (**12**).*

In addition, Alloc-S-Asp(*t*Bu)-OH is another suitable β^{3R3}-peptide diacid monomer, being attractive for selective side chains deprotection on solid support by the use of palladium(0) and an appropriate scavenger (Section 3.3). On the one hand, this allows for introducing specific branching points in selected positions on the backbone.[136] On the other hand, it also enhances the flexibility of the overall synthetic strategy as the *tert*-butyl ester of Alloc-S-Asp(*t*Bu)-OH can be selectively removed under acidic conditions in presence of the allyl ester of Fmoc mono-protected diamine building blocks, such as FmocNH-(S)*v*COOH(Allyl)-NH_2.HCl (**6**) and FmocNH-(R)*v*COOH(Allyl)-NH_2.HCl (**7**). However, Alloc-S-Asp(*t*Bu)-OH is not commercially available and therefore was synthesized through a straightforward two steps route starting from Fmoc-L-Asp(*t*Bu)-OH (scheme 3.9).

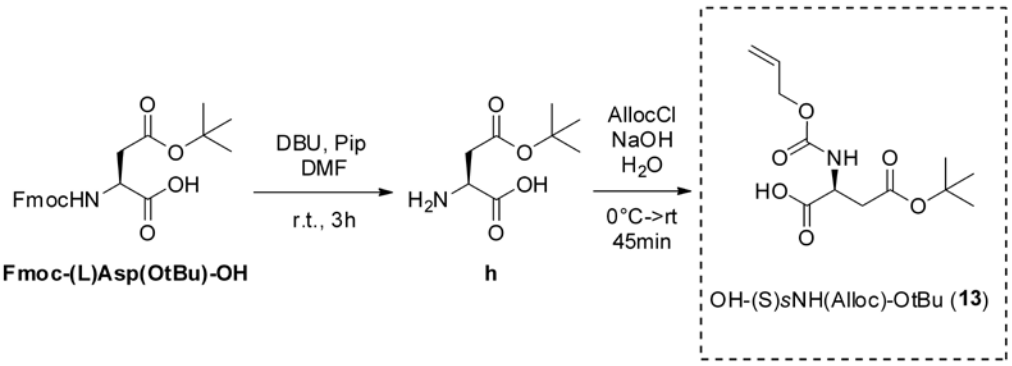

Scheme 3.9. *Synthetic scheme for the synthesis of the β^{3R3}-peptide diacid monomer OH-(S)sNH(Alloc)-OtBu (**13**).*

First, the Fmoc group was removed with 1,8-diazabi-cyclo[5.4.0]undec-7-ene (DBU)-piperidine (Pip)-DMF (1/1/48, v/v/v) followed by precipitation in Et_2O. Then the alloc protection reaction was performed in aqueous solution emplying NaOH as inorganic base. Overall, this route efficiently provided the desired Alloc-L-Asp(*t*Bu)-OH in high yield (47%) on high scale (30g) also employing only convenient purification protocols, such as precipitation and extraction.

Functionalized Hydroxy Diacid Building Blocks

Malic acid is another functionalized analogue of Succinic acid suitable as dimer building block. Indeed, as Asp can represent a Lys bioisoster in the β^{3R3}-peptides alphabet, malic acid can act as serine (Ser) and threonine (Thr) counterpart. This could be exploited for e.g. the O-glycosylation of β^{3R3}-peptide sequences with biomedically relevant sugars.

A convenient route was therefore applied towards the synthesis of a mono-protected derivative of malic acid suitable for the regioselective coupling with the Fmoc β-diamines (Scheme 3.10).[151] The Bn ester was here again chosen as temporary protective group for the carboxyl functionality in β position due to is good compatibility with Fmoc-chemistry.

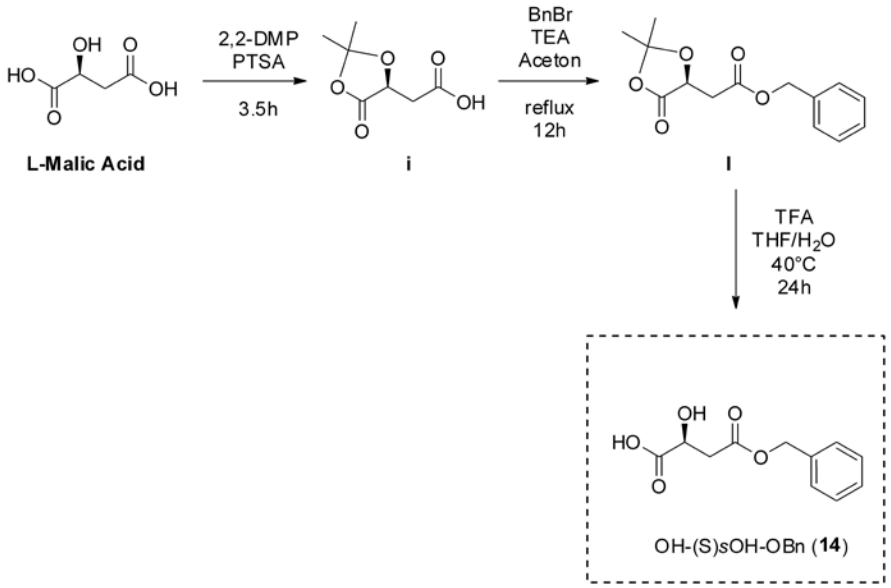

Scheme 3.10. *Synthetic scheme for the synthesis of the β^{3R3}-peptide diacid monomer OH-(S)sOH-OBn (**14**).*

First, the hydroxyl and carboxyl moieties in α position were simultaneously protected with 2,2-dimethoxypropane in presence of para-toluenesulfonic acid as Lewis acid catalyst. Here the regioselectively is kinetically driven favouring the formation of the five-membered ring rather than the six-membered ring which would imply the carboxyl functionality in β rather than in α position. Then the free carboxylic acid was protected as Bn ester using benzyl bromide (BnBr) in aceton with triethylamine as base. Finally, hydrolysis under acidic condition provided the diacid monomer **14** as succinic analogue OH-(S)sOH-OBn. Noteworthy, differently from the amino group of Asp, the free hydroxyl group should not interact with the chemoselective amide coupling of the free carboxyl moiety of OH-(S)sOH-OBn (**14**) and the amine of the Fmoc β-diamines building blocks.

Table 3.2. *Scale and yield for the synthesis of diacid monomers* ***8-14****.*

Diacid Building Block (n_o)	**Yield** [%]	**Scale** [g]
Suc (**8**)	*	*
OH-*s*Ala-O*t*Bu (**9**)	71	20
OH-*s*Phe-O*t*Bu (**10**)	64	20
OH-(S)*s*NH(Boc)-OBn (**11**)	*	*
OH-(R)*s*NH(Boc)-OBn (**12**)	*	*
OH-(S)*s*NH(Alloc)-O*t*Bu (**13**)	47	30
OH-(S)*s*OH-OBn (**14**)	37	20

** The compound was purchased as commercially available.*

Overall, an alphabet of properly protected β-diamine and β-diacid building blocks have been arranged and can be combined to design a variety of β^{3R3}-peptides with different physicochemical properties and biological activities.

3.2.3. Dimer Building Blocks

Alternatively to the coupling of diacid and diamine building blocks on solid support, the synthesized platform of β^{3R3}-peptide diamine and diacid building blocks also allows for the preparation of dimer building blocks to be applied for the SPS of β^{3R3}-peptide oligomers. In general, a dimer strategy for SPS consists in the coupling on solid support of dimer fragments of building blocks precedently prepared in solution. Such approach has been previously established also for the synthesis of β-peptide sequences.[21,152] A substantial difference in the case of β^{3R3}-peptides is that the dimer strategy implies the coupling in solution of monoprotected β-diamines and β-diacids rather than β-amino acids. Thus, different Fmoc protected chiral β diamines (*v*Xaa) and the ester mono-protected diacids (*s*Xaa) were coupled in solution to provide a designed library of dimer building blocks (Scheme 3.11).

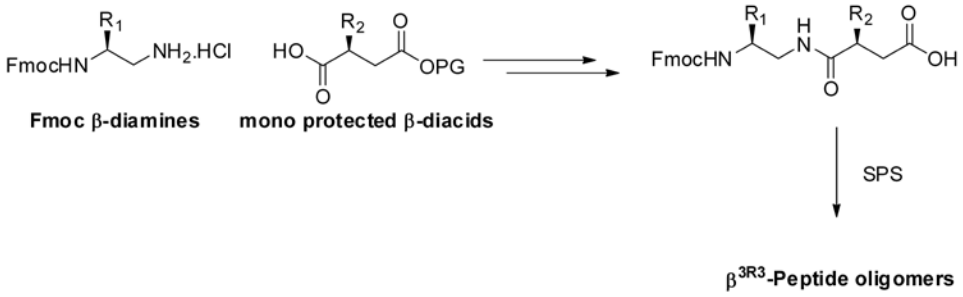

Scheme 3.11. *General synthetic scheme for the synthesis of β^{3R3}-peptide oligomers on solid support using the β^{3R3}-peptide dimer building blocks. The β^{3R3}-peptide dimer building blocks were prepared in solution combining Fmoc monoprotected β-diamines (vXaa) and properly monoprotected β-diacids (sXaa) monomers. The dimer building blocks obtained after deprotection of the carboxyl functionality was then applied for the SPS of β^{3R3}-peptide oligomers.*

Hydrophobic Proteinaceous Dimer Building Blocks

Hydrophobic side chains are generally employed for structural investigation on the folding propensity and structural properties of novel peptidomimetic backbones (see Chapter 5). Thus, using the hydrophobic β^{3R3}-peptides will allow evaluating the potential of the β^{3R3}-peptides to retain, modulate, and extend the structural space available to β-peptides with proteinaceous side chains. Therefore, hydrophobic β^{3R3}-peptide dimer building blocks have been prepared (Scheme 3.12).

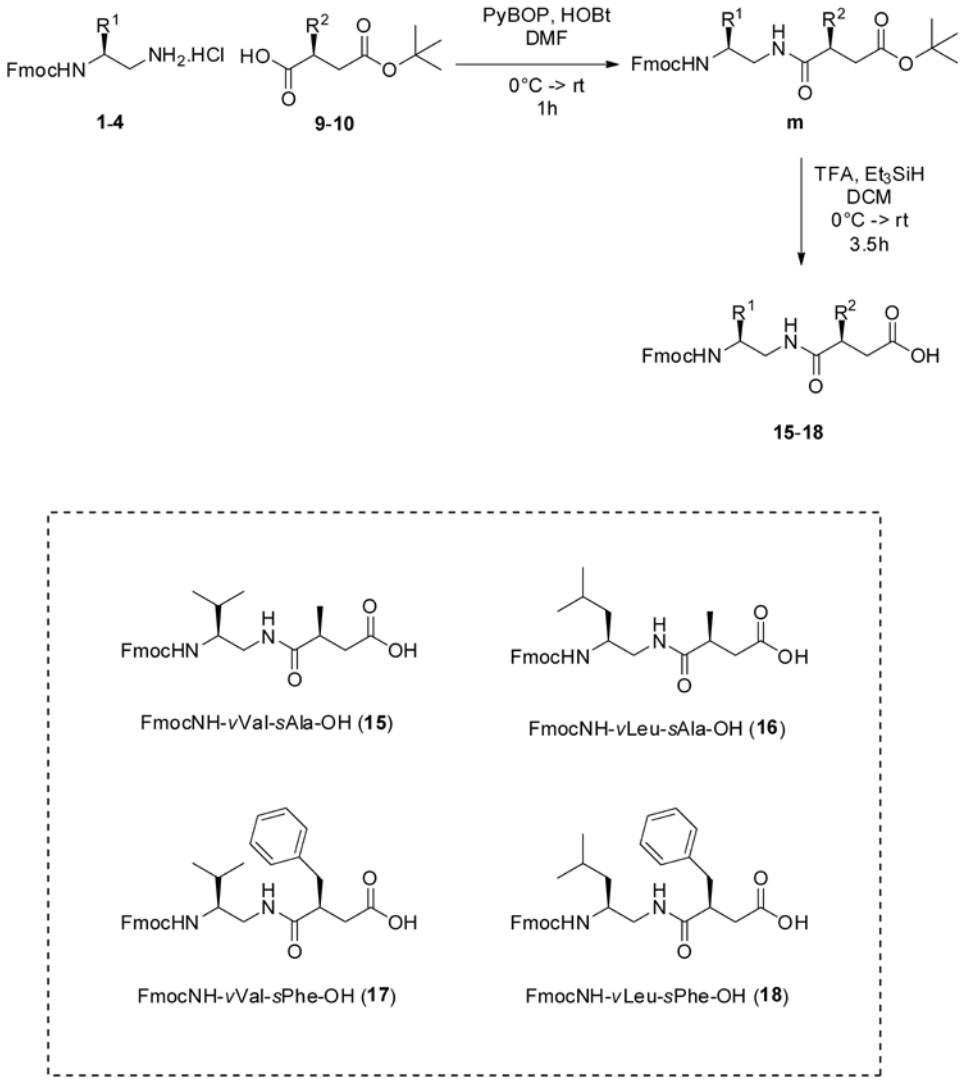

Scheme 3.12. *Synthetic scheme for the synthesis of the β^{3R3}-peptide dimer building blocks with hydrophobic proteinaceous side chains. Fmoc monoprotected β-diamines (vXaa)**1-4** and tert-Butyl ester minoprotected β-diacids (sXaa) **9-10** monomers were coupled in solution to afford after tert-Butyl ester deprotection the small library of dimer building blocks **15-18**.*

First, the Fmoc protected chiral β diamines (*v*Xaa) **1-4** were coupled in solution with the hydrophobic *tert*Butyl-ester mono-protected diacids (*s*Xaa) monomers **9** and **10**. Here the use of isobutyl chloroformate, the reagent of choice for large scale amide coupling in solution,[153] with *N*-methyl morpholine as base in DMF resulted in low reproducibility and significant amount of side products, mostly identified as isobutyl carbamate derivatives. Also screening different temperature and activation time did not lead to significant improvements. Gratifying, PyBOP/HOBt mediated coupling reaction in DMF with DIEA proved to be a reliable method providing all the products in

good yield. Finally, the *tert*-butyl ester (O*t*Bu) was deprotected under TFA acidic conditions affording small library of highly pure dimer building blocks **15**-**18** (Table 3.3 and Figure 3.3).

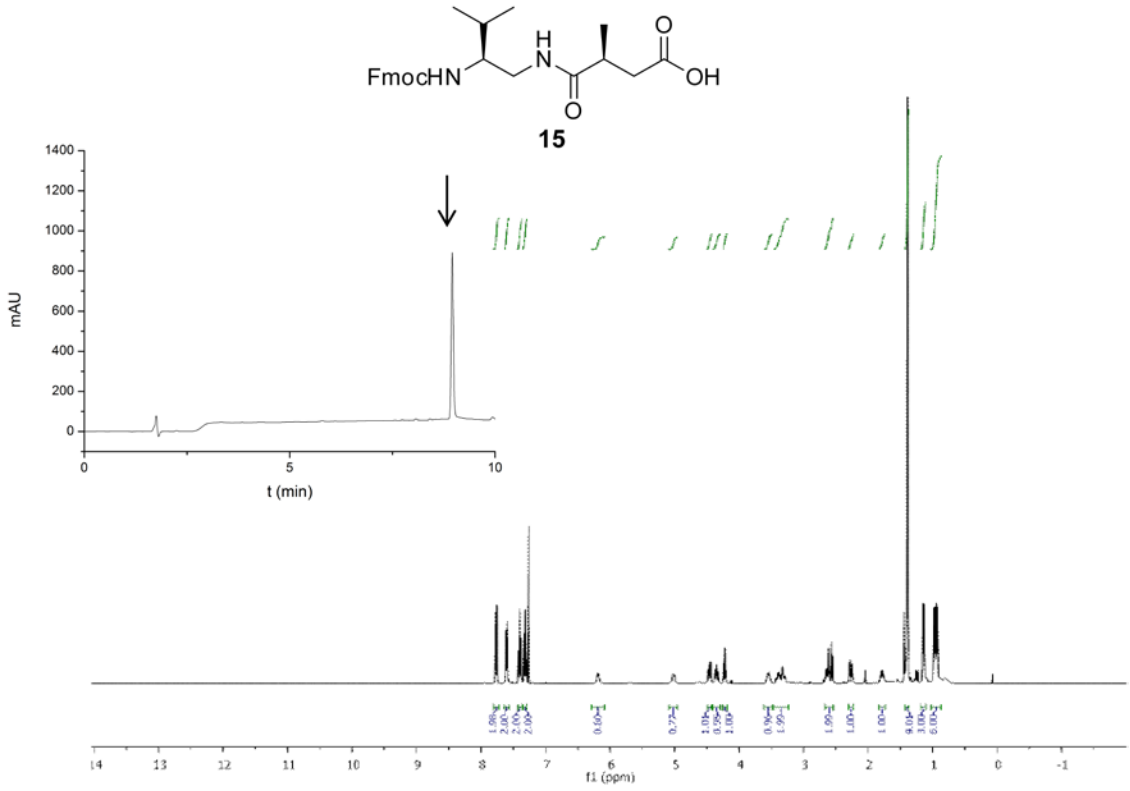

Figure 3.3. *HPLC trace (5 to 95% MeCN to H_2O in 10min) and NMR spectrum in d_6DMSO of FmocNH-vVal-sAla-OH (**15**), as representative example showing the efficiency of the purification protocols developed for the synthesis of β^{3R3}-peptide dimer building block with proteinaceous hydrophobic side chains.*

Dimer Building Blocks with Succinic Acid Unit

Suc can be directly employed as synthon for the β^{3R3}-peptide diacid derivative *s*Gly also for the synthesis in solution of β^{3R3}-peptide dimer building blocks. In particular, the β^{3R3}-peptide dimer building blocks **19**-**23** have been prepared combining Suc with the diamine building blocks **1**-**6** (Scheme 3.13).

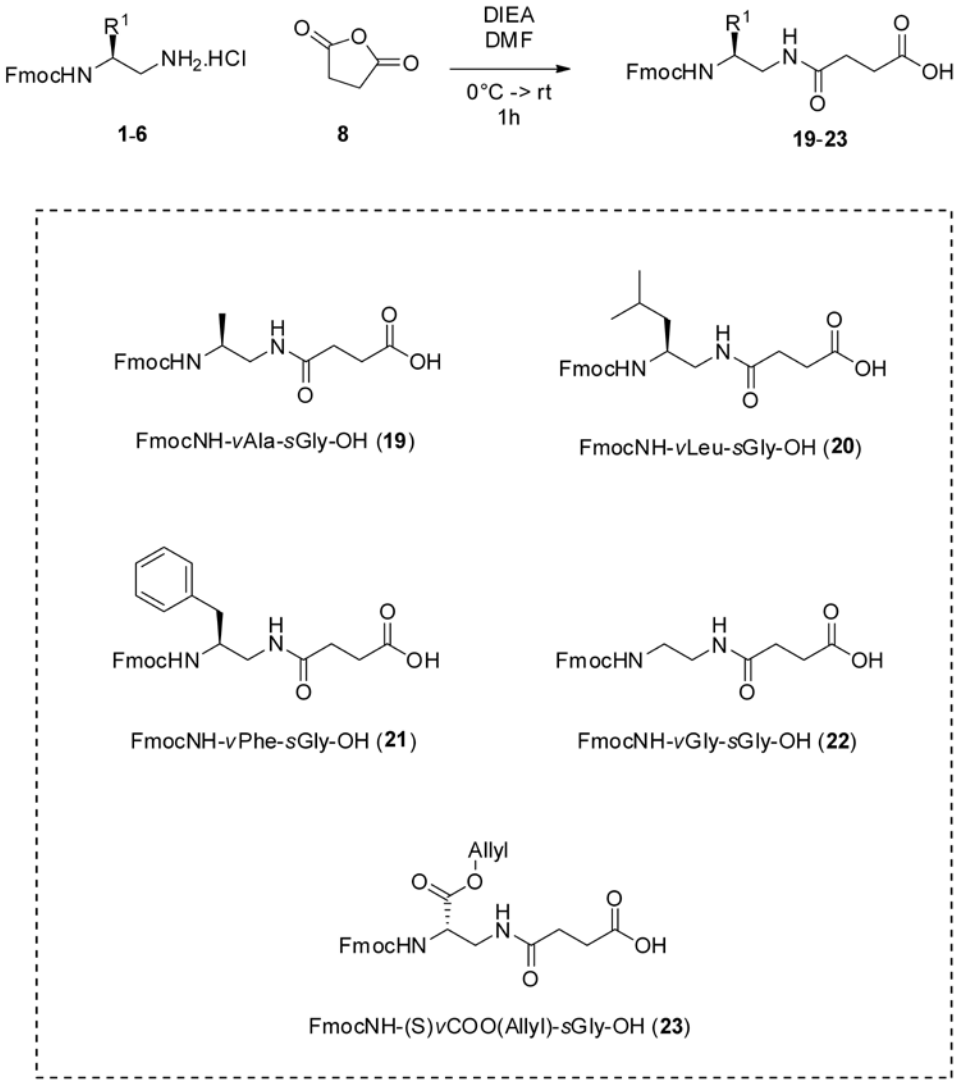

Scheme 3.13. *Synthetic route for the synthesis in solution the dimer building blocks presenting sGly as β-diacids unit. Fmoc monoprotected β-diamines (vXaa)* ***1-6*** *and Suc* ***(8)*** *as sGly monomer were coupled in solution to afford the small library of dimer building blocks* ***19-23****.*

Here, the coupling was achieved by adding Suc to the solution of the diamine building blocks (**1-6**) in DMF and DIEA as organic base. Thereby, the dimer building blocks **19-23** were produced with good yield and purity (Table 3.3 and Figure 3.4).

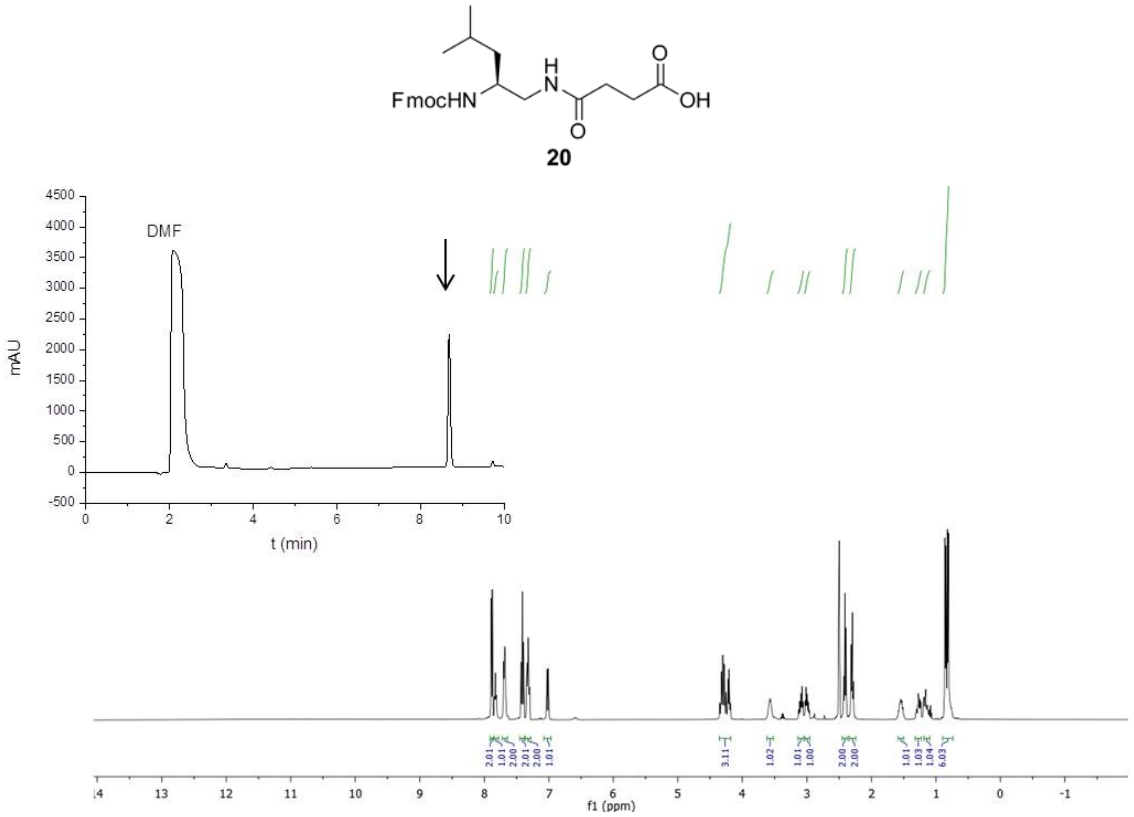

Figure 3.4 *HPLC trace (5 to 95% MeCN to H_2O in 10min) and NMR spectrum in d_6DMSO of FmocNH-vLeu-sGly-OH (**20**), as representative example showing the efficiency of the purification protocols developed for the synthesis of β^{3R3}-peptide dimer building blocks presenting sGly as β-diacids unit.*

Amphiphilic Cationic Dimer Building Blocks

Highly cationic and globally amphiphilic character are common and essential features of antimicrobial and cell-penetrating agents, which have acknowledge potential in the biomedical field and will be two major biomedical applications targeted with the β^{3R3}-peptides (Chapter 5). Therefore, amphiphilic cationic dimer building blocks have been also prepared.

For this purpose a synthetic protocol based on the PyBOP/HOBt coupling system was developed to employ commercially available Boc-L-Asp(Bn)-OH (**11**) and Boc-L-Asp(Bn)-OH (**12**) as diacid monomers to afford dimer building blocks presenting as β-diacid unit (S)-*s*NH(Boc)-OH (**24**-**28**) and (R)-*s*NH(Boc)-OH (**29**-**32**), respectively (Scheme 3.14 and 3.15). In particular, both the diastereoisomers were prepared as the the configuration of the chiral center of the diacid *s*NH_2 unit is expect to deeply influence the conformation of β^{3R3}-peptide sequences, as already discussed for the diacid building blocks Boc-Asp(Bn)-OH (**11** and **12**).

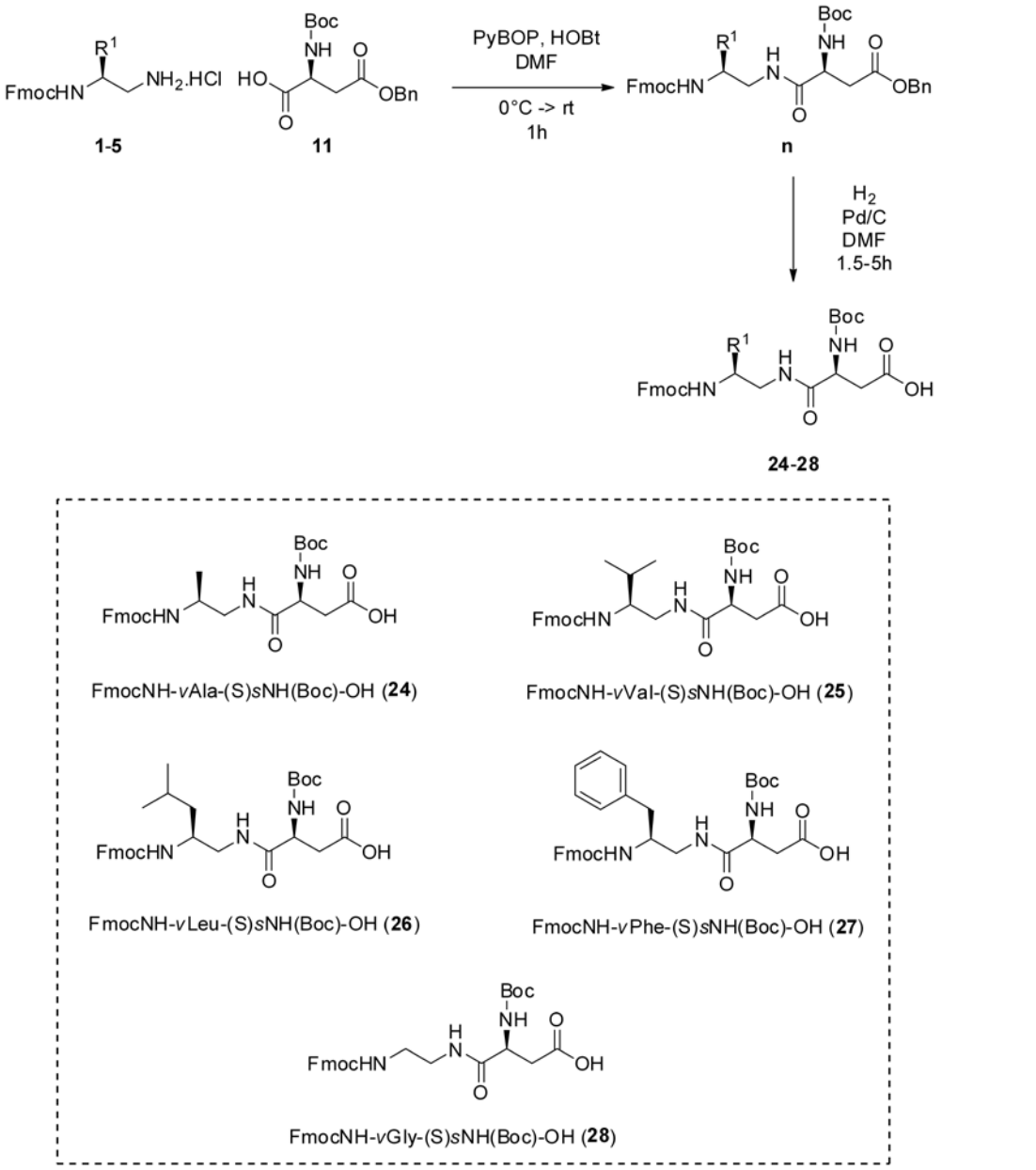

Scheme 3.14. *Synthetic route for the synthesis in solution the dimer building blocks presenting (S)-sNH(Boc) as β-diacids unit. Fmoc monoprotected β-diamines (vXaa)**1-5** and Boc-L-Asp(Bn)-OH (**11**) as (S)-sNH(Boc) monomer were coupled in solution to afford after Bn ester deprotection the small library of dimer building blocks **24-28**.*

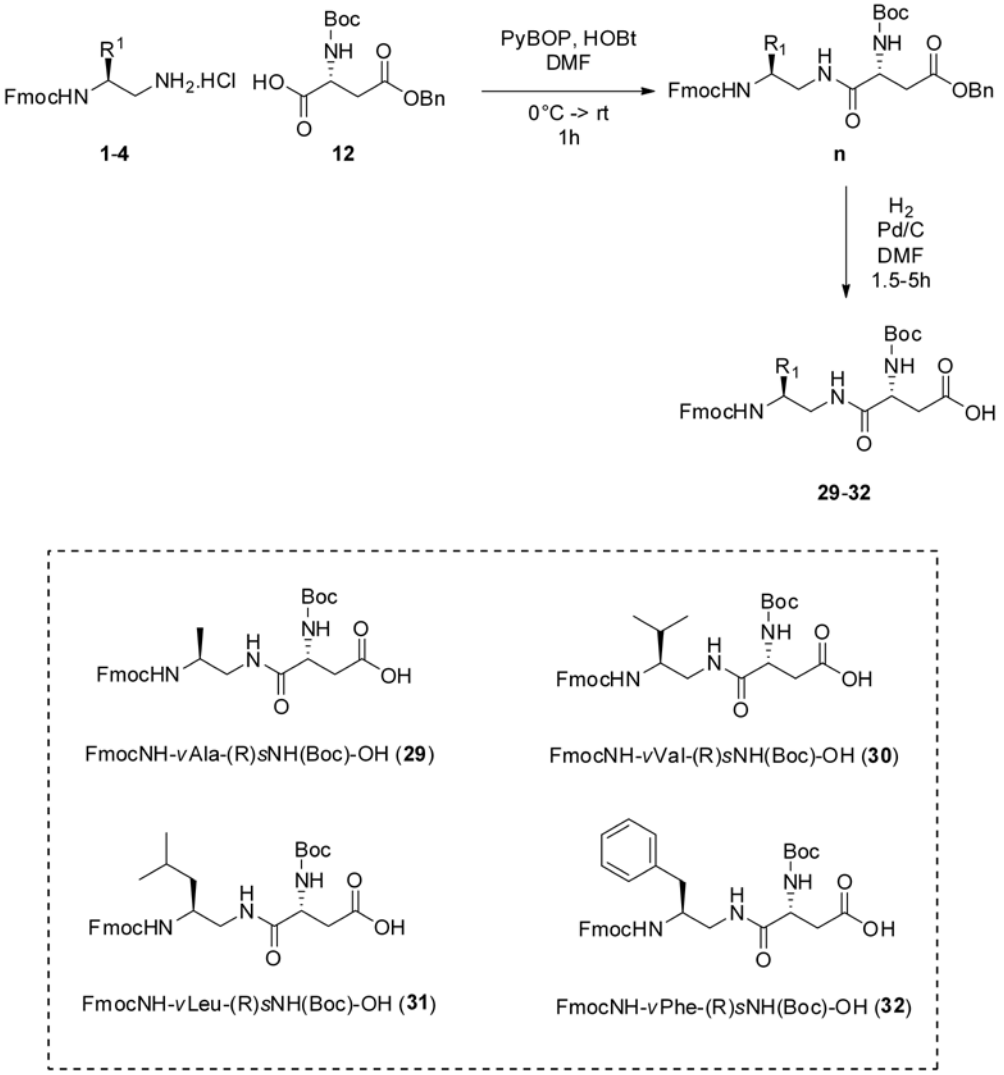

Scheme 3.15. *Synthetic route for the synthesis in solution the dimer building blocks presenting (R)-sNH(Boc) as β-diacids unit. Fmoc monoprotected β-diamines (vXaa)**1-4** and Boc-D-Asp(Bn)-OH (**12**) as (R)-sNH(Boc) monomer were coupled in solution to afford after Benzyl ester deprotection the small library of dimer building blocks **29-32**.*

After PyBOP/HOBT-mediated coupling reaction in solution, the Bn ester was deprocted via catalytic hydrogenation with Pd on carbon (Pd/C) in DMF. Here DMF proved to be a proper solvent avoiding solubility issue and precipitation of the product which can make more problematic the workup and the separation from the heterogeneous catalyst Pd/C. In addition, the Fmoc protecting group on the amino terminal proved to be less sensitive to the hydrogenation in DMF rather than in alcoholic media, such as EtOH. Nevertheless the reaction requires a constant monitoring as once the complete conversion is accomplished (generally 1.5-5 h), a not identified hydrophobic by-product can appear and increase steadily along the time. Thereby, the dimer building blocks **24-32** were produced with good yield and purity (Table 3.3 and Figure 3.5).

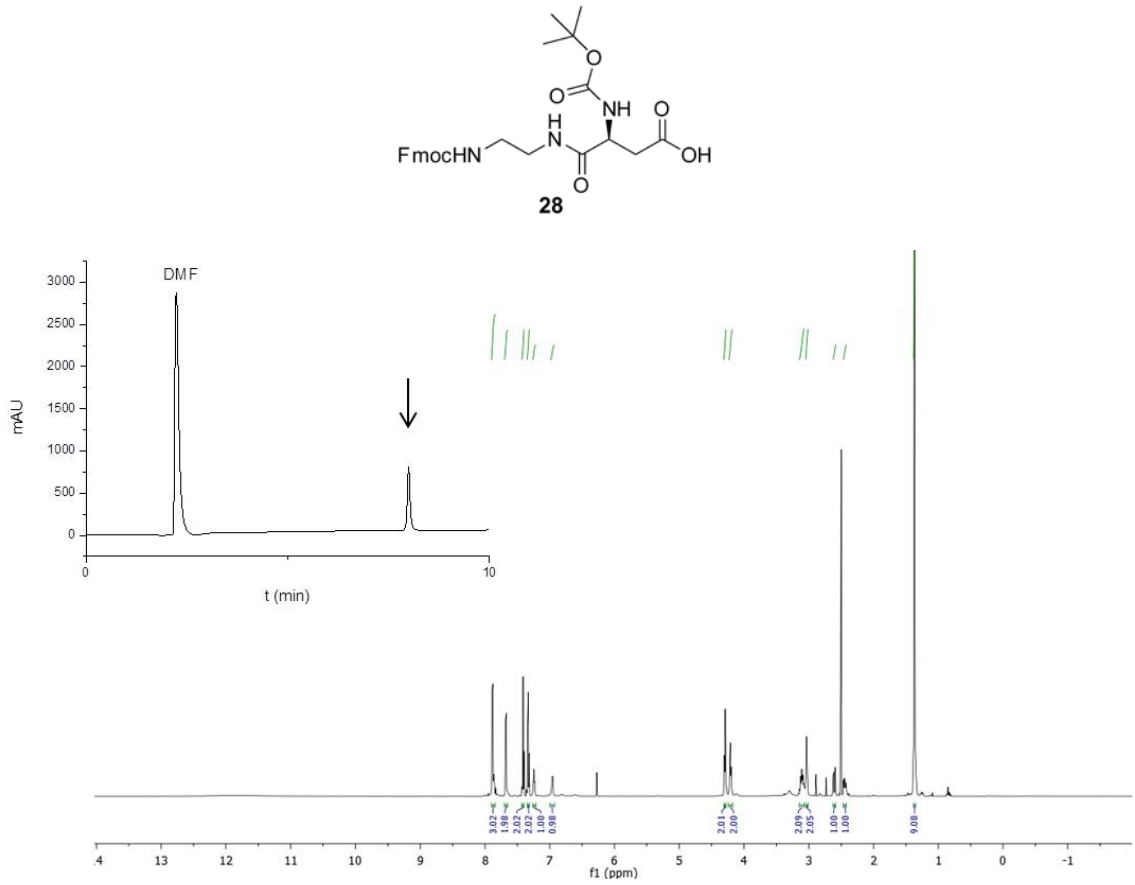

Figure 3.5. *HPLC trace (5 to 95% MeCN to H_2O in 10min) and NMR spectrum in d_6DMSO of FmocNH-vGly-(S)sNH(Boc)-OH (**28**), as representative example showing the efficiency of the purification protocols developed for the synthesis of β^{3R3}-peptide dimer building block with sNH(Boc) diacid monomers.*

Zwitterionic Dimer Building Blocks

Moreover, the diacid monomer (S)-*s*NH(Alloc)-OtBu (**13**) was conjugated with the Fmoc β-diamines *v*COO(Allyl) to prepared dimer building for zwitterionic β^{3R3}-peptides. Indeed, zwitterionic materials have been drawing much attention in the biomedical field as novel antifouling or ultralow-fouling materials to resist nonspecific protein adsorption and cell adhesion.[154] Thus, to also investigate the effect on conformational and biological properties of derived oligomers, the two diamine building blocks (S)-*v*COO(Allyl) (**6**) and (R)-*v*COO(Allyl) (**7**) have been specifically coupled to the diacid building block (S)-*s*NH(Alloc)-OtBu using the PyBOP/HOBT- coupling system (Scheme 3.16).

Thereby, the two diastereoisomer dimer building blocks were prepared, FmocNH-(S)*v*COO(Allyl)-*s*NH2(Alloc)-OH (**33)** and FmocNH-(S)*v*COO(Allyl)-*s*NH2(Alloc)-OH (**34)**, which are respectively homochiral (*v*S,*s*S) and heterochiral (*v*R,*s*S) (Table 3.3, Scheme 3.16 and Figure 3.6).

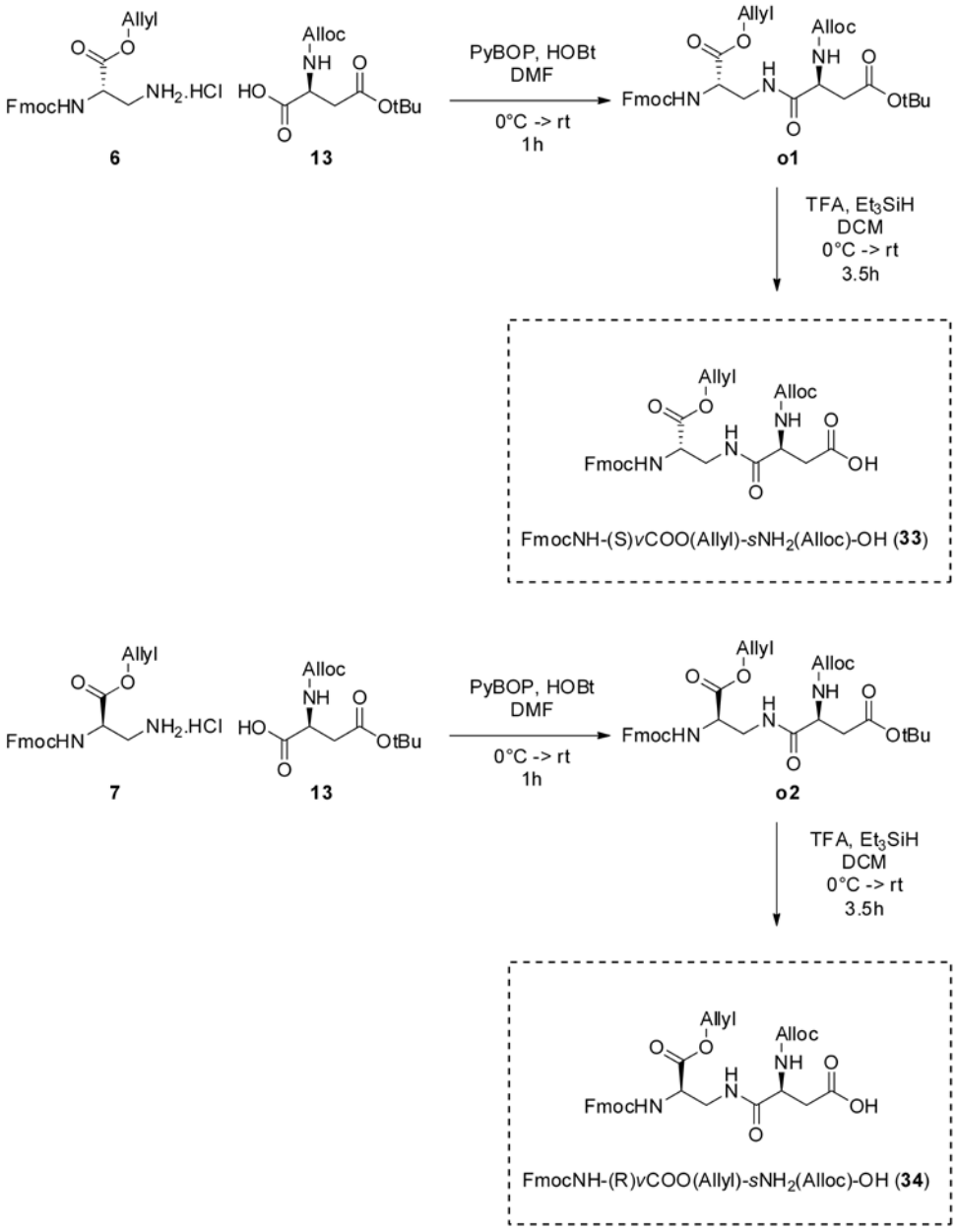

Scheme 3.16. *Synthetic route for the synthesis in solution the dimer building blocks presenting Fmoc mono-protected diamine monomers (S)-vCOO(Allyl)* ***(6)*** *and (R)-vCOO(Allyl)* ***(7)*** *and (S)-sNH(Alloc) as β-diacids unit. Fmoc monoprotected β-diamines* ***6*** *and* ***7*** *and Alloc-L-Asp(tBu)-OH)* ***(12)*** *as (S)-sNH(Alloc) monomer were coupled in solution to afford after tert-Butyl ester deprotection the dimer building blocks* ***33*** *and* ***34****.*

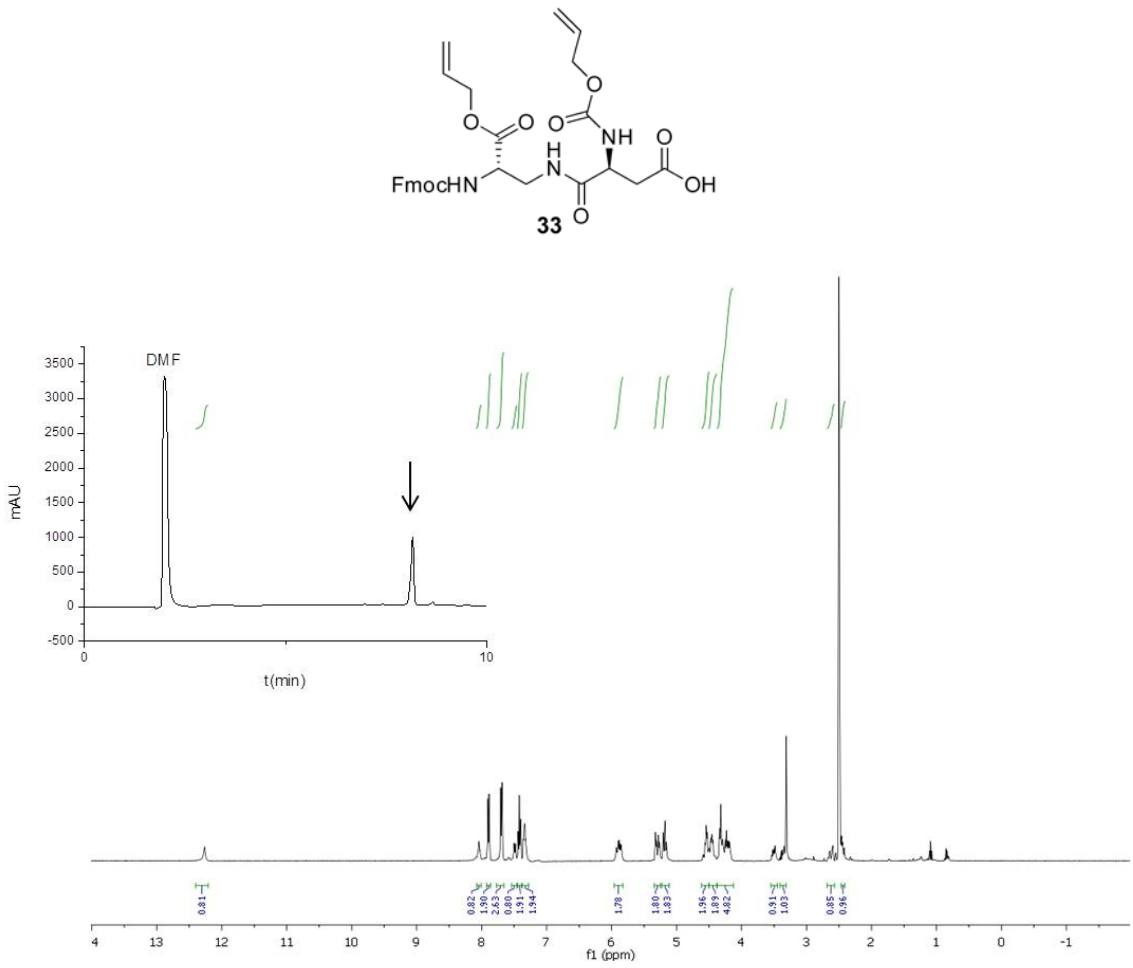

Figure 3.6 *HPLC trace (5 to 95% MeCN to H_2O in 10min) and NMR spectrum in d_6DMSO of FmocNH-(S)vCOO(Allyl)-sNH2(Alloc)-OH (**33**), as representative example showing the efficiency of the purification protocols developed for the synthesis of β^{3R3}-peptide dimer building block ofvCOO(Allyl) diamines and sNH(Boc) diacid monomers.*

Amphiphilic Dimer Building Blocks with Hydroxy Functionalities

Finally, it was proven that PyBOP/HOBT mediated coupling reaction is also suitable directly employing the diacid monomer **14** as succinic analogue (S)-sOH-OBn without the need for protection of the hydroxyl functionality (Scheme 3.17). Thus key intermediates **aa** and **bb** were synthesized providing a platform for different further modification before SPS. Indeed, the free alcoholic functionality is not applicable to SPS as the required excess of building blocks would partially produce esterification of the hydroxyl groups resulting in consistent amount of side products (Scheme 3.17). Nevertheless, the intermediates **aa** and **bb** represent a versatile and flexible platform for different protection or functionalization of the hydroxyl group aiming at different physicochemical

properties and biomedical applications (Scheme 3.17). For example, **aa** and **bb** can be therefore modified with protective groups compatible with solid phase Fmoc chemistry such as silyl ethers to produce β^{3R3}-peptide oligomers displaying free hydroxyl group as Ser/Thr bioisosters. Alternatively, glycosylation reaction can be also performed aiming at β^{3R3}-peptides presenting sugars with specific biological activities. Synthetic efforts aiming at such β^{3R3}-peptide structures are now on-going.

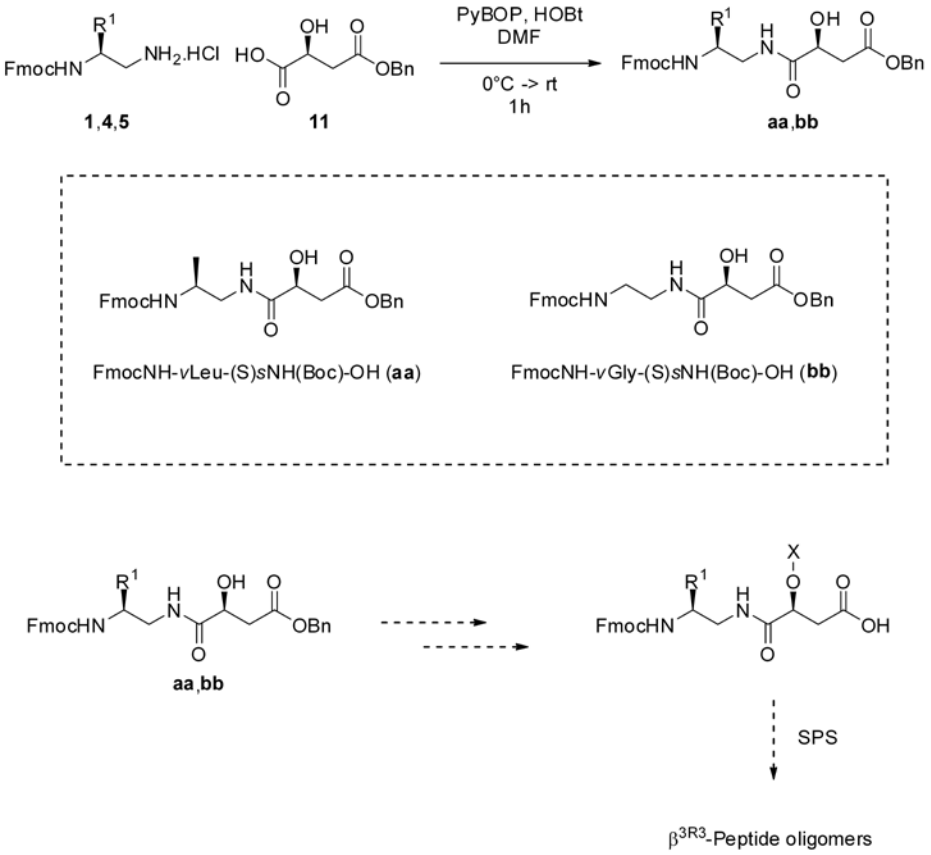

Scheme 3.17. *Synthetic route for the synthesis in solution the dimer building blocks presenting malic acid as succinic analogue (S)-sOH. Fmoc monoprotected β-diamines (vXaa)* ***1***, ***4*** *and* ***5*** *and Bn mono-protected diacid monomer (S)-sOH-OBn (****14****) were coupled in solution to afford the key intermediates (****aa*** *and* ***bb****). These can be then either protected or glycosylated with the chemical entity X allowing for SPS of specifically designed* β^{3R3}*-peptide structures.*

Conclusively, the synthetic protocols fulfill the requirements for the synthesis of building blocks suitable for SPS, giving high yield and purity on multigram scale (Table 3.3). Most notably, these procedures were developed to rely exclusively on simple and convenient purification methods avoiding scale-limiting and time consuming chromatographic purification.

Table 3.3. *Scale and yield for the synthesis of β^{3R3}-peptide dimer building blocks.*

Dimer Building Block (n_o)	**Yield [%]**	**Scale [g]**
FmocNH-*v*Val-*s*Ala-OH (**15**)	66	5
FmocNH-*v*Leu-*s*Ala-OH (**16**)	81	5
FmocNH-*v*Val-*s*Phe-OH (**17**)	67	5
FmocNH-*v*Leu-*s*Phe-OH (**18**)	73	5
FmocNH-*v*Ala-*s*Gly-OH (**19**)	82	3.5
FmocNH-*v*Leu-*s*Gly-OH (**20**)	84	5
FmocNH-*v*Phe-*s*Gly-OH (**21**)	96	4
FmocNH-*v*Gly-*s*Gly-OH (**22**)	92	10
FmocNH-(S)*v*COO(Allyl)-*s*Gly-OH (**23**)	92	3
FmocNH-*v*Ala-(S)*s*NH(Boc)-OH (**24**)	79	10
FmocNH-*v*Val-(S)*s*NH(Boc)-OH (**25**)	74	7
FmocNH-*v*Leu-(S)*s*NH(Boc)-OH (**26**)	72	6
FmocNH-*v*Phe-(S)*s*NH(Boc)-OH (**27**)	83	6
FmocNH-*v*Gly-(S)*s*NH(Boc)-OH (**28**)	71	9
FmocNH-*v*Ala-(R)*s*NH(Boc)-OH (**29**)	64	3
FmocNH-*v*Val-(R)*s*NH(Boc)-OH (**30**)	59	3.3
FmocNH-*v*Leu-(R)*s*NH(Boc)-OH (**31**)	59	3.4
FmocNH-*v*Phe-(R)*s*NH(Boc)-OH (**32**)	54	3.8
FmocNH-(S)*v*COO(Allyl)-*s*NH_2(Alloc)-OH (**33**)	66	4.4
FmocNH-(R)*v*COO(Allyl)-*s*NH_2(Alloc)-OH (**34**)	84	2.9

The alphabet of synthesized building blocks now allows for the design of a variety of sequences to target different biomedical applications. In the following chapter these building blocks will therefore be applied for the SPS of oligomers that will be ultimately evaluated for selected biomedical applications in Chapter 5.

4. Solid Phase Synthesis of β^{3R3}-Peptide Oligomers

In the previous chapter a variegated alphabet of building blocks has been prepared as either monomer diamine and diacid or dimer building blocks. These building blocks will now be applied for the SPS of different classes of β^{3R3}-peptides with designed physicochemical properties to target specific biomedical applications.

Specifically, the building blocks have been designed to be applicable for SPS of β^{3R3}-peptide oligomers using conventional Fmoc SPPS protocols. A major advantage of Fmoc chemistry are the very mild conditions required. Indeed, the removal of the Fmoc protecting group from the N-terminus of the peptidyl-resin is normally achieved by treatment with 20% v/v Pip in DMF.[49] Following the abstraction of the acidic proton at the 9-position of the fluorene ring system, β-elimination gives a highly reactive dibenzofulvene intermediate. Dibenzofulvene can be trapped by excess amine cleavage agents to form stable dibenzofulvene-Pip adduct (Scheme 4.1). When incomplete deprotection is observed, use of the stronger and more efficient base DBU at a concentration of 2% in DMF, is recommended. Typically, a solution of DBU-Pip-DMF (1:1:48) is effective, with the Pip component included to scavenge the dibenzofulvene species. Indeed, using the Fmoc approach in β-peptide synthesis generally requires that the coupling and deprotection times have to be greatly lengthened above chain lengths of about seven amino acids.[14] Therefore above the critical chain length DBU is added as an additional base to accelerate the Fmoc-removal step.[14] However, DBU can promote aspartimide formation, thus its use should be avoided for sequences containing Asp or Asn.[49]

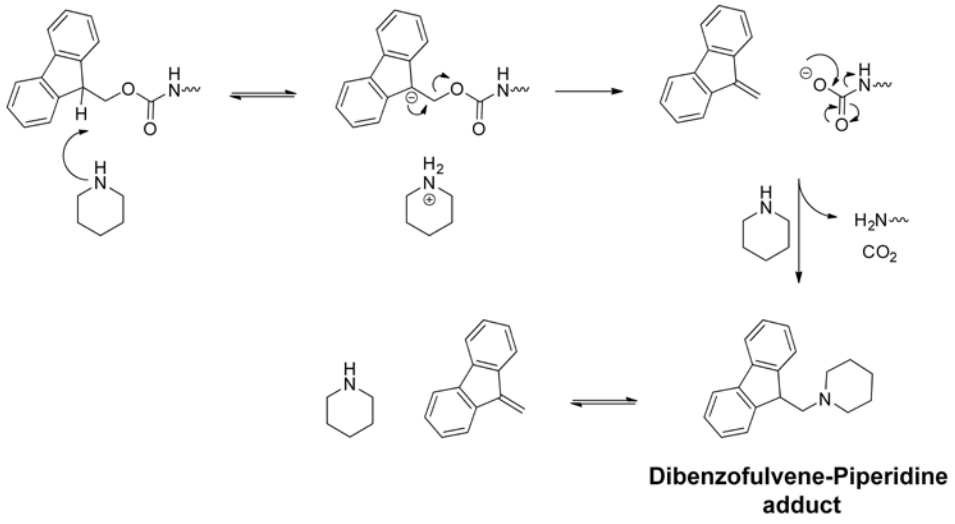

Scheme 4.1. *Reaction mechanism of Fmoc deprotection using Pip as base.*

Another advantage of Fmoc chemistry is the possibility of coupling protocols to be fully automated in a standard peptide synthesizer (Figure 4.1). This gives also the opportunity for on-line monitoring of the Fmoc deprotection efficiency using an UV detector, which surveys the presence of the UV active dibenzofulvene-Pip adduct.

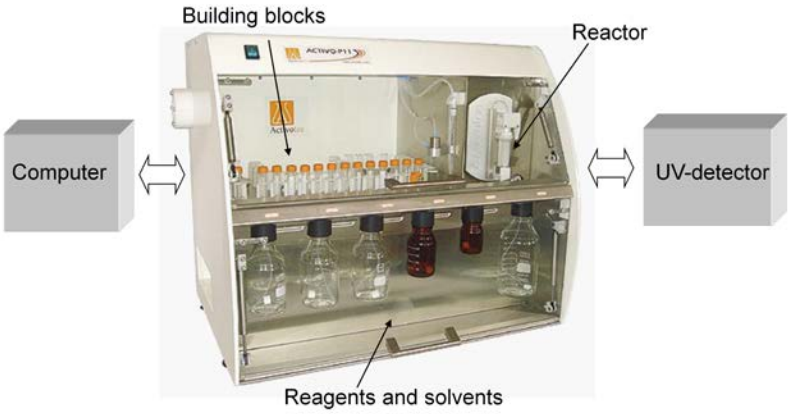

Figure 4.1. *Experimental set up of for the synthesis of β^{3R3}-peptide oligomers: The automated peptide synthesizer (Activotec P11) is control by an external computer; reaction monitoring was achieved by an UV detector, the reagents, solvent and the reaction vessel, containing resin are connected to the machinery; the building blocks are placed as solids under argon in a septum capped falcon, which is sorted into the specific position of the amino acid chain.*

Thus, in chapter 3 all the diamine units were equipped with an Fmoc-protective group. Nevertheless, different protocols have to be applied for the SPS of β^{3R3}-peptides using either monomer diamine and diacid building blocks, or dimer building blocks.

4.1. Diamine and Diacid Coupling Strategy

In contrast to SPPS, where N-protected amino acid building blocks are employed, the β^{3R3}-peptide backbone is constituted by alternating condensation of β-diamines and β-diacids (Scheme 3.1). Thus, the first step was to synthesize monoprotected β-diamine (*v*Xaa) and β-diacid (*s*Xaa) building blocks (Chapter 3).

Indeed, diamine and diacid building blocks in general can be assembled on solid support through alternating activation of the free carboxyl functionalities in solution and on the resin (Scheme 4.2).[144]

In the first step, an activated diacid building block is coupled to resin-bound amine functionalities. Following the activation of the resin-bound carboxylic moieties, the diamine building blocks are added. This sequence is repeated for the desired number of coupling cycles.

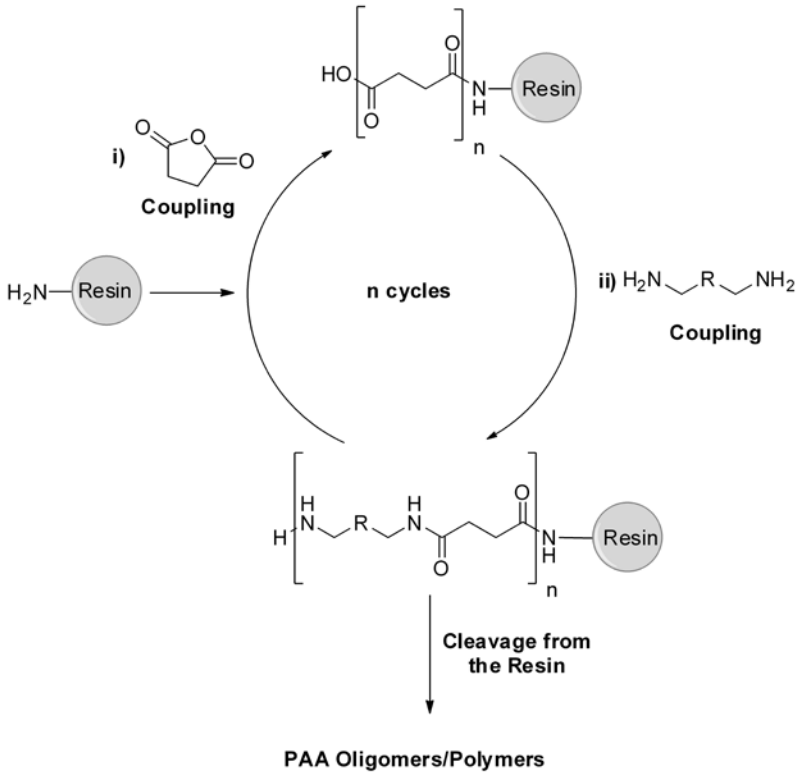

Scheme 4.2. *Original diamines and diacids SPS strategy for the preparation of monodisperse, sequence-defined PAAs segments via alternating assembly of symmetric diamines and Suc.*

This approach is rather convenient due to the easy accessibility to a wide range of suitable symmetrical diamine building blocks. In addition, it can be fully automated using a standard peptide synthesizer. However, inspired by polycondensation reactions, this approach has been designed and is actually suitable only for symmetric diamine and diacid building blocks.[144] Thus, using this protocol for the synthesis of β^{3R3}-peptides, only EDA and Suc could be applied as β-diamine and β-diacid building blocks, respectively. Therefore, two additional deprotection steps have to be enclosed within each coupling cycle for the SPS of different β^{3R3}-peptides employing monoprotected diamine and diacid building blocks (Scheme 4.3).

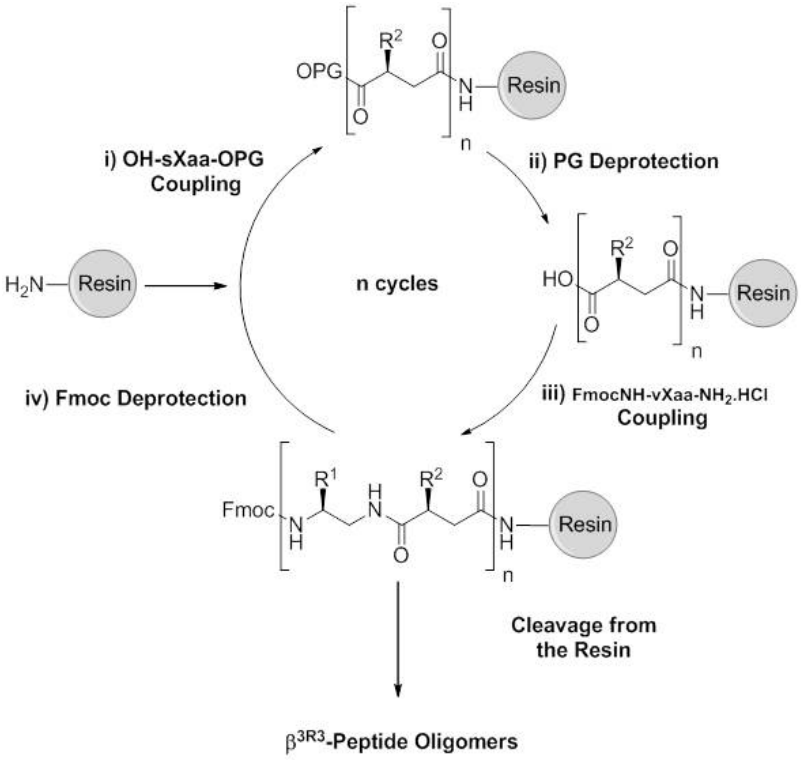

Scheme 4.3. *Designed diamines and diacids SPS strategy for the preparation of β^{3R3}-peptide oligomers.*

Nevertheless, the β^{3R3}-peptide diacid building blocks feature protective groups which are orthogonal to Fmoc, such as *tert*-butyl and Bn esters (table 3.2). Those require different conditions and variable time of the deprotection reactions, which needs to be specifically monitored. Consequently, the application of such monoprotected β-diacid building blocks directly for SPS makes the diamine and diacid approach significantly less convenient and precludes the possibility for full automation using a standard peptide synthesizer. However, different β^{3R3}-peptide sequences could be anyway targeted combining Suc as unique diacid with the library of different Fmoc-protected diamine building blocks (Scheme 4.4).

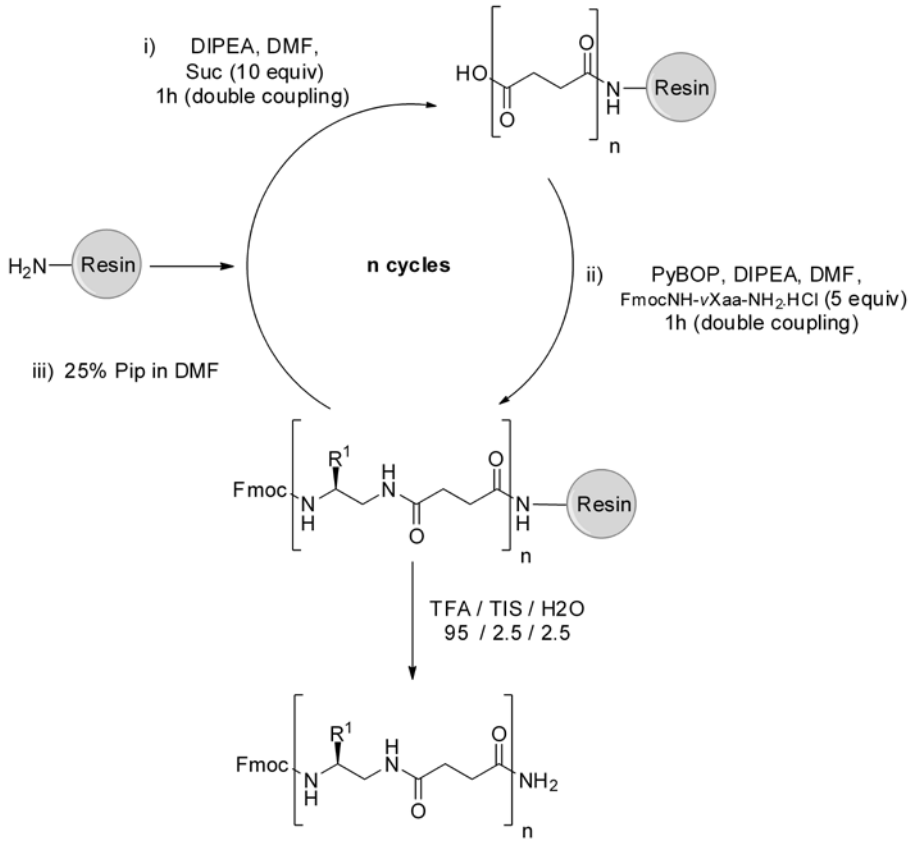

Scheme 4.4. *Diamines and diacids solid phase coupling strategy for the synthesis of β^{3R3}-peptide sequences with Suc as β-diacid (sXaa) analogue sGly.*

Thus, to evaluate the potential of this novel approach for the SPS polyamide and β^{3R3}-peptides in particular, a first oligomer **35** was synthesized using FmocNH-vAla-NH_2.HCl (**1**) as diamine building block. Tr-EDA Merrifield Resin (0.15mmol scale) was employed as solid support which releases EDA as terminal *v*Gly. 3 equiv. of diamine building block (**1**) and 10 equiv. of Suc with triple coupling of 1 h reaction time were applied. Specifically, PyBOP/HOBt/DIPEA was selected as system of choice for diamines and diacids solid phase coupling strategy.[155] Indeed, a major advantage of phosphonium salts such as PyBOP over aminium/uronium salts coupling agents is that the phosphonium does not react with the amino functionalities.[156] This is especially relevant in the diamines and diacids solid phase coupling strategy as an excess of the coupling reagent is required in order to accomplish complete activation of the on-resin carboxyl moieties.

However, no further chain elongation was witnessed after three repeating units without a consistent arising amount of side products, as shown for oligomers **35**, **36** and **37**, which respectively feature 3, 4 and 5 repeating units (Figure 4.2 and Figure 4.3).

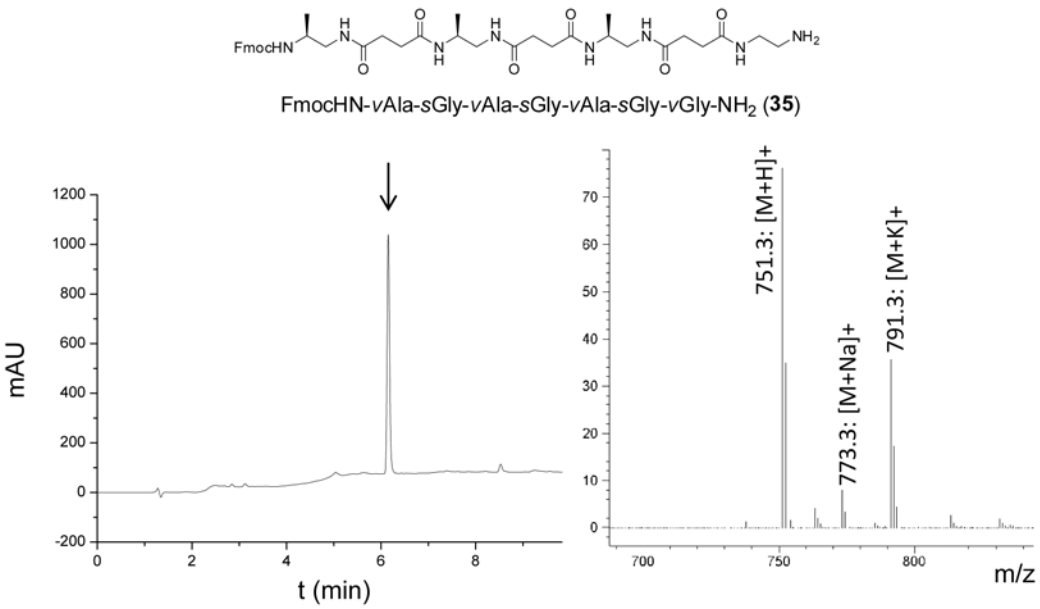

Figure 4.2. *Chemical structure, crude HPLC trace (5-95% H_2O to MeCN in 10 min) and ESI-MS of the β^{3R3}-peptide oligomer **35**.*

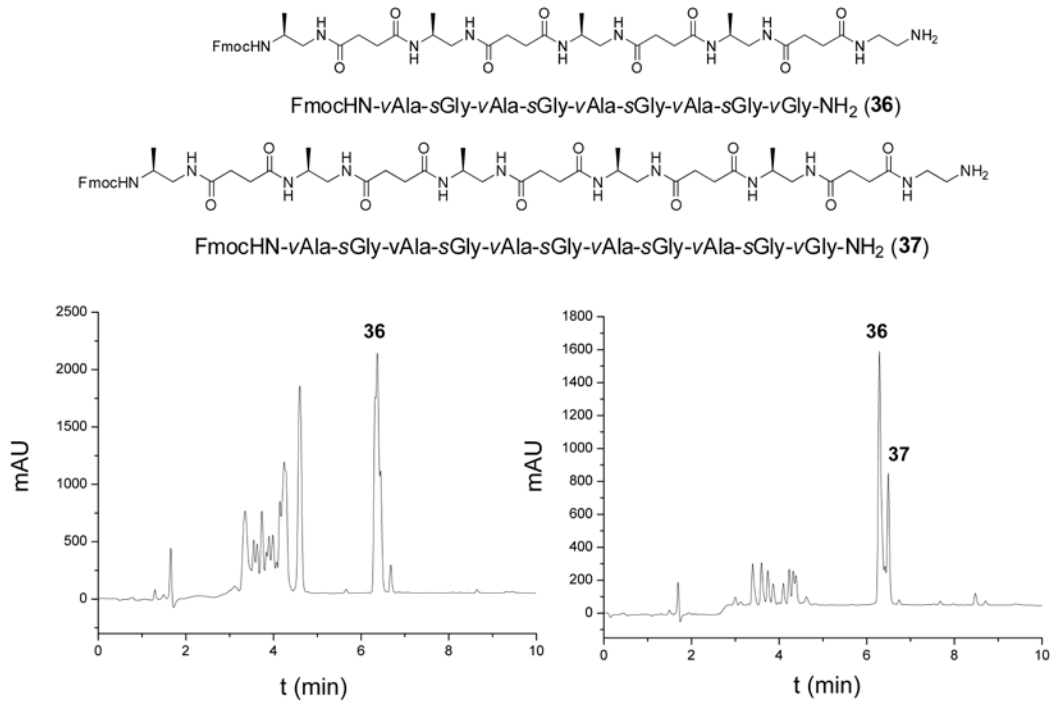

Figure 4.3. *Chemical structure and crude HPLC trace (5-95% H_2O to MeCN in 10 min) of the β^{3R3}-peptide oligomers **36** and **37**.*

It is well known from β-peptide sequences that starting from six/seven amino acids or building blocks, secondary structure can be induced.[133,157] This could be attributed to the hydrophobic properties of the *v*Ala units and the resulting oligomer inducing aggregation on and hydrophobic interactions with the solid support.[22] Thus, in order to minimize those hydrophobic interactions and target longer chain length, the hydrophilic Tentagel S RAM resin (loading 0.23 mmol/g) was employed. Thereby the β^{3R3}-peptide oligomer **38**, made up of 4 *v*Ala-*s*Gly repeating units, was synthesized overcoming the critical length of 3 repeating units (Figure 4.4).

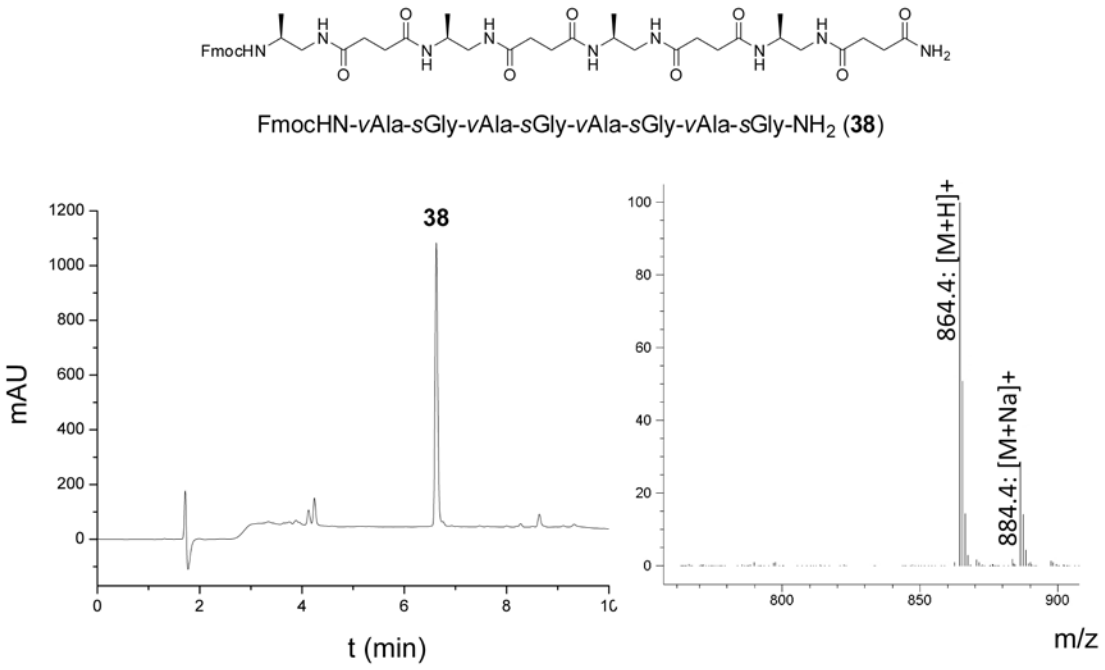

Figure 4.4. *Chemical structure, crude HPLC trace (5-95% H_2O to MeCN in 10 min) and ESI-MS of the β^{3R3}-peptide oligomer **38**.*

In conclusion, a novel approach for diamine and diacid coupling on solid phase has been designed and proved the potential for extending the earlier presented strategy towards chiral monodisperse, sequence-defined poly/oligo(amide) segments.[155]

Even though in general very appealing as synthetic strategy for an extended range of oligoamides, this is still quite limited for the synthesis of β^{3R3}-peptide sequences as it does not allow for the introduction of substituted diacid units *s*Xaa. Therefore, dimer building blocks were prepared from the diamine and diacid building blocks prior to SPS and will be applied for the synthesis of different classes of β^{3R3}-peptides in the next section.

4.2. Dimer Coupling Strategy

The β^{3R3}-peptide backbone is constituted by alternating condensation of β-diamines and β-diacids. In the previous section a novel approach for diamine and diacid coupling on solid support using β^{3R3}-peptide monomer building blocks has been attempted. However, this approach is not suitable for substituted diacid β^{3R3}-peptide building blocks, which significantly limits the versatility of β^{3R3}-peptides for different biomedical application.

Therefore, in chapter 3 substituted diacid building blocks have been coupled in solution with Fmoc-protected diamine building blocks to provide β^{3R3}-peptide dimer building blocks. These dimer building blocks will be now employed for SPS of different classes of β^{3R3}-peptides with design physicochemical properties to target specific biomedical applications.

In general, a dimer strategy for SPS consists in the coupling on solid support of dimer fragments of building blocks precedently prepared in solution. Here, the free carboxylic moiety of the β^{3R3}-peptide dimer building blocks gets activated in solution and conjugated to the N-terminus of chains linked to the solid support (Scheme 4.5).

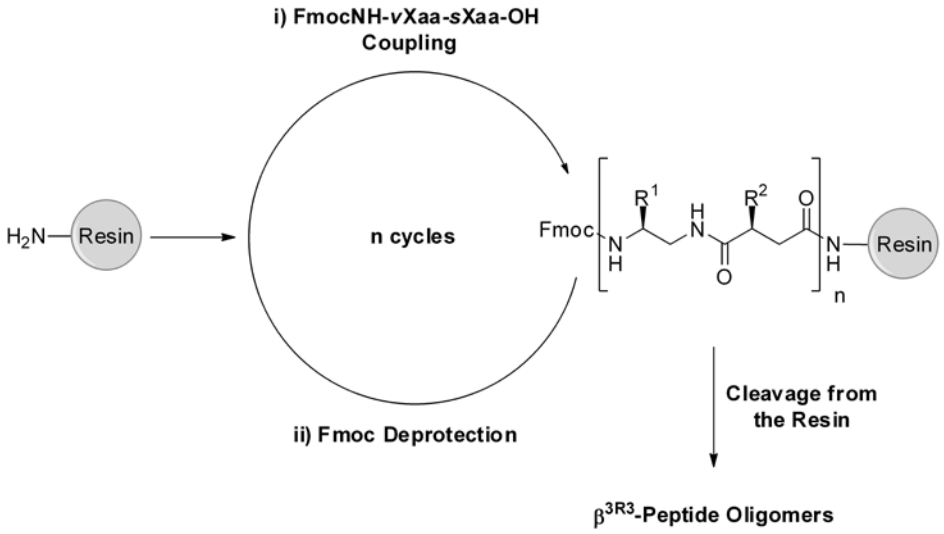

Scheme 4.5. *Dimer strategy for the SPS of β^{3R3}-peptide oligomers.*

Besides being more versatile and convenient allowing for the synthesis of multifunctional β^{3R3}-peptide sequences, this strategy offers other considerable advantages. Indeed, in contrast to the diamine and diacid strategy (Scheme 4.4), the Fmoc protected β^{3R3}-peptide dimer building blocks can be coupled following classic and extensively developed Fmoc peptide SPS protocols. In addition, this halves the number of coupling reactions on solid support, which can significantly improve the

efficiency of the SPS and gives access to longer oligomer chains. Finally, the protocols can be fully automated using a standard peptide synthesizer.

Thereby, specific protocols for the synthesis of three different classes of β^{3R3}-peptides with individual biomedical applications, namely hydrophobic proteinaceous, amphiphilic cationic and zwitterionic, have been developed and will be presented in the following sections.

Hydrophobic Proteinaceous Oligomers

First, β^{3R3}-peptide dimer building blocks with hydrophobic proteinaceous side chains were employed to synthesize β^{3R3}-peptide sequences with different hydrophobicity. On the one hand, this allows evaluating the general suitability and potential of the dimer strategy for SPS of β^{3R3}-peptides. Indeed, such building blocks can be considered as proper pilot system that avoid specific complexity related to specific functional side chains and different protective groups. On the other hand, specific hydrophobic sequences can allow for investigation on the intrinsic folding propensity and structural properties of the β^{3R3}-peptide backbone.[17,108]

Thus, dimer building blocks with hydrophobic proteinaceous side chains, both dichiral and monosubstituted with *s*Gly acid unit, were employed for SPS of β^{3R3}-peptides applying standard Fmoc coupling protocols, using an automated peptide synthesizer (Scheme 4.6).

HATU was chosen as activating agent because of high coupling efficiency,[14] and double coupling of 1 h with 5 equiv of building blocks was performed. Tentagel resins were selected as solid support for the hydrophilic properties, in order to minimize self-aggregation of hydrophobic chains that has been already observed using the diamines and diacids strategy for the SPS.[22]

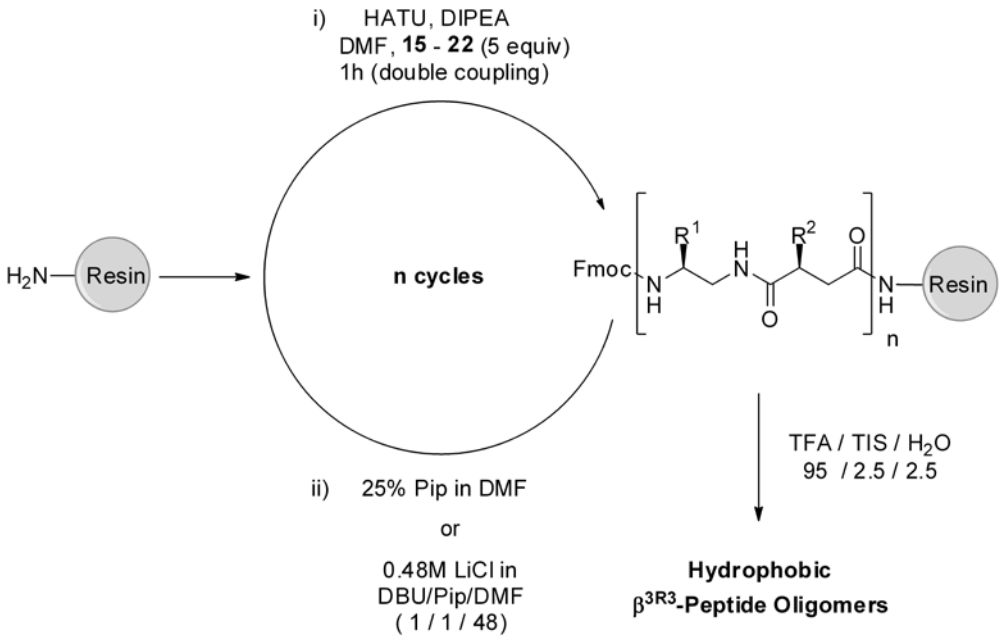

Scheme 4.6. *Synthetic route for the SPS of hydrophobic β^{3R3}-peptide sequences.*

Specifically, the hydrophobic β^{3R3}-peptide oligomers **39**-**44** have been prepared bringing the same side chain sequence of classical β-peptides used in folding studies (Scheme 4.7).[17,108] Thus, keeping the same side chains, these β^{3R3}-peptide oligomers (**39**-**44)** allow for a direct comparison of the conformational propensity of the classical β-peptide and β^{3R3}-peptide backbones, as it will be detailed in chapter 5.

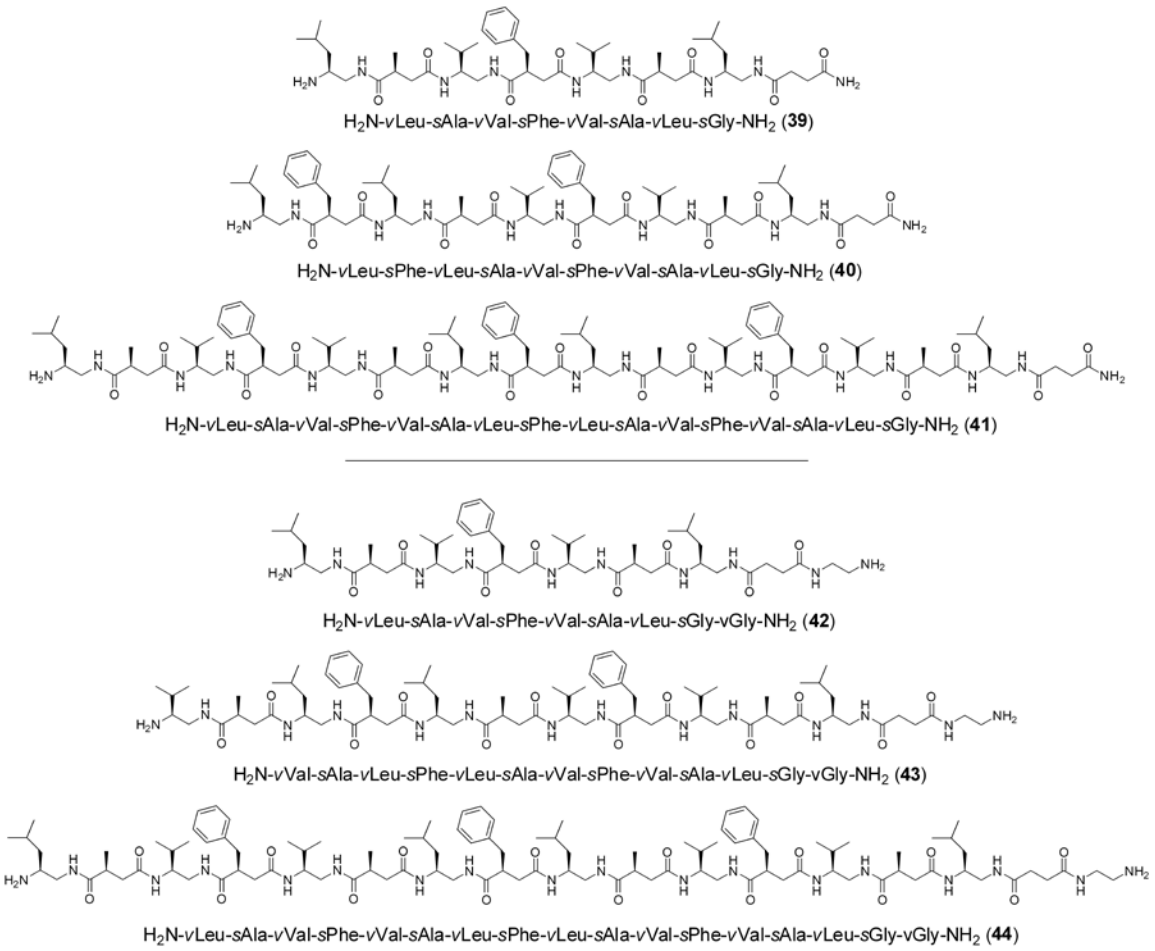

Scheme 4.7. *Hydrophobic β^{3R3}-peptide sequences synthesized employing dimer building blocks.*

First, a set of oligomers (**39**-**41**) differing in the chain length within a defined sequence of side chains was synthesized using Tentagel SRAM resin. In general, the use of 25% Pip in DMF as mixture for deprotection required extended time for complete removal of Fmoc groups. Gratifying, the time of deprotection could be considerably reduced by the use of the chaotropic salt LiCl in DBU, Pip and DMF mixture, as revealed by the Fmoc cleavage UV-patterns (Figure 4.5).

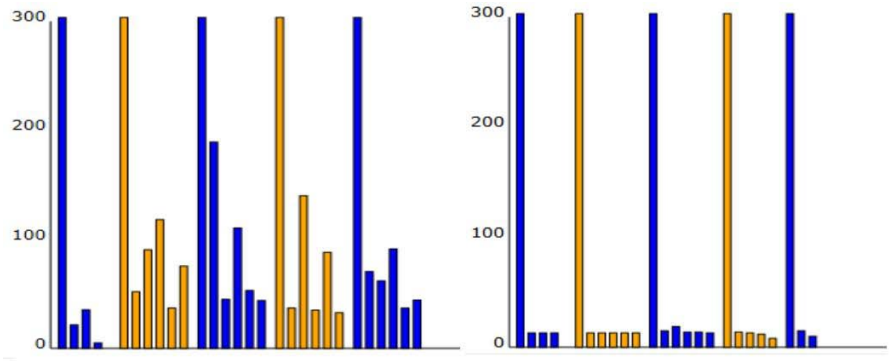

Figure 4.5. *Fmoc cleavage UV-patterns of oligomer **39** with 25% Pip in DMF (left) and 0.4M LiCl in DBU, Pip and DMF (right) as mixture for deprotection. The signals derived from the deprotection of the resin and the four couplings steps with dimer building blocks.*

Similarly to the parent β^3-peptides,[108] the obtained oligomers were insoluble in water and soluble only at low concentration (~1 mM) in MeOH, a common solvent for conformational investigations of hydrophobic β-peptides.[17] In order to improve the solubility and to investigate the effect of different terminal groups on the folding and aggregation behavior (Chapter 5), oligomers **42**-**44** were synthesized with similar side sequences and tagged with EDA as terminal *ν*Gly. In parallel to the diamines and diacids strategy (Section 4.1), this was achieved using Tr-EDA resin prepared by modification of a commercially available Tr-tentagel-OH resin with the EDA linker. Gratifyingly, oligomers **42**-**44** showed good solubility in MeOH (4 mM).

Remarkably, all the oligomers made of up to 8 dimer building blocks and a chain length corresponding to 17 β-aminoacids (**44**) were obtained in very high purity (>95%) directly after precipitation in cold Et_2O (Figure 4.6).

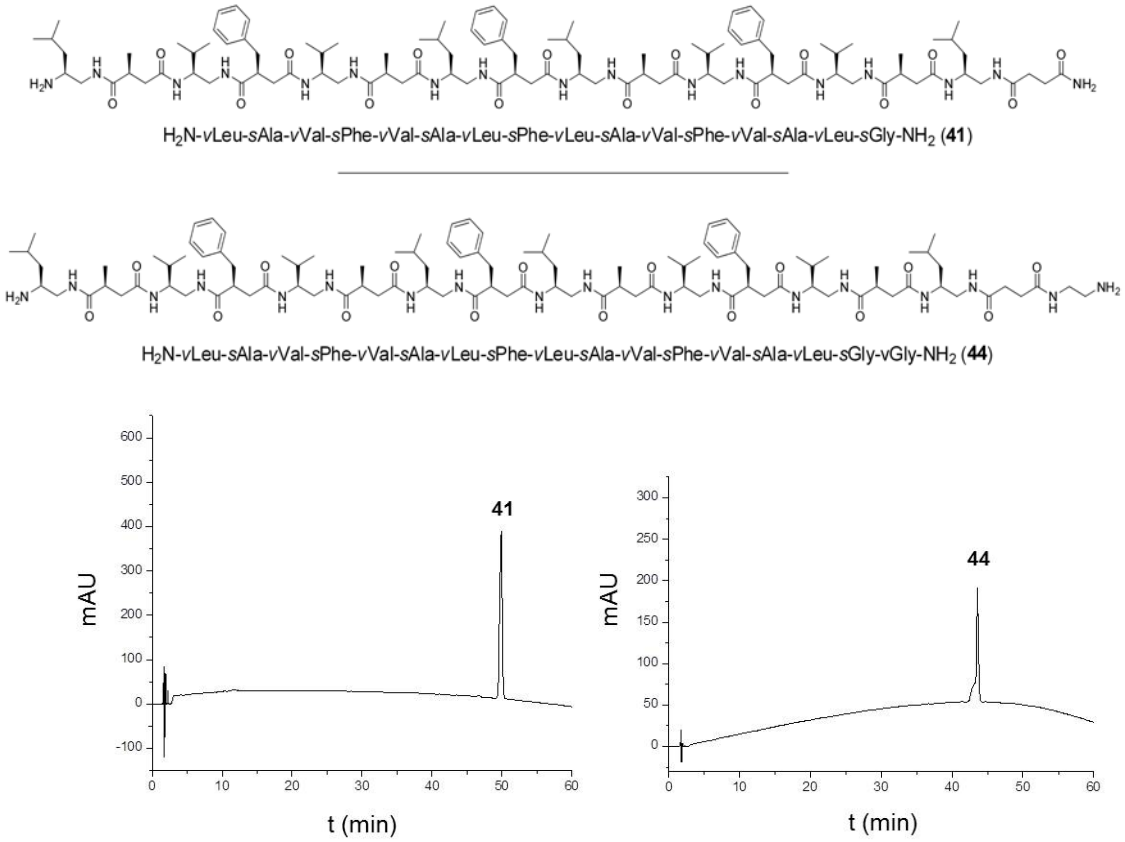

Figure 4.6. *Crude HPLC traces (5-95% H_2O to MeCN in 60 min) of oligomers **41** and **44**.*

Amphiphilic Cationic Oligomers

In the previous section, the efficiency and potential of the dimer strategy for SPS of β^{3R3}-peptides has been proven using dimer building blocks with hydrophobic proteinaceous side chains. Thus, the SPS of amphiphilic cationic β^{3R3}-peptide sequences was then directly attempted using dimer building blocks with hydrophobic β-diamines (*v*Xaa) and *s*NH(Boc) β-diacids (Chapter 3). In fact, amphiphilic cationic β^{3R3}-peptide are attractive target for biomedical applications as amphiphilicity and cationic character are physicochemical features that essentially determine the membrane activity of AMPs and CPPs (see Chapter 5).

In order to establish the conditions for SPS of amphiphilic cationic β^{3R3}-peptides, the dimer building blocks with (S)-*s*NH(Boc) diacid units were used as they are made up of the natural and less expensive (L) enantiomer of Asp. Specifically, two homosequences of *v*Ala-(S)*s*NH_2 (**45**) and *v*Gly-(S)*s*NH_2 (**46**), as well as a heterosequence with different *v*Xaa units and hydrophobic proteinaceous side chains (**47**), were targeted (Scheme 4.8).

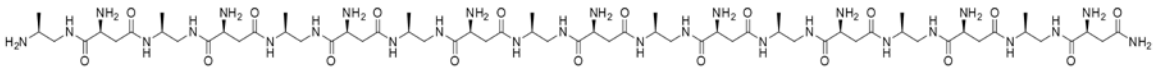

H_2N-*v*Ala-(S)*s*NH_2-*v*Ala-(S)*s*NH_2-*v*Ala-(S)*s*NH_2-*v*Ala-(S)*s*NH_2-*v*Ala-(S)*s*NH_2-*v*Ala-(S)*s*NH_2-*v*Ala-(S)*s*NH_2-*v*Ala-(S)*s*NH_2-NH_2 (**45**)

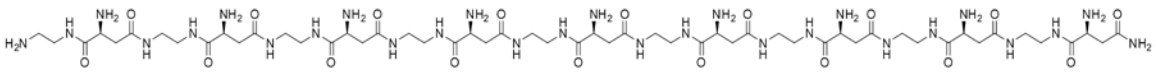

H_2N-*v*Gly-(S)*s*NH_2-*v*Gly-(S)*s*NH_2-*v*Gly-(S)*s*NH_2-*v*Gly-(S)*s*NH_2-*v*Gly-(S)*s*NH_2-*v*Gly-(S)*s*NH_2-*v*Gly-(S)*s*NH_2-*v*Gly-(S)*s*NH_2-NH_2 (**46**)

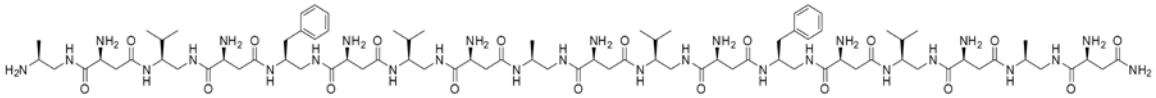

H_2N-*v*Ala-(S)*s*NH_2-*v*Val-(S)*s*NH_2-*v*Phe-(S)*s*NH_2-*v*Val-(S)*s*NH_2-*v*Ala-(S)*s*NH_2-*v*Val-(S)*s*NH_2-*v*Phe-(S)*s*NH_2-*v*Val-(S)*s*NH_2-*v*Ala-(S)*s*NH_2-NH_2 (**47**)

Scheme 4.8. *Sequence of the amphiphilic cationic β^{3R3}-peptide oligomers **45**, **46** and **47**.*

As successfully applied for the synthesis of hydrophobic proteinaceous sequences, double coupling with 5 equiv of building blocks and coupling times of 1 h with HATU as an activation agent were employed. Tentagel SRAM resin was again selected as solid support which intrinsically releases C-terminal carboxamide. As Tentagel resin, this was also preferred due to his hydrophilic properties which are expected to be beneficial for the coupling efficiency. However, first experiments resulted in limited purity of the oligomers, as shown from the cruse HPLC trace after precipitation in Et_2O. Also increasing the amount of building blocks from 5 to 8 equivalents did not lead to significant improvements (Figure 4.7). Therefore preparative HPLC was employed for purification of the oligomers. This inevitably resulted in significant drop of yield (around 40% on 0.025 scale). In addition, for homosequences, such as oligomers **45** and **46**, problematic purification and reduced purity of the product arose from HPLC peak overlap (Figure 4.7). Therefore, to reduce HPLC peak overlap, capping of unreacted chains on solid support was undertaken. This was done with the classical capping reagent acetic anhydride but not satisfactory improvements were achieved.

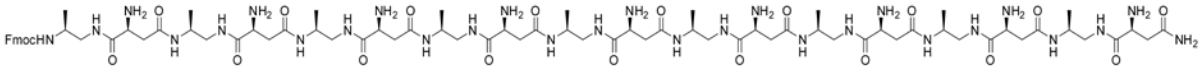

FmocHN-*v*Ala-(S)*s*NH_2-*v*Ala-(S)*s*NH_2-*v*Ala-(S)*s*NH_2-*v*Ala-(S)*s*NH_2-*v*Ala-(S)*s*NH_2-*v*Ala-(S)*s*NH_2-*v*Ala-(S)*s*NH_2-*v*Ala-(S)*s*NH_2-*v*Ala-(S)*s*NH_2-NH_2 (**45**)

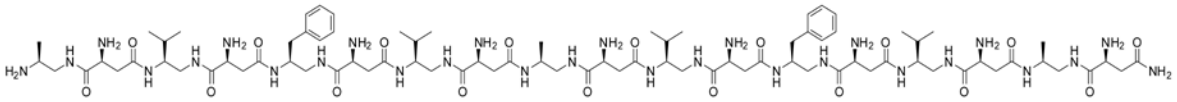

H_2N-*v*Ala-(S)*s*NH_2-*v*Val-(S)*s*NH_2-*v*Phe-(S)*s*NH_2-*v*Val-(S)*s*NH_2-*v*Ala-(S)*s*NH_2-*v*Val-(S)*s*NH_2-*v*Phe-(S)*s*NH_2-*v*Val-(S)*s*NH_2-*v*Ala-(S)*s*NH_2-NH_2 (**47**)

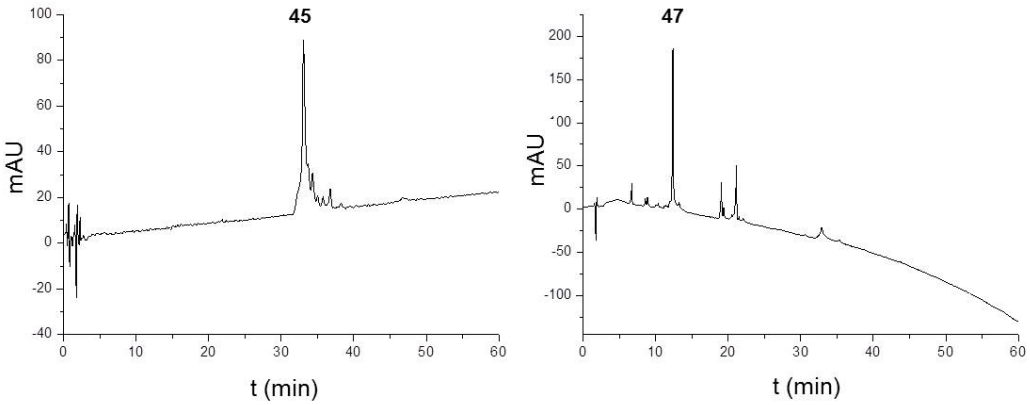

Figure 4.7. *Crude HPLC traces (5-95% H_2O to MeCN in 60 min) of oligomer **45** and **47** synthesized with 8 equiv. of building blocks and using 25% Pip in DMF as mixture for Fmoc deprotection. For oligomer **48** the HPLC of the Fmoc derivative is presented to show more directly the entity of peak overlap observed.*

Further optimization of the synthetic procedure was attempted aiming at highly pure samples directly from SPS in order to avoid elaborate HPLC purification. Indeed, residual Fmoc-entities were still revealed via HPLC after cleavage from the resin which hinted to problematic Fmoc deprotection (Figure 4.7). Similar difficulty was already reported for SPS of β-peptide for which above the critical chain length, typically about seven amino acids, DBU is added as an additional base to accelerate the Fmoc-removal step.[14] Here in particular the use of 25% Pip in DMF resulted in inefficient Fmoc deprotection, which could be attributed to a strong tendency of hydrophobic residues to aggregate on the solid support.[22] Differently from the hydrophobic β^{3R3}-peptides oligomers (**39-44**) previously synthesized, using dimer building blocks with *s*NH(Boc) as β-diacids unit, even extending considerably the time of deprotection did not produce complete removal of Fmoc groups (Figure 4.8). Gratifingly, this was overcome by the use of LiCl in DBU, Pip and DMF as mixture for Fmoc deprotection (Figure 4.8).[158] Finally, oligomer **47** was obtained in very high purity (>95%) after precipitation in cold Et_2O (Figure 4.9).

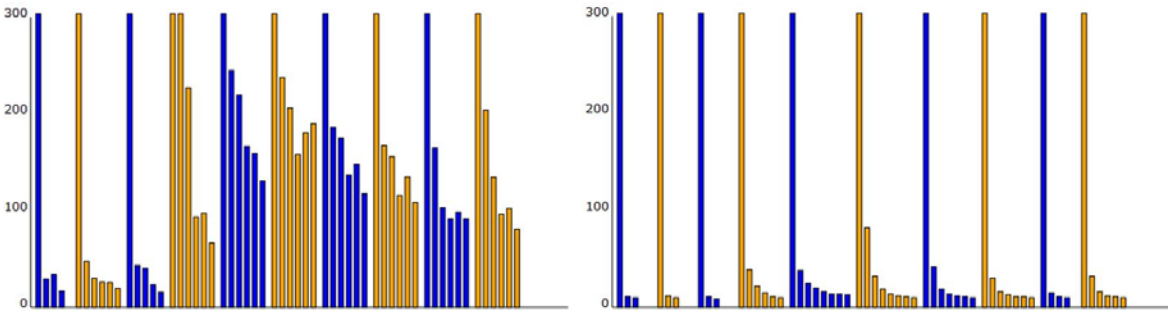

Figure 4.8. *Fmoc cleavage UV-patterns of oligomer* ***47*** *with 25% Pip in DMF (left) and 0.4M LiCl in DBU, Pip and DMF (right) as mixture for deprotection. The signals derived from the deprotection of the resin and the four couplings steps with dimer building blocks.*

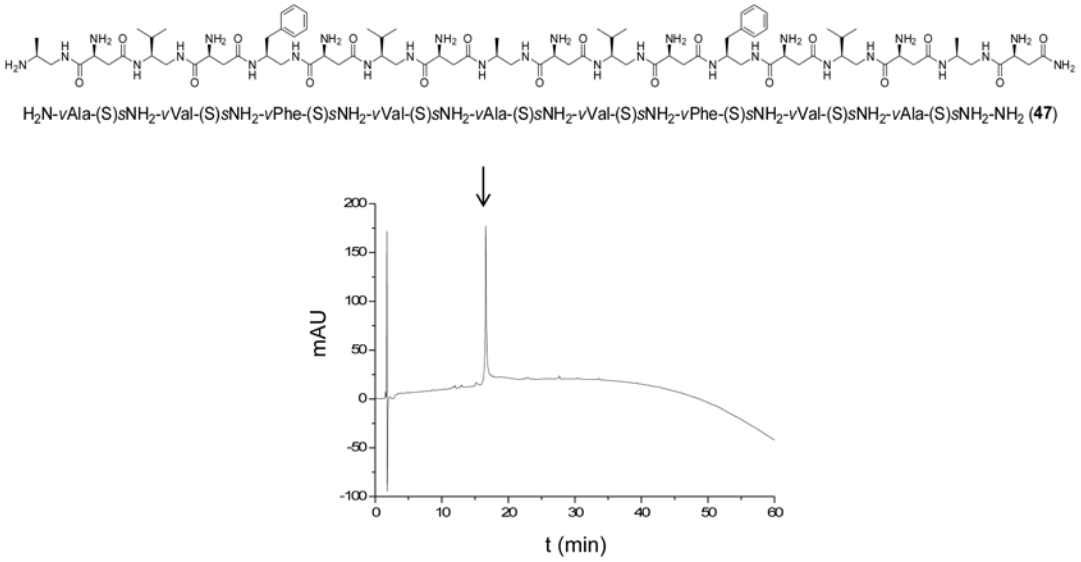

Figure 4.9. *Crude HPLC traces (5-95% H_2O to MeCN in 60 min) of oligomer* ***47*** *synthesized with 5 equiv. of building blocks and using 0.4M LiCl in DBU, Pip and DMF as mixture for Fmoc deprotection.*

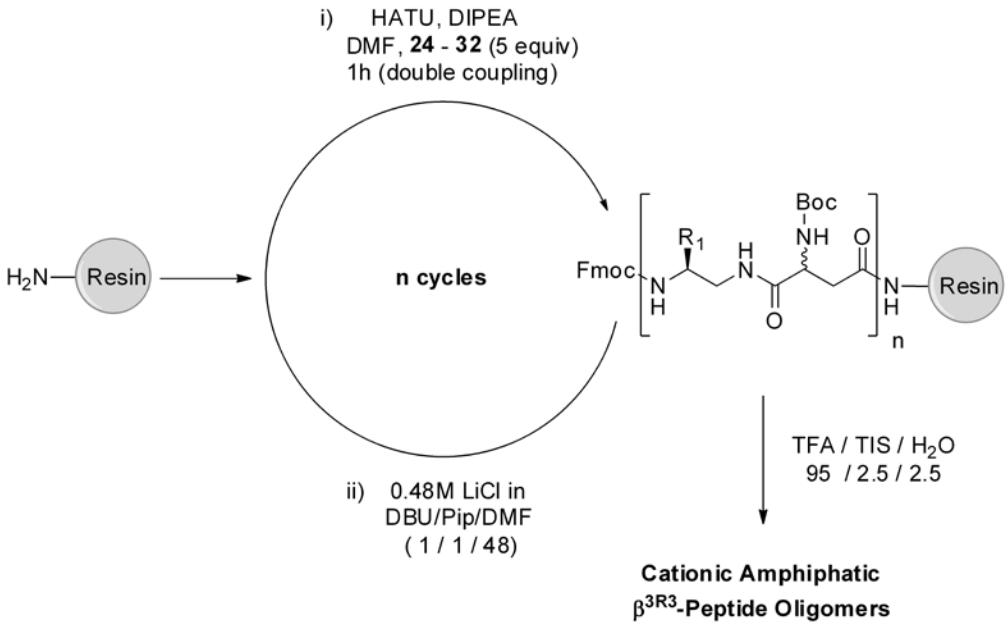

Scheme 4.9. *Synthetic route established for the SPS of cationic amphiphilic β^{3R3}-peptide sequences.*

Thereby, 11 designed sequences of amphiphilic cationic β^{3R3}-peptides (**46-56**) were synthesized employing dimer building blocks with the (S)-*s*NH(Boc) diacid unit and using 0.4M LiCl in DBU, Pip and DMF as mixture for Fmoc deprotection (Scheme 4.10). Thus, the efficiency and versatility of the developed protocols for the SPS of amphiphilic cationic β^{3R3}-peptides were demonstrated for chains made up of 9 (**46-52**), 5 (**53-54**), and 13 (**55**) dimer building blocks and a length corresponding to 18, 10, and 26 β-amino acids, respectively. Noteworthy, for the parent β^3-peptides, the successful synthesis of peptides made up of 24 amino acids is considered to be a good indication that every desired peptide sequence should be accessible.[14]

Within those chain lengths, the diamine units *v*Gly, *v*Ala, *v*Val, *v*Leu and *v*Phe were systematically interchanged to produce amphiphilic cationic β^{3R3}-peptide oligomers with variegated combinations of different proteinaceous side chains, aliphatic and aromatic, and different physicochemical features. This should ultimately allow for tuning their biological activity for specific biomedical application and will be investigated in chapter 5. In addition, the heterochiral sequence (*v*S,*s*R) **56** analogue of oligomer **50** was successfully synthesized, proving the versatility of this solid phase protocol also for the heterochiral dimer building blocks with the (R)-*s*NH(Boc) diacid unit (Scheme 4.10). Indeed, the effect of the chiral configuration of the sNH_2 diacid units on the conformational and biological properties of amphiphilic cationic β^{3R3}-peptides will be explored in chapter 5.

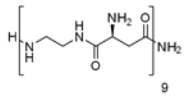

H_2N-(*v*Gly-(S)*s*NH_2)$_9$-NH_2 (**46**)

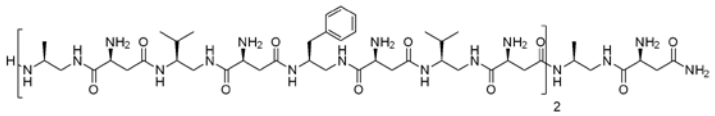

H_2N-(*v*Ala-(S)*s*NH_2-*v*Val-(S)*s*NH_2-*v*Phe-(S)*s*NH_2-*v*Val-(S)*s*NH_2)$_2$-*v*Ala-(S)*s*NH_2-NH_2 (**47**)

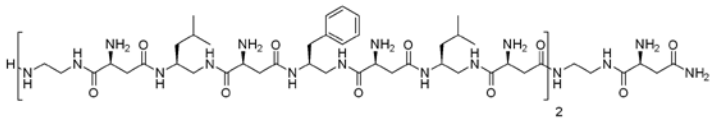

H_2N-(*v*Gly-(S)*s*NH_2-*v*Leu-(S)*s*NH_2-*v*Phe-(S)*s*NH_2-*v*Leu-(S)*s*NH_2)$_2$-*v*Gly-(S)*s*NH_2-NH_2 (**48**)

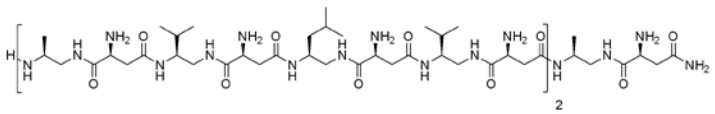

H_2N-(*v*Ala-(S)*s*NH_2-*v*Val-(S)*s*NH_2-*v*Leu-(S)*s*NH_2-*v*Val-(S)*s*NH_2)$_2$-*v*Ala-(S)*s*NH_2-NH_2 (**49**)

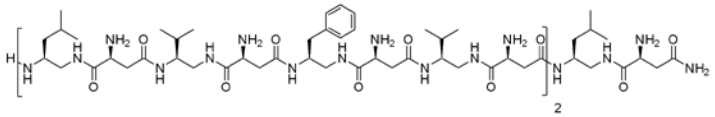

H_2N-(*v*Leu-(S)*s*NH_2-*v*Val-(S)*s*NH_2-*v*Phe-(S)*s*NH_2-*v*Val-(S)*s*NH_2)$_2$-*v*Leu-(S)*s*NH_2-NH_2 (**50**)

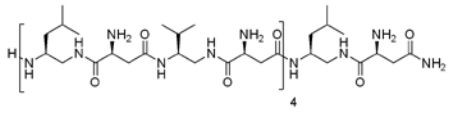

H_2N-(*v*Leu-(S)*s*NH_2-*v*Val-(S)*s*NH_2)$_4$-*v*Leu-(S)*s*NH_2-NH_2 (**51**)

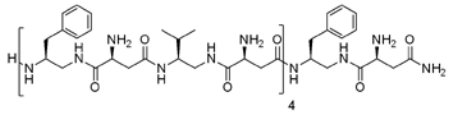

H_2N-(*v*Phe-(S)*s*NH_2-*v*Val-(S)*s*NH_2)$_4$-*v*Phe-(S)*s*NH_2-NH_2 (**52**)

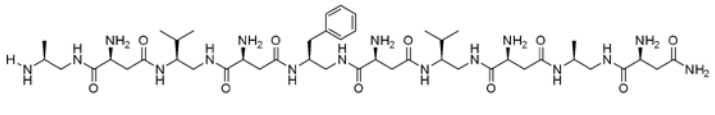

H_2N-*v*Ala-(S)*s*NH_2-*v*Val-(S)*s*NH_2-*v*Phe-(S)*s*NH_2-*v*Val-(S)*s*NH_2-*v*Ala-(S)*s*NH_2-NH_2 (**53**)

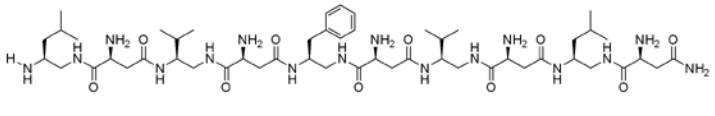

H_2N-(*v*Leu-(S)*s*NH_2-*v*Val-(S)*s*NH_2-*v*Phe-(S)*s*NH_2-*v*Val-(S)*s*NH_2)$_2$-*v*Leu-(S)*s*NH_2-NH_2 (**54**)

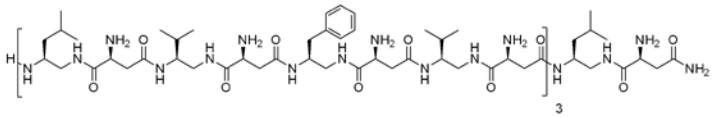

H_2N-(*v*Leu-(S)*s*NH_2-*v*Val-(S)*s*NH_2-*v*Phe-(S)*s*NH_2-*v*Val-(S)*s*NH_2)$_3$-*v*Leu-(S)*s*NH_2-NH_2 (**55**)

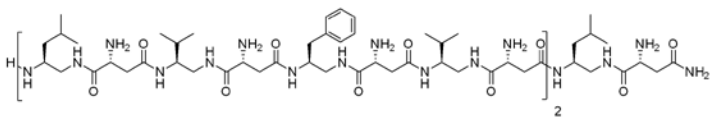

H_2N-(*v*Leu-(R)*s*NH_2-*v*Val-(R)*s*NH_2-*v*Phe-(R)*s*NH_2-*v*Val-(R)*s*NH_2)$_2$-*v*Leu-(R)*s*NH_2-NH_2 (**56**)

Scheme 4.10. *Sequences of the amphiphilic cationic β^{3R3}-peptide oligomers (**46-56**) synthesized.*

Remarkably, all the oligomers (**46**-**56**) were obtained in very high purity (>95%) after precipitation in cold Et_2O (Figure 4.11).

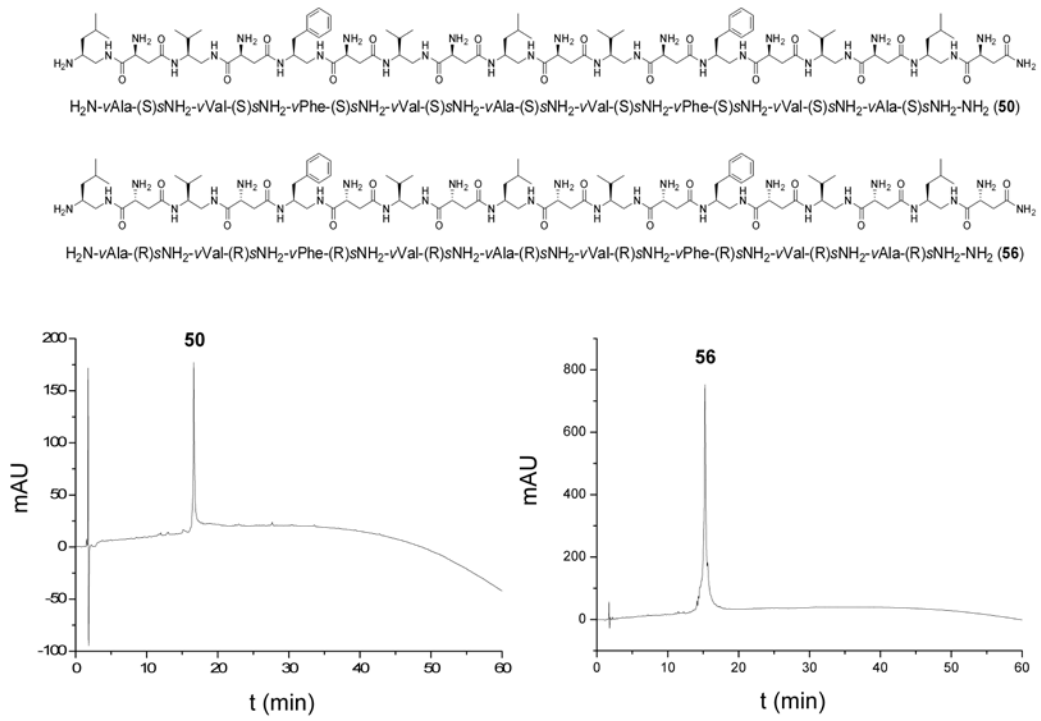

Figure 4.11. *Crude HPLC traces (5-95% H_2O to MeCN in 60 min) of oligomer **50** and its heterochiral (R,S) analogue oligomer **56**.*

Afterwards, all the amphiphilic cationic oligomers **46**-**56** were tagged with the fluorescent dye rhodamine B to afford oligomers **57**-**67** (Scheme 4.11). This allows for fluorescence-based investigation of the potential of amphiphilic cationic β^{3R3}-peptides for intracellular delivery of conjugated biomedical active cargos, as it will be detailed in chapter 5.

Gratifyingly, also the rhodamine B conjugated oligomers **57**-**67** were obtained in good yield and high puritiy after precipitation in cold Et_2O (Figure 4.12).

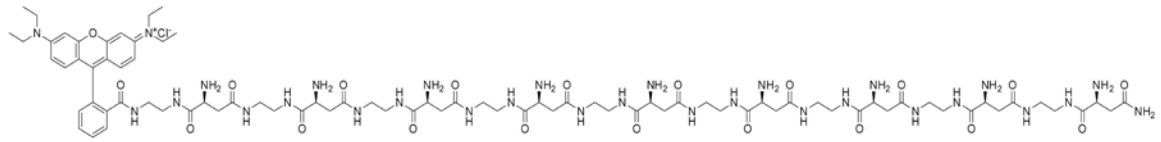

57

RhB-HN-(*v*Gly-(S)*s*NH$_2$)$_9$-NH$_2$ (**57**)

RhB-HN-(*v*Ala-(S)*s*NH$_2$-*v*Val-(S)*s*NH$_2$-*v*Phe-(S)*s*NH$_2$-*v*Val-(S)*s*NH$_2$)$_2$-*v*Ala-(S)*s*NH$_2$-NH$_2$ (**58**)

RhB-HN-(*v*Gly-(S)*s*NH$_2$-*v*Leu-(S)*s*NH$_2$-*v*Phe-(S)*s*NH$_2$-*v*Leu-(S)*s*NH$_2$)$_2$-*v*Gly-(S)*s*NH$_2$-NH$_2$ (**59**)

RhB-HN-(*v*Ala-(S)*s*NH$_2$-*v*Val-(S)*s*NH$_2$-*v*Leu-(S)*s*NH$_2$-*v*Val-(S)*s*NH$_2$)$_2$-*v*Ala-(S)*s*NH$_2$-NH$_2$ (**60**)

RhB-HN-(*v*Leu-(S)*s*NH$_2$-*v*Val-(S)*s*NH$_2$-*v*Phe-(S)*s*NH$_2$-*v*Val-(S)*s*NH$_2$)$_2$-*v*Leu-(S)*s*NH$_2$-NH$_2$ (**61**)

RhB-HN-(*v*Leu-(S)*s*NH$_2$-*v*Val-(S)*s*NH$_2$)$_4$-*v*Leu-(S)*s*NH$_2$-NH$_2$ (**62**)

RhB-HN-(*v*Phe-(S)*s*NH$_2$-*v*Val-(S)*s*NH$_2$)$_4$-*v*Phe-(S)*s*NH$_2$-NH$_2$ (**63**)

RhB-HN-*v*Ala-(S)*s*NH$_2$-*v*Val-(S)*s*NH$_2$-*v*Phe-(S)*s*NH$_2$-*v*Val-(S)*s*NH$_2$-*v*Ala-(S)*s*NH$_2$-NH$_2$ (**64**)

RhB-HN-*v*Leu-(S)*s*NH$_2$-*v*Val-(S)*s*NH$_2$-*v*Phe-(S)*s*NH$_2$-*v*Val-(S)*s*NH$_2$-*v*Leu-(S)*s*NH$_2$-NH$_2$ (**65**)

RhB-HN-(*v*Leu-(S)*s*NH$_2$-*v*Val-(S)*s*NH$_2$-*v*Phe-(S)*s*NH$_2$-*v*Val-(S)*s*NH$_2$)$_3$-*v*Leu-(S)*s*NH$_2$-NH$_2$ (**66**)

RhB-HN-(*v*Leu-(R)*s*NH$_2$-*v*Val-(R)*s*NH$_2$-*v*Phe-(R)*s*NH$_2$-*v*Val-(R)*s*NH$_2$)$_2$-*v*Leu-(R)*s*NH$_2$-NH$_2$ (**67**)

Scheme 4.11. *Rhodamine B conjugated oligomers* ***57-67*** *synthesized as derivatives of the amphiphilic cationic* β^{3R3}*-peptide oligomers* ***46-56****.*

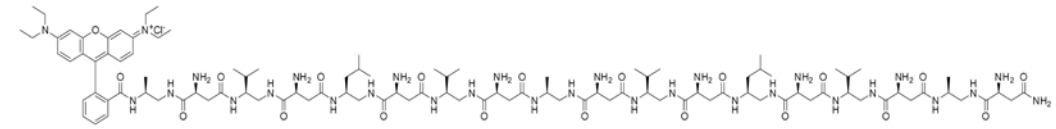

H$_2$N-*v*Ala-(S)*s*NH$_2$-*v*Val-(S)*s*NH$_2$-*v*Leu-(S)*s*NH$_2$-*v*Val-(S)*s*NH$_2$-*v*Ala-(S)*s*NH$_2$-*v*Val-(S)*s*NH$_2$-*v*Leu-(S)*s*NH$_2$-*v*Val-(S)*s*NH$_2$-*v*Ala-(S)*s*NH$_2$-NH$_2$ (**60**)

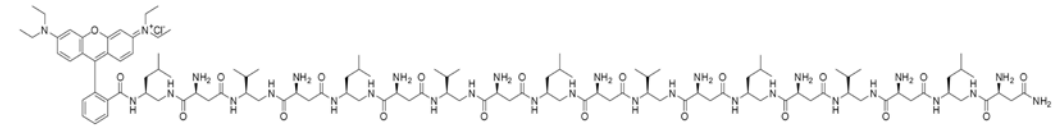

H$_2$N-*v*Leu-(S)*s*NH$_2$-*v*Val-(S)*s*NH$_2$-*v*Leu-(S)*s*NH$_2$-*v*Val-(S)*s*NH$_2$-*v*Leu-(S)*s*NH$_2$-*v*Val-(S)*s*NH$_2$-*v*Leu-(S)*s*NH$_2$-*v*Val-(S)*s*NH$_2$-*v*Leu-(S)*s*NH$_2$-NH$_2$ (**62**)

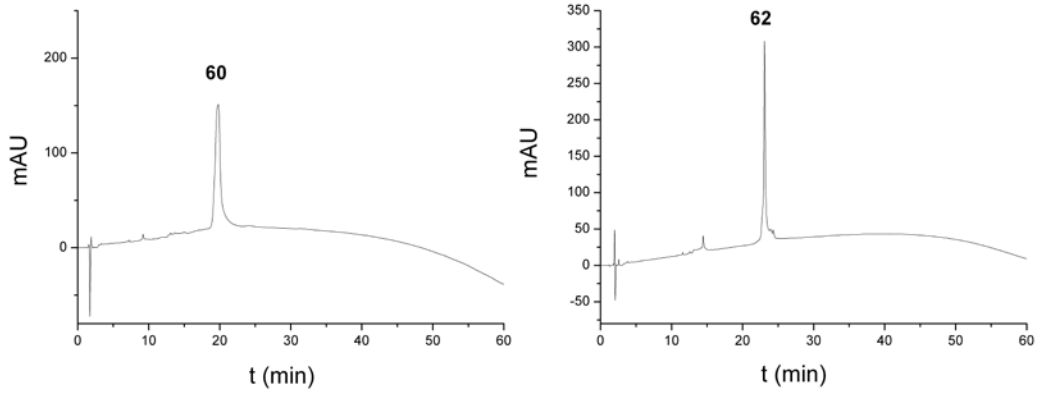

Figure 4.12. *Crude HPLC traces (5-95% H_2O to MeCN in 60 min) of rhodamine B conjugated amphiphilic cationic* β^{3R3}*-peptide oligomers* ***60*** *and* ***62****.*

Zwitterionic Oligomers

In the previous section, the synthetic protocol has been optimized for the SPS of amphiphilic cationic β^{3R3}-peptides using dimer building blocks with Boc protected amine group on the diacid unit *s*NH(Boc). Next, a specific protocol needs to be developed to apply dimer building blocks with *v*COO(Allyl) diamine and *s*NH(Alloc) diacid units (Chapter 3) for the SPS of zwitterionic β^{3R3}-peptides. Zwitterionic oligo/polymers feature unique biological antifouling property, i.e., those polymers can resist nonspecific protein adsorption, which makes them increasingly applied in a wide range of biomedical related fields.[159]

The key step for the synthesis of zwitterionic β^{3R3}-peptides is the removal of the *v*COO(Allyl) ester and Alloc protecting group of *s*NH(Alloc) after chain elongation. Specifically, the selected synthetic approach comprises the on-resin deprotection of the allyl species using catalytic amount of Tetrakis(triphenylphosphine)-palladium(0) ($Pd(Ph_3)_4$) (0.1 equiv per protecting group) and *N*,*N*-dimethylbarbituric acid (DMBA) as allyl scavenger (Scheme 4.12).

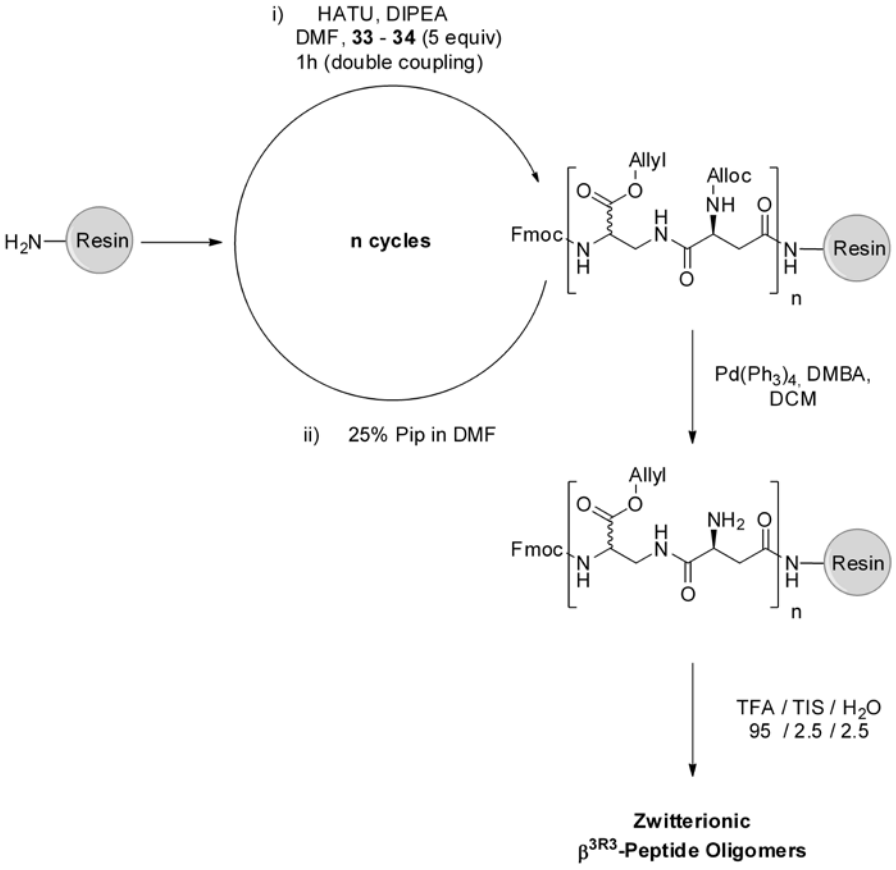

Scheme 4.12. *Synthetic route for the SPS of zwitterionic β^{3R3}-peptides.*

In order to optimize the SPS protocol for zwitterionic β^{3R3}-peptide, a homosequence of five repeating units (**68**) was targeted employing the homochiral (*v*S,*s*S) dimer building block FmocNH-(S)*v*COO(Allyl)-*s*NH_2(Alloc)-OH (Scheme 4.13). Indeed, this includes the (S)-*v*COO(Allyl) diamine unit which is prepared from the natural and less expensive (L) enantiomer of Asn (Chapter 3).

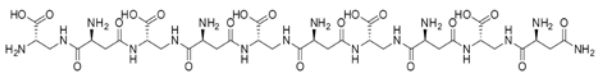

H_2N-(S)*v*COOH-(S)*s*NH_2-(S)*v*COOH-(S)*s*NH_2-(S)*v*COOH-(S)*s*NH_2-(S)*v*COOH-(S)*s*NH_2-(S)*v*COOH-(S)*s*NH_2-NH_2 (**68**)

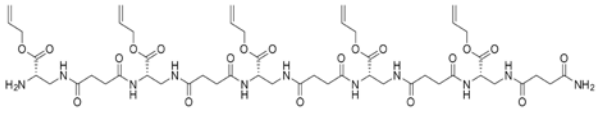

H_2N-(S)*v*COO(Allyl)-*s*Gly-(S)*v*COO(Allyl)-*s*Gly-(S)*v*COO(Allyl)-*s*Gly-(S)*v*COO(Allyl)-*s*Gly-(S)*v*COO(Allyl)-*s*Gly-NH_2 (**69**)

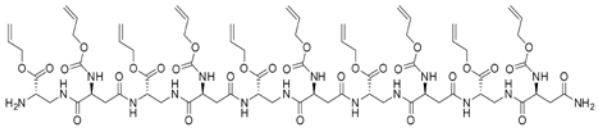

H_2N-(S)*v*COO(Allyl)-(S)*s*NH(Alloc)-(S)*v*COO(Allyl)-(S)*s*NH(Alloc)-(S)*v*COO(Allyl)-(S)*s*NH(Alloc)-(S)*v*COO(Allyl)-(S)*s*NH(Alloc)-(S)*v*COO(Allyl)-(S)*s*NH(Alloc)-NH_2 (**70**)

Scheme 4.13. *Zwitterionic oligomer **68** and related allyl and allyl-alloc derivatives **69** and **70**.*

Preliminarily, the synthesis of oligomer **69**, which presents exclusively allyl ester as side chains, was attempted to explore the complexity introduced by the ester moiety on the coupling and Fmoc-deprotection steps. The protocols developed for the SPS of amphiphilic cationic β^{3R3}-peptides was replicated, with 5 equiv. of building blocks and using 0.4M LiCl in DBU, Pip and DMF as mixture for Fmoc deprotection. However, HPLC analysis proved that such conditions are not suitable for the zwitterionic β^{3R3}-peptides (Figure 4.13). Indeed DBU can promote aspartimide formation and should be generally avoided for the synthesis of α-peptide sequences containing Asp or Asn. Additionally, the allyl ester could be not totally stable to a strong base such as DBU.

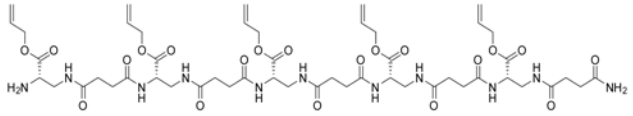

H_2N-(S)*v*COO(Allyl)-*s*Gly-(S)*v*COO(Allyl)-*s*Gly-(S)*v*COO(Allyl)-*s*Gly-(S)*v*COO(Allyl)-*s*Gly-(S)*v*COO(Allyl)-*s*Gly-NH_2 (**69**)

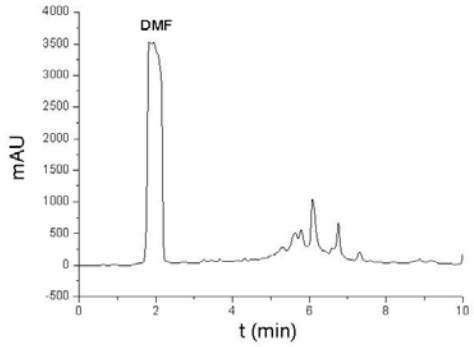

Figure 4.13. *Crude HPLC trace (5-95% H_2O to MeCN in 10 min) of synthesis of oligomer **69** with Allylester side chains using 0.4M LiCl in DBU, Pip and DMF as mixture for Fmoc deprotection.*

Therefore, 25% Pip in DMF was applied as Fmoc deprotection mixture for the synthesis of the zwitterionic β^{3R3}-peptide oligomer **68**. Gratifying, here the use of 25% Pip in DMF produced efficient Fmoc deprotection, even without the need for extended reaction time, as shown by the Fmoc cleavage UV-pattern (Figure 4.13). Indeed, the efficiency of this protocol for the SPS of the zwitterionic β^{3R3}-peptides was proved by HPLC analysis of the still protected sequence **70** (Figure 4.14). Finally, the simultaneous allyl ester and alloc deprotection was efficiently carried out on solid support with $Pd(Ph_3)_4$ and DMBA as allyl scavenger, as shown by MALDI analysis (Figure 4.15).

Thus, the synthetic protocols for the SPS of zwitterionic β^{3R3}-peptides have been established and can now be applied for the preparation of different sequences, with different chain length and chirality.

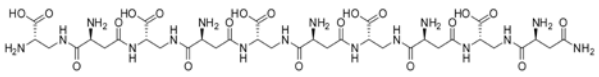

H_2N-(S)*v*COOH-(S)*s*NH_2-(S)*v*COOH-(S)*s*NH_2-(S)*v*COOH-(S)*s*NH_2-(S)*v*COOH-(S)*s*NH_2-(S)*v*COOH-(S)*s*NH_2-NH_2 (**69**)

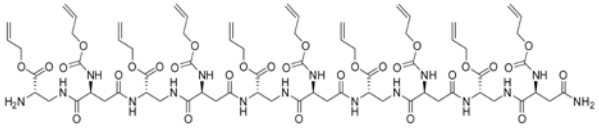

H_2N-(S)*v*COO(Allyl)-(S)*s*NH(Alloc)-(S)*v*COO(Allyl)-(S)*s*NH(Alloc)-(S)*v*COO(Allyl)-(S)*s*NH(Alloc)-(S)*v*COO(Allyl)-(S)*s*NH(Alloc)-(S)*v*COO(Allyl)-(S)*s*NH(Alloc)-NH_2 (**70**)

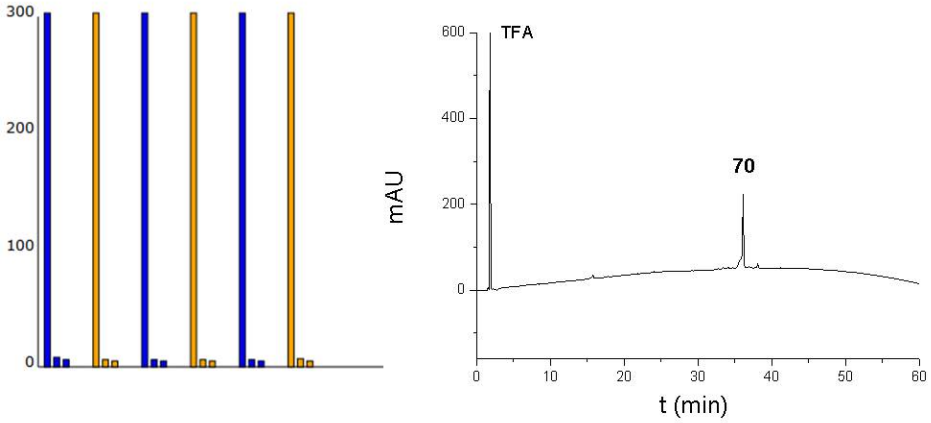

Figure 4.14. *Fmoc cleavage UV-pattern of the zwitterionic β^{3R3}-peptide oligomer* ***68*** *and crude HPLC trace (5-95% H_2O to MeCN in 60 min) of the protected precursor oligomer* ***70****.*

Overall, a potent and versatile synthetic platform has been developed for the SPS of three different classes of β^{3R3}-peptides: the hydrophobic, the amphiphilic cationic, and the zwitterionic β^{3R3}-peptides. This was achieved with dimer building blocks and selected combinations of Fmoc SPPS protocols which were fully automated using a standard peptide synthesizer. Thereby, libraries of hydrophobic and amphiphilic cationic β^{3R3}-peptides have been prepared.

The next step towards the development of these β^{3R3}-peptides as peptidomimetics for biomedical applications requires the investigation of primary properties related to their design and targeted application. Therefore, in the next chapter, specific structure-activity relationship studies comprising physicochemical and biological characterization will be detailed. In particular, the β^{3R3}-peptides with hydrophobic proteinaceous side chains will be presented with marked emphasis dedicated to their design and structural characterization at the air/water interface (Section 5.1). As a second class of β^{3R3}-peptides, the amphiphilic cationic β^{3R3}-peptides will be evaluated for their potential as antimicrobial and cell-penetrating agents (Section 5.2 and 5.3).

5. Biomedical Applications of β^{3R3}-Peptide Oligomers

The aim of this work is to introduce a novel class peptidomimetics and test for their potential for selected biomedical applications. In the previous chapter, an efficient and versatile synthetic platform has been developed for the SPS of the β^{3R3}-peptides, β-peptide analogues with proteinaceous side chains and different physicochemical properties. It is expected that due to novel qualities of the backbone with alternating direction of the amide bonds, the β^{3R3}-peptides can retain, modulate and extend essential structural, biochemical and biological properties of classical β-peptides. The next step towards the development of these β^{3R3}-peptides as peptidomimetics for biomedical applications requires the investigation of primary properties related to their design and targeted application. Essentially the synthesized β^{3R3}-peptide sequences can be grouped in different classes based on the inherent physicochemical features of the constitutive building blocks. Broadly, two main classes of these β^{3R3}-peptides for specific biomedical applications have been designed: the hydrophobic β^{3R3}-peptides and the amphiphilic cationic β^{3R3}-peptides,

Specifically, β^{3R3}-peptides with hydrophobic proteinaceous side chains will be presented with particular emphasis dedicated to the characterization of their folding and self-assembling properties at the air/water interface (Section 5.1). As a second set of oligomers, amphiphilic cationic β^{3R3}-peptides will be evaluated as membrane active peptidomimetics, namely antimicrobial and cell penetrating peptidomimetics (Section 5.2 and 5.3). Detailed SAR studies will be reported, comprising comprehensive physicochemical analysis, and fundamental biochemical and biological data.

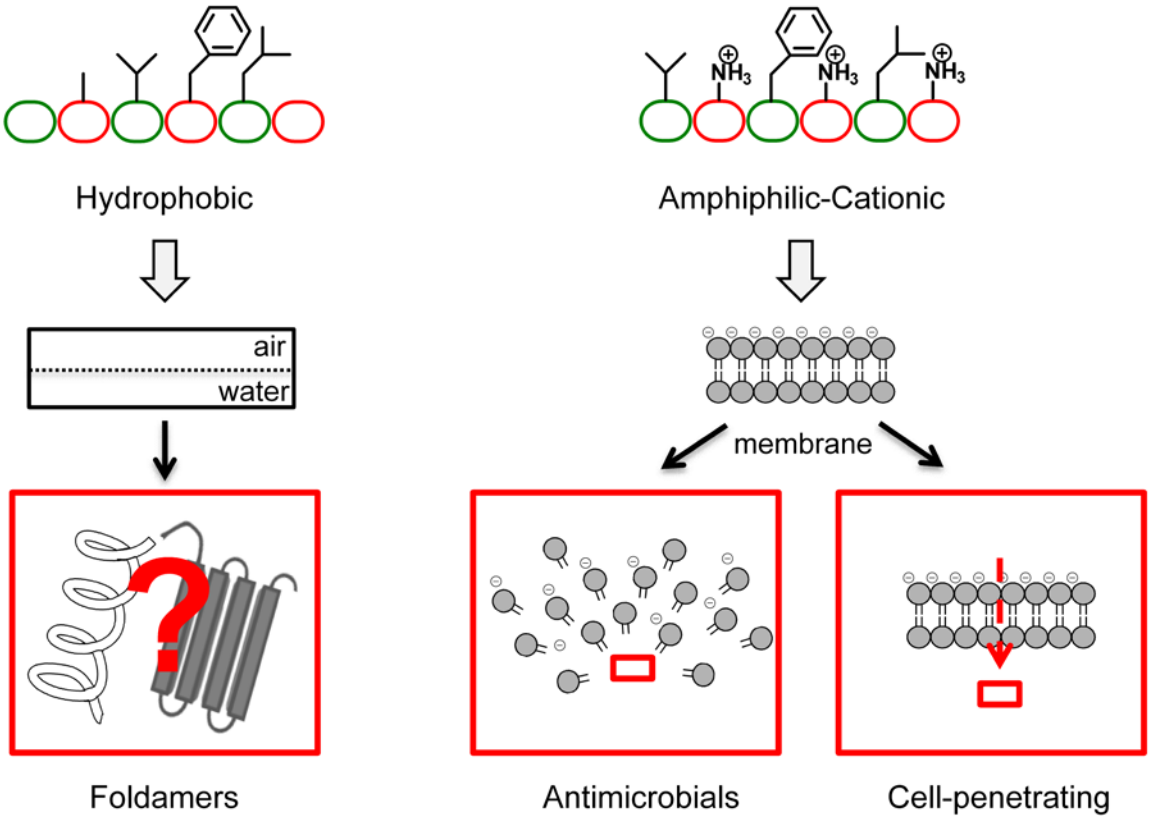

Figure 5.1. *Classes and applications of β^{3R3}-peptides investigated.*

5.1. β^{3R3}-Peptides with Hydrophobic Proteinaceous Side Chains and their Self-Assembling Properties at the Air/Water Interface

In the previous chapter, selected β^{3R3}-peptide dimer building blocks have been applied for the synthesis of hydrophobic β^{3R3}-peptides with proteinaceous side chains (Figure 4.2). Here, these sequences will be primarily employed for structural investigation to explore the possibility of long-range secondary structural order in the β^{3R3}-peptide backbone. Indeed, for foldamer development the most crucial types of secondary structure are those that display long-range order, helices and sheets.[7] Specifically, hydrophobic side chains are generally employed in the first phase of peptidomimetic foldamer development to assess the intrinsic folding propensity of a novel backbone.[7,14] Thus, using the hydrophobic β^{3R3}-peptides will now allow evaluating the potential of the β^{3R3}-peptides to retain, modulate, and extend the structural and thereby functional space available to β-peptides with proteinaceous side chains. Indeed, despite several β-peptide systems with helical conformation have been developed, only few examples of β-peptidic strands and sheets have been reported. The β-sheet conformation plays important biological and pathological roles.[32] For instance, β-strands aggregation ad sheet formation are crucial in the pathogenesis of several amyloidoses and mimicking β-strand have been proposed as a viable therapeutic strategy *e.g.* against Alzheimer's disease.[2] Therefore, novel building blocks have been designed to provide the β^{3R3}-peptide backbone with the potential to form apolar strand in extended conformation and to display orthogonal folding behaviour with respect to classical β-peptides (see Section 3.1).

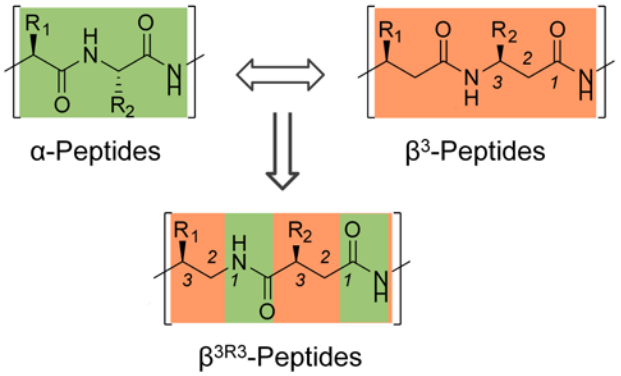

Figure 5.2. *Structural comparison among the α-, the β-, and the β^{3R3}-peptides backbone.*

Therefore, the folding and aggregation behaviour at the air/water interface of hydrophobic β^{3R3}-peptides will now be evaluated (Section 5.1.1). Indeed, alternating the directions of the amide bonds along the β-peptide chain, the β^{3R3}-peptide backbone has been designed to combine intrinsic physicochemical features of α- and β-peptides. Thereby and especially due to the potential to form apolar strand in extended conformation, β^{3R3}-peptides are expected to display orthogonal folding behaviour with respect to β-peptides and characteristic self-assembling properties.

The course of this study will be divided in two steps. First, the conformational properties of the hydrophobic β^{3R3}-peptides at the air/water interface will be evaluated by IRRAS (Section 5.1.1.a). Then, X-ray spectroscopy techniques for analysis at the air/water interface, namely GIXD and XR, will be applied to further investigate the self-assembling behaviour two-dimensional structure of β^{3R3}-peptide sheet monolayers (Section 5.1.1.b). In addition to the structural analysis, enzymatic stability assays on the hydrophobic β^{3R3}-peptide sequences will be considered in order to explore their potential as peptidomimetics for biomedical applications (Section 5.1.2).

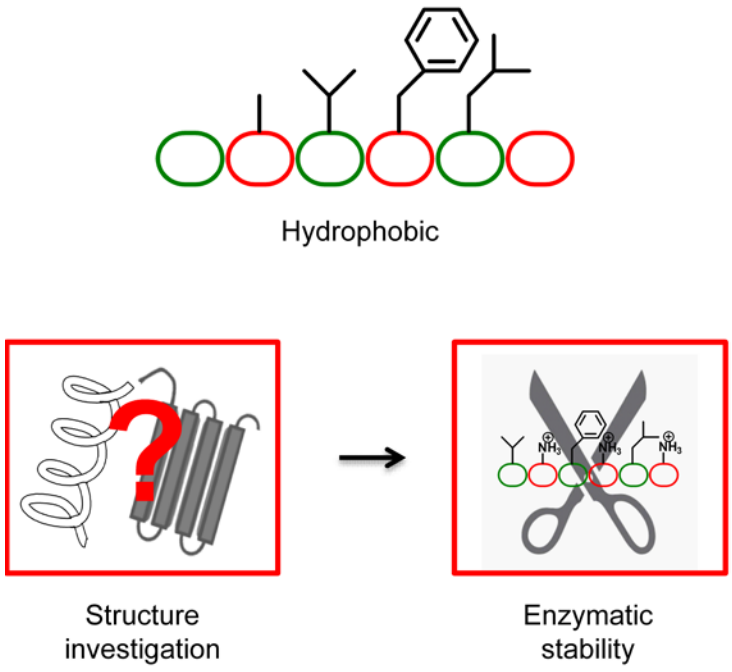

Figure 5.3. *Sequential steps towards the development of hydrophobic β^{3R3}-peptides for biomedical applications.*

5.1.1. Structural Characterization of Hydrophobic β^{3R3}-Peptides

In order to investigate the intrinsic folding propensity of the novel backbone and evaluate the potential to form strand conformation and β-sheet-like structures, hydrophobic β^{3R3}-peptide sequences have been designed and synthesized in Chapter 4 (Scheme 5.1). Specifically, these sequences are analogues of β^3-peptides used in folding studies and known to form stable 3_{14}-helix that emerged as the best documented conformation of β^3-peptides.[17,108] Indeed, sequence heterogeneity can contribute to govern the conformations of bio- and synthetic foldamers.[7] However, sequence heterogeneity is not required in the first phases of foldamer development, since heterogeneity is not necessary to explore the possibility of long-range secondary structural order in a given backbone.[7] Thus, keeping the same side chains allows for a comparison of the intrinsic folding propensity between the β^{3R3}-peptide and the β^3-peptide backbones. Similarly to the parent β^3-peptides,[108] oligomers **39**-**41** were insoluble in water and soluble only at low concentration (~1 mM) in MeOH, a common solvent for conformational investigations of hydrophobic β-peptides.[17] In order to improve the solubility and to investigate the effect of different terminal groups on the folding and aggregation behavior, similar sequences of β^{3R3}-peptides were tagged with EDA as terminal *v*Gly affording oligomers **42**-**44**. Gratifyingly, oligomers **42**-**44** showed good solubility in MeOH (4 mM).

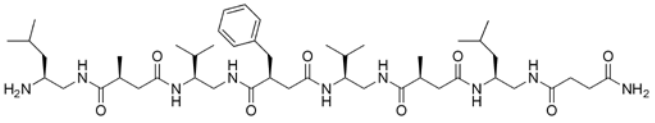

H_2N-*v*Leu-*s*Ala-*v*Val-*s*Phe-*v*Val-*s*Ala-*v*Leu-*s*Gly-NH_2 (**39**)

H_2N-*v*Leu-*s*Phe-*v*Leu-*s*Ala-*v*Val-*s*Phe-*v*Val-*s*Ala-*v*Leu-*s*Gly-NH_2 (**40**)

H_2N-*v*Leu-*s*Ala-*v*Val-*s*Phe-*v*Val-*s*Ala-*v*Leu-*s*Phe-*v*Leu-*s*Ala-*v*Val-*s*Phe-*v*Val-*s*Ala-*v*Leu-*s*Gly-NH_2 (**41**)

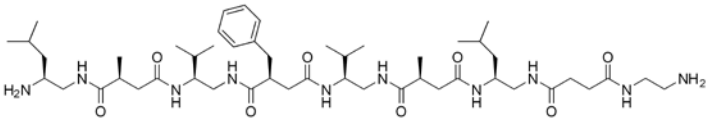

H_2N-*v*Leu-*s*Ala-*v*Val-*s*Phe-*v*Val-*s*Ala-*v*Leu-*s*Gly-*v*Gly-NH_2 (**42**)

H_2N-*v*Val-*s*Ala-*v*Leu-*s*Phe-*v*Leu-*s*Ala-*v*Val-*s*Phe-*v*Val-*s*Ala-*v*Leu-*s*Gly-*v*Gly-NH_2 (**43**)

H_2N-*v*Leu-*s*Ala-*v*Val-*s*Phe-*v*Val-*s*Ala-*v*Leu-*s*Phe-*v*Leu-*s*Ala-*v*Val-*s*Phe-*v*Val-*s*Ala-*v*Leu-*s*Gly-*v*Gly-NH_2 (**44**)

Scheme 5.1. *Hydrophobic β^{3R3}-peptide sequences synthesized and employed for structural investigation of the β^{3R3}-peptide backbone conformational propensity and self-assembling properties at the air/water interface.*

Thus, the β^{3R3}-peptides will be investigated for their structural properties, will particular focus dedicated to their folding and aggregation behavior at the air/water interface. On the one hand, the air/water interface has been established as a simplified model to mimic the physicochemical properties of the aqueous layer of a few nanometer thicknesses that exists at the interface of the cell membrane.[117-120] Thus the data obtained for the structural behavior at the air/water interface is relevant not only from a structural point of view but also for the potential interaction of the β^{3R3}-peptides with cell membranes and related biomedical targets. On the other hand, Langmuir monolayer techniques provide a unique and accurate methodology to investigate biomacromolecules at the air/water interface and establish relationships between chemical properties and assembly behavior.[119,121-127] Indeed, the use of a confined space at the hydrophilic/hydrophobic interface in combination with sophisticated surface sensitive techniques has been employed to investigate the self-assembly of α/β-peptides designed to form strands which can assemble through the formation of hydrogen-bonded sheets.[41,42] Thus the layers of the hydrophobic β^{3R3}-peptide oligomers (**39**-**44**) at the air/water interface were characterized by IRRAS, GIXD and XR, and the data will be presented in section 5.1.1.a and 5.1.1.b, respectively. In addition, preliminary analysis in bulk via CD spectroscopy will be treated in section 5.1.1.c.

5.1.1.a. IRRAS Analysis of Hydrophobic β^{3R3}-Peptides

IRRAS was employed to obtain information about the conformation of the β^{3R3}-peptides at the air/water interface. The experiments were performed with the help of Claudia Dannehl from the group of Prof. Gerald Brezesinski, an expert in the field of structural investigations at the air/water interface. The β^{3R3}-peptide oligomers **39**-**44** were dissolved in MeOH and spread onto a buffer solution. Due to the hydrophobicity of the oligomers, they form stable layers at the air/water interface which were further compressed to improve the signal-to-noise ratio. All oligomers contain a high amount of β-strands-like structures, as revealed by a Amide I band between 1625 and 1645 cm^{-1} in the IRRA spectra (Figure 5.4).[129,130] Indeed, bands around 1635 cm^{-1} have been reported as indicative of strong intermolecular H-bonds in α-peptides[120,124,126,129] as well as β-peptides.[33]

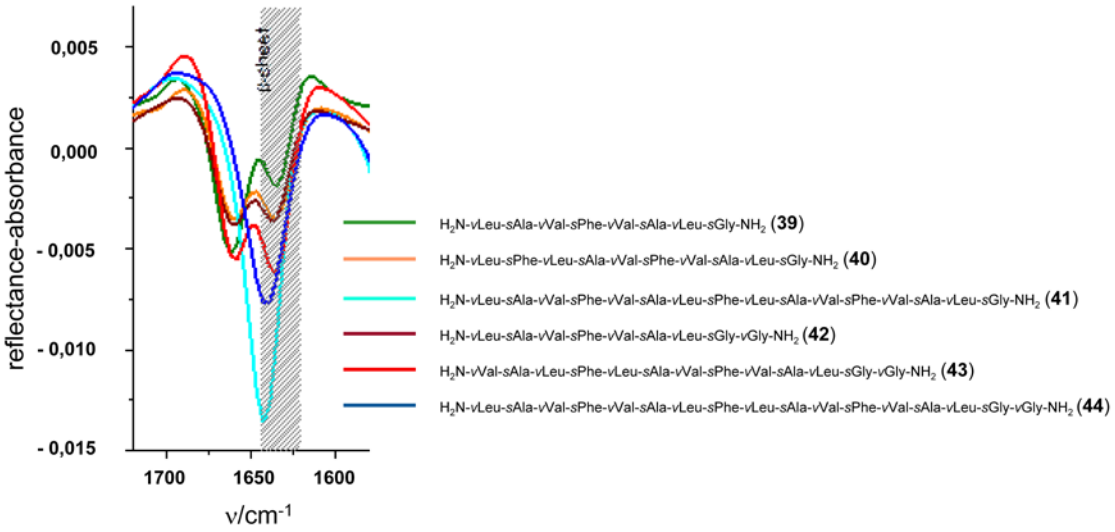

Figure 5.4. *Amide I band from IRRA spectra at the air/water interface after compression of the film.*

In particular, the oligomers **39**, **40**, **42**, and **43** show the maximum in the Amide I band around 1635 cm^{-1}, indicating the formation of a strong intermolecular hydrogen bond network typical for crystalline β-sheets at the air/water interface.[33,120,124,126,129,130] A second band appears at high frequency (around 1662 cm^{-1}) which is attributable to amide CO groups not involved as acceptors in H-bonding and can derive from non-specific aggregation.[33,129,130] The intensity ratio of these two bands changes along with the oligomer length. This indicates a changing ratio between the crystalline and non-crystalline parts of sheet monolayers. In contrast, the longest oligomers **41** and **44** exhibit a single and quite broad band around 1645 cm^{-1} which is characteristic for strands which self-assemble in less ordered intermolecular networks, as reported for both α-peptides and β-peptides.[33,129,130]

In conclusion, IRRAS clearly indicates that the β^{3R3}-peptides are able to form strands and sheet assemblies at the air/water interface. Here we can deduce a dependency of the assembling properties of the oligomers on the chain length: while the shortest oligomer, **39** shows limited strand and sheet formation and most likely undergoes non-specific aggregation, the longest oligomers, **41** and **44**, show distinct strand formation.

5.1.1.b. GIXD and XR Analysis of Hydrophobic β^{3R3}-Peptides

In order to further elucidate the two-dimensional structure of sheet monolayers, selected hydrophobic β^{3R3}-peptides were analyzed by GIXD, which is a direct method for structural analysis.[41,42] Indeed, GIXD has been also the method of choice for the investigation of α/β-peptides designed to form apolar strands which can assemble through the formation of hydrogen-bonded sheets at the air/water interface.[41] The oligomers **40**, **41** and **44** were selected and analyzed by GIXD, as their strands form sheets with different degrees of crystallinity at the air/water interface, as shown by IRRAS. The experiments were carried out at the DESY in Hamburg by Professor Gerald Brezesinski and evaluated with his help.

The short oligomer **40** exhibits Bragg peaks in the wide- as well as in the small-angle regions (Figure 5.5).

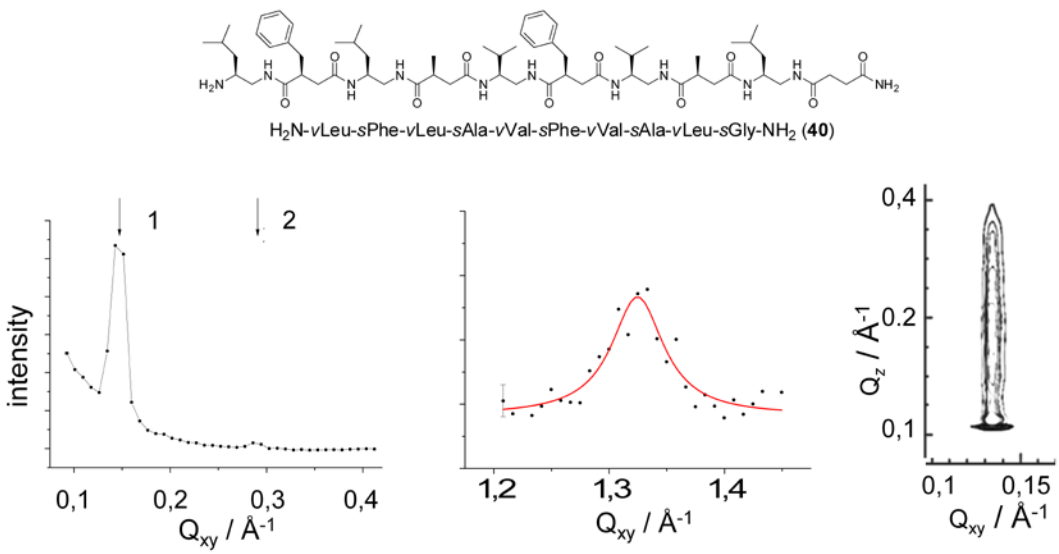

Figure 5.5. *GIXD spectra of the β^{3R3}-peptide oligomer **40**. Corrected X-ray intensities versus the in-plane scattering vector component Q_{xy} (left). Corrected X-ray intensities versus the out-of-plane (Q_z) scattering vector components (center). Contour plot of the corrected X-ray intensities as a function of in-plane (Q_{xy}) and out-of-plane (Q_z) scattering vector components(right).*

The weak Bragg peak at 1.327 Å^{-1} corresponds to the interstrand distance of 4.735 Å defined by the hydrogen bonds in crystalline β-sheets (proved by IRRAS experiments showing a band at 1635 cm^{-1}).[124,120,126] The correlation length in transversal direction amounts to 97 Å, corresponding to

20 molecular repeats. This excludes either any helical or unordered conformation. For the layer of oligomer **44**, no Bragg peak has been observed in this region in good agreement with the IRRAS data showing the amide I band only at a high wavenumber of 1641 cm^{-1}. This non-aggregated strand structure is characterized by the lack of long range correlation between the strands. Interestingly, oligomer **41** does not give any signal in GIXD thus indicating neither translational nor longitudinal long-range correlation between the strands. This is in agreement with IRRAS data where oligomer **40** exhibits a single band around 1645 cm-1 indicating the presence of strand conformations which do not assemble into sheets with an intermolecular network.[129,130,33]

The layers of oligomers **40** and **44** additionally exhibit two-dimensional smectic order (Bragg peaks in the small-angle region) (Figure 5.6).

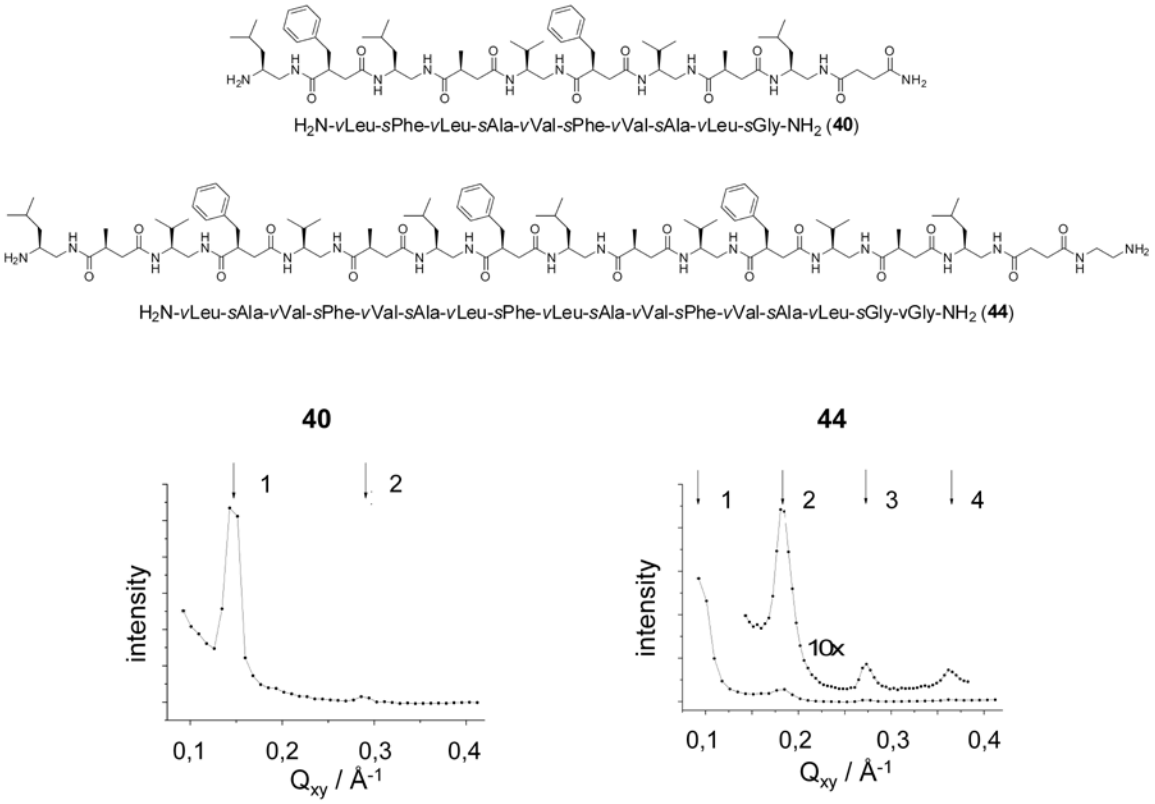

Figure 5.6. *Corrected X-ray intensities versus the in-plane scattering vector component Q_{xy} of oligomer **40** (left) and oligomer **44** (right).*

Thereby, oligomer **44** exhibits high order in the direction of the long repeat distance. 4 Bragg peaks have been observed at Q_{xy} values of 0.092, 0.182, 0.273 and 0.366 $Å^{-1}$ corresponding to a $d_{(01)}$ spacing of 68.7 Å and its higher order reflections. For oligomer **40**, two Bragg peaks are found at 0.144 and 0.287 $Å^{-1}$ corresponding to a $d_{(01)}$ spacing of 43.6 Å. The long repeat distances determined after compression of the film are shorter than expected for elongated strands (these distances were obtained by the addition of bond lengths with the structures presenting an all-trans linear conformation and were calculated by Chem3D Pro). The difference between the observed and the calculated values increases with increasing oligomer length. Specifically, a length of 43.6 Å was measured for oligomer **40** (89% of the calculated extended strand length of 49.1 Å), and 68.7 Å for oligomer **44** (86% of the calculated extended strand length of 80.2 Å) ruling out any helical or hairpin conformation and thus was assigned to a bended strand like secondary structure (Figure 5.7 and Figure 5.8).

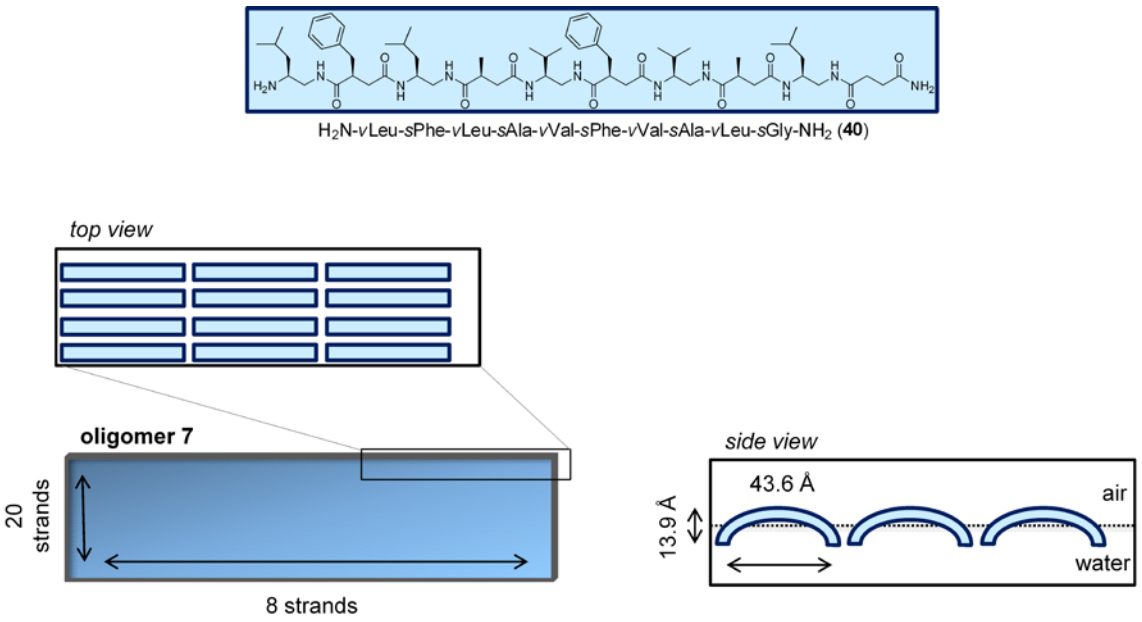

Figure 5.7. *Structural model for strand aggregation of oligomer **40** at the air/water interface to form sheets as derived from IRRAS, GIXD and XR data.*

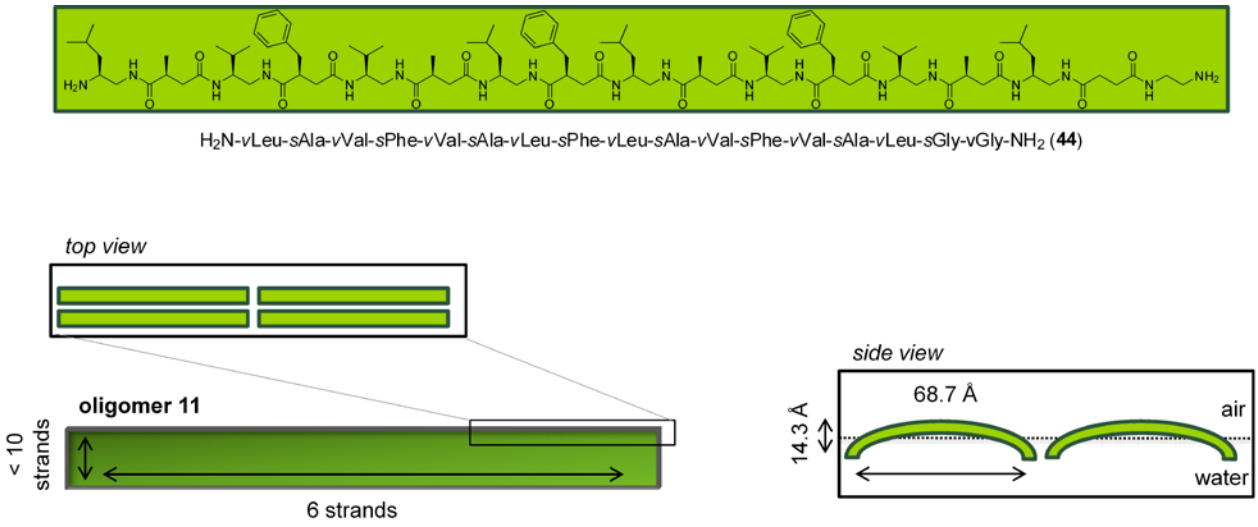

Figure 5.8. *Structural model for strand aggregation of oligomer **44** at the air/water interface to form sheets as derived from IRRAS and GIXD data.*

There are several possible arrangements of the oligomers that lead to a repeat distance shorter than the full length of the elongated molecule. The relative shorter length of **44** compared to **40** could be explained by the addition of the terminal *v*Gly which is flexible and hydrophilic and therefore tends to dive into the water. The correlation lengths in the direction of the long repeat distance are in the order of 400 Å, corresponding to 6 (oligomer **44**) or 8 (oligomer **40**) aligned strands. In addition, the analysis of the Bragg rods shows that the out-of-plane component of the scattering vector has clearly maximum intensity above the horizon which suggests that the strands are not lying entirely flat at the surface and more likely bend upon compression. To prove the bending, the layer thickness has been determined by XR experiments. The FWHM of the Gaussian-shaped curve amounts to 14.3 Å for oligomer **44** and 13.9 Å for oligomer **40**, which translates directly into the thickness of the corresponding films. This thickness is larger than expected for a layer of β-sheets lying flat at the air/water interface and the bending rigidity is smaller for the longer oligomer. These results support a structure model with bended strands being aggregated into sheet assemblies with different crystallinity. Similarly, D/L α-peptidic sequences also have side chains on one face and give rise to bending of the sheets eventually producing beta-helices instead of beta-sheets.[160] Therefore, the disposition of all side chains on one face might explain the bending of the backbone we observed by X-ray reflectivity experiments.

In summary, all three physical methods applied for structural investigations give consistent results showing the distinct formation of strands and sheets. Based on the data obtained so far, the self-assembling properties can be modulated by varying the chain length leading to a less ordered H-bond network with increasing oligomer chain length. We also see an influence of the end groups, *e.g.* oligomers **41** and **44** have a similar chain length but different end groups with both oligomers forming strands but only **44** forming sheets. These observations suggest stabilization of the strand conformation for oligomer **41** as a result of the lack of less-fixed terminal *v*Gly residues. Interestingly, specific residues at the terminal positions also promote alignment of α/β-peptides molecules along the H-bond direction within two dimensional sheet assemblies.[41] Thus, specific sequences of hydrophobic β^{3R3}-peptides with proteinaceous side chains could mimic β-strands and thereby antagonize hydrophobic β-sheet formation or recognition, which has been proposed as a viable therapeutic strategy e.g. against Alzheimer's disease.[2]

5.1.1.c. Preliminary Structural Analysis in Bulk of Hydrophobic β^{3R3}-Peptides

Lastly, the hydrophobic β^{3R3}-peptide oligomers **39**-**44** were investigated via CD spectroscopy as a convenient tool to obtain a first insight into their conformational and self-assembling properties in bulk (Figure 5.9). The CD analysis was performed in methanol, a common solvent for conformational investigations of hydrophobic β-peptides and peptidomimetics in general.[17] The oligomers **40**, **41**, **43** and **44** in MeOH exhibit two minima around 193 and 204 nm, which hint at the existence of chiral secondary structures. Interestingly, these traces could be attributed to nonpolar strand conformations according to literature data on β-peptides.[33,40] Nevertheless, the different backbones of β-peptides and α-peptides could lead to different conformational geometries which result in different CD spectra.[107] Similarly, the different intramolecular hydrogen bond patterns available to β^{3R3}-peptides and β-peptides (Figure 3.1.) can lead to alternative geometries and different CD spectra. Differently, oligomers **39** and **42** show strongly decreased CD signals indicating non-specific aggregation, which leads to a shading of chromophores and absorption flattening.[110-112]

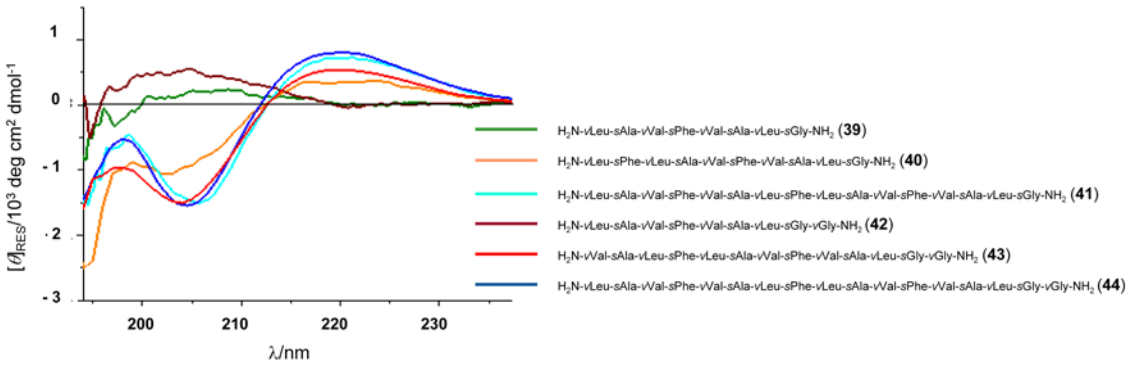

Figure 5.9. *CD spectra in methanol (c = 0.1 mM).*

Thus, it could be concluded that in bulk oligomers **40**, **41**, **43** and **44** tend to adopt a specific structure while oligomers **39** and **42** are more prone to non-specific aggregation. This is in agreement with the IRRAS data, where the intensity ratio of the second band at high frequency (around 1662 cm^{-1}) attributable to non-specific aggregation decreases along with the oligomer length. This indicates a changing ratio between the crystalline and non-crystalline parts of sheet monolayers.

Unfortunately, the complexity and the chain length of the β^{3R3}-oligomers investigated here did not allow us to corroborate the CD information using a conventional method of conformational analysis,

such as NMR. Indeed, only the incorporation of ^{13}C and/or ^{15}N labels in defined positions might allow for making assignments which is a basic prerequisite for the interpretation of 2D NOESY/ROESY spectra demanded for conformational analysis (Figure 5.10).

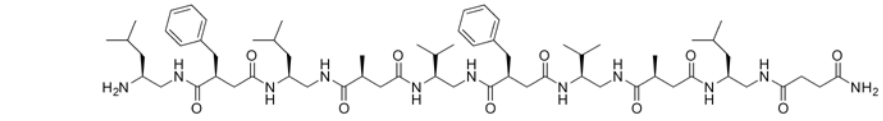

H_2N-*v*Leu-*s*Phe-*v*Leu-*s*Ala-*v*Val-*s*Phe-*v*Val-*s*Ala-*v*Leu-*s*Gly-NH_2 (**40**)

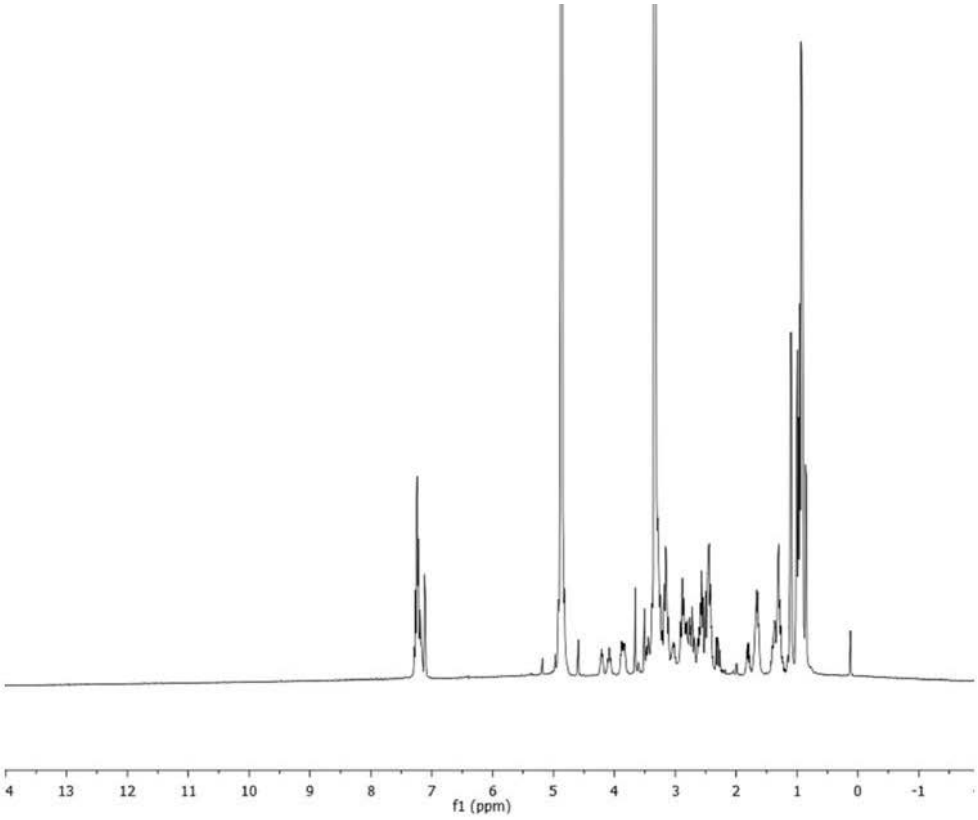

Figure 5.10. *NMR spectrum in d_4-MeOH of the hydrophobic β^{3R3}-oligomers oligomers* ***40***

Overall, via alternating directions of the amide bonds along β-peptide sequences, the β^{3R3}-peptides can indeed extend the structural space of β-peptides with proteinaceous side chains. Detailed analysis at the air/water interface shows strand conformations and the formation of sheet assemblies with different crystallinity. Ongoing work focuses on structural analysis in bulk using conventional high-resolution methods, such as NMR, which are required to draw further conclusions about the structural properties and functional potential of β^{3R3}-peptides.

5.1.2. Enzymatic Stability Assay with Hydrophobic β^{3R3}-Peptides

In addition to the structural analysis, the β^{3R3}-peptides have been also employed for enzymatic stability assays in order to primarily explore their potential as peptidomimetics for biomedical applications. It is well appreciated that β-peptides are highly interesting for applications where the use of natural peptides is limited due to their enzymatic susceptibility. Although tests with proteolytic enzymes of all types (from mammals, microorganisms or yeasts) showed β-peptides to be completely stable towards proteolysis, β^{3R3}-peptides could be expected to have higher proteolytic susceptibility as all the proteolytic enzymes (aspartic, serine, metallo, and cysteine proteases) bind their inhibitors/substrates in the same extended β-strand conformation.[2]

As model system, oligomer **44** was tested with pronase, a mixture of several endo- and exo-peptidase without sequence specificity and exclusive capability for digestion of α- and α/β-peptides.[14] Oligomer **44** was selected as it showed distinct strand formation and high enough solubility in 30% MeOH/aqueous buffer (25mM Tris HCl, 3mM $CaCl_2$) mixture required for the enzyme activity tests. The enzymatic stability assays were performed with the help of Uwe Möginger. Indeed, oligomer **44** is still detectable after 8 days without any signs of degradation. Therefore and due to the sequence aspecificity of pronase, it could be concluded that hydrophobic β^{3R3}-peptides have a high metabolic stability which makes them an interesting novel class of materials suitable for biomedical applications.

Thus in the next sections, a second set of oligomers, the amphiphilic cationic β^{3R3}-peptides will be evaluated for their potential as mimetics of MAPs with important applications in the biomedical field, namely antimicrobial and cell penetrating peptidomimetics (Section 5.2 and Section 5.3). Detailed SAR studies will be reported, comprising comprehensive physicochemical analysis, and fundamental biochemical and biological characterization.

5.2. Amphiphilic Cationic β^{3R3}-Peptides as Membrane Active Peptidomimetics for Biomedical Applications

In the previous section, β^{3R3}-peptide sequences with hydrophobic proteinaceous side chains have been employed to get a first insight into the structural properties and enzymatic stability of the β^{3R3}-peptide backbone. The next step towards the development of β^{3R3}-peptides as peptidomimetics requires the introduction of functional side chains to target specific applications in the biomedical field. Therefore, amphiphilic cationic β^{3R3}-peptides will be evaluated for their potential as membrane active peptidomimetics.

MAPs represent a variety of molecules which exert their biological functions by directly interacting with the cell membrane. MAPs generally share a highly cationic and globally amphiphilic character, which primarily determines their biological activity within the lipid membrane. AMPs and CPPs are two major classes of MAPs with acknowledged potential for biomedical applications. However, natural MAPs still suffer from major drawbacks, such as unfavorable pharmacokinetical profile and reduced therapeutic index. Indeed, natural MAPs tend to be quite protease sensitive and can display either low direct antimicrobial activity or significant cytotoxicity also against eukaryotic host cells. Therefore, different classes of membrane active peptidomimetics have been developed. In particular, cationic amphiphilc β-peptides with helical conformation have been attracted extensive research efforts and expectations,[132,12,11] as they can reproduce the physicochemical features of AMPs with improved proteolytic stability.[11,12] Indeed, despite their potential hemolytic activity,[19,21,22,23] β-peptides are good candidates for further research and development as membrane active peptidomimetics.

Thus, amphiphilic cationic β^{3R3}-peptide sequences have been synthesized in chapter 4 and will now be evaluated as membrane active peptidomimetics. Specifically, the amphiphilic cationic β^{3R3}-peptide oligomers will be first characterized for their physicochemical properties and studied as antimicrobial peptidomimetics in section 5.2.1. Afterwards, rhodamine B labeled derivatives of these amphiphilic cationic β^{3R3}-peptide sequences will be employed to investigate their cell-penetrating properties and discussed in section 5.2.2. In the last section, enzymatic stability assays for the amphiphilic cationic β^{3R3}-peptide oligomers and rhodamine B conjugates will be presented in section 5.2.3.

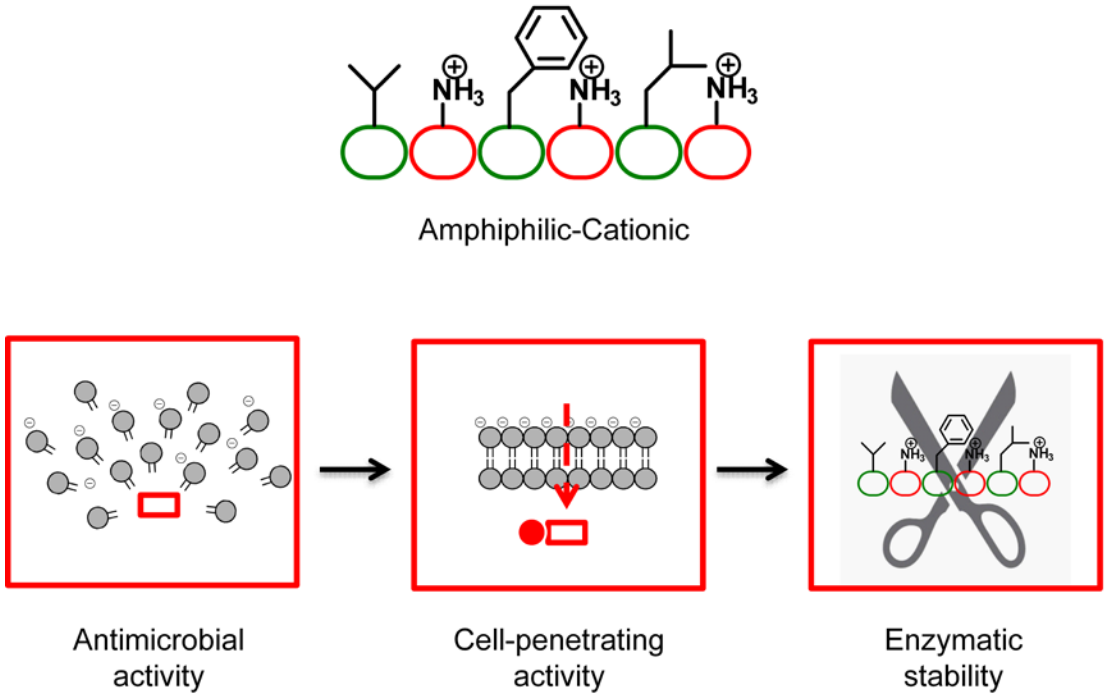

Figure 5.11. *Sequential steps towards the development of amphiphilic cationic β^{3R3}-peptide for biomedical applications.*

5.2.1. Amphiphilic Cationic β^{3R3}-Peptides as Antimicrobial Peptidomimetics

Here, the amphiphilic cationic β^{3R3}-peptides will be investigated for their potential as antimicrobial peptidomimetics. AMPs are amphiphilic cationic MAPs that can kill a broad range of microorganisms by perturbation of the cell membrane architecture. Due to the different mechanisms of action and decreased likelihood of resistance development compared to conventional antibiotics,[60,74] AMPs have been envisaged as a potential source of future antibiotics.[57] In order to overcome the major limitations related to the peptide formula of AMPs, different cationic amphiphilc β-peptides with helical conformation have been proposed as peptidomimetics with high antimicrobial activity. However, classical antimicrobial β-peptides are still affected by limited therapeutic index and indiscriminant cytotoxicity versus microbial targets and eukaryotic host cells.[19,21,22,23]

Therefore, the potential of the amphiphilic cationic β^{3R3}-peptides as a novel class of antimicrobial agents will be investigated. The full control over the building block chemical features and assembling allows us to perform a detailed structure-activity relationship study aiming at disclosing correlations between primary sequence, physicochemical and biological properties of the amphiphilic cationic β^{3R3}-peptides. This SAR study was performed in two steps. The first step consisted of the design and characterization of the physicochemical properties of amphiphilic cationic β^{3R3}-peptide sequences, which will be detailed in section 5.2.1.a. and section 5.2.1.b, respectively. In the second step, the potential of amphiphilic cationic β^{3R3}-peptide oligomers as antimicrobial peptidomimetics were evaluated *in vitro*. For this purpose, the antimicrobial activity against representative Gram + (*Micrococcus luteus*) and Gram – (*Escherichia coli*) bacteria have been tested and will be presented in section 5.2.1.c. Subsequently, their cytotoxicity towards eukaryotic cells will be discussed in section 5.2.1.d. with particular focus dedicated to the hemolytic activity.

5.2.1.a. Design of Amphiphilic Cationic β^{3R3}-Peptides as Membrane Active Peptidomimetics

Physicochemical factors rather than the specific primary sequence essentially determine the membrane activity and selectivity of AMPs.[60] These include sequence length, net charge, hydrophobicity, presence of aromatic side chains, as well as conformation and aggregation properties.[65] Therefore 12 different sequences of amphiphilic cationic β^{3R3}-peptides (**46-56**) were designed and synthesized in chapter 4 (Scheme 5.2). All the oligomers feature C-terminal carboxamide moiety, which generally enhances the activity of both natural and synthetic antimicrobial peptidic agents.[20,22] The goal of this study is to detect proper combinations of physicochemical determinants for the antimicrobial properties of the amphiphilic cationic β^{3R3}-peptides.

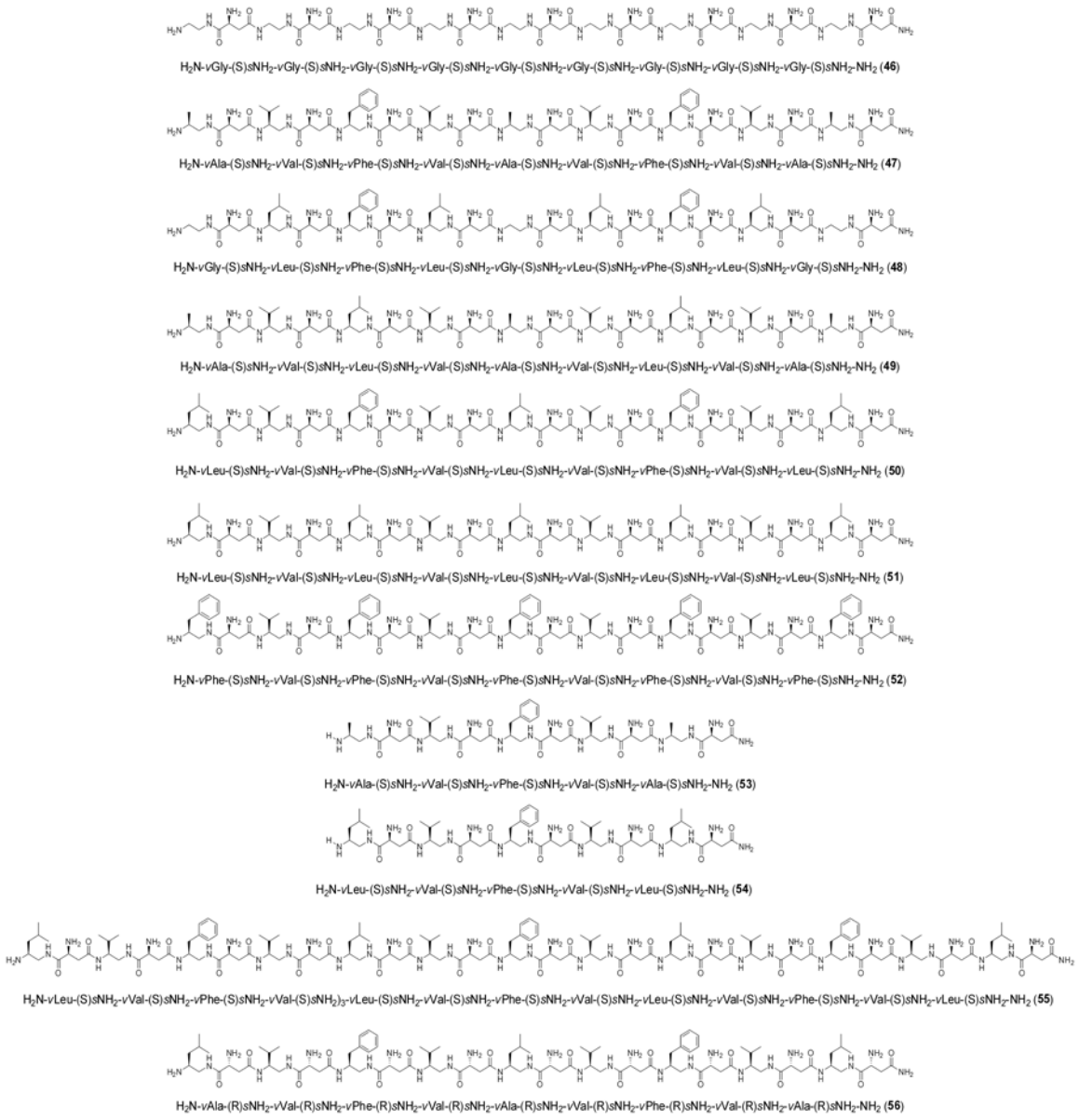

Scheme 5.2. *Amphiphilic cationic β^{3R3}-peptides investigated as antimicrobial peptidomimetics.*

The main chemical differences among the the amphiphilic cationic β^{3R3}-peptides are the chain length, side chain pattern and chiral configuration.

Chain length of 9 (**46-52, 56**), 5 (**53-54**), and 13 (**55**) dimer building blocks and parallel number of net charges were targeted (Scheme 5.2). Similar chain lengths feature many short AMPs with potent antimicrobial activity and most of β-peptides investigated as antimicrobial peptidomimetics.[65,19,20,21,22,23] Within those chain lengths the diamine units *v*Gly, *v*Ala, *v*Val, *v*Leu and *v*Phe were systematically interchanged to produce amphiphilic cationic β^{3R3}-peptide oligomers with variegated combinations of different proteinaceous side chains, aliphatic and aromatic, and

different physicochemical features. This should ultimately allow for tuning the biological properties and antimicrobial activity. Indeed, this set of side chains primarily features a fine scale of hydrophobicity. Hydrophobicity is fundamental for the interaction with membrane and the antimicrobial activity. On the other side, excessive hydrophobicity can lead to aspecific cytotoxicity and increased hemolytic activity.[21,20] Furthermore, the aggregation of hydrophobic side chains in aqueous media may result in reduced antimicrobial activity.[63]

Nevertheless, based on the available data, cationic and amphiphilic character alone cannot explain the selective bactericidal activity and strain selectivity of AMPs. Rather, the preference for a certain membrane or classes of membranes likely depends on specific residue composition. In particular, *v*Phe units can play an important role as aromatic rings can produce π-π interactions with *e.g.* unsaturated fatty acids which differentiate microbial and human cytoplasmic membranes.[64]

Structural factors also influences biological properties of AMPs.[60] The membrane activity of AMPs requires nascent or induced structural motifs producing amphiphilic macromolecular folds with spatial segregation of charges and hydrophobic moieties.[60,65] Specifically, the conformational properties of amphiphilic cationic β^{3R3}-peptides are expect to be hierarchically dictated to a significant extent by the configuration of the chiral center on the *s*NH_2 diacid units. The electrostatic interactions of the amino group in α position can produce a stronger influence on the backbone conformation than e.g. the amino group in ε position of Lys, where the flexible alkyl moiety can relieve the conformational drive of. Thus, both homochiral (*v*S,*s*S) (**46**-**55**) and heterochiral (*v*S,*s*R) (**56**) oligomers were synthesized. In this study a great majority of homochiral (*v*S,*s*S) sequences have been investigated as they imply the natural and less expensive L-Asp as diacid unit (S-*s*NH_2). In case the heterochiral (*v*S,*s*R) oligomer (**56**) will show particular potential, other heterochiral analogues can be eventually accessed using the synthetic platform developed in chapter 3 and chapter 4.

In section 5.1 it has been shown that the β^{3R3}-peptides backbone has an intrinsic propensity for extended conformation. However, homochiral amphiphilic cationic β^{3R3}-peptides cannot segregate cationic and hydrophobic moieties in extended conformation and therefore are forced to fold in order to adopt globally amphiphilic macromolecular fold (Figure 5.12). In contrast, the heterochiral sequence has been designed with globally amphiphilic structure in extended conformation and can therefore accommodate the folding propensity of the β^{3R3}-peptides backbone (Figure 5.12).

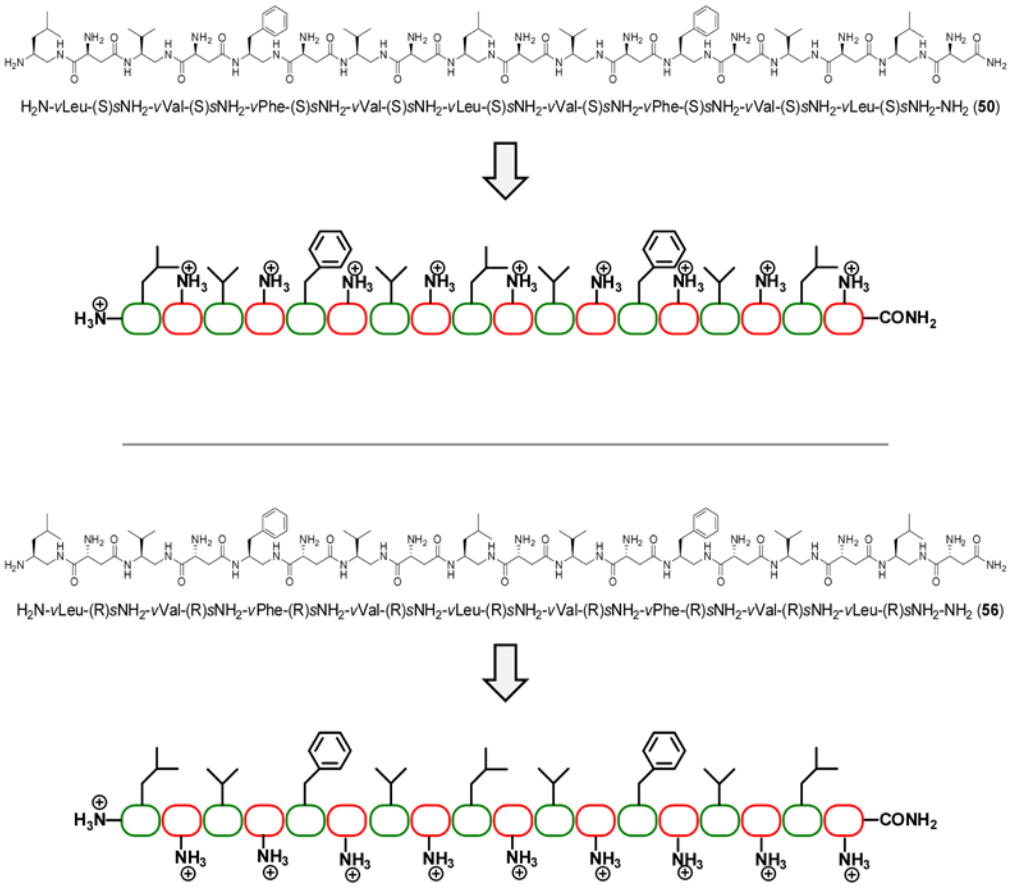

Figure 5.12. *Schematic representation of extended conformations of amphiphilic cationic β[3R3]-peptide oligomers* ***50*** *and* ***56****.*

Thus, in order to evaluate the efficacy of these design rules, in the next section the physicochemical properties of the amphiphilic cationic β[3R3]-peptide oligomers will be investigated by a selected combination of different techniques.

5.2.1.b. Physicochemical Characterization of Amphiphilic Cationic β^{3R3}-Peptides

Optimal efficacy of AMPs lies in the proper coordination of relevant physicochemical parameters. Thus the goal of this SAR study is to identify combinations of physicochemical features that can specifically tune the biological properties of amphiphilic cationic β^{3R3}-peptides as antimicrobial peptidomimetics. A set of amphiphilic cationic β^{3R3}-peptide sequences (**46**-**56**) has been designed and synthesized in chapter 4. As a next step, these oligomers will now be characterized for their physicochemical properties. Specifically RP-HPLC, Dynamic Light Scattering (DLS), and IRRAS have been employed (Table 5.1).

Table 5.1. *Chemical features, hydrophobicity and hydrodynamic diameter of the amphiphilic cationic β^{3R3}-peptide oligomers (**46**-**56**).*

Oligomer	n[a]	*[b]	Ar	H[c]	Ø[e]	π_{eq}[g]	Amid I[h]
46	9	*v*S,*s*S	0	0[d]	//[f]	0.2	1666
47	9	*v*S,*s*S	2	23.24	//	1.1	1667
48	9	*v*S,*s*S	2	26.6	//	3.6	1665
49	9	*v*S,*s*S	0	22.1	//	1.7	1664
50	9	*v*S,*s*S	2	29.9	0,72	6.8	1656
51	9	*v*S,*s*S	0	28.7	0,75	8.6	1663
52	9	*v*S,*s*S	4	29.9	2,52	5.4	1662
53	5	*v*S,*s*S	1	16.7	//	0.2	nn[i]
54	5	*v*S,*s*S	1	23.23	0,76	0.4	nn[i]
55	13	*v*S,*s*S	3	33.95	0,77	11.3	1655
56	9	*v*S,*s*R	2	27.95	0,86	13.3	1646

*[a]n stands for number of building blocks. [b] * refers to the absolute configuration of stereocenters in alternated positions, on the diamine (v) and diacid (s) units, respectively. [c]Hydrophobicity measure determined as percentage acetonitrile eluent in RP-HPLC analysis 5% to 95% MeCN in 60 min, using a C18 column. [d]Oligomer **46** is eluted within the injection peak. [e] Hydrodynamic diameter in nm measured by DLS. [f]The oligomer was not characterized. [g] Equilibrium surface pressure in mN/m obtained by IRRAS measurements. [h] Amide I band position in cm^{-1} observed by IRRAS.[i] The band was too weak to be univocally characterized.*

Hydrophobicity is perhaps the most critical parameters for membrane activity and selectivity of AMPs.[60,59] Therefore, the hydrophobicity of the amphiphilic cationic β^{3R3}-peptides was determined via RP-HPLC as percent of acetonitrile required to elute each oligomer from a C18 analytical column (Table 5.1). This approach has been established to measure the lipophilicity of various molecules,[161] including antimicrobial β-peptides.[22] In general, within the homochiral sequences **46**-**56** the relative values achieved can be linearly correlation to the hydrophobicity of the proteinaceous side chains on the diamine residues *v*Xaa that distinguish the oligomers. Remarkably, the RP-HPLC analysis showed higher hydrophobicity for the homochiral (*v*S,*s*S) oligomer **50** than the heterochiral (*v*S,*s*R) analogue **56**. Longer retention time generally correlates with a greater propensity to adopt a globally amphiphilic conformation, as observed for α- as well as β-peptides.[22,162]

Furthermore, since hydrophobic aggregation in aqueous media may result in decreased antimicrobial activity,[63] DLS was employed to determine the size distribution profile of the oligomer in solution (Table 5.1). Oligomers **50**, **51**, **52**, **54**, **55**, and **56** were analyzed. Here, oligomer **50** was taken as reference sequence with proper hydrophobicity and variegated pattern of side chains. In comparison, oligomers **54** and **55** present the same side chain pattern and different chain length. Differently, oligomer **51** features the same chain length but different side chains. Lastly, oligomer **56** (*v*S,*s*R) differs from oligomer **50** (*v*S,*s*S) by the chiral configuration of the diacid *s*NH_2 units. All these parameters are expected to influence the aggregation behavior of the amphiphilic cationic β^{3R3}-peptides. Regardless the chain length and side chains, the oligomers **50**, **51**, **54**, and **55** produce similar profile with average hydrodynamic diameter around 0.7-0.8 nm. Moreover, the heterochiral (*v*S,*s*R) oligomer **56** displays a slightly increased diameter of around 0,86. Although this could hint at different structural characteristics, the entity of the difference between the values is too limited for DLS analysis to be considered as a strong indication. In contrast, oligomer **52** displays a significantly increased hydrodynamic diameter of around 2.5 nm which can be attributed to the formation of aggregates. Such aggregation in aqueous media could derive from the sequence density of aromatic *v*Phe side chains which can generate both hydrophobic and π-π interactions.

In addition, IRRAS was employed to evaluate quantitative and qualitative physicochemical determinants of the amphiphilic cationic β^{3R3}-peptides at the air/water interface (Table 5.1). Indeed, the air/water interface can mimic the aqueous layer of a few nanometer thicknesses that exists at the interface of the cell membrane and allows establishing relationships between physicochemical properties in such environment.[41,42,117-127] The experiments were performed by Janos Keller from the group of Prof. Gerald Brezesinski, an expert in the field of structural investigations at the air/water interface.

First, the equilibrium surface pressure was measured as an alternative mean to estimate the hydrophobicity of the oligomers **46**-**56** (Table 5.1). A general trend parallel to the values of hydrophobicity obtained by RP-HPLC is observed. However, a stronger influence of the chain length and number of charges is observed compared to the hydrophobicity values achieved by RP-HPLC. In particular, the short oligomers **53** and **54** are not surface active. In addition, oligomer **52** shows a relatively reduced equilibrium surface pressure. This could correlate with the tendency of oligomer **52** to form aggregates, as seen in DLS experiments, which cannot extensively align and enlarge the pressure at the surface. In contrast, the heterochiral (*v*S,*s*R) oligomer **56** displays an extraordinary high equilibrium surface pressure. This could be explained with the potential to adopt globally amphiphilic structure with segregation of charges and hydrophobic moieties in extended conformation. Therefore oligomer **56** could form strands which can assemble through the formation of hydrogen-bonded sheets at the air/water interface and more uniformly absorb at the surface.

To further confirm this and provide qualitative structural information, the position of the amide I band in the IRRA spectra was analyzed (Table 5.1). All the homochiral (*v*S,*s*S) oligomers **46**-**55** present amide I at around 1660 cm^{-1} which is characteristic for conformations supported by intramolecular hydrogen bond network, such as helix. In contrast, the heterochiral (*v*S,*s*R) oligomer **56** displays the amide I at around 1645 cm^{-1}, typical for intermolecular hydrogen bond networks at the air/water interface.[120,124,126,129,130] Indeed, analogue values have been observed in section 5.1 for oligomers **41** and **44** which form strands that self-assemble in amorphous β-sheet-like structures.

In addition, IRRAS studies were performed with lipid monolayers at the air/water interface to quantify the interactions with model membranes and investigate the influence of diverse phospholipids on the ability of the amphiphilic cationic β^{3R3}-peptides to penetrate into lipidic media.[163] Oligomers **50**, **55**, and **56** were investigated. Besides measuring the surface activity of these oligomers (Table 5.1), this combination allows to univocally correlate the nature of the lipid–peptide interaction with essential physicochemical determinants of the amphiphilic cationic β^{3R3}-peptides. Specifically, oligomer **50** and **55** present different repeats of the same side chain pattern (Scheme 5.2), and therefore their comparison will reveal the effect of different chain length on the membrane activity of the amphiphilic cationic β^{3R3}-peptides. In contrast, based on the amide I position in the IRRA spectra, conformational properties mainly differentiate the heterochiral (*v*S,*s*R) oligomer **56** from the homochiral (*v*S,*s*S) analogue **50** and therefore the relevance of this on their membrane activity properties will be evaluated. As model membranes, the anionic 1-palmitoyl-2-oleoyl-*sn*-glycero-3-phospho-(1'-*rac*-glycerol) (POPG) and the zwitterionic 1-palmitoyl-2-oleoyl-*sn*-glycero-3-phosphocholine (POPC) lipids were employed to mimic prokaryotic and eukaryotic membranes,

respectively. Both lipids have one unsaturated acyl chain and thus form fluid monolayers in liquid disordered phase even in high surface pressures. Two sets of experiments were performed with different amount of lipid and different surface pressure. The experiments were carried out using a 10mM PBS at pH 7.4 with 150mM NaCl as aqueous subphase. In the first set of experiments 25µL of a 1mM lipid solution in $CHCl_3$ was spread on the air-buffer interface and compressed to form a monolayer of 30mN/m surface pressure, which is analogue to the surface pressure observed in biological membranes.[164] Thereafter the surface pressure was kept constant and changes in the lipid area monitored. In the second set of experiments 13µL of the lipid solutions were spread and compressed to the same area as in the first case obtaining a monolayer at 0mN/m. Here the area was kept constant and changes in the surface pressure monitored. After the measurement of the pure lipid film, 250-350µL of the amphiphilic cationic β^{3R3}-peptide oligomer dissolved in the same PBS were injected under the film to obtain a concentration of 500nM in the subphase and the new values registered at the equilibrium (Table 5.2).

Table 5.2. *IRRAS experiments with model membranes.*

		50	**55**	**56**
Oligomer[a]	π_{eq} [c]	6.8	11.3	13.3
POPC $\pi_{inj}0$[b]	$\Delta\pi$ [d]	7.9	13.9	12.5
POPG $\pi_{inj}0$	$\Delta\pi$	11.4	16.6	14.0
POPC $\pi_{inj}30$	A_{inj} [e]	86	85.5	80.9
	A_{eq} [f]	87.6	84.5	80.3
POPG $\pi_{inj}30$	A_{inj}	92.7	100.2	95.5
	A_{eq}	104.5	120.5	109.3

[a]*injected under the film to obtain a concentration of 500nM in the subphase* [b]π_{inj} *stands for initial surface pressure in (mN/m) of the lipid monolayer before the peptide injection.* [c]π_{eq} *stands for surface pressure in (mN/m) of the equilibrated mixed oligomer-lipid monolayer.* [d]$\Delta\pi$ *is the surface pressure change.* [e]A_{inj} *stands for initial surface area in* (cm^{-2}) *of the lipid monolayer before the peptide injection.* [f]A_{eq} *stands for surface area in* (cm^{-2}) *of the equilibrated mixed oligomer-lipid monolayer.*

In general, the equilibrium surface pressure after the injection of the oligomers below the zwitterionic eukaryotic-like POPC monolayer of 0mN/m is almost equal to the equilibrium surface pressure of the

oligomers alone. Moreover, the area of the compressed POPC monolayer at 30mN/m stays almost constant after the injection of the oligomers, which means that no insertion of the amphiphilic cationic β^{3R3}-peptide occurs. Differently, in the case of a POPG monolayer of 0mN/m, the equilibrium surface pressure observed after injection of the oligomers is significantly bigger than the value previously registered with the pure oligomers. Additionally, the amphiphilic cationic β^{3R3}-peptides also insert into the lipid monolayer at surface pressure of 30mN/m and the area of the equilibrated mixed peptide-lipid monolayer is increased. Specifically, oligomer **55** determines the larger effect with 20.3% of area increase.

Based on these results, the amphiphilic cationic β^{3R3}-peptides and especially oligomer **55** produces strong interaction and modify the lipid organization of the bacteria mimicking membrane. In contrast, no interaction was observed with human-like membrane. Therefore, the amphiphilic cationic β^{3R3}-peptides can potentially display high and selective antibacterial activity without cytotoxicity versus eukaryotic host cells.

Interestingly, an exclusive shift towards higher wavelength is observed in the amide I band of the heterochiral (*v*S,*s*R) oligomer **56** in presence of the bacterial mimicking membrane POPG (Figure 5.13).

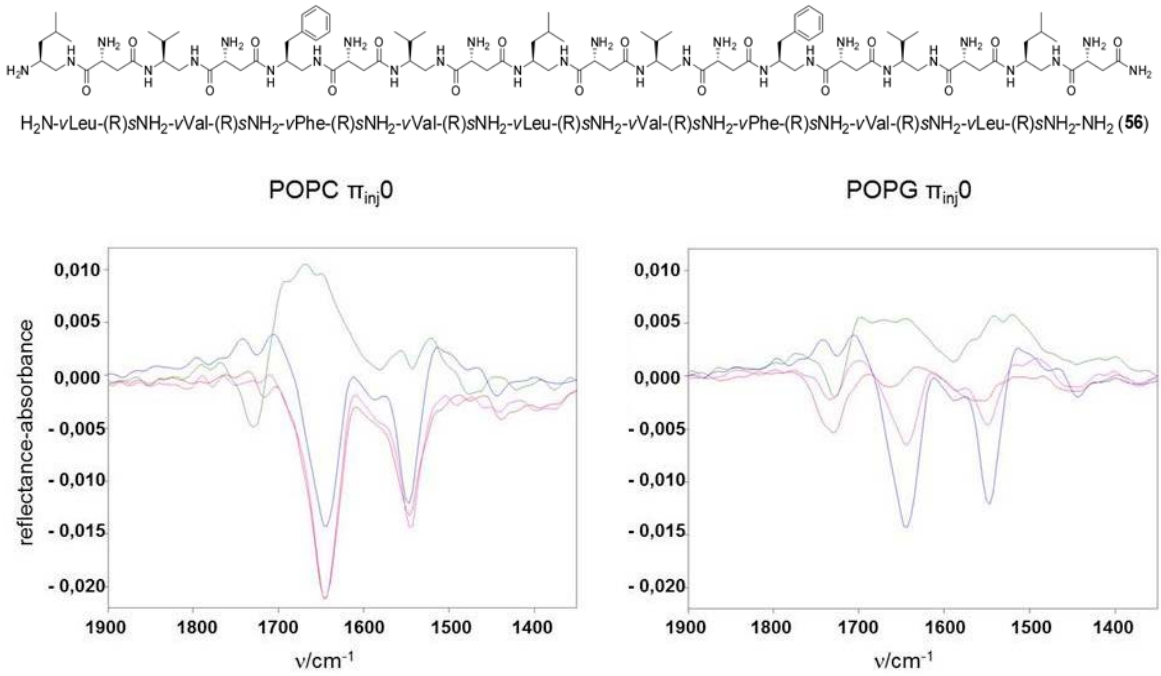

Figure 5.13. *IRRA spectra of the interaction of oligomer* ***56*** *with the zwitterionic monolayer POPC (left) and the anionic monolayer POPG (right) at 0mN/m initial surface pressure. Different spectra were registered with the pure oligomer (blue), the pure membrane (green line), and after the injection at short time (~1h) (pink line), and long time (~5,5h) (red line).*

Thus, similarly to several natural AMPs, lipid–peptide interactions can drive the conformational state(s) of the heterochiral amphiphilic cationic β^{3R3}-peptide.[60] As seen from the amide I band position (Table 5.1), oligomer **56** alone at the air/water interface forms strands that self-assemble in amorphous β-sheet-like structures supported by intermolecular hydrogen bond network. Indeed, water molecules play an important role in the stabilization of amorphous sheet layers rather than in more ordered crystalline sheet structures. In presence of membranes and along with closer proximity to lipid layers, such solvent contribution decays and therefore a conformational change is required to allow for the formation of intramolecular hydrogen bond networks with increased stability. Nevertheless, also for natural AMPs the globally amphiphilic macromolecular folds required for the antibacterial activity can derive from structural motifs that are either nascent or induced via peptide-membrane interaction.[60] Therefore, the specific outcome of these particular structural properties cannot be predicted and will be addressed in the next section.

5.2.1.c. Antibacterial Activity of Membrane Active β^{3R3}-Peptides

The goal of this study is to attain a SAR evaluation of amphiphilic cationic β^{3R3}-peptides to detect proper combinations of physicochemical properties promoting the antimicrobial activity and selectivity. In the previous section the physicochemical determinants of the designed oligomers **46**-**56** have been determined. The next step requires the *in vitro* evaluation of the properties of amphiphilic cationic β^{3R3}-peptides as antimicrobial peptidomimetics. Therefore antibacterial growth assays have been performed. The experiments were carried out by Dr. Nahid Azzouz, an expert in molecular biophysics of biomolecules implied in pathogen-host recognition processes. The Minimal Inhibitory Concentration (MIC) values were determined against *E. coli* (strain BL21) and *Micrococcus luteus* (type strain DSM 20030) as representative strains of Gram-negative and Gram-positive bacteria, respectively. Gratifyingly, specific sequences with an appropriate length and number of charges, hydrophobicity, aromatic residues and stereochemical configuration display high antimicrobial activity (Table 5.3).

Table 5.3. *MIC values of the amphiphilic cationic β^{3R3}-peptide oligomers (**46-56**).*

Oligomer	*M.luteus*	*E. coli*
46	No activity	No activity
47	> 20 µg/mL	No activity
48	No activity	> 120 µg/mL
49	No activity	~ 80 µg/mL
50	~ 14 µg/mL	~ 90 µg/mL
51	~18 µg/mL	~60 µg/mL
52	> 20 µg/mL	~ 100 µg/mL
53	No activity	No activity
54	No activity	No activity
55	~ 6 µg/mL	~ 60 µg/mL
56	> 20 µg/mL	> 120 µg/mL

In general, the amphiphilic cationic β^{3R3}-peptides shows higher activity against the Gram + bacterial. Within sequences with chain length of 9 repeating units (**46-52, 56**), hydrophobicity resulted indeed a critical parameter. The most hydrophobic are oligomer **50, 51** and **52** (Table 5.1). Indeed, **50** is the most active antibacterial oligomer with a MIC of ~14 μg/mL against *M. luteus*. In contrast, the oligomer **51** and **52** feature a reduced activity with MIC against *M. luteus* of ~18 μg/mL and > 20 μg/mL, respectively. Here, a correlation between the number of aromatic side chains and the antimicrobial activity can be deduced. The higher MIC value of oligomer **52** could derive from the aggregation in aqueous media related to the higher density of aromatic side chains and observed in DLS experiments (Table 5.1). Indeed, self-assembly in aqueous media may result in decreased antimicrobial activity.[63] Differently, oligomer **51** is slightly less hydrophobic and less active against *M. luteus* (Table 5.1 and Table 5.3). However, oligomer **51** has no aromatic side chains and shows the highest activity against the Gram - *E. coli* (Table 5.3). Thus, the aromatic *v*Phe units can play an important role driving the membrane selectivity of amphiphilic cationic β^{3R3}-peptides. Lastly, the chiral configuration of the *s*NH_2 diacid units can hierarchically influence the antimicrobial activity of amphiphilic cationic β^{3R3}-peptides, by driving the conformation (Section 5.2.1.b) and modulating the hydrophobicity (Table 5.1) of the sequences. Indeed, the heterochiral (*v*S,*s*R) oligomer **56** is less active than the homochiral (*v*S,*s*S) analogue **50** against both *M. luteus* and *E. coli* (Table 5.3).

In addition, the chain length and number of charges of amphiphilic cationic β^{3R3}-peptides extensively influence their antimicrobial activity which increases along with the number of repeating units (Table 5.1 and Table 5.3). Indeed, oligomers **50**, **54**, and **55** feature same side chain pattern and exclusively differ by the number of repeats (Scheme 5.2). Here, while the shortest oligomer **54** is not active, the longest oligomer **55** is the most active amphiphilic cationic β^{3R3}-peptide against both *M. luteus* and *E. coli*, with MIC of ~ 6 μg/mL (2.1μM) and ~ 60 μg/mL (21μM), respectively. Such values are comparable to the MIC of biologically important natural AMPs, such mammalian defensins[165] and the most active antimicrobial classical β-peptides.[166]

Thus, after it has been shown that amphiphilic cationic β^{3R3}-peptides can display potent antimicrobial activity, in the next section the cytotoxicity against human cells will be tested. Indeed, although classical β-peptides can also display high antimicrobial activity their biomedical application is often limited by their low therapeutic index, which is defined as the ratio between the amount of a therapeutic agent that causes the therapeutic effect to the amount that causes death (in animal studies) or toxicity (in human studies).

5.2.1.d. Cytotoxicity of Antibacterial Amphiphilic Cationic β^{3R3}-Peptides

Cell viability experiments have shown that amphiphilic cationic β^{3R3}-peptide sequences with appropriate combination of physicochemical properties display MIC values comparable to biologically important natural AMPs and the most active antimicrobial β-peptides. Nevertheless, both the natural AMPs and β-peptides with high antimicrobial activity can display indiscriminant cytotoxicity and high hemolytic activity,[19,57,167,21,22,23] which substantially hampers the development of these systems as therapeutics. Therefore, the hemolytic activity of the amphiphilic cationic β^{3R3}-peptide sequences has been evaluated. The experiments were carried out by Dr. Nahid Azzouz.

All the amphiphilic cationic β^{3R3}-peptide oligomers show no hemolytic activity at a concentration of 80μM, which is in the order of magnitude of the MIC values. In addition, the hemolytic activity of selected oligomers was tested in the range of concentrations between 0 to 2000 μM. The oligomers **50**, **51** and **55** were chosen as they display the highest antimicrobial activity. Furthermore, the hemolytic activity of the heterochiral (*v*S,*s*R) oligomer **56** was investigated as it presents peculiar conformational properties (Section 5.2.1.b) and this could potentially influence the hemolytic activity of antimicrobial peptidomimetics.[22] In general, all oligomers **50**, **51**, **55** and **56** show negligible hemolytic activity. For all compounds the concentration required for the lysis of 50% of the red blood cells (HD50) is higher than 1500 μM. This is significantly better than the best reported HD50 value (HD50 = 920 μM) for β-peptides with antimicrobial activity so far.[20]

Conclusively, the homochiral sequences (*v*S,*s*S) are superior as antimicrobial peptidomimetics displaying higher antibacterial activity while keeping irrelevant cytotoxicity, as observed with the analogues **50** (*v*S,*s*S) and **56** (*v*S,*s*R). In particular, oligomer **55** is the best candidate for further research and development as antimicrobial agent due to its high antimicrobial activity and therapeutic index (Figure 5.14).

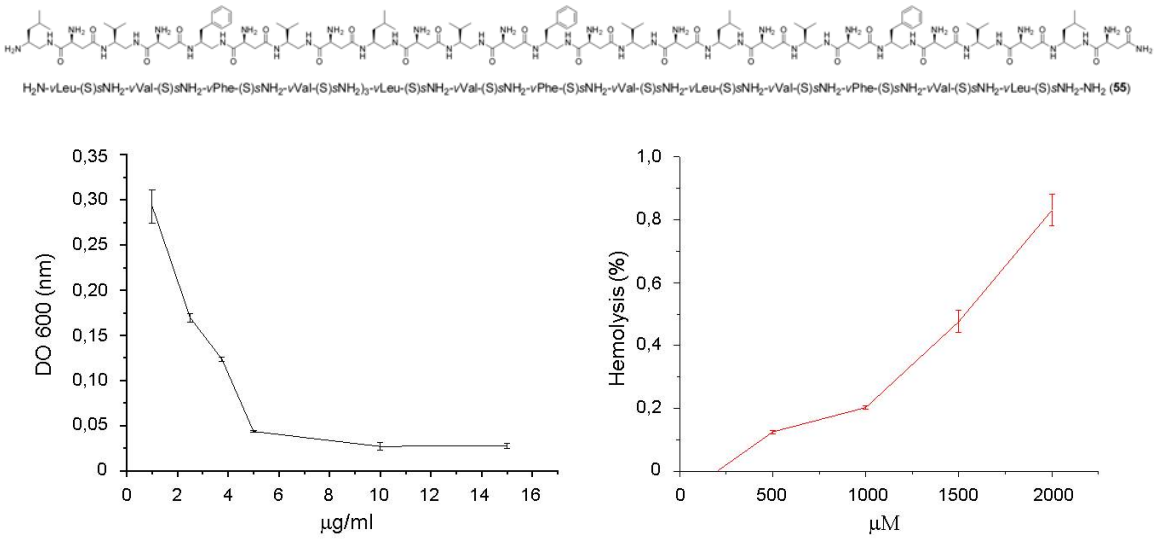

Figure 5.14. *MIC values versus M.luteus (~ 6µg/mL= 2.1µM) (left) and hemolytic activity (HD50 >1500 µM) (right) of the amphiphilic cationic β^{3R3}-peptide oligomer* ***55***

5.2.1. Cell-Penetrating Properties of Membrane Active Amphiphilic Cationic β^{3R3}-Peptides

In the previous sections, amphiphilic cationic β^{3R3}-peptides were shown to be membrane active compounds with high potential as antimicrobial peptidomimetics. In the following chapter these sequences of amphiphilic cationic β^{3R3}-peptides will be investigated for their cell-penetrating properties. CPPs represent a promising tool for intracellular delivery of biomedical active cargos.[75] Although AMPs and CPPs become functionally discriminated on the basis of the traditional nomenclature, comparative studies can emphasize the multifunctional aspects of membrane-active peptides. Indeed, many AMPs and CPPs show overlapping structural features and biological activities, i.e., certain AMPs can penetrate membranes, and some CPPs are good antibiotics.[51,52] Thus, the functional relationships between antimicrobial activity and cell-penetrating properties of amphiphilic cationic β^{3R3}-peptides are not so obvious and need to be explored.

In addition, the elucidation of cellular uptake mechanism is an essential step in the development of efficient cell-penetrating agents.[75] Most CPPs described so far have been designed to be covalently conjugated to the cargo.[76] Therefore, fluorescence-labeled derivatives of the amphiphilic cationic β^{3R3}-peptide sequences have been synthesized in chapter 4 and a SAR study will be now presented to their cell-penetrating properties. In particular, the physicochemical properties of the rhodamine labeled oligomers will be detailed in section 5.2.2.a. Then, fluorescence-activated cell sorting (FACS) experiments and inhibition assays to elucidate the cellular-uptake mechanism will be discussed in section 5.2.2.b.

5.2.2.a. Physicochemical Characterization of Rhodamine B Conjugates of Amphiphilic Cationic β^{3R3}-Peptides

The SAR study presented in section 5.2.1 has proven that amphiphilic cationic β^{3R3}-peptide sequences with appropriate combination of proteinaceous side chains and physicochemical properties have high membrane activity and great potential as antimicrobial peptidomimetics. Here, the amphiphilic cationic β^{3R3}-peptides will be evaluated for their potential cell-penetrating properties. For this purpose, rhodamine B has been selected as drug-like molecule to mimic biological active cargo and intrinsically allow for fluorescence-based investigation. Indeed, most CPPs described so far have been designed to be covalently conjugated to drugs for which the solubility and the efficient passage through cellular membranes remains a major hurdle.[76] Nevertheless, the conjugation of CPPs necessarily implies the alteration of physicochemical features that essentially determine the ability to interact with cell membrane and thereby the cellular uptake pathway of MAPs. Thus the evaluation of the amphiphilic cationic β^{3R3}-peptides as cell-penetrating agents to be covalently linked to bioactive cargo cannot just rely on the data achieved with the not conjugated analogues (Section 5.2.1). Therefore, all the β^{3R3}-peptide sequences investigated as antimicrobial peptidomimetics (Scheme 5.2) were conjugated with rhodamine B (Scheme 5.3) and their physicochemical properties have been characterized.

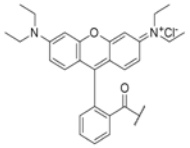

Rhodamine B (RhB)

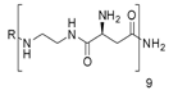

RhB-HN-(*v*Gly-(S)*s*NH$_2$)$_9$-NH$_2$ (**57**)

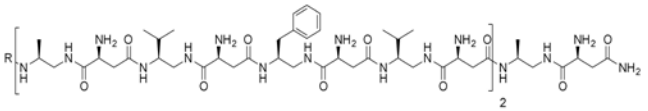

RhB-HN-(*v*Ala-(S)*s*NH$_2$-*v*Val-(S)*s*NH$_2$-*v*Phe-(S)*s*NH$_2$-*v*Val-(S)*s*NH$_2$)$_2$-*v*Ala-(S)*s*NH$_2$-NH$_2$ (**58**)

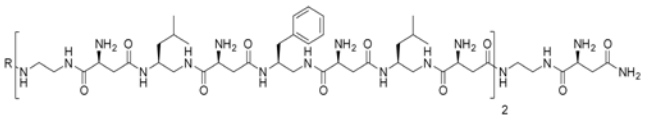

RhB-HN-(*v*Gly-(S)*s*NH$_2$-*v*Leu-(S)*s*NH$_2$-*v*Phe-(S)*s*NH$_2$-*v*Leu-(S)*s*NH$_2$)$_2$-*v*Gly-(S)*s*NH$_2$-NH$_2$ (**59**)

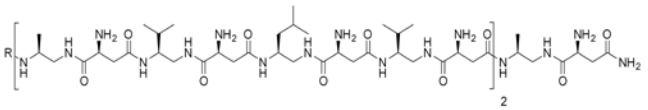

RhB-HN-(*v*Ala-(S)*s*NH$_2$-*v*Val-(S)*s*NH$_2$-*v*Leu-(S)*s*NH$_2$-*v*Val-(S)*s*NH$_2$)$_2$-*v*Ala-(S)*s*NH$_2$-NH$_2$ (**60**)

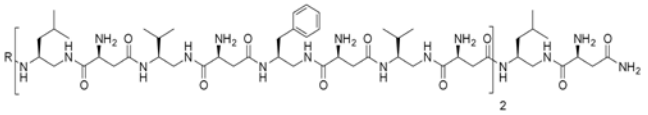

RhB-HN-(*v*Leu-(S)*s*NH$_2$-*v*Val-(S)*s*NH$_2$-*v*Phe-(S)*s*NH$_2$-*v*Val-(S)*s*NH$_2$)$_2$-*v*Leu-(S)*s*NH$_2$-NH$_2$ (**61**)

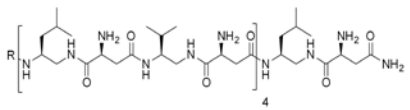

RhB-HN-(*v*Leu-(S)*s*NH$_2$-*v*Val-(S)*s*NH$_2$)$_4$-*v*Leu-(S)*s*NH$_2$-NH$_2$ (**62**)

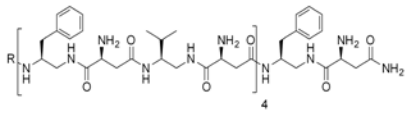

RhB-HN-(*v*Phe-(S)*s*NH$_2$-*v*Val-(S)*s*NH$_2$)$_4$-*v*Phe-(S)*s*NH$_2$-NH$_2$ (**63**)

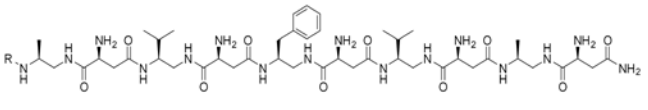

RhB-HN-*v*Ala-(S)*s*NH$_2$-*v*Val-(S)*s*NH$_2$-*v*Phe-(S)*s*NH$_2$-*v*Val-(S)*s*NH$_2$-*v*Ala-(S)*s*NH$_2$-NH$_2$ (**64**)

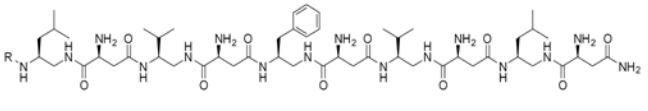

RhB-HN-(*v*Leu-(S)*s*NH$_2$-*v*Val-(S)*s*NH$_2$-*v*Phe-(S)*s*NH$_2$-*v*Val-(S)*s*NH$_2$)$_2$-*v*Leu-(S)*s*NH$_2$-NH$_2$ (**65**)

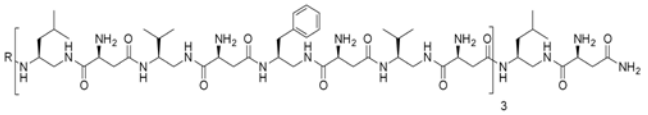

RhB-HN-(*v*Leu-(S)*s*NH$_2$-*v*Val-(S)*s*NH$_2$-*v*Phe-(S)*s*NH$_2$-*v*Val-(S)*s*NH$_2$)$_3$-*v*Leu-(S)*s*NH$_2$-NH$_2$ (**66**)

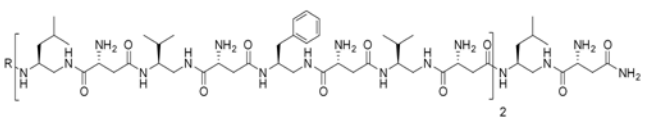

RhB-HN-(*v*Leu-(R)*s*NH$_2$-*v*Val-(R)*s*NH$_2$-*v*Phe-(R)*s*NH$_2$-*v*Val-(R)*s*NH$_2$)$_2$-*v*Leu-(R)*s*NH$_2$-NH$_2$ (**67**)

Scheme 5.3. *Synthesized rhodamine B labeled amphiphilic cationic β^{3R3}-peptides oligomers*

Specifically, RP-HPLC was employed as mean to quantify the hydrophobicity also for the conjugated oligomer **57**-**67** (table 5.4). Indeed, the covalent conjugation with hydrophobic fluorescent labels, such as rhodamine B, is expected to primarily alter the sequence hydrophobicity, which is definitely a critical parameter for membrane activity and selectivity of the amphiphilic cationic β^{3R3}-peptides (Section 5.2.1).

Table 5.4. *Comparison of hydrophobicity of the amphiphilic cationic β^{3R3}-peptide oligomers* ***46***-***56*** *and the rhodamine B conjugates* ***57***-***67****.*

Oligomer	n[a]	*[b]	Ar	H[c]	Ø[e]	Conjugate	H[c]
46	9	*v*S,*s*S	0	0[d]	//[f]	**57**	24.8
47	9	*v*S,*s*S	2	23.24	//	**58**	35.75
48	9	*v*S,*s*S	2	26.6	//	**59**	36.8
49	9	*v*S,*s*S	0	22.1	//	**60**	34.4
50	9	*v*S,*s*S	2	29.9	0,72	**61**	40.01
51	9	*v*S,*s*S	0	28.7	0,75	**62**	39.05
52	9	*v*S,*s*S	4	29.9	2,52	**63**	40.07
53	5	*v*S,*s*S	1	16.7	//	**64**	36.35
54	5	*v*S,*s*S	1	23.23	0,76	**65**	38.9
55	13	*v*S,*s*S	3	33.95	0,77	**66**	40.0
56	9	*v*S,*s*R	2	27.95	0,86	**67**	39.5

*[a]n stands for number of building blocks. [b] * refers to the absolute configuration of stereocenters in alternated positions, on the diamine (v) and diacid (s) units, respectively. [c]Hydrophobicity measure determined as percentage acetonitrile eluent in RP-HPLC analysis 5% to 95% MeCN in 60 min, using a C18 column. [d]Oligomer* ***46*** *is eluted within the injection peak. [e] Hydrodynamic diameter in nm measured by DLS. [f]The oligomer was not characterized.*

Indeed, a relevant increment of the hydrophobicity of the oligomers is observed after conjugation with rhodamine B. More interestingly, such hydrophobicity increase becomes less significant along with increasing hydrophobicity of the unlabeled amphiphilic cationic β^{3R3}-peptide precursors **46**-**56**. This was actually expected for sequences with different length, as the weight of the hydrophobic rhodamine B fraction decreases along with increasing length of the amphiphilic cationic sequences. Thus, also the rhodamine B conjugates of short and not membrane active oligomers **53** and **54** (Section 5.2.1) were prepared as they could display interesting activity as cell-penetrating peptidomimetics. In addition, the relative values observed for analogue oligomers with different

chiral configuration are consistent pre and after conjugation, with the homochiral oligomers (*v*S,*s*S) **50** and **55** being more hydrophobic than the heterochiral (*v*S,*s*R) **56** and **57**, respectively. In parallel, hydrophobicity increases after conjugation are observed for the analogue oligomers with different chirality, the homochiral (*v*S,*s*S) **50** and the heterochiral (*v*S,*s*R) **56**. Therefore, the covalent conjugation with hydrophobic cargos should not significantly influence the conformation of amphiphilic cationic β^{3R3}-peptides.

Overall, the conjugation with the fluorescent label rhodamine B as drug-like molecule significantly alters essential physicochemical features such as the hydrophobicity of amphiphilic cationic β^{3R3}-peptides. In the next section potential of these oligomers as cell-penetrating peptidomimetics will be evaluated i*n vitro* using a designed combination of eukaryotic cells and fluorescence-based techniques.

5.2.2.b. Cellular-Uptake Properties of Rhodamine B Labeled Amphiphilic Cationic β^{3R3}-Peptides

The goal of this study is to evaluate the cell-penetrating properties of hydrophobic conjugates of the amphiphilic cationic β^{3R3}-peptides. In the previous section the hydrophobicity has been quantified as an important physicochemical determinant of cellular interactions of cell-penetrating agents.

The next step towards the development of amphiphilic cationic β^{3R3}-peptides as cell-penetrating peptidomimetics requires *in vitro* investigation of their ability to penetrate cellular membranes and cellular uptake mechanism. Indeed, the elucidation of cellular uptake mechanism could improve the delivery efficacy of the amphiphilic cationic β^{3R3}-peptides and is an essential step in the development of cell-penetrating agents for biomedical applications.[75,168]

In general endocytosis is the dominant uptake pathway for CPP conjugates, although direct penetration of the plasma membrane could also occur.[100,169] The endocytic pathways are protein-mediated cell-uptake pathways and can be grouped in two major categories: clathrin-mediated endocytosis and clathrin-independent pathways, such as caveolin-dependent endocytosis and macropinocytosis.[88,89,91] Therefore, the cell-penetrating qualities of the rhodamine conjugates of amphiphilic cationic β^{3R3}-peptides were investigated on three different cell lines: HeLa cells, clathrin-dominant A10 cells, and MDCKII cells characterized by caveolae dominance. [76,84,88,90] This combination can allow for the elucidation of uptake mechanism and specific endocytic pathways involved. For this purpose, FACS experiments and fluorescence microscopy were employed. The experiments were carried out by Dr. Felicitas Lewrick, an expert on cell targeting and delivery agents at the Universität Freiburg.

First, FACS was employed to quantify the interaction of the oligomers with the three cell lines (Figure 5.15).

RhB-HN-(*v*Gly-(S)*s*NH_2)$_9$-NH_2 (**57**)

RhB-HN-(*v*Ala-(S)*s*NH_2-*v*Val-(S)*s*NH_2-*v*Phe-(S)*s*NH_2-*v*Val-(S)*s*NH_2)$_2$-*v*Ala-(S)*s*NH_2-NH_2 (**58**)

RhB-HN-(*v*Gly-(S)*s*NH_2-*v*Leu-(S)*s*NH_2-*v*Phe-(S)*s*NH_2-*v*Leu-(S)*s*NH_2)$_2$-*v*Gly-(S)*s*NH_2-NH_2 (**59**)

RhB-HN-(*v*Ala-(S)*s*NH_2-*v*Val-(S)*s*NH_2-*v*Leu-(S)*s*NH_2-*v*Val-(S)*s*NH_2)$_2$-*v*Ala-(S)*s*NH_2-NH_2 (**60**)

RhB-HN-(*v*Leu-(S)*s*NH_2-*v*Val-(S)*s*NH_2-*v*Phe-(S)*s*NH_2-*v*Val-(S)*s*NH_2)$_2$-*v*Leu-(S)*s*NH_2-NH_2 (**61**)

RhB-HN-(*v*Leu-(S)*s*NH_2-*v*Val-(S)*s*NH_2)$_4$-*v*Leu-(S)*s*NH_2-NH_2 (**62**)

RhB-HN-(*v*Phe-(S)*s*NH_2-*v*Val-(S)*s*NH_2)$_4$-*v*Phe-(S)*s*NH_2-NH_2 (**63**)

RhB-HN-(*v*Leu-(S)*s*NH_2-*v*Val-(S)*s*NH_2-*v*Phe-(S)*s*NH_2-*v*Val-(S)*s*NH_2)$_2$-*v*Leu-(S)*s*NH_2-NH_2 (**64**)

RhB-HN-(*v*Leu-(S)*s*NH_2-*v*Val-(S)*s*NH_2-*v*Phe-(S)*s*NH_2-*v*Val-(S)*s*NH_2)$_2$-*v*Leu-(S)*s*NH_2-NH_2 (**65**)

RhB-HN-(*v*Leu-(S)*s*NH_2-*v*Val-(S)*s*NH_2-*v*Phe-(S)*s*NH_2-*v*Val-(S)*s*NH_2)$_3$-*v*Leu-(S)*s*NH_2-NH_2 (**66**)

RhB-HN-(*v*Leu-(R)*s*NH_2-*v*Val-(R)*s*NH_2-*v*Phe-(R)*s*NH_2-*v*Val-(R)*s*NH_2)$_2$-*v*Leu-(R)*s*NH_2-NH_2 (**67**)

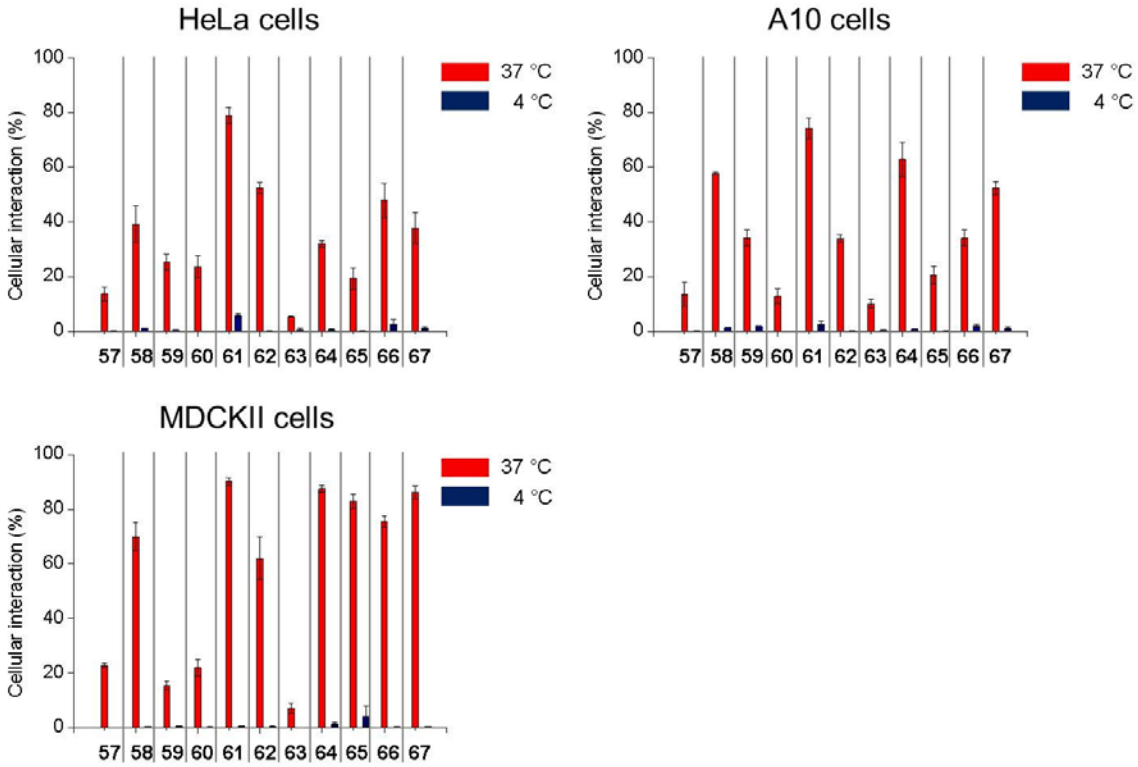

Figure 5.15. *Cellular interaction of rhodamine B conjugates of amphiphilic cationic β^{3R3}-peptides.*

Flow cytometry analysis revealed high cellular association in all three cell lines for several rhodamine B conjugates. In general, lack of cellular association at 4 °C is observed. Remarkably, despite their high membrane activity, the amphiphilic cationic β^{3R3}-peptide conjugates do not show any direct membrane translocation, as shown by the lack of binding or internalization in FACS experiments at 4°C (Figure 5.15). In contrast, most of CPPs undergo cellular internalization at 4 °C and in the presence of specific inhibitors of some endocytotic pathways. Indeed, this lack of specificity toward targets is a major weakness still encountered for the application of CPPs in the biomedical field.[80]

Gratifying, different oligomers show different cellular uptake in dependence of their primary sequence as well as overall length. Thus, the ability to interact with cell membrane is driven by physicochemical features of the amphiphilic cationic β^{3R3}-peptide sequence rather than the hydrophobic cargo.

Within sequences with chain length of 9 repeating units and homochiral (*v*S,*s*S) configuration (**57**-**63**), oligomer **61** displayed the highest interaction whereas oligomers **57** and especially **63** showed minor interaction. The low interaction of oligomers **57** and **63** is consistent with the low membrane activity of the not conjugated analogues **46** and **52** (Section 5.2.1). This can be once more explained by the limited hydrophobicity of the sequence of **57** and aggregation of aromatic side chains for **63,** respectively. Indeed, the aromatic rhodamine B moiety can further enhance hydrophobic and π-π interactions of sequence **52** resulting with **63** being the least membrane active conjugate. For all the other oligomers (**58**-**62**), the length and hydrophobicity of the β^{3R3}-peptide sequence itself becomes significantly less relevant compared to the membrane activity of the unlabeled analogues (Section 5.2.1). This can be actually correlated to the physicochemical analysis performed in section 5.2.1.b., where general increasing of hydrophobicity towards closer values was observed. However, the entity of membrane interaction is broadly parallel to the antimicrobial activity of the unlabeled analogues (**47**-**51**), with oligomer **61** being the most active, and **59** and **60** the least active ones.

In addition, the conjugation with rhodamine B did neither significantly influence the relative hydrophobicity nor the membrane activity of analogue amphiphilic cationic β^{3R3}-peptide sequences with different chirality. Indeed, as oligomer **50** (*v*S,*s*S) showed higher antimicrobial activity than **56** (*v*S,*s*R) (Section 5.2.1), also the rhodamine B derivative **61** (*v*S,*s*S) displays higher cellular interaction than **67** (*v*S,*s*R).

More significant is the effect of the conjugation with rhodamine B on the relative membrane activity of sequences featuring different number of repeats of same side chain patterns. The antimicrobial

activity increases along with the number of repeating units of oligomers **50**, **54**, and **55**, made of 9, 5 and 13 building blocks, respectively (Section 5.2.1). Differently, no linear trend is observed for the membrane activity of the rhodamine B labeled derivatives **61**, **65**, and **66** (Scheme 5.3). Here, oligomer **61** with average chain length is the most active on all the three cell lines. Among the others, the shortest analogue **65** is more active on MDCII cells, while the longest **66** is more active on HeLa and A10 cells. A different trend is observed for oligomers **58** and **64**, which feature different number of repeats of another side chain pattern (Scheme 5.3). Here, the longer **58** made of 9 repeating units is more active on HeLa cells, while **64** with 5 repeating units is more active on A10 and MDCII cell. So far these results cannot be rationalized and more specific investigations are required to gain a deeper insight.

In order to further elucidate the uptake mechanism of the rhodamine conjugates of amphiphilic cationic β^{3R3}-peptides, the experiments on caveolin-dominant MDCKII cells were repeated adding genistein, a selective inhibitor of caveolin (Figure 5.16). So far the highest cellular association for all oligomers was observed on MDCKII cells (Figure 5.15), which are characterized as caveolin-dominant. Oligomers **58**, **61**, and **64** were selected due to their high membrane activity (Figure 5.15).

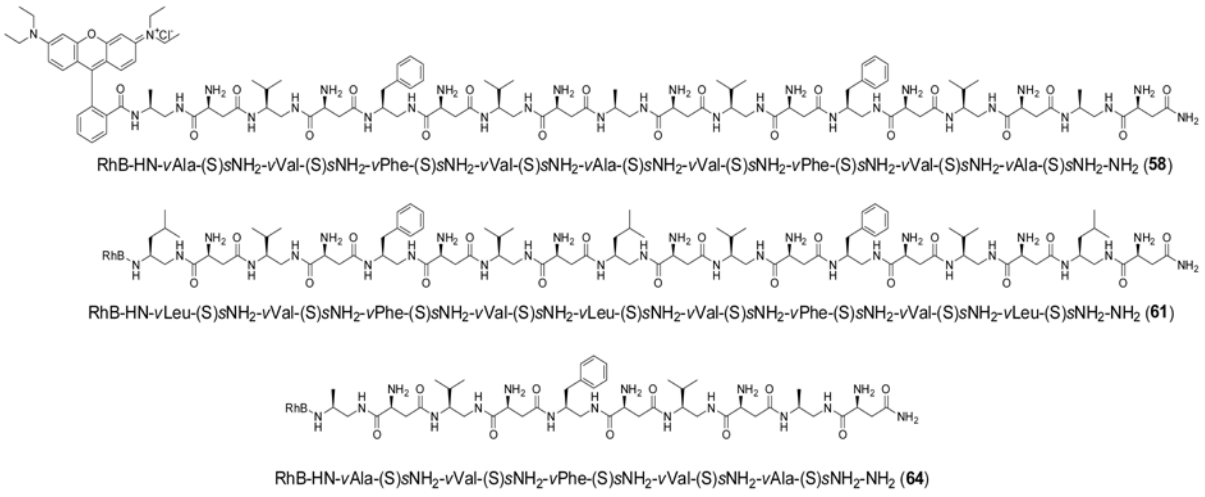

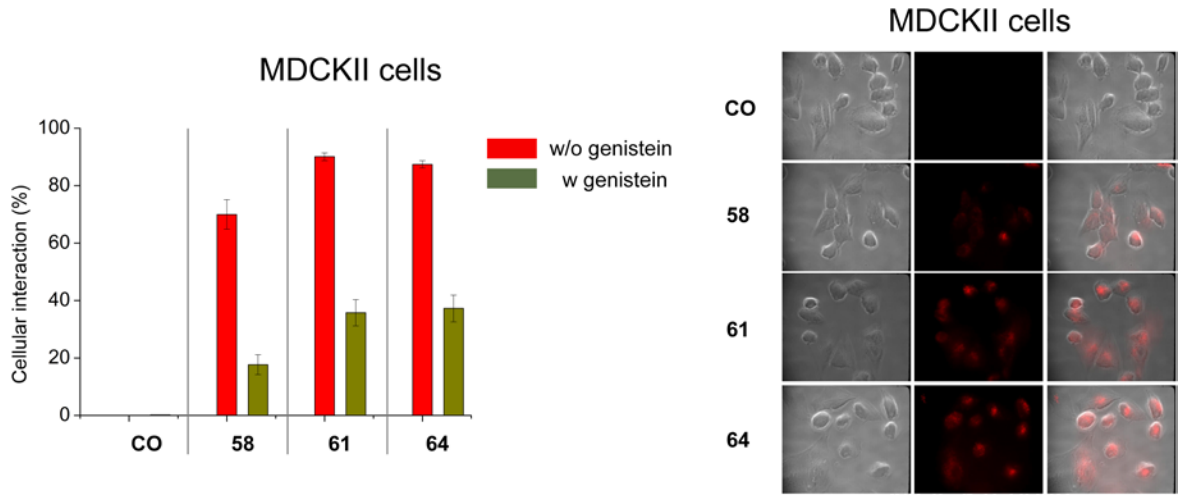

Figure 5.16. *Influence of genistein on the cellular uptake and fluorescence microscopy (100 X) pictures of oligomers* ***58***, ***61***, *and* ***64*** *in MDCKII cells.*

The FACS experiments in presence of genistein show significant contribution of caveolin-mediated endocytosis to the uptake for all rhodamine conjugates of amphiphilic cationic β^{3R3}-peptides. This is indeed an attractive feature as caveolae endocytosis can circumvent lysosomal degradation of acid sensitive cargo.

Lastly, fluorescence microscopy pictures were taken to further confirm that the oligomers do not just interact with but effectively penetrate the cellular membrane. Indeed, oligomers **58**, **61**, and **64** can definitely enter into the cells and are observed in both the cytoplasm and nucleus.

Based on these results, amphiphilic cationic β^{3R3}-peptides have high potential for the development as a new class of cell-penetrating peptidomimetics for drug delivery. Indeed, although it appears quite problematic and simplistic to provide a univocal scheme for their uptake mechanism, specific amphiphilic cationic β^{3R3}-peptide sequences can represent a potent tool to improve the uptake specificity of CPPs.

Thus, in the next section the rhodamine B conjugates of amphiphilic cationic β^{3R3}-peptides will be tested for their enzymatic stability, as an essential feature of peptidomimetics for biomedical applications.

5.2.3. Enzymatic Stability Assays with Amphiphilic Cationic β^{3R3}-Peptides

In the previous sections high potential of the amphiphilic cationic β^{3R3}-peptides have been proven as membrane active peptidomimetics with regards to their antimicrobial activity and the cell-penetrating properties of rhodamine B conjugates. Finally, enzymatic stability assays with the amphiphilic cationic β^{3R3}-peptides will be now performed. Indeed, improved enzymatic stability is acknowledged as a primary requirement of peptidomimetics for biomedical applications. Therefore, amphiphilic cationic β^{3R3}-peptide senquences and rhodamine B conjugates have been tested with different enzymes with different substrate specificity. Specifically trypsin, pepsin, and pronase were employed and different oligomers selected (Table 5.5). The experiments were performed with the help of Uwe Möginger.

Table 5.5. *Amphiphilic cationic β^{3R3}-peptide oligomers (**47**, **49**, **51**, **55**, ad **56**) and the rhodamine B conjugates (**61** and **67**) investigated for their proteolytic stability against trypsin, pepsin and pronase.*

Oligomer	Protease
*H_2N-(vAla-(S)sNH_2-vVal-(S)sNH_2-vPhe-(S)sNH_2-vVal-(S)sNH_2)$_2$-vAla-(S)sNH_2-NH_2 (**47**)*	Trypsin, Pronase
*H_2N-(vAla-(S)sNH_2-vVal-(S)sNH_2-vLeu-(S)sNH_2-vVal-(S)sNH_2)$_2$-vAla-(S)sNH_2-NH_2 (**49**)*	Trypsin, Pronase
*H_2N-(vLeu-(S)sNH_2-vVal-(S)sNH_2-vLeu-(S)sNH_2-vVal-(S)sNH_2)$_2$-vLeu-(S)sNH_2-NH_2 (**51**)*	Trypsin, Pepsin, Pronase
*H_2N-(vLeu-(S)sNH_2-vVal-(S)sNH_2-vPhe-(S)sNH_2-vVal-(S)sNH_2)$_3$-vLeu-(S)sNH_2-NH_2 (**55**)*	Pepsin, Pronase
*H_2N-(vLeu-(R)sNH_2-vVal-(R)sNH_2-vPhe-(R)sNH_2-vVal-(R)sNH_2)$_2$-vLeu-(R)sNH_2-NH_2 (**56**)*	Pepsin, Pronase
*RhB-HN-(vLeu-(S)sNH_2-vVal-(S)sNH_2-vPhe-(S)sNH_2-vVal-(S)sNH_2)$_2$-vLeu-(S)sNH_2-NH_2 (**61**)*	Pronase
*RhB-HN-(vLeu-(R)sNH_2-vVal-(R)sNH_2-vPhe-(R)sNH_2-vVal-(R)sNH_2)$_2$-vLeu-(R)sNH_2-NH_2 (**67**)*	Pronase

Trypsin is a serine endopeptidase that cleaves after cationic residues such as Lys or Arg. Indeed, the amphiphilic cationic β^{3R3}-peptides dysplay high density of cationic side chains as primary amino groups of the Asp moiety employed as succinic acid analogue within each repeating unit (Figure 5.17). This can act as bioisoster of Lys residues not just for the interaction cell membranes, which determines the antimicrobial activity of the oligomers, but potentially also for the affinity to enzymes and trypsin in particular. Nevertheless, no signs of degradation were detected on oligomers **47**, **49**, and **51** after 72h. Although oligomers **47**, **49**, and **51** were employed, here the choice was not critical as the different hydrophobic proteinaceous side chins discriminating among the sequences do not generally influence the substrate selectivity of trypsin. In contrast, pepsin, the principal protease of the stomach in higher organisms, is an endopeptidase with a preference for aromatic amino acids such as Phe. In addition, pepsin can also after other bulky hydrophobic residues such as Leu.[15] Therefore, oligomers **51**, **55**, and **56** were selected and tested for their stability against pepsyn. Indeed, the sequence of **51** is particularly enriched in *v*Leu units, whereas oligomers **55** and **56** present several aromatic *v*Phe residues (Figure 5.17). Additionally, **56** is heterochiral (*v*S,*s*R) and allows to analyzed the effect of the chiral configuration and conformational properties on the interaction with the enzyme. Nevertheless, all the oligomers **51**, **55**, and **56** were still detectable without any signs of degradation after 3 days.

Lastly, the amphiphilic cationic β^{3R3}-peptides were tested against pronase which is mixture of extracellular enzymes derived from the fungus Streptomyces griseus, and consists of both endo- and exopeptidases. Pronase can cleave almost any peptide bond and yields a large amount of free amino acids in the digestion of protein substrates within few minutes.[170] Although it has been shown in section 5.1.2 that hydrophobic β^{3R3}-peptides are completely stable towards pronase, these data cannot be directly extended to the amphiphilic cationic β^{3R3}-peptides. Indeed, pronase has an exclusive capability for digestion of α/β-peptides,[14] and the amphiphilic cationic β^{3R3}-peptides are actually made of the α-amino acid Asp employed as succinic acid analogue. Due to the sequence aspecificity of pronase, several amphiphilic cationic β^{3R3}-peptide oligomers (**47**, **49**, **51, 55** and **56**) with different side chain sequence and chiral configuration were investigated. In fact, regardless the side chain sequence the homochiral (*v*S,*s*S) amphiphilic cationic β^{3R3}-peptides got cleaved by pronase. However, the amphiphilic cationic β^{3R3}-peptides undergo exclusively exopeptidase cleavage and at a rate significantly slower than natural peptides. Indeed, after 1 h only the cleavage of the *s*NH_2 residue at the C-terminus is observed and 24h are generally needed for the following *v*Xaa unit. In addition, despite the sequence aspecificity of pronase, a different sequence susceptibility is observed for the amphiphilic cationic β^{3R3}-peptides, with oligomers **51** and **55** being the most stable one and still

detectable after 7h. In contrast, the heterochiral (*v*S,*s*R) **56** did not undergo pronase cleavage. Thus, due to the extreme substrate aspecificity of pronase, it could be concluded that the heterochiral (*v*S,*s*R) amphiphilic cationic β^{3R3}-peptides are extremely stable against enzymatic degradation.

In addition, also rhodamine B conjugates were investigated against pronase. Indeed, as potential agents for drug delivery, it is fundamental that the cargo and specifically rhodamine B does not get promptly disconnected from the β^{3R3}-peptide sequence by enzymatic hydrolysis. Oligomer **61** and **67** were tested. In particular oligomer **61** was selected as it displayed the most promising cell-penetrating activity (Section 5.2.2.b). Indeed, rhodamine B does not get removed and exclusively the cleavage of the C-terminal *s*NH_2 residue is observed. Furthermore, this occurs at a slower rate for oligomer **61** than for **47** and **49**. Thus, comparing the pronase susceptibility of oligomers **47**, **49**, **51** and **61**, it is observed an influence of the side chain on the *v*Xaa unit in P1 position to the rate of removal of the sensitive C-terminal *s*NH_2 residue. Indeed, while oligomers **47** and **49** present the Val side chain on the *v*Xaa unit, oligomers **51** and **61** display the more bulky isobutyl moiety of Leu and get slower hydrolyzed. Lastly, oligomer **67** was tested against pronase as heterochiral (*v*S,*s*R) analogue of oligomer **61**. Analogously to oligomer **56**, no signs of degradation are observed after 72h and therefore oligomer **67** is not substrate of pronase which confirm that the heterochiral (*v*S,*s*R) amphiphilic cationic β^{3R3}-peptides are extremely stable against enzymatic degradation.

Based on these results, the β^{3R3}-peptides in general feature a significantly improved enzymatic stability, which is a primary prerequisite for their development as peptidomimetics for biomedical applications. In addition, the enzymatic susceptibility towards proteases characterized by peculiarly low substrate specificity, such as pronase, can be tuned by the specific design of the β^{3R3}-peptide sequence. Indeed hydrophobic and heterochiral (*v*S,*s*R) amphiphilic cationic sequences are completely protease stable. Differently, homochiral (*v*S,*s*S) amphiphilic cationic β^{3R3}-peptides are fairly sensitive to C-terminal exopeptidase cleavage depending on the residue in P1 position. This is also an attractive feature for the development of peptidomimetics which can allow for specific tuning and targeting of selected biomedical applications.[14 14]

6. Conclusion and Outlook

In this thesis, a novel class of β-peptides, the β^{3R3}-peptides, have been presented with particular focus to their design, synthetic approach, physicochemical characterization and structure-activity relationships. β-peptides with proteinaceous side chains have great potential for biomedical applications such as inhibitors or modulators of peptide-protein interactions and antibacterial or cell-penetrating reagents. Besides their physicochemical and functional flexibility, the enthusiasm for β-peptides arises from their structural features ("foldamers"), as well as biochemical and pharmacological properties ("peptidomimetics"). However, to further develop the biomedical potential of classical β-peptides extensive research efforts are still devoted to extend their structural space towards non-helical conformations and to optimize their therapeutical index by reducing their cytotoxicity.

This thesis therefore presents the β^{3R3}-peptides as a novel class of peptidomimetic foldamers, which can retain, modulate, and extend structural and biological properties of classical β-peptides aiming at selected biomedical applications. To achieve this aim, a novel backbone based on alternating directions of the amide bonds along β-peptide sequences has been designed and installed into different classes of β^{3R3}-peptide oligomers. These oligomers are based on SPS using novel building blocks of β-diamines (*v*Xaa) and β-diacids (*s*Xaa) with proteinaceous side chains and different functional moieties.

Natural amino acids were used as a pool of chiral starting materials to give Fmoc-protected enantiomerically pure vicinal diamines with different side chains starting from L-Ala, L-Val, L-Leu and L-Phe. Moreover, the L-Gly analogue was synthesized from ethylendiamine. Lastly, Fmoc β-diamines with a carboxyl functionality in α position and both S- and R-configuration have been synthesized from L- and D-Asn, respectively. The diacid building blocks have been either prepared via asymmetric synthesis or selected from the pool of commercially available chiral β-diacids with bioactive functional side chains, such as aspartic and malic acids. Furthermore, the Fmoc-protected chiral β-diamines (*v*Xaa) were coupled in solution with the β-diacids (*s*Xaa) to provide a first library of novel dimer building blocks suitable for conventional Fmoc SPPS protocols, which can be fully automated using a standard peptide synthesizer. Conclusively, all synthetic routes fulfill the requirements for the synthesis of building blocks for SPS, employing readily available starting materials and giving high yields on a multigram scale. Most notably, these procedures were

developed to rely exclusively on simple and convenient purification methods and no chromatographic purification was required, allowing for performing reactions in parallel and for further scale up.

The dimer building blocks were then employed for SPS of different classes of β^{3R3}-peptides. Notably, the coupling protocols were optimized to afford oligomers made of up to 13 dimer building blocks and a chain length corresponding to 26 β-amino acids in very high purity (>95%) directly after precipitation in cold Et_2O. Thus, it is remarkable that the developed synthetic strategy gives access to long and highly pure β^{3R3}-peptide sequences directly from natural α-amino acids without the need for any chromatographic purification along the whole synthetic route.

First, representative examples of hydrophobic β^{3R3}-peptides with proteinaceous side chains have been synthesized in order to primarily explore the possibility of long-range secondary structural order and the aggregation behavior of the β^{3R3}-peptide backbone. Specifically, those oligomers were designed with side chain sequences analogues of β^3-peptides known to form stable 3_{14}-helix, which is the best documented conformation of classical β-peptides.[17] The novel qualities of β^{3R3}-peptide backbone and the potential to form stable apolar strands in extended conformation could lead to an orthogonal folding behavior in comparison to β^3-peptides. Detailed IR (IRRAS) and X-ray (GIXD and XR) analysis at the air/water interface showed strand conformations and the formation of sheet assemblies with different crystallinity. Thus, β^{3R3}-peptides proved the potential to extend the structural and thereby functional space of β-peptides with proteinaceous side chains. In addition such hydrophobic β^{3R3}-peptides have significantly higher proteolytic stability in comparison to natural peptides, which makes them particularly suitable for biomedical applications. Ongoing work focuses on structural analysis in bulk using high-resolution methods, such as NMR, which are required to draw further conclusions about the structural properties and the functional potential of hydrophobic β^{3R3}-peptides for appropriate biomedical applications such as mimicking β-strands to antagonize β-sheet formation as therapeutic strategy e.g. against Alzheimer's disease.

In a second part, the potential of amphiphilic cationic β^{3R3}-peptides as antimicrobial and cell-penetrating peptidomimetics was investigated. To achieve this, a second set of building blocks was synthesized combining the hydrophobic diamine units with proteinaceous side (*v*Xaa) and L- and D-Asp as chiral β-diacid units (*s*NH_2) which provides cationic charges as amino groups in α-position. Different amphiphilic cationic β^{3R3}-peptide sequences have been prepared varying in the building block chirality, primary sequence and chain length. These oligomers were characterized for their physicochemical properties via HPLC, DLS, and IRRAS, without and in presence of model prokaryotic and eukaryotic membranes. This allowed for elucidation of the relationships between the

building block and backbone features, the primary sequences and the overall physicochemical properties which conclusively determine membrane activity and selectivity of the oligomers. Indeed, different values of hydrophobicity were determined for the different oligomers by HPLC and IRRAS experiments. Moreover, excessive density of aromatic residue resulted in hydrophobic aggregation and reduced membrane activity, as respectively proven by DLS and IRRAS. In addition, the stereochemistry of the building blocks can dictate the conformational properties of β^{3R3}-peptide oligomers, with homochiral (*v*S,*s*S) and heterochiral (*v*S,*s*R) sequences promoting amphiphatic folding supported by intramolecular and intermolecular hydrogen bond networks, respectively. Interestingly, a conformational shift towards helical conformations upon contact with membranes was observed for the heterochiral (*v*S,*s*R) oligomer.

Then the amphiphilic cationic β^{3R3}-peptides were tested for their potential as antimicrobial peptidomimetics. AMPs are considered as a potential source of future antibiotics because of their particular mechanism of action and reduced likelihood of bacterial resistance compared to conventional antibiotics. Cell viability experiments showed that specific amphiphilic cationic β^{3R3}-peptides with appropriate physicochemical properties have very high antimicrobial activity especially against Gram+ bacteria (MIC < 10 µM). In addition, the amphiphilic cationic β^{3R3}-peptides show an extraordinary therapeutic index with high antimicrobial and yet extremely low hemolytic activity (HD_{50} > 1600 µM). On-going work focuses on targeting different clinically relevant microbes, such as bacteria, viruses and fungi.

Furthermore, cationic amphiphilic β^{3R3}-peptides have been investigated as analogues of CPPs. Therefore, β^{3R3}-peptide sequences were conjugated with rhodamine B as drug-like molecule which allowed for the investigation of the cell-uptake properties using fluorescence-based techniques. For sequences with appropriate physicochemical features, cellular uptake into HeLa, MDCKII and A10 cells as observed in flow cytometry was very high. Furthermore, inhibition assays were performed to elucidate the cellular uptake mechanism of cationic amphiphilic β^{3R3}-peptides. Taken together, the results indicate that there are several endocytotic uptake mechanisms including caveolae, clathrin dependent endocytosis and macropinocytosis processes, which have been already described for native CPPs. However, cationic amphiphilic β^{3R3}-peptides do not show any direct translocation which usually occurs for CPPs (high binding or internalization at 4°C) and display significantly increased proteolytic stability. Thus, cationic amphiphilic β^{3R3}-peptides can potentially overcome the major drawback of natural CPPs in terms of specificity of drug targeting. Lastly, the amphiphilic cationic β^{3R3}-peptides showed significantly increased and sequence-based tunable protease stability.

Based on these results β^{3R3}-peptides have a great potential for a variety of applications, especially in biomedicine such as β-strand mimetics and modulators/inhibitors of β-sheet peptide-proteins interactions. Moreover, the amphiphilic cationic β^{3R3}-peptides are very promising candidates for the development of novel antimicrobial and cell-penetrating therapeutic agents. In addition, β^{3R3}-peptides also have the potential to address other current biomedical issues, e.g. they are currently investigated as nonviral vectors for DNA complexation and delivery. Ultimately, the physicochemical and functional flexibility as well as their conformational and self-assembling properties make the β^{3R3}-peptides very interesting also for other fields and their application e.g. in nanobiotechnology, polymer and material sciences.

Appendix

Experimental Part

1. Materials

Commercial grade reagents and solvents were used as purchased without further purification, except as indicated below. Fmoc-α-amino acids, Boc-L-Asp-OBn and Boc-D-Asp-OBn were purchased from Iris Biotech, HATU, PyBOP and HOBt from Nova Biochem, all other reagents from Aldrich; all were used without further purification. All solvents were HPLC grade. Regarding DCM, amylene-stabilized HPLC grade was chosen. The solid-support resins were purchased from Rapp Polymers. Tentagel S RAM resin (loading 0.23 mmol/g) (Fmoc-protected) was used as purchased. A commercially available Tr-tentagel−OH resin was modified with EDA. Therfore, Tr-tentagel-OH resin was converted to Tr-tentagel chloride resin by addition of freshly distilled acetylchloride and heating the mixture at 60°C in toluene for 3 h. After cooling down, EDA was added and shaken for 48 h to obtain Tr-tentagel-EDA resin. Loading of Tr-tentagel-EDA resin was determined by standard loading test giving a loading of 0.2 mmol/g. The resin was swollen twice for 15 min in DCM before starting the initial Fmoc deprotection.

HeLa cells and A10 SMC cells were obtained from DSMZ (Heidelberg, Germany), MDCKII cells from ATCC (Manassas, USA). RPMI 1640 medium and DMEM medium, FCS, glutamine, sodium pyruvate, PBS buffer (10 mM with or without Ca^{2+} and Mg^{2+}) and trypsin/EDTA 0.05% / 0.25% were purchased from Biochrome (Berlin, Germany). FACSflow sheath fluid was provided by BD Biosciences (Heidelberg, Germany), CellTiter-Glo® luminescent cell viability assay from Promega (Mannheim, Germany) and genistein from A.G. Scientific, Inc. (San Diego, USA). MoBiGLOW® was obtained from MoBiTec (Göttingen, Germany), paraformaldehyde and gelatine from Sigma Aldrich (Munich, Germany).

2. Methods

Nuclear Magnetic Resonace Sectroscopy (NMR). **^{1}H-NMR** and **^{13}C-NMR** spectra were measured with a Varian 400-MR spectrometer. The proton signal of residual, non-deuterated solvent (δ 7.26 ppm for $CHCl_3$, δ 2.50 ppm for DMSO, δ 3.31 ppm for MeOD) was used as an internal reference for ^{1}H NMR spectra. For 13C NMR spectra, the chemical shifts are reported relative to the carbon signal of the solvent (δ 77.16 ppm for $CDCl_3$, δ 39.52 ppm for DMSO, δ 49.00 ppm for MeOD). Coupling constants are reported in Hertz (Hz). The following abbreviations are used to indicate the multiplicities: s, singlet, d, doublet; t, triplet; m multiplet.

Reversed-phase HPLC (RP-HPLC). RP-HPLC was performed with 214 nm UV detection on a C18 (Agilent Eclipse, 4.6 × 100 mm) analytical column at 60 °C and a flow rate of 1 mL/min. Eluent: (A) water + 0.1% TFA; (B) acetonitrile + 0.1% TFA. The purity was determined by integration of the UV-signal with the software ChemStation for LC from Agilent Technologies.

Solid phase synthesis (SPS). SPS was performed on an automated Activotec P11 Peptide Synthesizer. The deprotection was initially carried out for 5 min and checked by UV monitoring for the fluorenyl Pip adduct at 301 nm. This step was repeated with increasing deprotection time (10, 20, 30, 40, 60 min) until the deprotection was complete.

Circular Dichroism (CD). CD spectra in methanol were recorded on a Jasco J-715 (Japan) spectrometer by using a quartz cuvette with an optical path length of 0.1 cm. The spectra were recorded in the wavelength interval from 190 to 260 nm, with 0.5 nm step resolution. 3 scans were accumulated for one spectrum. The peptide concentration was 100 µM. The spectra of the pure subphase were subtracted. The measured CD signal was transformed to mean residue molar ellipticity [θ] and divided by the number of peptide bonds to obtain $[\theta]_{RES}$.

Infrared Reflection-Absorption Spectroscopy (IRRAS). IRRA spectra were recorded with a Vertex 70 FT-IR spectrometer (Bruker, Germany) coupled with a Langmuir film balance (Riegler & Kirstein, Potsdam, Germany). The trough and the external reflectance unit (XA 511) were flushed with dry air in a sealed container to obtain a stable atmosphere. To measure the surface pressure, a filter paper as a Wilhelmy plate was used. The peptide was spread from a methanol solution onto the subphase (10 mM PBS, pH 7.4, 20 °C) to obtain high surface pressure (referred as 'single shot method'), which corresponds to a theoretical bulk solution of 0.2 µM. The film was compressed symmetrically by two barriers with a velocity of 8.2 cm^2/min. After relaxation for one hour, the reflected IR beam was detected at the same angles as incidence (40°) with a liquid nitrogen cooled MCT (Mercury Cadmium Telluride) detector with a resolution of 8 cm^{-1}.

800 scans were made for a p-polarization beam to obtain a sample spectrum R (scanner velocity 20 kHz), apodized using Blackman-Harris 3-term function and fast Fourier transformed after one level of zero filling. Due to the shuttle technique, a pure subphase spectrum R_0 is recorded before each sample spectrum is measured. The reflectance-absorbance RA is plotted as $-\lg(R/R_0)$. Therefore, the strong absorption bands from water can be eliminated.

Grazing Incidence X-Ray Diffraction (GIXD). GIXD measurements were carried out at the undulator beamline BW1 using the liquid surface diffractometer at HASYLAB, DESY (Hamburg, Germany). The setup is equipped with a temperature controlled Langmuir trough (Riegler and Kirstein, Potsdam, Germany), which is enclosed in a sealed, helium-filled container. The synchrotron X-ray beam is monochromated to a wavelength of 1.304 Å and is adjusted to strike the helium/water interface at a grazing incidence angle $\alpha_i = 0.85\alpha_c$ ($\alpha_c = 0.13°$ is the critical angle for total reflection) illuminating approximately 2×50 mm^2 of the monolayer surface. A MYTHEN detector system (PSI, Villigen, Switzerland) measures the diffracted signal and is rotated to scan the in-plane Q_{xy} component of the scattering vector. A Soller collimator in front of the MYTHEN restricted the in-plane divergence of the diffracted beam to 0.09°. The vertical strips of the MYTHEN measure the out-of-plane Q_z component of the scattering vector between 0.0 and 0.75 Å^{-1}. The diffraction data consist of Bragg peaks at diagnostic Q_{xy} values obtained by summing the diffracted intensity over a defined vertical angle or Q_z-window. The in-plane lattice repeat distances d of the ordered structures in the monolayer are calculated from the Bragg peak positions: $d = 2\pi/Q_{xy}$. To estimate the extent of the crystalline order in the monolayer, the in-plane coherence length L_{xy}, is approximated from the full-width at half-maximum (fwhm) of the Bragg peaks using $L_{xy} \sim 0.9(2\pi)/\text{fwhm}(Q_{xy})$ using the measured fwhm(Q_{xy}) corrected for the instrumental resolution. Integrating the diffracted intensity normal to the interface over the Q_{xy} window of the diffraction peak yields the corresponding Bragg rod. The thickness of the scattering unit is estimated from the fwhm of the Bragg rod using $0.9(2\pi)/\text{fwhm}(Q_z)$. All experiments have been performed at the air/water interface at 20 °C and 20 mN/m.

X-Ray Reflectivity (XR). XR measurements were carried out at the same beamline as GIXD experiments. The specular XR data collection was performed by using a NaI scintillation detector. The X-ray reflectivity was measured with the geometry, $\alpha_i = \alpha_f = \alpha$, where α_i is the vertical incidence angle and α_f is the vertical exit angle of the reflected X-rays. XR data were collected as a function of the incidence angle, α_i, varied in the range of 0.06° - 3.5°, corresponding to a range of 0.01 Å^{-1} - 0.6 Å^{-1} of the vertical scattering vector component Q_z. The background scattering from the subphase was measured at $2\theta_{xy} = 0.7°$ and subtracted from the signal measured at $2\theta_{xy} = 0$.

The electron density profile has been obtained with a model-independent method. From the experimentally observed reflectivity curve, the corresponding profile correlation function is estimated via indirect Fourier transformation. For this profile correlation function the matching electron density profile is then derived by square-root deconvolution. No a priori assumptions on the shape of the electron-density profile have to be made.

The X-ray reflectivity can be inverted to yield the laterally averaged electron density ρ(z) of the monolayer as a function of the vertical z coordinate.

Dynamic Light Scattering (DLS). DLS spectra in H2O were recorded on a Zetasizer Nano ZS (ZEN3500) spectrometer by using a quartz cuvette with an optical path length of 1 cm. 3 scans were accumulated for one spectrum. The peptide concentration was 100 µg/mL. The spectra of the pure subphase were subtracted. The signal was converted Nano Application 6.12.1.0 Software (Malvern Instruments Ltd).

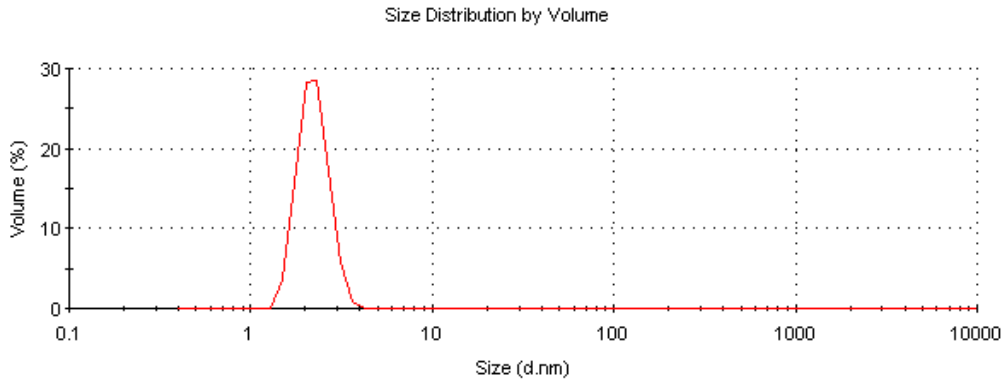

Figure 1. *DLS spectrum of oligomer* ***52***

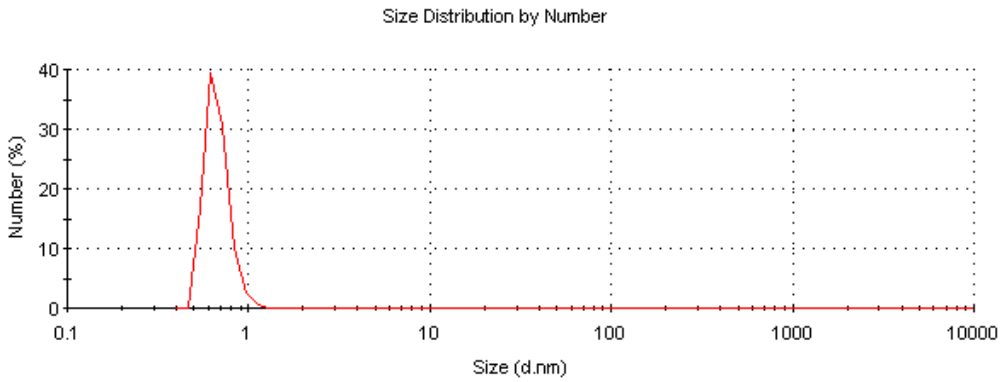

Figure 2. *DLS spectrum of oligomer* ***55***

Enzymatic stability assays. The mixture was analyzed using a Bruker Autoflex MALDI TOF system and as Matrix DHB (2,5-dihydroxybenzoic acid). The samples were incubated at 37°C.
For pronase, 100ng Pronase/digest and 1pmol/µl peptide concentration were employed. 25mM TRIS HCl, 3mM $CaCl_2$ as buffer and a peptide with the sequence NVFVHPNYSK (m/z=1219.6106) was used as control. For Pepsin, 100ng pepsin/sample and 40µl sample volume were used. The buffer was 0.25% TFA and BSA 10µg the control peptide.10ng were spotted. Lastly, 25mM ammonium bicarbonate buffer, 40µl volume and spotting 10nmol/µl were selected for Trypsin.

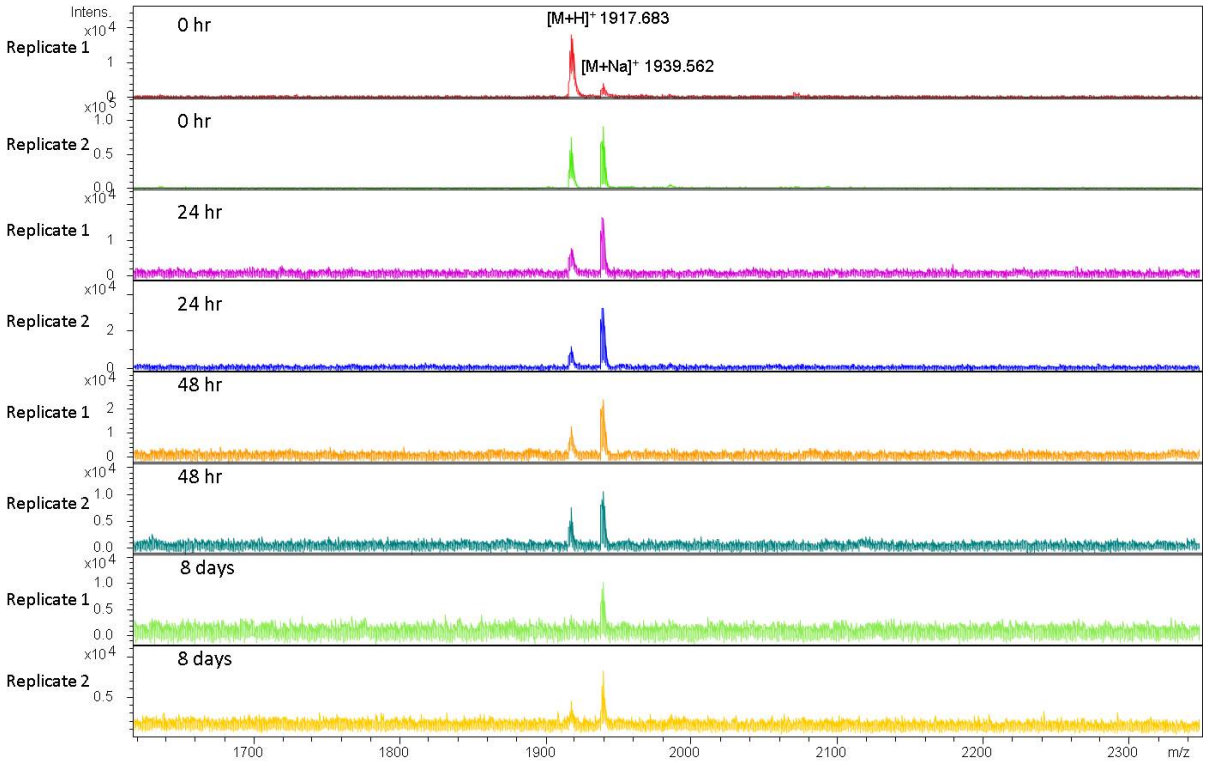

Figure 3. *MALDI spectra of pronase digestion of oligomer* ***44****.*

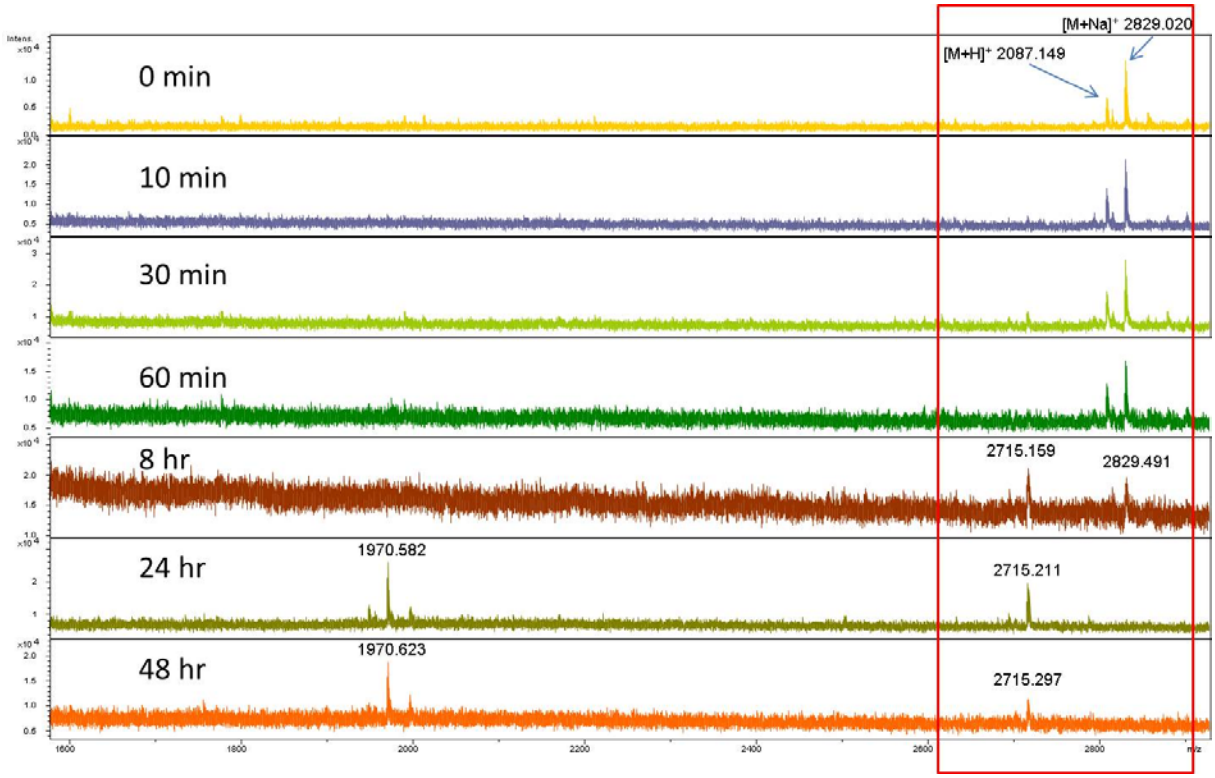

Figure 4. *MALDI spectra of pronase digestion of oligomer* ***55****.*

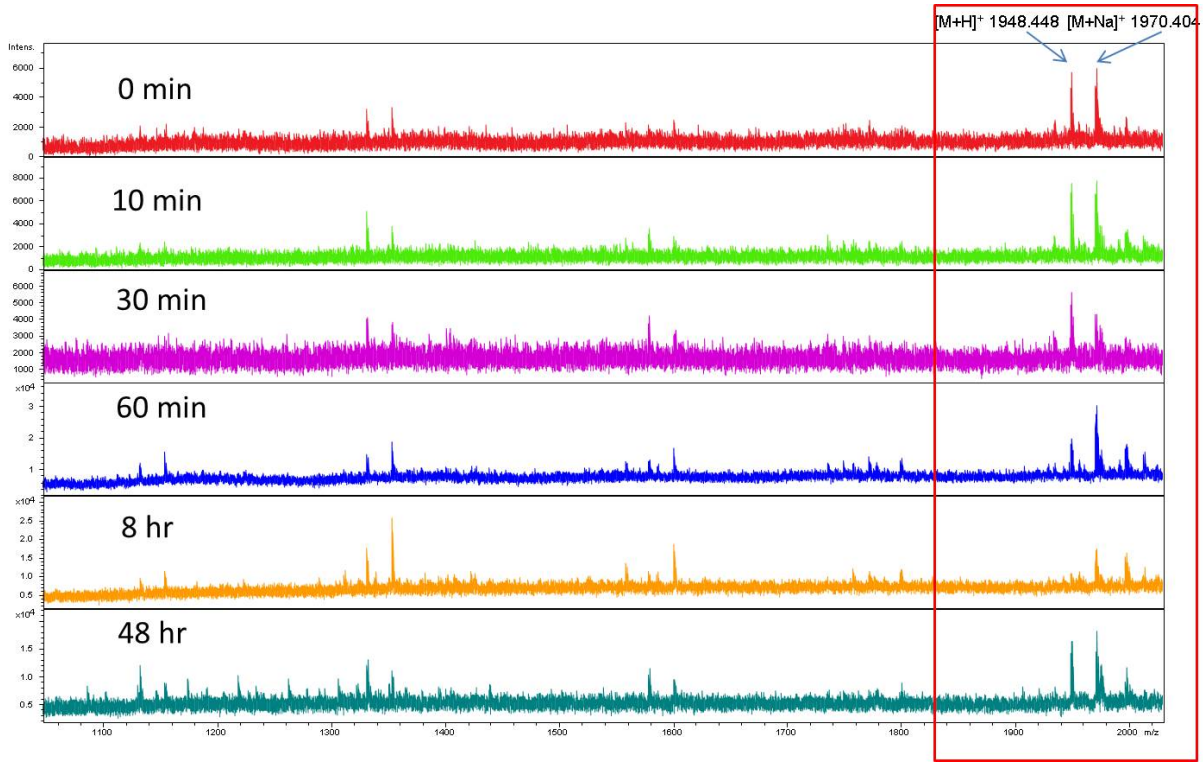

Figure 5. *MALDI spectra of pronase digestion of oligomer* ***56****.*

Antibacterial growth assay. Liquid pre-culture bacteria were inoculated with a single colonies picked from LB agar streaked plates of Gram-negative *Escherichia coli* strain BL21 (Invitogen) or of Gram-positive *Micrococcus luteus* (type strain DSM 20030). Bacteria were grown in 3 ml LB medium (Roth) in sterile plastic tubes (Greiner) in a Multitron incubator shaker (Infors) at 220 rpm at 37 °C for *E. coli* or 28 °C for *M. luteus*. Bacteria were grown overnight and were then directly used for the experiments. For antibacterial assays the different compounds were dissolved in 80% ethanol in sterile phosphate buffer saline (PBS) to ensure their sterility. For the assays, different compounds were added at the given concentration in sterile plastic tubes under sterile bench and were let open for 1 h to remove maximum of ethanol. Each measurement was performed in duplicate. The control incubations contain the same amount of 80% of ethanol in PBS. 1 ml of LB medium was then added to each incubation tube. The incubation tubes were inoculated with 3 µl from the liquid pre-culture bacteria and incubated over night at 37 °C (*E. coli*) or at 28 °C (*M. luteus*) with shaking at 220 rpm. Bacterial growth was monitored by measuring the absorbance at a wavelength of 600 nm with a spectrophotometer (Ultrospec 6300pro, Amersham).

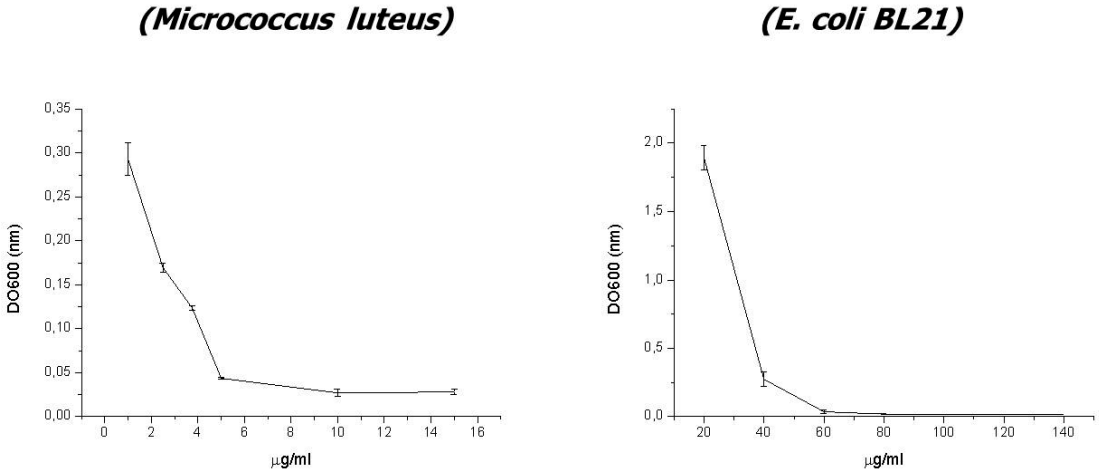

Figure 6. *Antibacterial activity of oligomer* ***55****.*

Hemolysis assay. Five hundred microliter of fresh human blood (German Red Cross; DRK Berlin) was drawn into a 1 ml and centrifuged at 4000 rpm for 5 minutes. Following centrifugation, the supernatant was discarded and the pelleted containing human red blood cells (hRBCs) were suspended in 1 mL of PBS buffer and centrifuged at 6000 rpm for 5 minutes. The washing process was repeated 3 times or 4 until the supernatant become completely clear displaying a negligible absorbance at 415 nm. The pellet was then suspended in 1 mL of PBS buffer representing a stock hRBCs solution. To each test tube 2 µl of hRBCs stock solution was suspended in 98 µl PBS buffer to adjust the final volume to 100 µl. Each incubation test tube was

then supplemented with 100 µl PBS containing different compounds at the desired concentration. Complete hemolysis of the hRBCs was accomplished by adding a Triton-X-100 (Sigma) at finale concentration of 0.1 %. Samples were incubated at 37 ºC under maximum shaking conditions (Eppendorf Thermomixer) for 1 h. The tubes were then centrifuged at 14,000 rpm for 10 min. Hemoglobin released, as a result of hRBC lysis, was assessed by measuring the absorbance at 415 nm. All essays were performed in duplicate. The value of a blank incubation without any compound was subtracted from the values of the incubation test tubes. The integrity and intact of the hRBC was checked for the coupounds **9** by taking images before and after treatments using 20 x magnification Zeiss Axiovert 40C microscope.

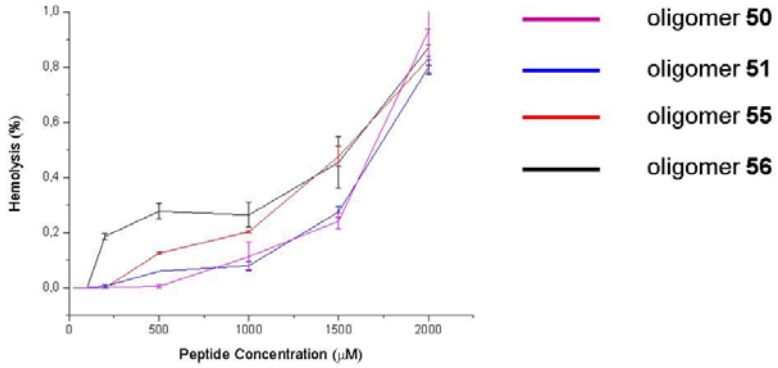

Figure 7. *Hemolytic activity of oligomers* ***50****,* ***51****,* ***55*** *and* ***56****.*

Cytotoxicity assay. Human foreskin fibroblasts (HFF; ATCC CRL-1635), were cultured in a 24-well cell culture plate in DMEM medium supplemented with 10% heat-inactivated FCS, 2mM glutamine, 100 units/ml penicillin and 0.1 mg/ml streptomycin. Cultures were incubated at 37°C and 5% CO_2 in humidified air. Compounds in 80% ethanol in sterile water were dried and suspended in 200 ml DMEM medium followed by the addition of 300 µL containing 10,000 fibroblasts/cm^2 pro-well. Images of fibroblasts growth in the presence or absence of compounds of were recorded at t = 24, 48 and 72 h using 20 x magnification Zeiss Axiovert 40C microscope. The data in figure was recorded at t = 24 h and t = 48 h.

Cell cultures. HeLa cells were cultured in RPMI 1640 medium supplemented with 10 % FCS and 2 mM glutamine. MDCKII cells were grown in DMEM medium supplemented with 10 % FCS. For A10 cells, DMEM medium supplemented with 20 % FCS and additionally 1 % sodium pyruvate was used. Cells were seeded into 24-well culture plates 24 h prior to the experiment at a density of 7.5 x 10^4 cells per well for HeLa cells and 4 x 10^4 for MDCKII as well as A10 cells and were maintained at 37 °C in a humidified incubator with 5% CO_2 atmosphere. The culture medium was renewed 1 h prior to incubation and the cells were then incubated with different

Rhodamine B-labeled β^{3R3}-peptidess at a final concentration of 15 µM for 2 h for HeLa cells and 4 h for MDCKII and A10 cells, respectively, each at 37 °C and 4 °C. For inhibition studies cells were pretreated with 200 µM solution of the caveolae inhibitor genistein for 60 min.

Flow cytometry and viability assays. After incubation, the cells were prepared for flow cytometry. First, fluorescently labeled samples and medium were removed. Cells were then washed with 1 ml PBS (once for HeLa and MDCKII, twice for A10). MDCKII were also washed once with 1 ml trypsin. Cells were then harvested by trypsinization for 2-8 minutes, depending on the cell line. All supernatants were collected and centrifuged (5 min at 1200 x g), washed and resuspended in 200 µl Ca^{2+}/Mg^{2+} containing PBS. These samples were stored on ice in the dark until used. Flow cytometry analysis was performed using a 4-color FACS Calibur® (Becton-Dickinson, Heidelberg, Germany) in combination with Lysis II software for calculation. For determination of cell-associated fluorescence of rhodamine-B, 10,000 cells were analyzed from each sample.

For determination of cell viability the CellTiter-Glo® luminescent cell viability assay was performed. Cells were prepared and incubated as described above. After incubation the 24-well plates and their contents were equilibrated to room temperature for 15 min. The samples were stored in the dark during the whole procedure, as described below. A volume of 500 µl of the CellTiter-Glo® reagent was added to each well and followed by mixing on an orbital shaker for 2 min. The plates were then incubated again at room temperature for an additional 10 min. Three 200 µl samples of each well were transferred into a luminometer-compatible multiwell plate and luminescence was recorded (MicroLumat Plus LB 96V luminometer, Win Glow software Version 1.24 from EG&G Berthold GmbH, Bad Wildbach, Germany).

Fluorescence microscopy. 24 h prior to the experiment cells were seeded onto sterilized 12 mm gelatine coated coverslips in 24 well plates at a density of 2 x 10^4 cells per well. The culture medium was renewed 1 h prior to incubation and MDCKII or A10 cells were then incubated with the corresponding rhodamine-PE labeled peptides (15 µM) for 4 h at 37 °C. Thereafter, cells were washed three times with warm PBS w/o Ca^{2+}/Mg^{2+} (37 °C). Cells were then fixed using 1 ml of a freshly prepared paraformaldehyde solution (4%) for 20 min at 37 °C. Subsequently, cells were washed again three times with warm PBS w/o Ca^{2+}/Mg^{2+}. Afterwards, cover slips were embedded with MoBiGLOW® on a slide. The cells were analyzed using a fluorescent microscope (Axiovert 100 Zeiss, Jena, Germany with a 100X/1.3 NA).

3. Experimental Procedures

Building block synthesis and characterization

Synthesis of the diamine monomers 1-4

General procedure for the preparation of compounds **a(1-4)**.

N-methylmorpholine (NMM) (1.1 equiv) and isobutylchloroformate (1.1 equiv) were added to a cold (-15°C) solution of Boc-L-aminoacid (1 equiv) in dry THF (0.8 mM) under Ar. After 10 min, the precipitated NMM hydrochloride salt was removed by filtration; washed with THF and cooled to -78°C. A solution of sodium borohydride ($NaBH_4$) (1.5 equiv) in water (2.6 M) was added at once, resulting in strong hydrogen gas formation. The reaction mixture was stirred 20 min at room temperature and the solvent was evaporated at 40°C. The solid was dissolved in DCM and 5% aqueous citric acid. The organic layer was washed with brine, $NaHCO_3$ saturated aqueous solution and again brine, dried over $MgSO_4$, filtered and evaporated to give a solid. The final product was isolated as a colorless solid after drying in high vacuum.

Boc-Protected-(*S*)-Alanine Alcohol (**a1**) (R= CH_3)

Compound **a1** was prepared from Boc-L-Alanine (30g, 159 mmol) and isolated as a white solid (Yield: 21.95g, 125 mmol, 79%). ^{1}H NMR (400 MHz, cdcl$_3$) δ 3.82 – 3.69 (m, 1H), 3.64 (dd, *J* = 10.9, 3.8 Hz, 1H), 3.50 (dd, *J* = 10.9, 6.2 Hz, 1H), 1.44 (s, 10H), 1.14 (d, *J* = 6.8 Hz, 3H); ^{13}C NMR (100 MHz, cdcl$_3$) δ 157.01, 79.71, 64.46, 58.26, 29.49, 28.52, 19.63, 18.65.

Boc-Protected-(*S*)-Valine Alcohol (**a2**) (R= $CH(CH_3)_2$)

Compound **a2** was prepared from Boc-L-Valine (30g, 138 mmol) and isolated as a white solid (Yield: 24.42g, 120 mmol, 87%). ^{1}H NMR (400 MHz, cdcl$_3$) δ 4.77 (d, *J* = 8.4 Hz, 1H), 3.70 – 3.54 (m, 2H), 3.49 – 3.28 (m, 1H), 2.85 (s, 1H), 1.89 – 1.70 (m, 1H), 1.42 (s, 9H), 0.94 – 0.88 (m, 6H); ^{13}C NMR (100 MHz, cdcl$_3$) δ 156.95, 79.60, 64.15, 58.13, 29.39, 28.49, 19.62, 18.61.

Boc-Protected-(*S*)-Leucine Alcohol (**a3**) (R= $CH_2CH(CH_3)_2$)

Compound **a3** was prepared from Boc-L-Leucine hydrate (30g, 120 mmol) and isolated as a white solid (Yield: 22.23g, 102 mmol, 85%). ^{1}H NMR (400 MHz, cdcl$_3$) δ 4.70 (d, *J* = 6.8 Hz, 1H), 3.74 – 3.57 (m, 2H), 3.53 – 3.40 (m, 1H), 2.98 (b s, 1H), 1.70 – 1.56 (m, 1H), 1.42 (s, 9H), 1.29 (dd, *J* = 8.2, 6.3 Hz, 2H), 0.91 – 0.88 (m, 6H); ^{13}C NMR (100 MHz, cdcl$_3$) δ 156.65, 79.63, 66.43, 51.02, 40.64, 28.49, 24.90, 23.15, 22.32.

Boc-Protected-(*S*)-Phenylalanine Alcohol (**a4**) (R= $CH(C_6H_5)$

Compound **a4** was prepared from Boc-L-Phenyalanine (30g, 113 mmol) and isolated as a white solid (Yield: 24.72g, 98 mmol, 87%). ^{1}H NMR (400 MHz, cdcl$_3$) δ 7.33 – 7.27 (m, 2H), 7.25 – 7.18 (m, 3H), 3.87 (s, 1H), 3.67 (dd, *J* = 11.0, 3.7 Hz, 1H), 3.56 (dd, *J* = 11.0, 5.3 Hz, 1H), 2.84 (d, *J* = 7.2 Hz, 2H), 1.41 (s, 9H); ^{13}C NMR (100 MHz, cdcl$_3$) δ 137.92, 129.42, 128.71, 126.70, 64.63, 37.64, 28.49.

General procedure for the preparation of compounds **b(1-4).**

Under Ar, to a solution of compound 1 (1 equiv) in dry DCM cooled to 0°C, triethylamine (Et_3N) (1 equiv) and methanesulfonyl chloride (MsCl) (1 equiv) were added dropwise. The reaction mixture was stirred at 0°C for 1h and then 1h at room temperature. Ice-water was added and the organic layer was washed with water, 5% citric acid, brine, $NaHCO_3$ saturated aqueous solution and again brine, dried over $MgSO_4$, filtered and evaporated. The final product was isolated after drying in high vacuum.

Boc-Protected-(*S*)-Alanine-methanesulfonate (**b1**)

Compound **b1** was prepared from compound **a1** (21.90g, 125 mmol) and isolated as a white crystalline solid (Yield: 31.25g, 124 mmol, 99%). ^{1}H NMR (400 MHz, cdcl$_3$) δ 4.61 (s), 4.29 – 4.18 (m), 4.15 (dd, *J* = 10.0, 4.3 Hz), 4.02 – 3.89 (m), 3.03 (s), 1.44 (s), 1.23 (d, *J* = 6.9 Hz); ^{13}C NMR (100 MHz, cdcl$_3$) δ 142.53, 110.58, 72.18, 71.80, 48.37, 45.69, 37.47, 28.46, 24.24, 20.92, 17.30.

Boc-Protected-(*S*)-Valine methanesulfonate (**b2**)

Compound **b2** was prepared from compound **a2** (24.42g, 120 mmol) and isolated as a white crystalline solid (Yield: 33.4g, 119 mmol, 99%). ^{1}H NMR (400 MHz, cdcl$_3$) δ 4.62 (d, *J* = 8.2 Hz), 4.26 (d, *J* = 4.2 Hz), 3.62 (b s, *J* = 6.5 Hz), 3.03 (s), 1.90 – 1.81 (m), 1.45 (s), 0.98 (dd, *J* = 10.2, 6.8 Hz); ^{13}C NMR (100 MHz, cdcl$_3$) δ 155.76, 69.85, 55.05, 37.55, 29.23, 28.49, 19.54, 18.60.

Boc-Protected-(*S*)-Leucine methanesulfonate (**b2)**

Compound **b3** was prepared from compound **a3** (22.23g, 102 mmol) and isolated as a white crystalline solid (Yield: 28.6g, 97 mmol, 95%). ^{1}H NMR (400 MHz, cdcl$_3$) δ 4.54 (d), 4.26 (dd), 4.14 (dd, *J* = 10.0, 4.1 Hz), 3.92 (b s), 3.02 (s), 1.72 – 1.62 (m), 1.44 (s), 0.93 (dd, *J* = 6.6, 3.7 Hz); ^{13}C NMR (100 MHz, cdcl$_3$) δ 155.41, 71.74, 48.07, 40.28, 37.44, 28.48, 24.77, 23.05, 22.16; *m/z* (ESI-HRMS) found $[M + Na]^+$, 318.1339 $C_{12}H_{25}NNaO_5S$ requires $[M + Na]^+$, 318.1346.

Boc-Protected-(*S*)-Phenyalanine methanesulfonate (**b4)**

Compound **b4** was prepared from compound **a4** (24.32g, 97 mmol) and isolated as a white crystalline solid (Yield: 30.52g, 93 mmol, 96%). ^{1}H NMR (400 MHz, cdcl$_3$) δ 7.36 – 7.28 (m), 7.28 – 7.16 (m), 4.73 (d, *J* = 6.2 Hz), 4.28 – 4.21 (m), 4.12 (dd, *J* = 10.4, 3.3 Hz), 3.02 (s), 2.87 (d, *J* = 7.7 Hz), 1.42 (s). ^{13}C NMR (100 MHz, cdcl$_3$) δ 155.24, 136.71, 129.40, 128.92, 127.11, 69.94, 37.43, 28.45.

General procedure for the preparation of compounds **c(1-4).**

To a solution of compound **b** (1 equiv) in DMF sodium azide (NaN_3) (3 equiv) was added and the reaction mixture was stirred at 80°C for 8h. The solvent was removed under reduced pressure and the residue was re-dissolved in hexane (Hex) and washed with water, 5% citric acid and brine, dried over $MgSO_4$, filtered and evaporated to give colorless oil.

Boc-Protected-(*S*)-Alanine Azide (**c1**)

Compound **c1** was prepared from compound **b1** (31.25g, 124 mmol) and isolated as a white crystalline solid (Yield: 19.22g, 96 mmol, 77.4%). ^{1}H NMR (400 MHz, cdcl$_3$) δ 4.56 (b s, 1H), 3.84 (b s, 1H), 3.39 (dd, *J* = 11.2, 3.3 Hz, 1H), 3.30 (dd, *J* = 12.1, 4.6 Hz, 1H), 1.44 (s, 9H), 1.17 (d, *J* = 6.8 Hz, 3H); ^{13}C NMR (100 MHz, cdcl$_3$) δ 155.16, 79.83, 56.19, 46.35, 28.49, 18.43.

Boc-Protected-(*S*)-Valine Azide (**c2**)

Compound **c2** was prepared from compound **b2** (33.4g, 119 mmol) and isolated as a white crystalline solid (Yield: 19.64g, 86 mmol, 72.3%). ^{1}H NMR (400 MHz, cdcl$_3$) δ 4.55 (d, *J* = 7.3 Hz), 3.59 – 3.45 (m), 3.41 (d, *J* = 4.5 Hz), 1.86 – 1.73 (m), 1.45 (s), 0.93 (t, *J* = 7.0 Hz); ^{13}C NMR (100 MHz, cdcl$_3$) δ 155.69, 79.71, 55.68, 53.20, 29.94, 28.50, 19.63, 18.53.

Boc-Protected-(*S*)-Leucine Azide (**c3**)

Compound **c3** was prepared from compound **b3** (28.6g, 97 mmol) and isolated as a white crystalline solid (Yield: 19.71g, 81 mmol, 84%). ^{1}H NMR (400 MHz, cdcl$_3$) δ 4.46 (s, 1H), 3.80 (s, 1H), 3.44 (dd, *J* = 8.5 Hz, 1H), 3.31 (dd, *J* = 12.1, 3.9 Hz, 1H), 1.64 (dt, *J* = 18.3, 5.6 Hz, 1H), 1.45 (s, 9H), 1.38 – 1.25 (m, 2H), 0.93 (d, *J* = 6.7 Hz, 6H); ^{13}C NMR (100 MHz, cdcl$_3$) δ 155.38, 79.75, 55.33, 48.67, 41.46, 28.50, 24.89, 23.08, 22.28.

Boc-Protected-(*S*)-Phenyalanine Azide (**c4**)

Compound **c4** was prepared from compound **b4** (30.12g, 91 mmol) and isolated as a white crystalline solid (Yield: 19.56g, 71 mmol, 77.4%). ^{1}H NMR (400 MHz, cdcl$_3$) δ 7.32 (ddd, *J* = 7.5, 4.5, 1.2 Hz, 2H), 7.27 – 7.16 (m, 3H), 4.65 (s, 1H), 3.97 (s, 1H), 3.42 (dd, *J* = 12.3, 4.2 Hz, 1H), 3.31 (dd, *J* = 12.3, 4.4 Hz, 1H), 2.88 (dd, *J* = 13.4, 6.3 Hz, 1H), 2.79 (dd, *J* = 13.6, 7.9 Hz,

1H), 1.43 (s, 9H); ^{13}C NMR (100 MHz, cdcl$_3$) δ 155.20, 137.26, 129.41, 128.81, 126.89, 79.93, 53.29, 51.50, 38.31, 28.47.

General Procedure for the preparation of compounds **d(1-4).**

A mixture of THF: HCl(aq) (12M) = 10:4 (0.2 M) cooled to 0°C, was slowly added to compound **c**. The reaction mixture was stirred for 1h and then the solvent was evaporated *in vacuo* and then lyophilized to afford the hydrochloride salt as a crystalline residue. The residue in was dissolved in a mixture of THF-water (3/5, v/v, 0.1 M) and treated with Na_2CO_3 (5 equiv). The resulting suspension was cooled to 0°C and fluorenyl chloroformate (FmocCl) (1 equiv) was added. The reaction mixture was stirred 24h at room temperature and then THF was removed under reduced pressure. The resulting yellow solid was dissolved by adding Et_2O. The organic layer was washed with water, 5% citric acid and brine. The solvent was concentrated and precipitation in Hex afforded compound **d**.

Fmoc-(*S*)-Alanine Azide (**d1**)

Compound **d1** was prepared from compound **c1** (19.22g, 96 mmol) and isolated as a white solid (Yield: 29.7g, 92 mmol, 96%). ^{1}H NMR (400 MHz, cdcl$_3$) δ 7.77 (d, *J* = 7.6 Hz, 2H), 7.59 (d, *J* = 7.5 Hz, 2H), 7.41 (dd, *J* = 9.4, 5.5 Hz, 2H), 7.32 (td, *J* = 7.5, 0.9 Hz, 2H), 4.78 (d, *J* = 4.1 Hz, 1H), 4.42 (dt, *J* = 16.3, 9.8 Hz, 2H), 4.22 (t, *J* = 6.7 Hz, 1H), 3.93 (s, 1H), 3.45 (d, *J* = 8.3 Hz, 1H), 3.35 (d, *J* = 9.3 Hz, 1H), 1.22 (d, *J* = 5.8 Hz, 3H); ^{13}C NMR (100 MHz, cdcl$_3$) δ 155.68, 144.00, 141.48, 127.85, 127.19, 125.13, 120.14, 110.15, 66.86, 56.05, 47.41, 46.84, 18.43.

Fmoc-(*S*)-Valine Azide (**d2**)

Compound **d2** was prepared from compound **c2** (19.64g, 86 mmol) and isolated as a white solid (Yield: 29.5, 84 mmol, 98%). ^{1}H NMR (400 MHz, cdcl$_3$) δ 7.77 (d, *J* = 7.6 Hz, 2H), 7.61 (d, *J* = 7.5 Hz, 2H), 7.41 (t, *J* = 7.5 Hz, 2H), 7.33 (t, *J* = 7.4 Hz, 2H), 4.82 (d, *J* = 9.2 Hz, 1H), 4.45 (d, *J* = 6.8 Hz, 2H), 4.24 (t, *J* = 6.8 Hz, 1H), 3.64 – 3.52 (m, 1H), 3.44 (d, *J* = 4.8 Hz, 2H), 1.90 – 1.73 (m, 1H), 0.94 (dd, *J* = 10.5, 6.8 Hz, 6H), 0.81 (b, *J* = 4.9 Hz, 1H); ^{13}C NMR (100 MHz, cdcl$_3$) δ 156.21, 143.97, 143.95, 141.44, 127.80, 127.16, 127.14, 125.12, 120.09, 120.08, 66.75, 56.30, 53.12, 47.42, 29.83, 19.58, 18.64.

Fmoc-(*S*)-Leucine Azide (**d3**)

Compound **d3** was prepared from compound **c3** (19.64g, 86 mmol) and isolated as a white solid (Yield: 29.5, 84 mmol, 98%). ^{1}H NMR (400 MHz, cdcl$_3$) δ 7.77 (d, *J* = 7.6 Hz, 2H), 7.61 (d, *J* = 7.5 Hz, 2H), 7.41 (t, *J* = 7.5 Hz, 2H), 7.33 (t, *J* = 7.4 Hz, 2H), 4.82 (d, *J* = 9.2 Hz, 1H), 4.45 (d, *J* = 6.8 Hz, 2H), 4.24 (t, *J* = 6.8 Hz, 1H), 3.64 – 3.52 (m, 1H), 3.44 (d, *J* = 4.8 Hz, 2H), 1.90 – 1.73

(m, 1H), 0.94 (dd, *J* = 10.5, 6.8 Hz, 6H), 0.81 (b, *J* = 4.9 Hz, 1H); ^{13}C NMR (100 MHz, cdcl$_3$) δ 156.21, 143.97, 143.95, 141.44, 127.80, 127.16, 127.14, 125.12, 120.09, 120.08, 66.75, 56.30, 53.12, 47.42, 29.83, 19.58, 18.64.

Fmoc-(*S*)-Phenylalanine Azide (**d4**)

Compound **d4** was prepared from compound **c4** (19.56g, 71 mmol) and isolated as a white solid (Yield: 35.5, 89 mmol, 97%). ^{1}H NMR (400 MHz, cdcl$_3$) δ 7.78 (d, *J* = 7.5 Hz, 2H), 7.59 – 7.54 (m, 2H), 7.42 (td, *J* = 7.5, 0.6 Hz, 2H), 7.32 (t, *J* = 7.1 Hz, 4H), 7.28 – 7.15 (m, 3H), 4.91 (d, *J* = 8.3 Hz, 1H), 4.48 – 4.34 (m, 2H), 4.21 (t, *J* = 6.7 Hz, 1H), 4.13 – 3.97 (m, 1H), 3.46 (dd, *J* = 12.6, 4.5 Hz, 1H), 3.35 (dd, *J* = 12.3, 4.2 Hz, 1H), 3.09 – 2.78 (m, 2H); ^{13}C NMR (100 MHz, cdcl$_3$) δ 155.73, 143.92, 143.90, 141.44, 136.94, 129.36, 128.87, 127.84, 127.18, 127.01, 125.14, 120.12, 66.85, 53.24, 51.94, 47.33, 38.16.

General Procedure for the preparation of compounds **1**-**4**.

Compound **d** (1 equiv) dissolved in a mixture of MeOH-THF-CHCl$_3$ (40/10/1, v/v, 0.2 M), was hydrogenated in the presence of 10% Pd/C (10% w/w) at room temperature till RP-HPLC indicates completion of the reaction (approximately 48 h). The reaction mixture was filtered over GHP membrane (0.2 µm). The filtrate was evaporated to afford a solid. The solid was dissolved in a minimal amount of hot EtOH and precipitated by dropwise addition to cold diethyl ether to yield compound **5** as white powder.

Fmoc-(*S*)-Alanine amine hydrochloride salt (FmocNH-*v*Ala-NH$_2$.HCl) (**1**)

Compound **1** was prepared from compound **d1** (29.7g, 92 mmol) and isolated as a white solid (Yield: 23.9g, 71.8 mmol, 78%). ^{1}H NMR (400 MHz, cd$_3$od) δ 7.79 (d, *J* = 7.5 Hz), 7.66 (d, *J* = 7.4 Hz), 7.39 (t, *J* = 7.4 Hz), 7.31 (t, *J* = 7.4 Hz), 4.47 (dd, *J* = 10.5, 6.7 Hz), 4.36 (dd, *J* = 10.5, 6.6 Hz), 4.21 (t, *J* = 6.5 Hz), 3.99 – 3.84 (m), 2.97 (ddd, *J* = 22.1, 12.9, 6.7 Hz), 2.15 (s), 1.22 (d, *J* = 6.8 Hz); ^{13}C NMR (100 MHz, cd$_3$od) δ 149.24, 135.80, 135.72, 133.14, 119.30, 118.63, 116.65, 116.59, 111.45, 58.35, 57.39, 37.15, 36.38, 8.92, 5.96; HRMS (ESI): *m/z* calcd for $C_{18}H_{21}N_2O_2$: 297.1598 $[M–Cl]^+$, found: 297.1612; RP-HPLC analysis 5% to 95% MeCN in 10 min, T_R = 6.5 min.

Fmoc-(*S*)-Valine amine hydrochloride salt (FmocNH-*v*Val-NH$_2$.HCl) (**2**)

Compound **2** was prepared from compound **d2** (29.5g, 84 mmol) and isolated as a white solid (Yield: 26.4g, 73.1 mmol, 87%). ^{1}H NMR (400 MHz, cd$_3$od) δ 7.82 (d, *J* = 7.5 Hz), 7.70 (dd, *J* = 7.5, 0.9 Hz), 7.41 (t, *J* = 7.4 Hz), 7.33 (t, *J* = 7.4 Hz), 4.61 (dd, *J* = 10.6, 6.4 Hz), 4.36 (dd, *J* = 10.6, 6.3 Hz), 4.25 (t, *J* = 6.4 Hz), 3.63 – 3.57 (m), 3.15 (dd, *J* = 13.0, 3.2 Hz), 2.85 (dd, *J* = 12.9,

10.8 Hz), 1.84 – 1.76 (m), 0.94 (dd, *J* = 13.7, 6.8 Hz); ^{13}C NMR (100 MHz, cd_3od): δ 157.78, 143.95, 143.70, 141.24, 127.36, 126.68, 124.73, 124.61, 119.52, 119.50, 66.30, 54.91, 41.65, 30.70, 18.13, 17.07; HRMS (ESI): *m/z* calcd for $C_{20}H_{25}N_2O_2$: 325.1911 $[M–Cl]^+$, found: 325.1920; RP-HPLC analysis 5% to 95% MeCN in 10 min, T_R = 7.1 min.

Fmoc-(*S*)-Leucine amine hydrochloride salt (FmocNH-*v*Leu-NH_2.HCl) (**3**)

Compound **3** was prepared from compound **d3** (28.3g, 78 mmol) and isolated as a white solid (Yield: 26.6g, 71 mmol, 91%). ^{1}H NMR (400 MHz, cd_3od) δ 7.82 (d, *J* = 7.6 Hz, 2H), 7.68 (dd, 2H), 7.42 (t, *J* = 7.5 Hz, 2H), 7.33 (tt, 2H), 4.63 (dd, *J* = 10.7, 6.6 Hz, 1H), 4.36 (dd, *J* = 10.7, 6.3 Hz, 1H), 4.25 (t, *J* = 6.4 Hz, 1H), 3.70 – 3.62 (m, 1H), 3.15 (dd, *J* = 13.0, 3.0 Hz, 1H), 2.84 (dd, *J* = 12.9, 11.0 Hz, 1H), 1.60 – 1.53 (m, 1H), 1.50 – 1.43 (m, 1H), 1.20 – 1.14 (m, 1H), 0.96 – 0.89 (m, 6H); ^{13}C NMR (100 MHz, cd_3od) δ = 145.38, 142.70, 128.81, 128.11, 126.00, 120.94, 67.62, 45.70, 42.20, 25.66, 23.52, 21.91; HRMS (ESI): *m/z* calcd for $C_{21}H_{27}N_2O_2$: 339.2067 $[M–Cl]^+$, found: 339.2071; RP-HPLC analysis 5% to 95% MeCN in 10 min, T_R = 7.4 min.

Fmoc-(*S*)-Phenyalanine amine hydrochloride salt (FmocNH-*v*Phe-NH_2.HCl) (**4**)

Compound **4** was prepared from compound **d4** (35.2g, 89 mmol) and isolated as a white solid (Yield: 30.7g, 75 mmol, 85%). ^{1}H NMR (400 MHz, cd_3od) δ 7.82 (d, *J* = 7.6 Hz, 2H), 7.60 (d, *J* = 7.5 Hz, 2H), 7.44 – 7.39 (m, 2H), 7.35 – 7.28 (m, 4H), 7.23 (dd, *J* = 14.0, 7.1 Hz, 3H), 4.47 (dd, *J* = 10.6, 6.5 Hz, 1H), 4.24 (dd, *J* = 10.6, 6.7 Hz, 1H), 4.15 (t, *J* = 6.6 Hz, 1H), 4.05 (dt, *J* = 9.8, 6.7 Hz, 1H), 3.11 (dd, *J* = 13.0, 3.6 Hz, 1H), 2.95 (dd, *J* = 12.9, 10.5 Hz, 1H), 2.84 (ddd, *J* = 22.4, 13.8, 7.4 Hz, 2H); ^{13}C NMR (100 MHz, cd_3od) δ 158.75, 145.23, 145.19, 142.62, 142.59, 138.36, 130.31, 129.65, 128.78, 128.14, 128.10, 127.88, 126.23, 126.04, 120.92, 67.88, 52.59, 44.37, 39.51; HRMS (ESI): *m/z* calcd for $C_{24}H_{25}N_2O_2$: 373.1911 $[M–Cl]^+$, found: 373.1955; RP-HPLC analysis 5% to 95% MeCN in 10 min, T_R = 7.5 min.

Synthesis of the diamine monomer FmocNH-vGly-NH_2.TFA (5)

Preparation of *N*-tritylethane-1,2-diamine (**e**)

Ethylenediamine (96 mL, 1.435 mol, 8 equiv) was dissolved in 1.75 L of DCM and cooled to 0 °C. Trityl chloride (TrCl) (50 g, 179 mmol, 1 equiv) was dissolved in 250 mL of DCM and added dropwise to diethylenetriamine solution at 0 °C. After 2 h, the mixture was slowly warmed to room temperature and stirred for an additional 3 h. After 5 h reaction time, the mixture was concentrated under reduced pressure to 0.5 L and washed with 3 × 500 mL $NaHCO_3$ saturated aqueous solution. The organic layer was dried over $MgSO_4$, filtered, and evaporated under reduced pressure to give **e** as colorless oil in quantitative yield (54.2 g, 179 mmol): ^{1}H NMR (400 MHz, $cdcl_3$) δ 7.56 – 7.48 (m, 5H), 7.32 – 7.26 (m, 5H), 7.22 – 7.17 (m, 2H), 5.28 (s, 1H), 2.81 (t,

J = 6.0 Hz, 2H), 2.23 (t, *J* = 6.0 Hz, 2H); ^{13}C NMR (100 MHz, cdcl$_3$) δ 146.25, 128.81, 128.79, 128.78, 128.77, 128.75, 127.96, 127.90, 126.34, 70.77, 46.65, 42.91.

Preparation of N^1-(((2-(9H-Fluoren-9-yl)methoxy)carbonyl))-N^2-tritylethane-1,2-diamine (**f**)

Compound **e** (54 g, 179 mmol, 1 equiv) was dissolved in DCM (900 mL, 0.2 M) and *N*,*N*-Diisopropylethylamine (DIEA) (62.4 mL, 2 equiv) was added. The resulting suspension was cooled to 0°C and fluorenyl chloroformate (FmocCl) (1 eq) was added. The reaction mixture was stirred 24h at room temperature and then the reaction mixture was washed with water, 5% citric acid and brine. The organic layer was dried over $MgSO_4$, filtered, and evaporated under reduced pressure to give **f** as white powder in quantitative yield (86.2 g, 164 mmol, 82%): ^{1}H NMR (400 MHz, cdcl$_3$) δ 7.77 (d, *J* = 7.5 Hz), 7.61 (d, *J* = 7.2 Hz), 7.46 (d, *J* = 7.5 Hz), 7.40 (t, *J* = 7.4 Hz), 7.33 – 7.23 (m), 7.19 (t, *J* = 7.3 Hz), 5.06 (s), 4.42 (d, *J* = 7.0 Hz), 4.24 (t, *J* = 6.8 Hz), 3.32 (d, *J* = 5.5 Hz), 2.31 (t, *J* = 5.5 Hz); ^{13}C NMR (100 MHz, cdcl$_3$) δ 156.67, 145.89, 144.12, 141.44, 128.83, 128.67, 128.04, 127.93, 127.81, 127.38, 127.19, 126.54, 125.16, 120.11, 70.85, 66.84, 47.43, 43.81, 41.87.

Preparation of Fmoc-Glycine amine trifluoroacetate Salt (FmocNH-*v*Gly-NH_2.TFA) (**5**)

To a solution of **f** (86 g, 164 mmol, 1 equiv) in 5% Trifluoroacetic Acid (TFA) in DCM (600 mL, 0.1 M) stirred at 0'C was added Triethylsilane (52.4 mL, 2 equiv). The solution was stirred at r.t for 1h and toluene was added; the contents were concentrated *in vacuo*, precipitated and deeply washed with cold Et_2O. The precipitate powder was filtered and dry *in vacuo* to yield compound **5** as white powder (Yield: 56.8g, 150 mmol, 91%): ^{1}H NMR (400 MHz, cd$_3$od) δ 7.82 (d, *J* = 7.6 Hz, 2H), 7.67 (d, *J* = 7.5 Hz, 2H), 7.42 (t, *J* = 7.5 Hz, 2H), 7.34 (t, *J* = 7.4 Hz, 2H), 4.49 – 4.40 (m, 2H), 4.24 (t, *J* = 6.6 Hz, 1H), 3.43 – 3.36 (m, 2H), 3.05 (t, *J* = 5.8 Hz, 2H); ^{13}C NMR (100 MHz, cd$_3$od) δ 157.95, 143.81, 141.23, 127.39, 126.70, 124.64, 119.53, 66.56, 46.96, 39.72, 38.01; HRMS (ESI): *m/z* calcd for $C_{24}H_{25}N_2O_2$: 283.1441 $[M–CF_3COO^-]^+$, found: 283.1462; RP-HPLC analysis 5% to 95% MeCN in 10 min, T_R = 6.3 min.

Synthesis of the diamine monomers FmocNH-(S)*v*COO(Allyl)-NH_2.HCl (6) and FmocNH-(R)*v*COO(Allyl)-NH_2.HCl (7)

General Procedure for the preparation of compounds **g(1-2).**

To a solution of Fmoc-Asn-OH (10 g, 28.2 mmol, 1 equiv) in a mixture of DMF-water (3/1, v/v, 280 mL, 0.1 M) was added bis(trifluoroacetoxy)iodobenzene (IBFTA) (13.35 g, 31 mmol, 1.1 equiv) at 0°C. The reaction was stirred for 10 min at this temperature and pyridine (7.75 mL, 95.8 mmol, 3.0 eq) was added at 0°C. After being stirred for 24 h at room temperature, the reaction mixture was concentrated under reduced pressure. To the residue was added water

(100 mL) and the pH was adjusted to 6 with 4N NaOH. After one hour at 0°C a precipitation was observed. The product was filtered and washed with $NaHCO_3$, H_2O, EtOH, Et_2O and dried under reduced pressure.

(2S)-3-amino-2-(((9H-fluoren-9-ylmethoxy)carbonyl)amino)propanoic acid hydrochloride (**g1**)

Compound **g1** was prepared from Fmoc-L-Asn-OH and isolated as a white solid (Yield: 6.83 g, 18.82 mmol, 66.7%). TFA addition was required for the dissolution in DMSO and NMR analysis. ^{1}H NMR (400 MHz, dmso) δ 13.26 (bs, 1H), 8.10 (bs, 3H), 7.90 (d, *J* = 7.5 Hz, 2H), 7.76 (dd, *J* = 20.7, 7.9 Hz, 3H), 7.43 (t, *J* = 7.4 Hz, 2H), 7.34 (t, *J* = 7.4 Hz, 2H), 4.45 – 4.16 (m, 4H), 3.29 – 3.16 (m, 1H), 3.10 – 2.93 (m, 1H); ^{13}C NMR (100 MHz, dmso) δ 170.81, 156.15, 143.73, 143.69, 140.71, 127.67, 127.10, 125.31, 125.28, 120.13, 65.98, 64.90, 51.77, 46.54, 34.04, 15.17.

(2R)-3-amino-2-(((9H-fluoren-9-ylmethoxy)carbonyl)amino)propanoic acid hydrochloride (**g2**)

Compound **g2** was prepared from Fmoc-D-Asn-OH and isolated as a white solid (Yield: 6.05 g, 16.68 mmol, 59.1%). TFA addition was required for the dissolution in DMSO and NMR analysis. ^{1}H NMR (400 MHz, dmso) δ 7.92 (bs, 3H), 7.88 (d, *J* = 7.5 Hz, 2H), 7.71 (d, *J* = 7.1 Hz, 2H), 7.41 (t, *J* = 7.4 Hz, 2H), 7.32 (t, *J* = 7.4 Hz, 2H), 4.46 – 4.20 (m, 4H), 3.32 – 3.18 (m, 1H), 3.11 – 2.96 (m, 1H). ^{13}C NMR (100 MHz, dmso) δ 171.30, 156.71, 144.19, 144.14, 141.21, 128.02, 127.45, 125.59, 120.46, 66.32, 52.20, 47.00.

General Procedure for the preparation of compounds **6**-**7**.

To a stirred suspension of compound **g** (1 equiv) in allylalcohol (Allyl-OH) (0.15 M) under argon conditions was added dropwise chlortrimethylsilane (2.5 equiv) at 0°C. The reaction mixture was warmed to room temperature and stirring was continued for 48 hours. The reaction mixture was filtered with a syringe and added dropwise to cold Et_2O (400 mL) and stirred at 0°C for two hours. The mixture was put in fridge overnight and the precipitate was filtered and dried under reduced pressure to afford the product.

(2S)-3-amino-2-(((9H-fluoren-9-ylmethoxy)carbonyl)amino)propanoic acid allyl ester hydrochloride (FmocNH-(S)*v*COO(Allyl)-NH_2.HCl) (**6**)

Compound **6** was prepared from compound **g1** (6.8 g, 18.74 mmol) and isolated as a white powder (Yield: 6.05g, 15.01 mmol, 80.1%). ^{1}H NMR (400 MHz, dmso) δ 8.19 (s, 3H), 7.94 (d, *J* = 8.3 Hz, 1H), 7.90 (d, *J* = 7.5 Hz, 2H), 7.72 (d, *J* = 7.5 Hz, 2H), 7.43 (t, *J* = 7.3 Hz, 2H), 7.34 (td, *J* = 7.4, 1.0 Hz, 2H), 5.96 – 5.82 (m, 1H), 5.31 (dq, *J* = 17.3, 1.7 Hz, 1H), 5.21 (ddd, *J* = 10.6, 2.9, 1.4 Hz, 1H), 4.66 – 4.55 (m, 2H), 4.51 – 4.29 (m, 3H), 4.25 (t, *J* = 6.7 Hz, 1H), 3.24 (dd, *J* = 13.0, 4.6 Hz, 1H), 3.08 (dd, *J* = 13.0, 9.5 Hz, 1H); ^{13}C NMR (100 MHz, dmso) δ 168.98, 156.12,

143.68, 143.63, 140.73, 132.01, 127.66, 127.08, 125.16, 120.14, 117.95, 65.97, 65.57, 51.86, 46.52.

(2R)-3-amino-2-(((9H-fluoren-9-ylmethoxy)carbonyl)amino)propanoic acid allyl ester hydrochloride (FmocNH-(R)*v*COO(Allyl)-NH_2.HCl) (**7**)

Compound **7** was prepared from compound **g2** (6 g, 16.54 mmol) and isolated as a white powder (Yield: 4.94 g, 12.25 mmol, 74.1%).^{1}H NMR (400 MHz, dmso) δ 8.27 (bs), 7.98 (d, *J* = 8.3 Hz), 7.90 (d, *J* = 7.5 Hz), 7.73 (dd, *J* = 7.5, 1.0 Hz), 7.43 (t, *J* = 7.3 Hz), 7.34 (t, *J* = 7.4 Hz), 5.97 – 5.78 (m), 5.31 (dq, *J* = 17.3, 1.7 Hz), 5.26 – 5.19 (m), 4.66 – 4.56 (m), 4.52 – 4.41 (m), 4.41 – 4.29 (m), 4.25 (t, *J* = 6.7 Hz), 3.98 – 3.83 (m), 3.31 – 3.17 (m), 3.16 – 3.01 (m); ^{13}C NMR (100 MHz, dmso) δ 169.03, 156.14, 143.71, 143.67, 140.75, 139.07, 132.05, 127.70, 127.12, 125.26, 125.22, 120.18, 117.97, 113.32, 109.57, 66.01, 65.60, 61.76, 51.89, 46.53.

Synthesis of the diacid monomers OH-*s*Ala-O*t*Bu (9) and OH-*s*Phe-O*t*Bu (10)

The diacid monomers **9-10** were prepared through protocols presented in literature.[145] Analytical data were in accordance with the previously reported.

(S)-4-(*tert*-Butoxy)-2-methyl-4-oxobutanoic acid (OH-*s*Ala-O*t*Bu) (**9**)

Compound **9** was prepared from (4R)-4-Benzyl-1,3-Oxazolidin-2-one (20 g, 113 mmol) and isolated as a white powder (Overall Yield: 15.06 g, 80 mmol, 71%); ^{1}H NMR (400 MHz, cdcl$_3$) δ 2.95 – 2.84 (m), 2.64 (ddd, *J* = 16.4, 8.1, 0.6 Hz), 2.40 – 2.33 (m), 1.44 (s), 1.24 (d, *J* = 7.2 Hz); ^{13}C NMR (100 MHz, cdcl$_3$) δ 181.26, 171.14, 81.18, 38.83, 35.94, 28.15, 16.85.

(R)-4-(*tert*-Butoxy)-4-oxo-2-(1-phenylmethyl)butanoic acid (OH-*s*Phe-O*t*Bu) (**10**)

Compound **10** was prepared from (4R)-4-Benzyl-1,3-Oxazolidin-2-one (20 g, 113 mmol) and isolated as a white powder (Overall Yield: 19.12 g, 72.3 mmol, 64%); ^{1}H NMR (400 MHz, cdcl$_3$) δ 7.34 – 7.27 (m, 2H), 7.26 – 7.14 (m, 3H), 3.16 – 3.03 (m, 2H), 2.77 (dd, *J* = 15.4, 10.5 Hz, 1H), 2.56 (dd, *J* = 16.9, 8.7 Hz, 1H), 2.36 (dd, *J* = 16.9, 4.6 Hz, 1H), 1.42 (s, 9H); ^{13}C NMR (100 MHz, cdcl$_3$) δ 178.74, 171.15, 138.21, 129.22, 128.75, 126.90, 81.34, 43.00, 37.50, 36.26, 28.16.

Synthesis of the diacid monomer OH-(S)*s*NH(Alloc)-O*t*Bu (13)

Preparation of L-Asp(*t*Bu)-OH (**h**)

Fmoc-L-Asp(*t*Bu)-OH (30.0 g, 72.9 mmol, 1.0 eq) was dissolved in Pip-DBU-DMF (1/1/48 v/v, 242.6 mL, 0.3 M) and the reaction mixture was stirred at room temperature for 3 h. The reaction mixture was reduced under reduced pressure. The residue was dissolved with a minimal volume of DMF and precipitate by addition to cold Et_2O. The precipitate was filtered, dried under reduced pressure, dissolved with water and lyophilized to afford compound **h** as white needles (Overall Yield: 8.28 g, 43.7 mmol, 60%): ^{1}H NMR (400 MHz, D_2O) δ 3.96 (t, *J* = 5.5 Hz, 1H), 2.91 (d, *J* = 5.5 Hz, 2H), 1.46 (s, 9H); ^{13}C NMR (100 MHz, D_2O) δ 172.94, 171.12, 83.91, 35.67, 27.14.

Preparation of Alloc-L-Asp(*t*Bu)-OH (OH-(S)*s*NH(Alloc)-O*t*Bu) (**13**)

To an ice-cooled solution of compound **h** (9.0 g, 47.8 mmol, 1.0 eq) in aqueous NaOH (3.8 g, 96.0 mmol, 2.0 eq, in 159 mL water) allylchloroformate (5.1 mL, 5.8 g, 47.8 mmol, 1.0 eq) was added dropwise within 20 minutes. The reaction mixture was stirred at this temperature for 30 minutes, allowed to get to room temperature and stirred for further 15 minutes. The reaction mixture was washed with diethyl ether (50 mL) and the aqueous layer was acidified at 0°C to pH 2 with 6N HCl. The precipitate was extracted with DCM (300mL) and dried over $MgSO_4$, filtered and concentrated under reduced pressured to yield compound 13 as colorless oil (Yield: 10.1 g,

36.6 mmol, 77%): ^{1}H NMR (400 MHz, cdcl$_3$) δ 8.29 (s, 1H), 5.99 – 5.83 (m, 1H), 5.76 (d, *J* = 8.6 Hz, 1H), 5.38 – 5.28 (m, 1H), 5.22 (dq, *J* = 10.5, 1.3 Hz, 1H), 4.68 – 4.55 (m, 3H), 2.97 (dd, *J* = 17.1, 4.5 Hz, 1H), 2.76 (dd, *J* = 17.1, 4.8 Hz, 1H), 1.44 (s, 9H); ^{13}C NMR (100 MHz, cdcl$_3$) δ 175.89, 170.37, 156.11, 132.55, 118.12, 82.43, 66.22, 50.38, 37.74, 28.14.

Synthesis of the diacid monomer OH-(S)*s*OH-OBn (14)

The diacid monomer **14** was prepared through protocols presented in literature.[151] Analytical data were in accordance with the previously reported.

Synthesis of 2-(2,2-Dimethyl-5-oxo-1,3-dioxolan-4-yl)acetic Acid (**i**).

To a mixture of L-malic acid (20 g, 0.15 mol, 1 equiv) and 2,2-dimethoxypropane (2,2-DMP) (74 mL, 0.60 mol, 4 equiv) under argon was added *p*-toluenesulfonic acid monohydrate (0.29 g, 1.5 mmol, 1 equiv), and the solution was stirred at room temperature for 3.5 h. $NaHCO_3$ saturated aqueous solution (100mL) was added to the reaction mixture, the aqueous layer was separated and extracted with DCM (5×100mL). The combined organic layers were dried with Na_2SO_4 and filtered, and the solvent was removed under reduced pressure. The resulting solid was recrystallized from Et_2O, yielding compound **i** as white solid (15.33 g, 149 mmol, 59%): ^{1}H NMR (400 MHz, cdcl$_3$) δ 4.71 (dd, *J* = 6.6, 3.8 Hz, 1H), 2.99 (dd, *J* = 17.3, 3.8 Hz, 1H), 2.86 (dd, *J* = 17.3, 6.6 Hz, 1H), 1.62 (s, 3H), 1.57 (s, 3H); ^{13}C NMR (100 MHz, cdcl$_3$) δ 174.97, 171.91, 111.47, 70.47, 36.08, 26.84, 25.91.

Synthesis of 2-(2,2-Dimethyl-5-oxo-1,3-dioxolan-4-yl)acetic Acid Benzyl Ester (**l**)

To a solution of **i** (15.3 g, 88 mmol, 1 equiv) in dry acetone under argon was added dry NEt_3 (14.69 mL, 105 mmol, 1.2 equiv) followed by benzyl bromide (11.49 mL, 97 mmol, 1.1 equiv). The solution was refluxed for 60 h at 50 °C before being cooled to room temperature. The solids were removed by filtration and washed with acetone before the volatile organic solvents were removed under reduced pressure. The residue was dissolved in EtOAc (400 mL) and H_2O (200 mL). The aqueous layer was further extracted with EtOAc (2 × 200 mL) before the combined organic layers were dried with $MgSO_4$, filtered, and reduced in vacuo. The resultant solid was recrystallized from Et_2O to afford compound **l** as white crystals (14.39 g, 54.5 mmol, 62%): ^{1}H NMR (400 MHz, cdcl$_3$) δ 7.41 – 7.29 (m), 5.18 (d, *J* = 2.1 Hz, 5H), 4.74 (dd, *J* = 6.5, 3.9 Hz, 2H), 2.98 (dd, *J* = 17.0, 3.9 Hz, 1H), 2.85 (dd, *J* = 17.0, 6.5 Hz, 1H), 1.58 (s, 3H), 1.56 (s, 3H) ; ^{13}C NMR (100 MHz, cdcl$_3$) δ 172.10, 169.16, 135.42, 128.73, 128.56, 128.48, 111.31, 70.78, 67.15, 36.41, 26.83, 25.99.

Synthesis of 2-Hydroxysuccinic Acid 4-Benzyl Ester (OH-(S)*s*OH-OBn) (**14**)

A solution of **l** (14.35 g, 54.3 mmol, 1 equiv) was dissolved in AcOH/THF/H2O (1:1:1) (260 mL) and heated for 24 h at 40 °C. The solvent was removed under reduced pressure, and the resulting colorless oil was freeze-dried to give compound **14** as white solid in quantitative yield (12.17 g, 54.3 mmol, quant): ^{1}H NMR (400 MHz, cdcl$_3$) δ 7.42 – 7.29 (m, 5H), 5.22 – 5.13 (m, 2H), 4.61 – 4.54 (m, 1H), 2.95 (qd, *J* = 17.0, 5.4 Hz, 2H); ^{13}C NMR (100 MHz, cdcl$_3$) δ 171.18, 135.29, 128.81, 128.69, 128.49, 67.36, 67.10, 38.32.

Synthesis of the hydrophobic proteinaceous dimer building blocks FmocNH-*v*Xaa-*s*Xaa-OH (15-18)

General procedure for the synthesis of compounds **m1-4**.

To a solution of the diacid *tert*-butyl mono-ester (**9-10**) (1 equiv) in dryDMF (0.1 M) stirred at 0°C under argon was added PyBOP (1 equiv), HOBt.H$_2$O and DIEA (3 equiv). After 5min the diamine monomer (**1-4)** was added. The solution was stirred at 0 °C for 15min and then allowed to warm to room temperature. After 1h water was added *via* a syringe till the reaction mixture got turbid and then put at 4°C overnight. The precipitated white powder was filtered, washed with water, dissolved with DCM and washed with brine (x3); dried over MgSO$_4$, filtered, and concentrated *in vacuo* to yield a vitreous solid which was precipitated from AcOEt/Hex mixture. The precipitate powder was filtered and dry *in vacuo* to yield compound **m** as white powder.

FmocHN-*v*Val-*s*Ala-O*t*Bu (**m1**)

Compound **m1** was prepared from FmocNH-*v*Val-NH$_2$.HCl (**2**) (7.86g, 21.78 mmol) and OH-*s*Ala-O*t*Bu (**9**) (4.1g, 21.78 mmol) and isolated as white powder (Yield: 9.37g, 18.94 mmol, 87%). ^{1}H NMR (400 MHz, cdcl$_3$) δ 7.76 (d, *J* = 7.5 Hz, 2H), 7.61 (d, *J* = 7.4 Hz, 2H), 7.40 (t, *J* = 7.3 Hz, 2H), 7.32 (td, *J* = 7.4, 0.9 Hz, 2H), 6.18 (b s, 1H), 5.02 (d, *J* = 4.7 Hz, 1H), 4.46 (dd, *J* = 10.6, 7.1 Hz, 1H), 4.35 (dd, *J* = 10.5, 7.1 Hz, 1H), 4.22 (t, *J* = 6.9 Hz, 1H), 3.61 – 3.48 (m, 1H), 3.47 – 3.23 (m, 2H), 2.67 – 2.54 (m, 2H), 2.26 (dd, *J* = 16.0, 5.1 Hz, 1H), 1.83 – 1.74 (m, 1H), 1.39 (s, 9H), 1.14 (d, *J* = 6.7 Hz, 3H), 0.95 (dd, *J* = 14.7, 6.8 Hz, 6H); ^{13}C NMR (100 MHz, cdcl$_3$) δ 176.12, 171.96, 157.17, 144.06, 144.04, 141.46, 127.82, 127.19, 125.26, 125.19, 120.09, 120.09, 80.92, 66.88, 57.25, 47.43, 41.93, 39.52, 37.22, 30.68, 28.17, 19.40, 18.47, 17.49; HRMS (ESI): *m/z* calcd for $C_{29}H_{38}N_2NaO_5$: 517.2673 $[M+Na]^+$, found: 517.2700.

FmocHN-*v*Leu-*s*Ala-O*t*Bu (**m2**)

Compound **m2** was prepared from FmocNH-*v*Leu-NH$_2$.HCl (**3**) (7.37g, 19.66 mmol) and OH-*s*Ala-O*t*Bu (**9**) (3.7g, 19.66 mmol) and isolated as white powder (Yield: 9.10g, 17.89 mmol, 91%). ^{1}H NMR (400 MHz, cdcl$_3$) δ 7.72 (d, *J* = 7.5 Hz, 2H), 7.57 (dd, *J* = 7.5, 0.7 Hz, 2H), 7.35 (t, *J* = 7.3 Hz, 2H), 7.27 (t, *J* = 7.4 Hz, 2H), 6.58 (t, *J* = 5.0 Hz, 1H), 5.40 (d, *J* = 8.6 Hz, 1H), 4.43

(dd, *J* = 10.5, 7.2 Hz, 1H), 4.31 (dd, *J* = 10.4, 7.1 Hz, 1H), 4.17 (t, *J* = 6.8 Hz, 1H), 3.89 – 3.72 (m, 1H), 3.38 – 3.18 (m, 2H), 2.68 – 2.58 (m, 2H), 2.25 (dd, *J* = 15.4, 4.9 Hz, 1H), 1.69 – 1.58 (m, 1H), 1.37 (s, 9H), 1.28 – 1.22 (m, 1H), 1.13 (d, *J* = 6.5 Hz, 3H), 0.77 (d, *J* = 23.8 Hz, 6H); ^{13}C NMR (100 MHz, cdcl$_3$) δ 175.90, 171.74, 156.70, 143.89, 143.86, 141.23, 127.61, 126.96, 125.06, 125.00, 119.89, 80.56, 66.49, 49.84, 47.22, 44.18, 41.69, 39.24, 37.09, 27.99, 24.72, 23.00, 22.12, 17.51; HRMS (ESI): *m/z* calcd for $C_{30}H_{41}N_2O_5$: 509.3010 $[M+H]^+$, found: 509.3032.

FmocHN-*v*Val-*s*Phe-O*t*Bu (**m3**)

Compound **m3** was prepared from FmocNH-*v*Val-NH$_2$.HCl (**2**) (7.65g, 21.19 mmol) and OH-*s*Phe-O*t*Bu (**10**) (5.6g, 21.19 mmol) and isolated as white powder (Yield: 11.25g, 19.70 mmol, 93%). ^{1}H NMR (400 MHz, cdcl$_3$) δ 7.72 (d, *J* = 7.5 Hz, 2H), 7.59 (d, *J* = 7.4 Hz, 2H), 7.35 (t, *J* = 7.4 Hz, 2H), 7.27 (t, *J* = 7.4 Hz, 2H), 7.21 – 7.16 (m, 2H), 7.15 – 7.09 (m, 3H), 6.26 (b s, 1H), 5.22 (d, *J* = 8.5 Hz, 1H), 4.46 (dd, *J* = 10.4, 7.1 Hz, 1H), 4.27 (dd, *J* = 10.4, 7.1 Hz, 1H), 4.18 (t, *J* = 6.9 Hz, 1H), 3.41 – 3.11 (m, 3H), 2.91 (dd, *J* = 12.5, 8.6 Hz, 1H), 2.87 – 2.76 (m, 1H), 2.74 – 2.57 (m, 2H), 2.34 (dd, *J* = 16.8, 5.2 Hz, 1H), 1.58 – 1.48 (m, 1H), 1.36 (s, 9H), 0.84 (dd, *J* = 15.4, 6.7 Hz, 6H); ^{13}C NMR (100 MHz, cdcl$_3$) δ 174.46, 171.45, 156.60, 143.85, 143.79, 141.13, 138.93, 128.94, 128.84, 128.28, 127.49, 126.87, 126.34, 126.25, 125.03, 124.91, 119.77, 80.55, 66.32, 60.19, 56.88, 47.11, 44.86, 40.97, 38.11, 37.40, 29.61, 27.85, 19.18, 18.21; HRMS (ESI): *m/z* calcd for $C_{35}H_{43}N_2O_5$: 571.3166 $[M+H]^+$, found: 571.3173.

FmocHN-*v*Leu-*s*Phe-O*t*Bu (**m4**)

Compound **m4** was prepared from FmocNH-*v*Leu-NH$_2$.HCl (**3**) (7.37g, 19.67 mmol) and OH-*s*Phe-O*t*Bu (**10**) (5.2g, 19.67 mmol) and isolated as white powder (Yield: 11.04g, 18.88 mmol, 96%). ^{1}H NMR (400 MHz, cdcl$_3$) δ 7.78 (d, *J* = 7.5 Hz, 2H), 7.62 (t, *J* = 6.5 Hz, 2H), 7.40 (t, *J* = 7.2 Hz, 2H), 7.33 (tdd, *J* = 9.6, 6.9, 2.9 Hz, 2H), 7.23 – 7.15 (m, 3H), 7.15 – 7.11 (m, 2H), 5.72 (b s, 1H), 4.59 (d, *J* = 7.8 Hz, 1H), 4.51 (dd, *J* = 10.7, 6.6 Hz, 1H), 4.38 (dd, *J* = 10.5, 6.6 Hz, 1H), 4.21 (t, *J* = 6.5 Hz, 1H), 3.64 – 3.43 (m, 1H), 3.36 – 3.22 (m, 1H), 3.16 – 3.05 (m, 1H), 2.91 – 2.82 (m, 1H), 2.80 – 2.63 (m, 3H), 2.37 (dd, *J* = 16.6, 4.2 Hz, 1H), 1.58 – 1.46 (m, 1H), 1.41 (d, *J* = 4.4 Hz, 9H), 1.22 – 1.11 (m, 1H), 1.04 (ddd, *J* = 13.8, 8.2, 5.6 Hz, 1H), 0.85 (dd, *J* = 9.8, 6.7 Hz, 6H); ^{13}C NMR (100 MHz, cdcl$_3$) δ 174.37, 171.78, 156.28, 144.19, 144.03, 141.51, 141.47, 139.27, 129.28, 129.15, 128.66, 128.47, 127.78, 127.17, 127.11, 126.63, 125.24, 125.14, 120.06, 120.04, 81.00, 66.26, 49.90, 47.54, 45.46, 43.50, 41.19, 38.53, 37.79, 28.21, 28.19, 24.78, 23.02, 22.17; HRMS (ESI): *m/z* calcd for $C_{36}H_{45}N_2O_5$: 585.3323 $[M+H]^+$, found: 585.3325.

General procedure for the preparation of compounds (**15-18**).

To a solution of **m** (1 equiv) in 70:30 (v/v) DCM/TFA (0.1 M) stirred at 0'C was added Triethylsilane Et_3SiH (4 equiv). The solution was stirred at r.t till TLC revelead completion of the reaction (approximately 3.5h) and toluene was added; the contents were concentrated *in vacuo*, precipitated and deeply washed with cold Et_2O. The filtrate was evaporated *in vacuo* to afford the product.

FmocHN-*v*Val-*s*Ala-OH (**15**)

Compound **15** was prepared from **m1** (9.37g, 18.94 mmol) and isolated as white powder (Yield: 7.39g, 16.85 mmol, 89%). ^{1}H NMR (400 MHz, dmso) δ 12.04 (b s, 1H), 7.89 (d, *J* = 7.6 Hz, 2H), 7.76 (t, *J* = 5.6 Hz, 1H), 7.71 (dd, *J* = 7.1, 5.1 Hz, 2H), 7.41 (t, *J* = 7.4 Hz, 2H), 7.32 (tt, 2H), 6.99 (d, *J* = 9.4 Hz, 1H), 4.36 – 4.30 (m, 1H), 4.26 – 4.19 (m, 2H), 3.44 – 3.39 (m, 1H), 3.26 – 3.18 (m, 1H), 3.03 – 2.94 (m, 1H), 2.67 – 2.60 (m, 1H), 2.49 – 2.44 (m, 1H), 2.16 (dd, *J* = 16.3, 6.6 Hz, 1H), 1.75 – 1.64 (m, 1H), 0.99 (d, *J* = 7.0 Hz, 3H), 0.80 (dd, 6H); ^{13}C NMR (100 MHz, dmso) δ 174.67, 173.15, 156.17, 143.99, 143.81, 140.71, 127.57, 127.01, 125.21, 120.07, 65.19, 55.54, 46.81, 40.44, 37.54, 35.86, 29.28, 19.48, 17.84, 17.80; HRMS (ESI): *m/z* calcd for $C_{25}H_{31}N_2O_5$: 439.2227 $[M+H]^+$, found: 439.2258;RP-HPLC analysis 5% to 95% MeCN in 10 min + 95% MeCN for 4 min, T_R = 8.5 min.

FmocHN-*v*Leu-*s*Ala-OH (**16**)

Compound **16** was prepared from **m2** (9.10g, 17.89 mmol) and isolated as white powder (Yield: 7.37g, 16.28 mmol, 91%). ^{1}H NMR (400 MHz, dmso) δ 12.03 (b s, 1H), 7.89 (d, *J* = 7.5 Hz, 2H), 7.84 (t, *J* = 5.8 Hz, 1H), 7.69 (dd, *J* = 7.3, 4.2 Hz, 2H), 7.41 (t, *J* = 7.4 Hz, 2H), 7.32 (tdd, *J* = 7.4, 2.5, 0.9 Hz, 2H), 7.00 (d, *J* = 9.0 Hz, 1H), 4.36 – 4.18 (m, 3H), 3.65 – 3.51 (m, 1H), 3.18 – 3.03 (m, 1H), 2.98 – 2.86 (m, 1H), 2.69 – 2.57 (m, 1H), 2.49 – 2.43 (m, 1H), 2.16 (dd, *J* = 16.3, 6.5 Hz, 1H), 1.61 – 1.47 (m, 1H), 1.31 – 1.20 (m, 1H), 1.20 – 1.12 (m, 1H), 1.00 (d, *J* = 7.0 Hz, 3H), 0.83 (dd, *J* = 15.5, 6.6 Hz, 6H); ^{13}C NMR (100 MHz, dmso) δ 174.66, 173.13, 155.78, 144.01, 143.79, 140.72, 140.71, 127.56, 127.00, 126.97, 125.15, 120.08, 120.07, 65.03, 48.69, 46.84, 43.01, 40.79, 37.52, 35.89, 24.21, 23.29, 21.76, 17.90; HRMS (ESI): *m/z* calcd for $C_{26}H_{32}N_2O_5$: 453.2384 $[M+H]^+$, found: 453.2429; RP-HPLC analysis 5% to 95% MeCN in 10 min + 95% MeCN for 4 min, T_R = 9.0 min.

FmocHN-*v*Val-*s*Phe-OH (**17**)

Compound **17** was prepared from **m3 (**11.25g, 19.70 mmol) and isolated as white powder (Yield: 9.12g, 17.73 mmol, 90%). ^{1}H NMR (400 MHz, dmso) δ 12.07 (b s, 1H), 7.88 (d, *J* = 5.3 Hz, 1H), 7.84 (t, *J* = 5.7 Hz, 1H), 7.69 (t, 2H), 7.41 (t, *J* = 7.5 Hz, 2H), 7.31 (td, *J* = 7.4, 0.6 Hz, 1H), 7.26 – 7.22 (m, 2H), 7.19 – 7.14 (m, 3H), 6.92 (d, *J* = 9.4 Hz, 1H), 4.36 – 4.28 (m, 1H), 4.25 – 4.18

(m, 2H), 3.40 – 3.34 (m, 1H), 3.24 – 3.15 (m, 1H), 3.00 – 2.91 (m, 1H), 2.89 – 2.79 (m, 2H), 2.54 (dd, *J* = 12.5, 6.8 Hz, 1H), 2.46 (d, *J* = 8.5 Hz, 1H), 2.14 – 2.06 (m, 1H), 1.62 – 1.49 (m, 1H), 0.77 (dd, *J* = 9.5, 6.8 Hz, 3H); ^{13}C NMR (100 MHz, dmso) δ 173.32, 173.05, 156.13, 144.00, 143.78, 140.70, 139.27, 128.87, 128.13, 127.56, 127.00, 126.07, 125.19, 120.06, 65.20, 55.38, 46.80, 43.25, 40.43, 37.88, 35.43, 28.81, 19.53, 17.52; HRMS (ESI): *m/z* calcd for $C_{31}H_{34}N_2O_5$: 515.2540 $[M+H]^+$, found: 515.2598; RP-HPLC analysis 5% to 95% MeCN in 10 min + 95% MeCN for 4 min, T_R = 9.5 min.

FmocHN-*v*Leu-*s*Phe-OH (**18**)

Compound **18** was prepared from **m4** (11.04g, 18.88 mmol) and isolated as white powder (Yield: 9.28g, 17.55 mmol, 93%). ^{1}H NMR (400 MHz, dmso) δ 12.05 (b s, 1H), 7.93 (t, *J* = 5.6 Hz, 1H), 7.88 (d, *J* = 7.5 Hz, 2H), 7.67 (t, *J* = 7.9 Hz, 2H), 7.41 (t, *J* = 7.4 Hz, 2H), 7.31 (t, *J* = 7.4 Hz, 2H), 7.24 (t, 2H), 7.19 – 7.14 (m, 3H), 6.91 (d, *J* = 9.0 Hz, 1H), 4.36 – 4.18 (m, 3H), 3.60 – 3.50 (m, 1H), 3.13 – 3.03 (m, 1H), 2.95 – 2.81 (m, 3H), 2.54 (dd, *J* = 14.5, 8.9 Hz, 1H), 2.46 (d, *J* = 8.4 Hz, 1H), 2.09 (dd, *J* = 16.7, 4.6 Hz, 1H), 1.56 – 1.45 (m, 1H), 1.26 – 1.12 (m, 1H), 1.09 – 1.02 (m, 1H), 0.80 (dd, *J* = 21.8, 6.5 Hz, 6H);^{13}C NMR (100 MHz, dmso): δ 173.32, 173.03, 155.74, 144.02, 143.76, 140.72, 139.34, 128.87, 128.16, 127.55, 126.99, 126.09, 125.12, 120.08, 65.04, 48.61, 46.83, 43.24, 43.08, 40.58, 37.88, 35.38, 24.14, 23.26, 21.65; HRMS (ESI): *m/z* calcd for $C_{32}H_{37}N_2O_5$: 529.2697 $[M+Na]^+$, found: 529.2730; RP-HPLC analysis 5% to 95% MeCN in 10 min + 95% MeCN for 4 min, T_R = 9.9 min.

Synthesis of the dimer building blocks presenting *s*Gly as β-diacid unit (19-23)

General procedure for the synthesis of compounds **19-23**.

To a solution of the diamine monomer (**1-6**, 1 equiv) in dryDMF (0.1 M) stirred at 0 °C under Ar was added Succinic anhydride (Suc, **8**) (1 eq.) and DIEA (3 equiv). The solution was stirred at 0 °C for 15min and then allowed to warm to room temperature. After 1h water was added via a syringe till the reaction mixture got turbid and then stored at 4°C overnight. The white precipitated powder was filtered, washed with water, dissolved with DCM and washed with 5% HCl(aq) (x3); dried over $MgSO_4$, filtered, and concentrated *in vacuo* to yield a vitreous solid which was precipitated from $CHCl_3$/Hex mixture. The precipitate powder was filtered and dry *in vacuo* to yield compounds **19-23**.

FmocHN-*v*Ala-*s*Gly-OH (**19**).

Compound **19** was prepared from **1** (3.5g, 10.52 mmol) and isolated as white powder (Yield: 3.42g, 8.62 mmol, 82%). ^{1}H NMR (400 MHz, dmso): δ 12.04 (bs, 1H), 7.89 (d, *J* = 7.5 Hz, 2H), 7.85 (t, *J* = 5.9 Hz, 1H), 7.69 (dd, *J* = 7.3, 2.4 Hz, 2H), 7.41 (td, *J* = 7.4, 0.5 Hz, 2H), 7.33 (tt, *J* =

7.4, 0.9 Hz, 2H), 7.12 (d, *J* = 8.2 Hz, 1H), 4.34 – 4.25 (m, 2H), 4.24 – 4.18 (m, 1H), 3.62 – 3.52 (m, 1H), 3.05 (t, *J* = 6.1 Hz, 2H), 2.45 – 2.39 (m, 2H), 2.31 (t, *J* = 7.1 Hz, 2H), 0.99 (d, *J* = 6.6 Hz, 3H); ^{13}C NMR (100 MHz, dmso) δ 173.76, 171.17, 155.46, 143.93, 143.85, 140.71, 127.58, 127.03, 125.13, 120.09, 65.19, 46.74, 46.41, 43.53, 30.03, 29.14, 18.11.

FmocHN-(*v*Leu-*s*Gly-OH (**20**).

Compound **20** was prepared from **3** (8g, 21.34 mmol) and isolated as white powder (Yield: 7.86g, 17.92 mmol, 84%). ^{1}H NMR (400 MHz, dmso) δ 11.97 (b s, 1H), 7.89 (d, *J* = 7.5 Hz, 2H), 7.79 – 7.60 (m, 3H), 7.41 (t, *J* = 7.4 Hz, 2H), 7.32 (td, *J* = 7.4, 3.1 Hz, 2H), 7.02 (d, *J* = 9.1 Hz, 1H), 4.49 – 3.99 (m, 3H), 3.48 – 3.38 (m, 1H), 3.26 – 3.16 (m, 1H), 3.09 – 2.97 (m, 1H), 2.40 (t, *J* = 7.0 Hz, 2H), 2.30 (t, *J* = 6.8 Hz, 2H), 1.53 – 1.25 (m, 2H), 1.09 – 0.99 (m, 1H), 0.86 – 0.71 (m, 6H); ^{13}C NMR (100 MHz, dmso) δ 173.79, 171.08, 155.80, 144.01, 143.79, 140.72, 127.56, 127.00, 126.98, 125.17, 120.08, 120.07, 65.05, 48.76, 46.84, 43.10, 40.81, 30.09, 29.21, 24.22, 23.27, 21.74; *m/z* (ESI-HRMS) found $[M + H]^+$, 439.2242 $C_{25}H_{31}N_2O_5$ requires $[M + H]^+$, 439.2233; RP-HPLC analysis 5% to 95% MeCN in 10 min + 95% MeCN for 4 min, T_R = 8.7 min.

FmocHN-*v*Phe-*s*Gly-OH (**21**).

Compound **21** was prepared from **4** (4g, 9.78 mmol) and isolated as white powder (Yield: 4.46g, 9.43 mmol, 96%). ^{1}H NMR (400 MHz, dmso) δ 12.05 (bs, 1H), 7.92 (t, *J* = 5.8 Hz, 1H), 7.88 (d, *J* = 7.6 Hz, 1H), 7.62 (d, *J* = 7.5 Hz, 1H), 7.41 (t, *J* = 7.4 Hz, 1H), 7.35 – 7.12 (m, 5H), 4.26 – 4.10 (m, 2H), 3.76 – 3.64 (m, 1H), 3.25 – 3.14 (m, 1H), 3.11 – 3.01 (m, 1H), 2.76 (dd, *J* = 13.7, 4.9 Hz, 1H), 2.64 – 2.55 (m, 1H), 2.47 – 2.40 (m, 1H), 2.36 – 2.28 (m, 1H); ^{13}C NMR (100 MHz, dmso) δ 173.82, 171.24, 155.57, 143.79, 140.66, 138.91, 129.12, 128.01, 127.56, 127.00, 125.91, 125.14, 120.06, 65.21, 52.40, 46.68, 30.08, 29.16.

FmocHN-*v*Gly-*s*Gly-OH (**22**).

Compound **22** was prepared from **5** (10g, 31.4 mmol) and isolated as white powder (Yield: 10.98g, 28.7 mmol, 92%). ^{1}H NMR (400 MHz, dmso) δ 11.91 (bs, 1H), 7.92 – 7.84 (m, 3H), 7.68 (d, *J* = 7.4 Hz, 2H), 7.41 (t, *J* = 7.4 Hz, 2H), 7.33 (td, *J* = 7.4, 0.9 Hz, 2H), 7.27 (t, *J* = 5.5 Hz, 1H), 4.30 (d, *J* = 6.8 Hz, 2H), 4.21 (t, *J* = 6.8 Hz, 1H), 3.15 – 3.05 (m, 2H), 3.03 (t, *J* = 5.5 Hz, 2H), 2.42 (t, *J* = 6.9 Hz, 2H), 2.30 (t, *J* = 7.0 Hz, 2H); ^{13}C NMR (100 MHz, dmso) δ 143.88, 142.54, 140.71, 139.39, 137.40, 128.91, 127.27, 121.37, 120.01, 109.75, 98.59.

FmocNH-(S)*v*COO(Allyl)-*s*Gly-OH (**23**).

Compound **23** was prepared from **6** (3g, 7.45 mmol) and isolated as white powder (Yield: 3.20g, 6.85 mmol, 92%). ^{1}H NMR (400 MHz, dmso) δ 12.06 (bs, 1H), 7.99 (t, *J* = 5.5 Hz, 1H), 7.90 (d, *J*

= 7.5 Hz, 2H), 7.71 (d, *J* = 7.5 Hz, 2H), 7.42 (t, *J* = 7.4 Hz, 2H), 7.34 (t, *J* = 7.3 Hz, 2H), 5.89 (qd, *J* = 10.4, 5.2 Hz, 1H), 5.30 (d, *J* = 17.3 Hz, 1H), 5.19 (d, *J* = 10.5 Hz, 1H), 4.55 (bs, 2H), 4.40 – 4.26 (m, 2H), 4.27 – 4.15 (m, 2H), 3.54 – 3.40 (m, 1H), 3.40 – 3.24 (m, 2H), 2.40 (t, *J* = 6.9 Hz, 2H), 2.30 (t, *J* = 6.9 Hz, 2H); ^{13}C NMR (100 MHz, dmso) δ 173.70, 171.54, 170.34, 155.94, 143.73, 140.72, 132.33, 127.63, 127.07, 125.16, 120.12, 117.70, 65.76, 65.05, 53.82, 46.58, 29.96, 29.06.

Synthesis of the dimer building blocks FmocNH-*v*Xaa-*s*NH(Boc)-OH (24-32)

General procedure for the synthesis of compounds FmocNH-*v*Xaa-*s*NH(Boc)-OBn **n(1-9)**.

To a solution of Boc-Asp-OBn (**11-12**) (1 equiv) in dryDMF (0.1 M) stirred at 0°C under Ar was added PyBOP (1 equiv), HOBt.H_2O (1 equiv) and DIEA (3 equiv). The solution was stirred at 0 °C for 5min and then the diamine counterpart (**1-5**) was added. The solution was stirred at 0°C for 15min and then allowed to warm to room temperature. After 1h water was added via a syringe till the reaction mixture got turbid and then put at 4°C overnight. The white precipitated powder was filtered, washed with water, dissolved with DCM and washed with brine (x3); dried over $MgSO_4$, filtered, and concentrated *in vacuo* to yield a vitreous solid. The solid was dissolved in $CHCl_3$ and precipitated in Hex at 0°C. The resulting suspension was stored at 4°C for at least 24h. The powder was filtered and dried *in vacuo* to yield compound **n(1-9)**.

FmocHN-*v*Ala-(S)*s*NHBoc-OBn (**n1**):

Compound **n1** was prepared from **1** (10 g, 30.0 mmol) and Boc-L-Asp-OBn (**11**) (9.72 g, 30.0 mmol) and isolated as white powder (Yield: 16.77 g, 27.9 mmol, 93 %). ^{1}H NMR (400 MHz, $cdcl_3$) δ 7.76 (d, *J* = 7.6 Hz, 2H), 7.61 – 7.56 (m, 2H), 7.41 – 7.37 (m, 2H), 7.35 – 7.25 (m, 7H), 6.89 – 6.81 (m, 1H), 5.66 – 5.56 (m, 1H), 5.10 (q, *J* = 12.3 Hz, 2H), 5.06 – 4.98 (m, 1H), 4.50 (bs, 1H), 4.36 (d, *J* = 6.7 Hz, 2H), 4.20 (t, *J* = 6.9 Hz, 1H), 3.85 – 3.78 (m, 1H), 3.41 – 3.34 (m, 1H), 3.30 – 3.24 (m, 1H), 3.06 (dd, *J* = 17.2, 4.3 Hz, 1H), 2.71 (dd, *J* = 17.2, 6.3 Hz, 1H), 1.43 (s, 9H), 1.14 (d, *J* = 6.2 Hz, 3H); ^{13}C NMR (100 MHz, $cdcl_3$) δ 171.95, 171.64, 156.36, 144.11, 144.07, 141.45, 135.46, 128.73, 128.52, 128.41, 127.81, 127.19, 125.24, 120.09, 67.04, 66.89, 50.81, 47.74, 47.37, 45.03, 36.47, 28.44, 18.54; HRMS (ESI): *m/z* calcd for $C_{34}H_{39}N_3NaO_7$: 624.2680 $[M+Na]^+$, found: 624.2729.

FmocHN-*v*Val-(S)*s*NHBoc-OBn (**n2**):

Compound **n2** was prepared from **2** (7 g, 19.40 mmol) and Boc-L-Asp-OBn (**11**) (6.27 g, 19.40 mmol) and isolated as white powder (Yield: 11.6 g, 18.43 mmol, 95%). ^{1}H NMR (400 MHz, $cdcl_3$): δ 7.75 (dd, *J* = 7.5, 2.1 Hz, 2H), 7.58 (t, *J* = 7.4 Hz, 2H), 7.39 (td, *J* = 7.4, 3.4 Hz, 2H), 7.35 – 7.25 (m, 7H), 6.84 – 6.78 (m, 1H), 5.64 – 5.52 (m, 1H), 5.09 (s, 2H), 4.91 (d, *J* = 8.9 Hz,

1H), 4.48 (s, 1H), 4.41 (dd, *J* = 10.4, 7.4 Hz, 1H), 4.32 (dd, *J* = 10.3, 7.3 Hz, 1H), 4.21 (t, *J* = 7.1 Hz, 1H), 3.58 – 3.52 (m, 1H), 3.40 – 3.32 (m, 2H), 3.02 (dd, *J* = 17.2, 3.9 Hz, 1H), 2.67 (dd, *J* = 17.2, 6.4 Hz, 1H), 1.76 (dt, *J* = 13.3, 6.6 Hz, 1H), 1.42 (s, 9H), 0.94 (dd, *J* = 16.6, 6.8 Hz, 6H); ^{13}C NMR (100 MHz, cdcl$_3$) δ 171.97, 171.55, 157.02, 144.15, 144.04, 141.45, 135.47, 128.71, 128.49, 128.40, 127.81, 127.19, 125.29, 125.23, 120.09, 120.07, 67.04, 66.93, 56.95, 50.71, 47.39, 41.92, 36.59, 30.59, 28.43, 19.44, 18.42; HRMS (ESI): *m/z* calcd for $C_{36}H_{44}N_3O_7$: 630.3174 $[M+H]^+$, found: 630.3241.

FmocHN-*v*Leu-(S)*s*NHBoc-OBn (**n3**):

Compound **n3** was prepared from **3** (6 g, 16.0 mmol) and Boc-L-Asp-OBn (**11**) (5.17 g, 16.0 mmol) and isolated as white powder (Yield: 9.69 g, 15.04 mmol, 94%). ^{1}H NMR (400 MHz, cdcl$_3$): δ 7.76 (dd, *J* = 7.5, 0.5 Hz, 2H), 7.59 (dd, *J* = 7.4, 2.5 Hz, 2H), 7.38 (tt, *J* = 5.9, 3.0 Hz, 2H), 7.36 – 7.25 (m, 7H), 6.85 – 6.74 (m, 1H), 5.57 (bs, 1H), 5.13 – 5.04 (m, 2H), 4.78 (d, *J* = 8.6 Hz, 1H), 4.48 (bs, 1H), 4.43 – 4.33 (m, 2H), 4.21 (t, *J* = 6.9 Hz, 1H), 3.84 – 3.74 (m, 1H), 3.42 – 3.34 (m, 1H), 3.30 – 3.21 (m, 1H), 3.04 (dd, *J* = 17.2, 4.3 Hz, 1H), 2.69 (dd, *J* = 17.2, 6.3 Hz, 1H), 1.61 (d, *J* = 16.6 Hz, 3H), 1.43 (s, 9H), 1.34 – 1.21 (m, 2H), 0.91 (dd, *J* = 6.2, 3.5 Hz, 6H); ^{13}C NMR (100 MHz, cdcl$_3$) δ 171.97, 171.39, 156.64, 144.09, 143.99, 141.43, 135.42, 128.70, 128.49, 128.39, 127.78, 127.16, 125.23, 120.07, 120.06, 80.61, 67.00, 66.78, 50.74, 49.77, 47.36, 44.34, 41.76, 36.54, 28.42, 24.89, 23.19, 22.26; HRMS (ESI): *m/z* calcd for $C_{37}H_{46}N_3O_7$: 644.3330 $[M+H]^+$, found: 644.3326.

FmocHN-*v*Phe-(S)*s*NHBoc-OBn (**n4**):

Compound **n4** was prepared from **4** (6 g, 14.67 mmol) and Boc-L-Asp-OBn (**11**) (4.74 g, 14.67 mmol) and isolated as white powder (Yield: 9.27 g, 13.68 mmol, 93%). ^{1}H NMR (400 MHz, cdcl$_3$) δ 7.76 (d, *J* = 7.5 Hz, 2H), 7.54 (t, *J* = 8.4 Hz, 2H), 7.39 (t, *J* = 7.4 Hz, 2H), 7.35 – 7.16 (m, 12H), 6.82 – 6.72 (m, 1H), 5.57 (d, *J* = 7.5 Hz, 1H), 5.19 (d, *J* = 7.9 Hz, 1H), 5.12 – 5.04 (m, 2H), 4.50 (bs, 1H), 4.39 – 4.33 (m, 1H), 4.31 – 4.24 (m, 1H), 4.18 (t, *J* = 7.0 Hz, 1H), 4.02 – 3.93 (m, 1H), 3.47 – 3.39 (m, 1H), 3.34 – 3.25 (m, 1H), 3.09 (dd, *J* = 17.3, 3.9 Hz, 1H), 2.88 (dd, *J* = 13.7, 6.6 Hz, 1H), 2.77 (dd, *J* = 13.7, 7.1 Hz, 1H), 2.69 (dd, *J* = 17.3, 6.1 Hz, 1H), 1.44 (s, 9H); ^{13}C NMR (100 MHz, cdcl$_3$) δ 171.82, 156.36, 144.01, 143.99, 141.41, 140.20, 137.37, 135.37, 129.38, 128.83, 128.72, 128.53, 128.41, 127.80, 127.18, 127.17, 126.93, 126.91, 125.29, 125.27, 120.08, 67.09, 66.90, 53.06, 50.76, 47.29, 42.75, 38.81, 36.41, 28.44; HRMS (ESI): *m/z* calcd for $C_{40}H_{44}N_3O_7$: 678.3174 $[M+H]^+$, found: 678.3248.

FmocHN-*v*Gly-(S)*s*NHBoc-OBn (**n5**):

Compound **n5** was prepared from **5** (9 g, 28.2 mmol) and Boc-L-Asp-OBn (**11**) (9.13 g, 28.2 mmol) and isolated as white powder (Yield: 15.89 g, 27.0 mmol, 96%). ^{1}H NMR (400 MHz, cdcl$_3$) δ 7.76 (d, *J* = 7.5 Hz, 2H), 7.63 – 7.56 (m, 2H), 7.39 (t, *J* = 7.5 Hz, 2H), 7.37 – 7.26 (m, 7H), 6.81 – 6.71 (m, 1H), 5.55 (d, *J* = 6.1 Hz, 1H), 5.29 – 5.20 (m, 1H), 5.09 (q, *J* = 12.2 Hz, 2H), 4.49 (bs, 1H), 4.44 – 4.36 (m, 2H), 4.22 (t, *J* = 7.0 Hz, 1H), 3.45 – 3.38 (m, 1H), 3.38 – 3.26 (m, 3H), 3.08 (dd, *J* = 17.2, 4.5 Hz, 1H), 2.74 (dd, *J* = 17.2, 6.0 Hz, 1H), 1.44 (s, 9H); ^{13}C NMR (100 MHz, cdcl$_3$) δ 171.96, 171.52, 156.97, 144.10, 144.07, 141.46, 135.41, 128.75, 128.57, 128.38, 127.82, 127.19, 125.25, 120.10, 67.06, 66.97, 50.92, 47.39, 40.77, 40.16, 36.41, 28.44; HRMS (ESI): *m/z* calcd for $C_{33}H_{38}N_3O_7$: 588.2704 $[M+H]^+$, found: 588.2715.

FmocHN-*v*Ala-(R)*s*NHBoc-OBn (**n6**):

Compound **n6** was prepared from **1** (3 g, 9.0 mmol) and Boc-D-Asp-OBn (**12**) (2.91 g, 9.0 mmol) and isolated as white powder (Yield: 3.97 g, 6.60 mmol, 73.2%). ^{1}H NMR (400 MHz, cdcl$_3$) δ 7.80 – 7.69 (m, 2H), 7.60 (d, *J* = 7.4 Hz, 2H), 7.44 – 7.36 (m, 2H), 7.35 – 7.26 (m, 7H), 6.86 (bs, 1H), 5.52 (bs, 1H), 5.14 – 5.04 (m, 2H), 5.03 – 4.97 (m, 1H), 4.50 (bs, 1H), 4.43 – 4.32 (m, 2H), 4.22 (t, *J* = 7.0 Hz, 1H), 3.84 (bs, 1H), 3.41 – 3.21 (m, 2H), 3.01 (dd, *J* = 17.1, 4.7 Hz, 1H), 2.75 (dd, *J* = 17.0, 6.1 Hz, 1H), 1.43 (s, 10H), 1.15 (d, *J* = 6.0 Hz, 3H);^{13}C NMR (100 MHz, cdcl$_3$) δ 171.57, 144.13, 141.47, 135.53, 128.72, 128.49, 128.36, 127.83, 127.21, 125.26, 120.11, 66.94, 47.68, 47.43, 45.24, 29.85, 28.43, 18.63; HRMS (ESI): *m/z* calcd for $C_{34}H_{39}N_3NaO_7$: 624.2680 $[M+Na]^+$, found:624.2695.

FmocHN-*v*Val-(R)*s*NHBoc-OBn (**n7**):

Compound **n7** was prepared from **2** (3.25 g, 9.0 mmol) and Boc-D-Asp-OBn (**12**) (2.91 g, 9.0 mmol) and isolated as white powder (Yield: 4.17 g, 6.62 mmol, 73.6 %). ^{1}H NMR (400 MHz, cdcl$_3$) δ 7.75 (dd, *J* = 7.5, 3.5 Hz, 2H), 7.60 (d, *J* = 7.5 Hz, 2H), 7.43 – 7.35 (m, 2H), 7.35 – 7.24 (m, 7H), 6.81 (bs, 1H), 5.43 (bs, 1H), 5.10 – 4.98 (m, 2H), 4.88 (d, *J* = 8.9 Hz, 1H), 4.54 – 4.41 (m, 2H), 4.40 – 4.30 (m, 1H), 4.23 (t, *J* = 7.0 Hz, 1H), 3.64 – 3.52 (m, 1H), 3.47 – 3.34 (m, 1H), 3.35 – 3.24 (m, 1H), 2.97 (dd, *J* = 17.0, 4.7 Hz, 1H), 2.74 (dd, *J* = 17.0, 6.2 Hz, 1H), 1.84 – 1.71 (m, 1H), 1.40 (s, 9H), 0.95 (dd, *J* = 9.9, 6.9 Hz, 6H); ^{13}C NMR (100 MHz, cdcl$_3$) δ 171.53, 144.08, 144.05, 141.40, 135.46, 128.61, 128.37, 128.25, 127.75, 127.75, 127.14, 127.12, 125.24, 125.14, 120.04, 120.02, 66.89, 66.78, 56.81, 47.37, 30.52, 28.32, 19.32, 18.33; HRMS (ESI): *m/z* calcd for $C_{36}H_{44}N_3O_7$: 630.3174 $[M+H]^+$, found:630.3130.

FmocHN-*v*Leu-(R)*s*NHBoc-OBn (**n8**):

Compound **n8** was prepared from **3** (3.37 g, 9.0 mmol) and Boc-D-Asp-OBn (**12**) (2.91 g, 9.0 mmol) and isolated as white powder (Yield: 4.46 g, 6.93 mmol, 77%). ^{1}H NMR (400 MHz, cdcl$_3$)

δ 7.79 – 7.71 (m, 2H), 7.63 – 7.57 (m, 2H), 7.42 – 7.34 (m, 2H), 7.34 – 7.23 (m, 7H), 6.83 (bs, 1H), 5.58 – 5.40 (m, 1H), 5.11 – 4.96 (m, 2H), 4.86 – 4.72 (m, 1H), 4.58 – 4.31 (m, 3H), 4.29 – 4.16 (m, 1H), 3.90 – 3.72 (m, 1H), 3.36 – 3.17 (m, 3H), 3.06 – 2.90 (m, 1H), 2.81 – 2.66 (m, 1H), 1.92 – 1.83 (m, 1H), 1.41 (s, 9H), 1.35 – 1.22 (m, 2H), 0.97 – 0.81 (m, 6H); ^{13}C NMR (100 MHz, $cdcl_3$) δ 171.48, 171.17, 156.56, 155.47, 143.98, 143.92, 141.30, 135.36, 128.52, 128.28, 128.15, 127.63, 127.01, 125.05, 119.91, 66.68, 49.63, 47.28, 46.76, 44.40, 41.70, 36.13, 28.24, 26.30, 26.22, 24.76, 22.97, 22.10; HRMS (ESI): *m/z* calcd for $C_{37}H_{46}N_3O_7$: 644.3330 $[M+H]^+$, found:644.3304.

FmocHN-*v*Phe-(R)*s*NHBoc-OBn (**n9**):

Compound **n9** was prepared from **4** (3.68 g, 9.0 mmol) and Boc-D-Asp-OBn (**12**) (2.91 g, 9.0 mmol) and isolated as white powder (Yield: 4.49 g, 6.62 mmol, 73.6%). ^{1}H NMR (400 MHz, $cdcl_3$) δ 7.75 (dd, *J* = 7.6, 0.7 Hz, 2H), 7.54 (t, *J* = 6.8 Hz, 2H), 7.42 – 7.36 (m, 2H), 7.37 – 7.12 (m, 12H), 6.83 (s, 1H), 5.52 (d, *J* = 6.3 Hz, 1H), 5.18 (d, *J* = 6.5 Hz, 1H), 5.05 (q, *J* = 12.3 Hz, 2H), 4.50 (s, 1H), 4.45 – 4.36 (m, 1H), 4.33 – 4.25 (m, 1H), 4.19 (t, *J* = 7.0 Hz, 1H), 3.98 (d, *J* = 4.8 Hz, 1H), 3.36 (s, 1H), 3.23 – 3.13 (m, 2H), 3.02 (dd, *J* = 17.1, 4.7 Hz, 1H), 2.75 (dd, *J* = 16.8, 6.0 Hz, 2H), 1.49 – 1.37 (m, 9H); ^{13}C NMR (100 MHz, $cdcl_3$) δ 171.77, 171.67, 156.47, 155.64, 144.09, 144.07, 141.44, 137.37, 135.48, 129.36, 128.81, 128.70, 128.48, 128.34, 127.81, 127.20, 126.89, 125.24, 120.08, 80.77, 66.92, 53.13, 50.88, 47.38, 46.62, 46.57, 43.00, 38.86, 36.30, 28.42, 26.55, 26.48; HRMS (ESI): *m/z* calcd for $C_{40}H_{44}N_3O_7$: 678.3174 $[M+H]^+$, found:678.3129.

General procedure for the preparation of compounds FmocNH-*v*Xaa-*s*NH(Boc)-OH **(24-32)**.

Compound **n** (1 equiv) dissolved in DMF (0.1 M), was hydrogenated in the presence of 10% Pd/C (10% w/w) at room temperature till RP-HPLC indicates completion of the reaction (1.5-5 h). The solution was filtered over GHP membrane (0.2 µm). The filtrate was evaporated at 65'C to afford a solid. The solid was dissolved in a minimal amount of DMF at 65'C and precipitated in a stirred 1:1 Et_2O:Hex mixture. The resulting suspension was stored at 4°C for few hours, and moved to -20'C for at least 24h. The powder was filtered and dried *in vacuo* to yield compound **24**-**32**.

FmocHN-*v*Ala-(S)*s*NHBoc-OH (**24**):

Compound **24** was prepared from **n1** (16.76 g, 27.9 mmol) and isolated as white powder (Yield: 12.11 g, 23.68 mmol, 85%). ^{1}H NMR (400 MHz, dmso) δ 11.81 (s, 1H), 7.89 (d, *J* = 7.5 Hz, 2H), 7.87 – 7.78 (m, 1H), 7.68 (d, *J* = 7.0 Hz, 2H), 7.41 (t, *J* = 7.4 Hz, 2H), 7.33 (t, *J* = 7.4 Hz, 2H), 7.15 (d, *J* = 7.9 Hz, 1H), 6.99 (d, *J* = 7.7 Hz, 1H), 4.28 (d, *J* = 6.2 Hz, 2H), 4.21 (d, *J* = 6.4 Hz, 2H), 3.66 – 3.52 (m, 1H), 3.13 – 3.01 (m, 2H), 2.60 (dd, *J* = 16.3, 4.7 Hz, 1H), 2.47 – 2.38 (m, 1H), 1.36 (s, 9H), 0.98 (d, *J* = 6.2 Hz, 3H); ^{13}C NMR (101 MHz, dmso) δ 176.17, 171.94, 155.47,

155.12, 143.95, 143.83, 143.24, 140.71, 127.58, 127.04, 125.14, 120.10, 78.17, 65.23, 51.16, 46.74, 46.35, 43.64, 36.46, 28.14, 17.93; HRMS (ESI): *m/z* calcd for $C_{27}H_{34}N_3O_7$: 512.2391 $[M+H]^+$, found: 512.2387.

FmocHN-*v*Val-(S)*s*NHBoc-OH (**25**):

Compound **25** was prepared from **n2** (11.6 g, 18.43 mmol) and isolated as white powder (Yield: 7.75 g, 14.37 mmol, 78%). ^{1}H NMR (400 MHz, dmso) δ 7.88 (d, *J* = 7.5 Hz, 2H), 7.75 – 7.61 (m, 3H), 7.41 (t, *J* = 7.5 Hz, 2H), 7.32 (tdd, *J* = 7.4, 2.6, 1.1 Hz, 2H), 7.03 (d, *J* = 9.2 Hz, 1H), 6.96 (d, *J* = 7.9 Hz, 1H), 4.37 – 4.31 (m, 1H), 4.27 – 4.15 (m, 3H), 3.44 – 3.38 (m, 1H), 3.21 – 3.08 (m, 2H), 2.59 (dd, *J* = 16.3, 5.3 Hz, 1H), 2.44 (dd, *J* = 16.3, 8.4 Hz, 1H), 1.75 – 1.66 (m, 1H), 1.35 (s, 9H), 0.85 – 0.69 (m, 6H); ^{13}C NMR (100 MHz, DMSO) δ 171.94, 171.90, 171.09, 156.22, 155.13, 144.04, 143.77, 140.73, 127.59, 127.04, 125.22, 120.09, 78.18, 65.27, 55.51, 46.81, 40.56, 36.42, 36.36, 29.02, 28.13, 19.42, 17.81; HRMS (ESI): *m/z* calcd for $C_{29}H_{38}N_3O_7$: 540.2704 $[M+H]^+$, found: 540.2689.

FmocHN-*v*Leu-(S)*s*NHBoc-OH (**26**):

Compound **26** was prepared from **n3** (9.69 g, 15.04 mmol) and isolated as white powder (Yield: 6.33 g, 11.43 mmol, 76%). ^{1}H NMR (400 MHz, dmso) δ 7.89 (d, *J* = 7.4 Hz), 7.69 (t, *J* = 7.4 Hz), 7.41 (t, *J* = 7.4 Hz), 7.32 (td, *J* = 7.3, 3.2 Hz), 7.05 (d, *J* = 9.0 Hz), 6.97 (d, *J* = 7.5 Hz), 4.35 (dd, *J* = 13.0, 10.2 Hz), 4.28 – 4.10 (m), 3.44 (dd, *J* = 13.7, 6.8 Hz), 3.25 – 3.15 (m), 3.15 – 3.04 (m), 2.58 (dd, *J* = 16.4, 5.1 Hz), 2.43 (dd, *J* = 16.3, 8.5 Hz), 1.51 – 1.43 (m), 1.35 (s), 1.07 – 1.00 (m), 0.86 – 0.71 (m); ^{13}C NMR (100 MHz, $CDCl_3$); HRMS (ESI): *m/z* calcd for $C_{30}H_{40}N_3O_7$: 554,2861 $[M+H]^+$, found: 554.2870.

FmocHN-*v*Phe-(S)*s*NHBoc-OH (**27**):

Compound **27** was prepared from **n4** (9.27 g, 13.68 mmol) and isolated as white powder (Yield: 7.15 g, 12.17 mmol, 89%). ^{1}H NMR (400 MHz, dmso) δ 7.96 – 7.89 (m, 1H), 7.90 – 7.83 (m, 2H), 7.61 (dd, *J* = 7.3, 4.6 Hz, 2H), 7.44 – 7.36 (m, 2H), 7.35 – 7.28 (m, 2H), 7.19 (tt, *J* = 14.3, 7.7 Hz, 5H), 7.00 (d, *J* = 7.9 Hz, 1H), 4.28 – 4.17 (m, 2H), 4.18 – 4.11 (m, 2H), 3.77 – 3.68 (m, 1H), 3.32 (s, 2H), 3.21 – 3.15 (m, 1H), 3.13 – 3.07 (m, 1H), 2.77 – 2.72 (m, 1H), 2.64 – 2.55 (m, 2H), 2.49 – 2.43 (m, 1H), 1.35 (s, 9H); ^{13}C NMR (100 MHz, dmso) δ 171.97, 155.61, 143.86, 143.76, 140.67, 139.39, 137.40, 129.16, 128.90, 127.98, 127.56, 127.27, 127.02, 125.90, 125.18, 125.12, 121.36, 120.07, 120.01, 109.74, 78.17, 65.24, 52.28, 51.22, 46.67, 42.49, 40.06, 36.54, 28.15; HRMS (ESI): *m/z* calcd for $C_{33}H_{38}N_3O_7$: 588.2704 $[M+H]^+$, found: 588.2753.

FmocHN-*v*Gly-(S)*s*NHBoc-OH (**28**):

Compound **28** was prepared from **n5** (15.88 g, 27.0 mmol) and isolated as white powder (Yield: 9.95 g, 20.0 mmol, 74%).^{1}H NMR (400 MHz, dmso) δ 7.90 – 7.84 (m, 3H), 7.68 (d, *J* = 7.5 Hz, 2H), 7.41 (t, *J* = 7.4 Hz, 2H), 7.33 (t, *J* = 7.2 Hz, 2H), 7.24 (t, *J* = 5.3 Hz, 1H), 6.96 (d, *J* = 7.9 Hz, 1H), 4.30 (d, *J* = 7.0 Hz, 2H), 4.21 (t, *J* = 6.8 Hz, 2H), 3.15 – 3.07 (m, 2H), 3.03 (dd, *J* = 12.0, 6.0 Hz, 2H), 2.61 (dd, *J* = 16.3, 5.3 Hz, 1H), 2.44 (dd, *J* = 16.0, 8.1 Hz, 1H), 1.37 (s, 9H); ^{13}C NMR (100 MHz, dmso) δ 171.94, 171.05, 156.15, 155.08, 143.86, 140.69, 128.88, 127.56, 127.02, 125.10, 121.34, 120.07, 78.15, 65.35, 51.12, 46.69, 40.06, 38.74, 36.60, 28.14; HRMS (ESI): *m/z* calcd for $C_{26}H_{32}N_3O_7$: 498,2235 $[M+H]^+$, found: 498.2211.

FmocHN-*v*Ala-(R)*s*NHBoc-OH (**29**):

Compound **29** was prepared from **n6** (3.92 g, 6.60) and isolated as white powder (Yield: 2.94 g, 5.74 mmol, 87%). ^{1}H NMR (400 MHz, dmso) δ 9.16 (s, 1H), 7.88 (d, *J* = 7.1 Hz, 3H), 7.84 (d, *J* = 7.3 Hz, 2H), 7.68 (bs, 1H), 7.41 (t, *J* = 7.2 Hz, 3H), 7.35 – 7.31 (m, 2H), 4.51 – 3.92 (m, 3H), 3.80 – 3.48 (m, 1H), 3.49 – 3.29 (m, 1H), 3.22 (bs, 1H), 3.12 – 2.98 (m, 1H), 2.62 – 2.52 (m, 1H), 2.45 – 2.24 (m, 1H), 1.37 (d, *J* = 5.9 Hz, 9H), 0.98 (s, 3H); ^{13}C NMR (101 MHz, dmso) δ 172.80, 154.80, 142.52, 139.37, 137.38, 128.86, 127.51, 127.23, 124.17, 121.32, 119.96, 109.65, 78.76, 78.20, 52.10, 52.08, 46.92, 42.33, 41.07, 28.11, 28.05, 16.35; HRMS (ESI): *m/z* calcd for $C_{27}H_{34}N_3O_7$: 512.2391 $[M+H]^+$, found:512.2361.

FmocHN-*v*Val-(R)*s*NHBoc-OH (**30**):

Compound **30** was prepared from **n7** (4.13 g, 6.62mmol) and isolated as white powder (Yield: 2.86 g, 5.30 mmol, 80%): ^{1}H NMR (400 MHz, dmso) δ 7.88 (dd, *J* = 7.5, 0.6 Hz, 2H), 7.69 (dd, *J* = 17.8, 10.0 Hz, 2H), 7.45 – 7.38 (m, 2H), 7.38 – 7.29 (m, 2H), 7.03 (d, *J* = 9.2 Hz, 1H), 4.39 – 4.28 (m, 1H), 4.27 – 4.04 (m, 3H), 3.50 – 3.34 (m, 1H), 3.29 – 3.20 (m, 1H), 2.99 (ddd, *J* = 25.2, 12.4, 5.9 Hz, 1H), 2.58 (dd, *J* = 16.3, 4.9 Hz, 1H), 2.43 (dd, *J* = 16.2, 8.2 Hz, 1H), 1.90 – 1.65 (m, 1H), 1.40 – 1.35 (m, 9H), 0.92 (d, *J* = 6.9 Hz, 1H), 0.90 – 0.67 (m, 6H); ^{13}C NMR (100 MHz, dmso) δ 172.03, 171.19, 156.16, 155.08, 144.02, 143.73, 142.54, 140.68, 139.37, 137.38, 128.87, 127.54, 127.23, 126.98, 125.17, 121.32, 120.03, 119.97, 109.66, 78.10, 65.24, 55.45, 46.74, 40.57, 29.06, 28.61, 28.10, 19.39; HRMS (ESI): *m/z* calcd for $C_{29}H_{38}N_3O_7$: 540.2704 $[M+H]^+$, found:540.2672.

FmocHN-*v*Leu-(R)*s*NHBoc-OH (**31**):

Compound **31** was prepared from **n8** (4.42 g, 6.93 mmol) and isolated as white powder (Yield: 2.9 g, 5.24 mmol, 77%): ^{1}H NMR (400 MHz, dmso) δ 7.88 (d, *J* = 7.5 Hz, 2H), 7.84 – 7.76 (m, 1H), 7.68 (t, *J* = 6.7 Hz, 2H), 7.41 (t, *J* = 7.4 Hz, 2H), 7.37 – 7.27 (m, 2H), 7.02 (d, *J* = 8.9 Hz, 1H), 6.93 (d, *J* = 7.8 Hz, 1H), 4.37 – 4.25 (m, 2H), 4.25 – 4.16 (m, 2H), 3.67 – 3.54 (m, 1H), 3.26

– 3.08 (m, 1H), 3.04 – 2.93 (m, 1H), 2.59 (dd, *J* = 16.4, 4.9 Hz, 1H), 2.48 – 2.38 (m, 1H), 1.61 – 1.46 (m, 1H), 1.29 – 1.11 (m, 2H), 0.83 (dd, *J* = 15.7, 6.5 Hz, 6H); ^{13}C NMR (101 MHz, dmso) δ 171.92, 171.15, 155.78, 155.05, 144.02, 143.73, 140.69, 128.86, 127.51, 126.96, 125.11, 121.32, 120.04, 120.02, 78.06, 65.08, 51.15, 48.53, 46.81, 43.22, 40.62, 28.12, 24.15, 23.18, 21.70; HRMS (ESI): *m/z* calcd for $C_{30}H_{40}N_3O_7$: 554,2861 $[M+H]^+$, found:554.2871.

FmocHN-*v*Phe-(R)*s*NHBoc-OH (**32**):

Compound **32** was prepared from **n9** (4.45g, 6.62 mmol) and isolated as white powder (Yield: 2.8 g, 4.76 mmol, 73.4%): ^{1}H NMR (400 MHz, dmso) δ 11.87 (bs, 1H), 7.95 – 7.84 (m, 3H), 7.61 (d, *J* = 7.4 Hz, 2H), 7.41 (t, *J* = 7.1 Hz, 2H), 7.36 – 7.28 (m, 2H), 7.26 – 7.14 (m, 6H), 7.00 (d, *J* = 7.8 Hz, 1H), 4.30 – 4.20 (m, 2H), 4.20 – 4.10 (m, 2H), 3.81 – 3.67 (m, 1H), 3.28 – 3.17 (m, 1H), 3.10 – 2.99 (m, 1H), 2.76 (dd, *J* = 13.7, 4.8 Hz, 1H), 2.69 – 2.54 (m, 2H), 2.46 (d, *J* = 8.2 Hz, 1H), 1.36 (s, 9H); ^{13}C NMR (101 MHz, dmso) δ 171.89, 171.18, 155.57, 155.12, 143.85, 143.75, 140.64, 138.85, 129.14, 127.94, 127.52, 126.98, 125.88, 125.14, 125.08, 120.03, 78.15, 65.22, 52.14, 51.15, 46.67, 42.52, 37.21, 36.34, 28.12; HRMS (ESI): *m/z* calcd for $C_{33}H_{37}N_3NaO_7$: 610.2524 $[M+Na]^+$, found:610.2534.

Synthesis of the dimer zwitterionic building blocks FmocNH-*v*COO(Allyl)-*s*NH$_2$(Alloc)-OH (33-34)

General procedure for the synthesis of compounds **o1**-**2**.

To a solution of the diacid OH-*s*NH(Alloc)-O*t*Bu (**13**) (1 equiv) in dryDMF (0.1 M) stirred at 0°C under argon was added PyBOP (1 equiv), HOBt.H_2O and DIEA (3 equiv). After 5min the diamine monomer FmocNH-*v*COO(Allyl)-NH_2.HCl (**6**-**7**) was added. The solution was stirred at 0 °C for 15min and then allowed to warm to room temperature. After 1h water was added *via* a syringe till the reaction mixture got turbid and then put at 4°C overnight. The precipitated white powder was filtered, washed with water, dissolved with DCM and washed with brine (x3); dried over $MgSO_4$, filtered, and concentrated *in vacuo* to yield a vitreous solid which was precipitated from $CHCl_3$/Hex mixture. The precipitate powder was filtered and dry *in vacuo* to yield compound **o** as white powder.

FmocNH-(S)*v*COO(Allyl)-*s*NH$_2$(Alloc)-O*t*Bu (**o1**)

Compound **o1** was prepared from FmocNH-(S)*v*COO(Allyl)-NH_2.HCl (**6**) (4.42 g, 10.98 mmol) and OH-(S)*s*NH(Alloc)-O*t*Bu (**13**) (3 g, 10.98 mmol) and isolated as white powder (Yield: 5.06 g, 8.15 mmol, 74.2%). ^{1}H NMR (400 MHz, cdcl$_3$) δ 7.77 (d, *J* = 7.5 Hz, 2H), 7.62 (dd, *J* = 7.3, 3.2 Hz, 2H), 7.40 (t, *J* = 7.4 Hz, 2H), 7.32 (tdd, *J* = 7.5, 1.8, 1.3 Hz, 2H), 6.91 (t, *J* = 5.6 Hz, 1H), 5.96 – 5.84 (m, 3H), 5.39 – 5.17 (m, 4H), 4.72 – 4.61 (m, 2H), 4.59 (d, *J* = 5.4 Hz, 2H), 4.53 –

4.43 (m, 2H), 4.43 – 4.31 (m, 2H), 4.24 (t, *J* = 7.2 Hz, 1H), 3.79 – 3.64 (m, 2H), 2.88 (dd, *J* = 17.1, 4.5 Hz, 1H), 2.64 (dd, *J* = 17.1, 6.3 Hz, 1H), 1.42 (s, 9H); ^{13}C NMR (100 MHz, cdcl$_3$) δ 171.66, 171.26, 143.91, 141.42, 132.47, 131.53, 127.86, 127.23, 125.35, 120.11, 119.38, 118.35, 82.15, 67.51, 66.70, 66.37, 54.30, 47.21, 41.72, 37.12, 28.17; HRMS (ESI): *m/z* calcd for $C_{33}H_{39}N_3NaO_9$:644.2579 $[M+Na]^+$, found:644.2602.

FmocNH-(R)*v*COO(Allyl)-*s*NH$_2$(Alloc)-O*t*Bu (**o2**)

Compound **o2** was prepared from FmocNH-(R)*v*COO(Allyl)-NH$_2$.HCl (**7**) (2.95 g, 7.32 mmol) and OH-(S)*s*NH(Alloc)-O*t*Bu (**13**) (2 g, 7.32 mmol) and isolated as white powder (Yield: 3.13 g, 5.03 mmol, 89%): ^{1}H NMR (400 MHz, cdcl$_3$) δ 7.76 (d, *J* = 7.5 Hz, 2H), 7.61 (d, *J* = 7.1 Hz, 2H), 7.40 (t, *J* = 7.4 Hz, 2H), 7.31 (tt, *J* = 7.4, 0.9 Hz, 2H), 7.02 – 6.90 (m, 1H), 5.96 – 5.82 (m, 3H), 5.41 – 5.18 (m, 4H), 4.66 (t, *J* = 5.8 Hz, 2H), 4.58 (d, *J* = 5.3 Hz, 2H), 4.56 – 4.44 (m, 2H), 4.36 (d, *J* = 7.2 Hz, 2H), 4.23 (t, *J* = 7.2 Hz, 1H), 3.83 – 3.61 (m, 2H), 2.94 (dd, *J* = 17.3, 4.2 Hz, 1H), 2.61 (dd, *J* = 17.3, 6.6 Hz, 1H), 1.43 (s, 9H); ^{13}C NMR (100 MHz, cdcl$_3$) δ 171.67, 170.14, 156.13, 143.90, 141.40, 132.46, 131.51, 127.84, 127.23, 125.35, 120.10, 119.41, 118.34, 82.26, 67.51, 66.66, 66.31, 54.45, 47.18, 41.40, 28.16.

General procedure for the preparation of compounds **33-34**.

To a solution of **o** (1 equiv) in 80:20 (v/v) DCM/TFA (0.1 M) stirred at 0'C was added Et$_3$SiH (3 equiv). The solution was stirred at r.t till TLC revelead completion of the reaction (approximately 3.5h) and toluene was added; the contents were concentrated *in vacuo*, precipitated and deeply washed with cold Et$_2$O. The filtrate was evaporated *in vacuo* to afford the product.

FmocNH-(S)*v*COO(Allyl)-*s*NH$_2$(Alloc)-OH (**33**)

Compound **33** was prepared from **o1** (5.04 g, 8.11 mmol) and isolated as white powder (Yield: 4.08 g, 7.22 mmol, 89%): ^{1}H NMR (400 MHz, dmso) δ 12.26 (bs), 8.04 (t, *J* = 5.6 Hz), 7.90 (d, *J* = 7.5 Hz), 7.70 (d, *J* = 7.5 Hz), 7.49 (d, *J* = 7.8 Hz), 7.42 (t, *J* = 7.4 Hz), 7.34 (td, *J* = 7.3, 3.5 Hz), 5.89 (ddd, *J* = 16.9, 10.6, 5.3 Hz), 5.29 (dd, *J* = 17.5, 6.8 Hz), 5.18 (t, *J* = 9.6 Hz), 4.62 – 4.50 (m), 4.50 – 4.38 (m), 4.38 – 4.13 (m), 3.55 – 3.45 (m), 3.41 – 3.32 (m), 2.62 (dd, *J* = 16.7, 4.2 Hz), 2.47 – 2.41 (m); ^{13}C NMR (101 MHz, dmso) δ 172.18, 170.60, 156.35, 144.15, 141.14, 133.85, 132.77, 128.06, 127.52, 125.21, 120.57, 118.19, 117.54, 66.16, 65.53, 65.02, 64.76, 54.08, 46.99; HRMS (ESI): *m/z* calcd for $C_{29}H_{32}N_3O_9$:566.2133 $[M+H]^+$, found:566.2149.

FmocNH-(R)*v*COO(Allyl)-*s*NH$_2$(Alloc)-OH (**34**)

Compound **34** was prepared from **o2** (3.12 g, 5.02 mmol) and isolated as white powder (Yield: 2.68 g, 4.73 mmol, 94%): ^{1}H NMR (400 MHz, dmso) δ 12.32 (bs, 1H), 8.05 (t, *J* = 5.9 Hz, 1H), 7.90 (d, *J* = 7.5 Hz, 2H), 7.73 – 7.68 (m, 2H), 7.70 (d, *J* = 6.7 Hz, 2H), 7.52 (d, *J* = 8.1 Hz, 1H), 7.42 (t, *J* = 7.4 Hz, 2H), 7.34 (tdd, *J* = 7.4, 2.4, 1.1 Hz, 2H), 5.89 (ddd, *J* = 22.5, 10.6, 5.4 Hz, 2H), 5.36 – 5.25 (m, 2H), 5.18 (td, *J* = 10.2, 1.4 Hz, 2H), 4.61 – 4.50 (m, 2H), 4.49 – 4.40 (m, 2H), 4.38 – 4.16 (m, 5H), 3.54 – 3.34 (m, 3H), 2.63 (dd, *J* = 16.6, 4.6 Hz, 1H), 2.49 – 2.38 (m, 1H); ^{13}C NMR (101 MHz, dmso) δ 171.76, 171.19, 155.96, 155.61, 143.74, 140.74, 133.44, 132.36, 127.67, 127.13, 125.18, 120.17, 117.84, 117.14, 65.81, 65.15, 64.61, 51.42, 46.58, 36.33.

Synthesis of the dimer building blocks presenting malic acid as β-diacid unit (aa, bb)

General procedure for the synthesis of compounds **aa** and **bb.**

To a solution of the diacid OH-(S)*s*OH-OBn (**14**) (1 equiv) in dryDMF (0.1 M) stirred at 0°C under argon was added PyBOP (1 equiv), HOBt.H_2O and DIEA (3 equiv). After 5min the diamine monomer FmocNH-*v*Xaa-NH_2.HCl (**1-5**) was added. The solution was stirred at 0°C for 15min and then allowed to warm to room temperature. After 1h water was added *via* a syringe till the reaction mixture got turbid and then put at 4°C overnight. The precipitated white powder was filtered, washed with water, dissolved with DCM and washed with brine (x3); dried over $MgSO_4$, filtered, and concentrated *in vacuo.* The resulting white solid was washed with MeOH to yield the product as white powder.

FmocNH-*v*Ala-*s*OH-OBn (**aa**)

Compound **aa** was prepared from FmocNH-*v*Ala-NH_2.HCl (**1**) (2 g, 6.01 mmol) and OH-(S)*s*OH-OBn) (**14**) (1.35 g, 6.01 mmol) and isolated as white powder (Yield:2.98 g, 5.93 mmol, quant). ^{1}H NMR (400 MHz, $cdcl_3$) δ 7.76 (d, *J* = 7.6 Hz, 2H), 7.60 – 7.55 (m, 2H), 7.41 – 7.37 (m, 2H), 7.37 – 7.28 (m, 7H), 7.15 (bs, 1H), 5.03 (d, *J* = 7.2 Hz, 1H), 4.45 – 4.40 (m, 1H), 4.40 – 4.33 (m, 2H), 4.21 (t, *J* = 6.9 Hz, 1H), 3.85 (dd, *J* = 11.9, 6.2 Hz, 1H), 3.65 (d, *J* = 4.0 Hz, 1H), 3.41 – 3.26 (m, 2H), 2.99 (dd, *J* = 17.4, 3.8 Hz, 1H), 2.79 (dd, *J* = 17.3, 8.0 Hz, 1H), 1.17 (d, *J* = 6.4 Hz, 3H); ^{13}C NMR (151 MHz, $cdcl_3$) δ 172.74, 144.05, 128.79, 128.63, 128.40, 127.84, 127.19, 120.12, 68.61, 67.11, 47.37, 38.36, 18.71.

FmocNH-*v*Gly-*s*OH-OBn (**bb**)

Compound **bb** was prepared from FmocNH-*v*Gly-NH_2.HCl (**5**) (4.98 g, 15.61 mmol) and ((*S*)-(*s*Ala)-O*t*Bu) (**9**) (3.5 g, 15.61 mmol) and isolated as white powder (Yield: 6.22 g, 12.72 mmol, 81%). ^{1}H NMR (400 MHz, $cdcl_3$) δ 7.76 (d, *J* = 7.5 Hz), 7.59 (d, *J* = 7.4 Hz), 7.42 – 7.27 (m), 7.12 (s), 5.18 – 5.09 (m), 4.47 – 4.35 (m), 4.21 (t, *J* = 6.9 Hz), 3.64 (bs), 3.44 – 3.39 (m), 3.38 – 3.29 (m), 3.00 (dd, *J* = 17.4, 3.7 Hz), 2.80 (dd, *J* = 17.4, 7.9 Hz).

Oligomer SPS and Characterization

General Procedure for SPS Coupling

Diamines and Diacids Coupling Strategy

Succinic anhydride (Suc) (0.15 g, $1.5x10^{-3}$ mol, 10 eq) was dissolved in DMF (3 mL) and coupled to the free amino group (0.15 mmol) with a 1M solution of DIEA (0.513 mL, 20 eq) in DMF (2.5 mL) at room temperature for 25 min; the coupling was repeated three times. DMF (5 mL) and DIEA (2 mL) were added and shaken for 8 min to cleave the anhydride by-product eventually formed on the growing chain; this step was repeated three times. The mono Fmoc-protected diamine FmocNH-vAla-NH_2.HCl (**1**) (0.15g, $0.45x10^{-3}$ mol, 3 eq) was dissolved in DMF (3mL) and added to the resin-bound carboxylic function preactivated with a DMF solution (1mL) of PyBOP (1.171g, $1.5x10^{-3}$ mol, 0,5M DMF sol, 10 eq) and HOBt (0.115 g, $0.75x10^{-3}$ mol, 0.25M DMFsol, 5 eq) in the presence of DIEA (1mL of 1M DMF sol, 20 eq); the reaction mixture was shaken for 45min and the coupling step was repeated three times.

Dimer Coupling Strategy

The resin (0.025 mmol, 1 equiv) was swollen twice for 15 min in DCM before starting the initial Fmoc deprotection. The selected building block **1**-**5** (5 equiv) and O-(7-azabenzotriazol-1-yl)-N,N,N,N-tetramethyluronium hexafluorophosphate (HATU) (46.5 mg, 4.9 equiv) were placed as powder in the amino acid vial and placed in the peptide synthesizer. The solids were dissolved in 2 mL of DMF with a gentle nitrogen stream. Then 10 equiv of 1 M DIEA solution in DMF was added. Preactivation was carried out for 3 min in the amino acid vial before the solution was transferred to the resin. Afterward the resin with the coupling solution was shaken carefully for 1 h, the reaction vessel was emptied and washed with DMF. Then the whole procedure was repeated once.

Fmoc-Deprotection Protocol

Hydrophobic proteinaceous oligomers

Fmoc deprotection was performed using 3mL of a solution of 25% Pip in DMF. The deprotection was initially carried out for 5 min and checked by UV monitoring for the fluorenyl-Pip adduct at 301 nm. This step was repeated with increasing deprotection time (10, 20, 30, 40, 60 min) until the deprotection was complete. The deprotection time was considerably reduced by the use of 3mL of 0.4M LiCl in DBU-Pip-DMF (1/1/48, v/v) mixture.

Amphiphilic cationic oligomers

Fmoc deprotection was performed using 3mL of 0.4M LiCl in DBU-Pip-DMF (1/1/48, v/v) mixture. The deprotection was initially carried out for 5 min and checked by UV monitoring for the fluorenyl-Pip adduct at 301 nm. This step was repeated with increasing deprotection time (10, 20, 30, 40, 60 min) until the deprotection was complete.

Zwitterionic oligomers

Fmoc deprotection was performed using 3mL of a solution of 25% Pip in DMF.. The deprotection was initially carried out for 5 min and checked by UV monitoring for the fluorenyl-Pip adduct at 301 nm. This step was repeated with increasing deprotection time (10, 20, 30, 40, 60 min) until the deprotection was complete.

Final Cleavage from Solid Support.

The final cleavage was performed in two different ways based on the resin. For Tentagel S RAM resin, the cleavage cocktail (95% TFA-triisopropylsilane(TIS)-H_2O, 95/2.5/2.5, 1 mL/50 mg resin) was added to the resin and allowing it to react for 70 min. In the case of Tr-EDA resin, the cleavage was performed by the addition of a solution of 30% TFA in DCM and shaking for 30 min.The cleavage solution was filtered and purged into ice-cold diethyl ether. The precipitate was isolated. The residue was dissolved in H_2O and/or MeOH, diluted with water and lyophilized overnight, giving the final product and the corresponding yield.

Oligomer Characterization

Hydrophobic proteinaceous oligomers

FmocHN-vAla-sGly-vAla-sGly-vAla-sGly-vGly-NH₂ (35)

Compound **35** (60 mg, 0.08 mmol) was prepared on obtained with a yield of 53%.

ESI *m/z* calcd for $C_{38}H_{55}N_8O_8^+$ $[M+H]^+$ 750.4, found 751.3; RP-HPLC analysis 5% to 95% MeCN in 10 min, T_R = 6.15 min.

FmocHN-vAla-sGly-vAla-sGly-vAla-sGly-vAla-sGly-NH₂ (38)

Compound **38** (79 mg, 0.092 mmol) was obtained with a yield of 61%.

ESI *m/z* calcd for $C_{43}H_{62}N_9O_{10}^+$ $[M+H]^+$ 864.4, found 864.4; RP-HPLC analysis 5% to 95% MeCN in 10 min, T_R = 6.6 min.

H₂N-vLeu-sAla-vVal-sPhe-vVal-sAla-vLeu-sGly-NH₂ (39)

Compound **39** (17 mg, 0.019 mmol) was obtained with a yield of 76%.

ESI-HRMS *m/z* calcd for $C_{47}H_{82}N_9O_8^+$ $[M+H]^+$ 900.6281, found 900,6296; RP-HPLC analysis 5% to 95% MeCN in 60 min, T_R = 21.5 min.

H₂N-vLeu-sPhe-vLeu-sAla-vVal-sPhe-vVal-sAla-vLeu-sGly-NH₂ (40)

Compound **40** (23 mg, 0.019 mmol) was obtained with a yield of 77%.

ESI-HRMS *m/z* calcd for $C_{64}H_{106}N_{11}O_{10}^+$ $[M+H]^+$ 1188.8119, found 1188.8106; RP-HPLC analysis 5% to 95% MeCN in 60 min, T_R = 28.2 min.

H_2N-vLeu-sAla-vVal-sPhe-vVal-sAla-vLeu-sPhe-vLeu-sAla-vVal-sPhe-vVal-sAla-vLeu-sGly-NH_2 (41)

Compound **41** (39 mg, 0.021 mmol) was obtained with a yield of 83%.

ESI-HRMS *m/z* calcd for $C_{101}H_{166}N_{17}O_{16}^+$ $[M+H]^+$ 1873.2693 found 1873.2819; RP-HPLC analysis 5% to 95% MeCN in 60 min, T_R = 51.0 min.

H_2N-vLeu-sAla-vVal-sPhe-vVal-sAla-vLeu-sGly-vGly-NH_2 (42)

Compound **42** (18 mg, 0.019 mmol) was obtained with a yield of 76%.

ESI-HRMS *m/z* calcd for $C_{49}H_{87}N_{10}O_8^+$ $[M+H]^+$ 943.6703, found 943.6656; RP-HPLC analysis 5% to 90% MeCN in 30 min, T_R = 12.6 min.

H_2N-vVal-sAla-vLeu-sPhe-vLeu-sAla-vVal-sPhe-vVal-sAla-vLeu-sGly-vGly-NH_2 (43)

Compound **43** (23 mg, 0.016 mmol) was obtained with a yield of 64.3%.

ESI-HRMS *m/z* calcd for $C_{76}H_{129}N_{14}O_{12}^+$ $[M+H]^+$ 1429.9909, found 1429.9905; RP-HPLC analysis 5% to 90% MeCN in 30 min, T_R = 18.4 min.

H_2N-vLeu-sAla-vVal-sPhe-vVal-sAla-vLeu-sPhe-vLeu-sAla-vVal-sPhe-vVal-sAla-vLeu-sGly-vGly-NH_2 (44)

Compound **44** (24 mg, 0.017 mmol) was obtained with a yield of 73.4%.

ESI-HRMS *m/z* calcd for $C_{103}H_{171}N_{18}O_{16}^+$ $[M+H]^+$ 1916.3115, found 1916.3096; RP-HPLC analysis 5% to 95% MeCN in 60 min, T_R = 43.5 min.

Amphiphilic cationic oligomers

H_2N-vGly-(S)sNH_2-vGly-(S)sNH_2-vGly-(S)sNH_2-vGly-(S)sNH_2-vGly-(S)sNH_2-vGly-(S)sNH_2-vGly-(S)sNH_2-vGly-(S)sNH_2-vGly-(S)sNH_2-NH_2 (46)

Compound **46** (27 mg, 0.019 mmol) was obtained with a yield of 75%.

ESI-HRMS *m/z* calcd for $C_{54}H_{103}N_{28}O_{18}^+$ $[M+H]^+$ 1431.8000, found 1431.8013; RP-HPLC analysis 5% to 95% MeCN in 60 min, T_R = 0 min.

H_2N-vAla-(S)sNH_2-vVal-(S)sNH_2-vPhe-(S)sNH_2-vVal-(S)sNH_2-vAla-(S)sNH_2-vVal-(S)sNH_2-vPhe-(S)sNH_2-vVal-(S)sNH_2-vAla-(S)sNH_2-NH_2 (47)

Compound **47** (42 mg, 0.023mmol) was obtained with a yield of 92%.

ESI-HRMS *m/z* calcd for $C_{83}H_{145}N_{28}O_{18}^+$ $[M+H]^+$ 1821.1213, found 1822.1258; RP-HPLC analysis 5% to 95% MeCN in 60min, T_R = 12.3 min.

H_2N-vGly-(S)sNH_2-vLeu-(S)sNH_2-vPhe-(S)sNH_2-vLeu-(S)sNH_2-vGly-(S)sNH_2-vLeu-(S)sNH_2-vPhe-(S)sNH_2-vLeu-(S)sNH_2-vGly-(S)sNH_2-NH_2 (48)

Compound **48** (39 mg, 0.021 mmol) was obtained with a yield of 85%.

ESI-HRMS *m/z* calcd for $C_{84}H_{148}N_{28}O_{18}^{2+}$ $[M+2H]^{2+}$ 918.5685, found 918.5810; RP-HPLC analysis 5% to 95% MeCN in 60min, T_R = 14.4 min.

H_2N-vAla-(S)sNH$_2$-vVal-(S)sNH$_2$-vLeu-(S)sNH$_2$-vVal-(S)sNH$_2$-vAla-(S)sNH$_2$-vVal-(S)sNH$_2$-vLeu-(S)sNH$_2$-vVal-(S)sNH$_2$-vAla-(S)sNH$_2$-NH$_2$ (49)

Compound **49** (38 mg, 0.022 mmol) was obtained with a yield of 86%.

ESI-HRMS *m/z* calcd for $C_{77}H_{149}N_{28}O_{18}^{+}$ $[M+H]^{+}$ 1754.1599, found 1754.1628; RP-HPLC analysis 5% to 95% MeCN in 60min, T_R = 11.4 min.

H_2N-vLeu-(S)sNH$_2$-vVal-(S)sNH$_2$-vPhe-(S)sNH$_2$-vVal-(S)sNH$_2$-vLeu-(S)sNH$_2$-vVal-(S)sNH$_2$-vPhe-(S)sNH$_2$-vVal-(S)sNH$_2$-vLeu-(S)sNH$_2$-NH$_2$ (50)

Compound **50** (42 mg, 0.022 mmol) was obtained with a yield of 86%.

ESI-HRMS *m/z* calcd for $C_{92}H_{163}N_{28}O_{18}^{+}$ $[M+H]^{+}$ 1948.2695, found 1948.2499; RP-HPLC analysis 5% to 95% MeCN in 60min, T_R = 16.6 min.

H_2N-vLeu-(S)sNH$_2$-vVal-(S)sNH$_2$-vLeu-(S)sNH$_2$-vVal-(S)sNH$_2$-vLeu-(S)sNH$_2$-vVal-(S)sNH$_2$-vLeu-(S)sNH$_2$-vVal-(S)sNH$_2$-vLeu-(S)sNH$_2$-NH$_2$ (51)

Compound **51** (41 mg, 0.022 mmol) was obtained with a yield of 88%.

ESI-HRMS *m/z* calcd for $C_{86}H_{168}N_{28}O_{18}^{+}$ $[M+H]^{+}$ 1880.3008, found 1880.3045; RP-HPLC analysis 5% to 95% MeCN in 60min, T_R = 15.8 min.

H_2N-vPhe-(S)sNH$_2$-vVal-(S)sNH$_2$-vPhe-(S)sNH$_2$-vVal-(S)sNH$_2$-vPhe-(S)sNH$_2$-vVal-(S)sNH$_2$-vPhe-(S)sNH$_2$-vVal-(S)sNH$_2$-vPhe-(S)sNH$_2$-NH$_2$ (52)

Compound **52** (46 mg, 0.022 mmol) was obtained with a yield of 90%.

ESI-HRMS *m/z* calcd for $C_{101}H_{157}N_{28}O_{18}^{+}$ $[M+H]^{+}$ 2050.2225, found 2050.2185; RP-HPLC analysis 5% to 95% MeCN in 60min, T_R = 16.6 min.

H_2N-vAla-(S)sNH$_2$-vVal-(S)sNH$_2$-vPhe-(S)sNH$_2$-vVal-(S)sNH$_2$-vAla-(S)sNH$_2$-NH$_2$ (53)

Compound **53** (21 mg, 0.021 mmol) was obtained with a yield of 84%.

ESI-HRMS *m/z* calcd for $C_{45}H_{81}N_{16}O_{10}^{+}$ $[M+H]^{+}$ 1005.6316, found ; RP-HPLC analysis 5% to 95% MeCN in 60min, T_R = 8.34 min.

H_2N-vLeu-(S)sNH$_2$-vVal-(S)sNH$_2$-vPhe-(S)sNH$_2$-vVal-(S)sNH$_2$-vLeu-(S)sNH$_2$-NH$_2$ (54)

Compound **54** (24 mg, 0.022 mmol) was obtained with a yield of 88%.

ESI-HRMS *m/z* calcd for $C_{51}H_{93}N_{16}O_{10}^{+}$ $[M+H]^{+}$ 1089.7255, found ; RP-HPLC analysis 5% to 95% MeCN in 60min, T_R = 12.15 min.

H_2N-vLeu-(S)sNH$_2$-vVal-(S)sNH$_2$-vPhe-(S)sNH$_2$-vVal-(S)sNH$_2$)$_3$-vLeu-(S)sNH$_2$-vVal-(S)sNH$_2$-vPhe-(S)sNH$_2$-vVal-(S)sNH$_2$-vLeu-(S)sNH$_2$-vVal-(S)sNH$_2$-vPhe-(S)sNH$_2$-vVal-(S)sNH$_2$-vLeu-(S)sNH$_2$-NH$_2$ (55)

Compound **55** (67 mg, 0.024 mmol) was obtained with a yield of 96%.

ESI-HRMS *m/z* calcd for $C_{133}H_{233}N_{40}O_{26}^{+}$ $[M+H]^{+}$ 2806.8134, found ; RP-HPLC analysis 5% to 95% MeCN in 60min, T_R = 19.3 min.

H_2N-vLeu-(R)sNH$_2$-vVal-(R)sNH$_2$-vPhe-(R)sNH$_2$-vVal-(R)sNH$_2$-vLeu-(R)sNH$_2$-vVal-(R)sNH$_2$-vPhe-(R)sNH$_2$-vVal-(R)sNH$_2$-vLeu-(R)sNH$_2$-NH$_2$ (56)

Compound **56** (42 mg, 0.022 mmol) was obtained with a yield of 86%.

ESI-HRMS *m/z* calcd for $C_{92}H_{163}N_{28}O_{18}^{+}$ $[M+H]^{+}$ 1948.2695, found; RP-HPLC analysis 5% to 95% MeCN in 60min, T_R = 15.3 min.

RhB-HN-(vGly-(S)sNH$_2$)9-NH$_2$ (57)

Compound **57** (37 mg, 20 mmol) was obtained with a yield of 79%.

ESI-HRMS *m/z* calcd for $C_{82}H_{132}N_{30}O_{20}^{2+}$ $[M-Cl+H]^{2+}$ 928.5111, found 928.5074; RP-HPLC analysis 5% to 95% MeCN in 60min, T_R = 13.2 min.

RhB-HN-(vAla-(S)sNH$_2$-vVal-(S)sNH$_2$-vPhe-(S)sNH$_2$-vVal-(S)sNH$_2$)$_2$-vAla-(S)sNH$_2$-NH$_2$ (58)

Compound **58** (34 mg, 0.015 mmol) was obtained with a yield of 59%.

ESI-HRMS *m/z* calcd for $C_{111}H_{174}N_{30}O_{20}^{2+}$ $[M-Cl+H]^{2+}$ 1123.6755, found 1123.6694; RP-HPLC analysis 5% to 95% MeCN in 60min, T_R = 20.5 min.

RhB-HN-(vGly-(S)sNH$_2$-vLeu-(S)sNH$_2$-vPhe-(S)sNH$_2$-vLeu-(S)sNH$_2$)$_2$-vGly-(S)sNH$_2$-NH$_2$ (59)

Compound **59** (34 mg, 0.015 mmol) was obtained with a yield of 60%.

ESI-HRMS *m/z* calcd for $C_{112}H_{176}N_{30}O_{20}^{2+}$ $[M-Cl+H]^{2+}$ 1130.6833, found 1130.6780; RP-HPLC analysis 5% to 95% MeCN in 60min, T_R = 21.2 min.

RhB-HN-(vAla-(S)sNH$_2$-vVal-(S)sNH$_2$-vLeu-(S)sNH$_2$-vVal-(S)sNH$_2$)$_2$-vAla-(S)sNH$_2$-NH$_2$ (60)

Compound **60** (47 mg, 0.021 mmol) was obtained with a yield of 84%.

ESI-HRMS *m/z* calcd for $C_{105}H_{178}N_{30}O_{20}^{2+}$ $[M-Cl+H]^{2+}$ 1089.6911, found 1089.6978; RP-HPLC analysis 5% to 95% MeCN in 60min, T_R = 19.6 min.

RhB-HN-(vLeu-(S)sNH$_2$-vVal-(S)sNH$_2$-vPhe-(S)sNH$_2$-vVal-(S)sNH$_2$)$_2$-vLeu-(S)sNH$_2$-NH$_2$ (61)

Compound **61** (35 mg, 0.015 mmol) was obtained with a yield of 58%.

ESI-HRMS *m/z* calcd for $C_{120}H_{192}N_{30}O_{20}^{2+}$ $[M-Cl+H]^{2+}$ 1186.7459, found 1186.7396; RP-HPLC analysis 5% to 95% MeCN in 60min, T_R = 23.4 min.

RhB-HN-(vLeu-(S)sNH$_2$-vVal-(S)sNH$_2$)$_4$-vLeu-(S)sNH$_2$-NH$_2$ (62)

Compound **62** (50 mg, 0.022 mmol) was obtained with a yield of 86%.

ESI-HRMS *m/z* calcd for $C_{114}H_{196}N_{30}O_{20}^{2+}$ $[M-Cl+H]^{2+}$ 1152.7615, found 1152.7660; RP-HPLC analysis 5% to 95% MeCN in 60min, T_R = 22.7 min.

RhB-HN-(vPhe-(S)sNH$_2$-vVal-(S)sNH$_2$)$_4$-vPhe-(S)sNH$_2$-NH$_2$ (63)

Compound **63** (40 mg, 0.016 mmol) was obtained with a yield of 63%.

ESI-HRMS *m/z* calcd for $C_{129}H_{186}N_{30}O_{20}^{2+}$ $[M-Cl+H]^{2+}$ 1237.7224, found 1237.7169; RP-HPLC analysis 5% to 95% MeCN in 60min, T_R = 23.8 min.

RhB-HN-vAla-(S)sNH$_2$-vVal-(S)sNH$_2$-vPhe-(S)sNH$_2$-vVal-(S)sNH$_2$-vAla-(S)sNH$_2$-NH$_2$ (64)

Compound **64** (24 mg, 0.017 mmol) was obtained with a yield of 66%.

ESI-HRMS *m/z* calcd for $C_{73}H_{109}N_{18}O_{12}^{+}$ $[M-Cl]^{+}$ 1429.8467, found 1429.8394; RP-HPLC analysis 5% to 95% MeCN in 60min, T_R = 20.9 min.

RhB-HN-vLeu-(S)sNH$_2$-vVal-(S)sNH$_2$-vPhe-(S)sNH$_2$-vVal-(S)sNH$_2$-vLeu-(S)sNH$_2$-NH$_2$ (65)

Compound **65** (27 mg, 0.017 mmol) was obtained with a yield of 69%.

ESI-HRMS *m/z* calcd for $C_{79}H_{121}N_{18}O_{12}^{+}$ $[M\text{-}Cl]^{+}$ 1513.9406, found 1513.9366; RP-HPLC analysis 5% to 95% MeCN in 60min, T_R = 20.9 min.

RhB-HN-(vLeu-(S)sNH$_2$-vVal-(S)sNH$_2$-vPhe-(S)sNH$_2$-vVal-(S)sNH$_2$)$_3$-vLeu-(S)sNH$_2$-NH$_2$ (66)

Compound **66** (58 mg, 0.018 mmol) was obtained with a yield of 71%.

ESI-HRMS *m/z* calcd for $C_{161}H_{263}N_{42}O_{28}^{3+}$ $[M\text{-}Cl+2H]^{3+}$ 1077.6810, found 1077.6811; RP-HPLC analysis 5% to 95% MeCN in 60min, T_R = 23.3 min.

RhB-HN-(vLeu-(R)sNH$_2$-vVal-(R)sNH$_2$-vPhe-(R)sNH$_2$-vVal-(R)sNH$_2$)$_2$-vLeu-(R)sNH$_2$-NH$_2$ (67)

Compound **67** (41 mg, 0.017 mmol) was obtained with a yield of 68%.

ESI-HRMS *m/z* calcd for $C_{120}H_{192}N_{30}O_{20}^{2+}$ $[M\text{-}Cl+H]^{2+}$ 1186.7459, found 1186.7456; RP-HPLC analysis 5% to 95% MeCN in 60min, T_R = 23.0 min.

Zwitterionic oligomers

H$_2$N-(S)vCOOH-(S)sNH$_2$-(S)vCOOH-(S)sNH$_2$-(S)vCOOH-(S)sNH$_2$-(S)vCOOH-(S)sNH$_2$-(S)vCOOH-(S)sNH$_2$-NH$_2$ (68)

Compound **68** (21 mg, 0.021 mmol) was obtained with a yield of 82%.

MALDI *m/z* calcd for $C_{35}H_{59}N_{16}O_{20}^{+}$ $[M+H]^{+}$ 1023.409, found 1023.584; RP-HPLC analysis 5% to 95% MeCN in 60min, T_R = 0 min (eluted within the injection peak).

H$_2$N-(S)vCOO(Allyl)-(S)sNH(Alloc)-(S)vCOO(Allyl)-(S)sNH(Alloc)-(S)vCOO(Allyl)-(S)sNH(Alloc)-(S)vCOO(Allyl)-(S)sNH(Alloc)-(S)vCOO(Allyl)-(S)sNH(Alloc)-NH$_2$ (70)

Compound **70** was isolated in analytical amount.

RP-HPLC analysis 5% to 95% MeCN in 60min, T_R = 36.1 min.

List of Abbreviations

Ala	Alanine
Alloc	Allylchloroformate
AllOH	Allylalcohol
AMP	Antimicrobial peptide
Asn	Asparagine
Asp	Aspartic acid
Bn	Benzyl
Boc	*tert*-Butoxycarboyl
BuLi	Buthyllithium
CD	Circular dichroism
CPP	Cell-penetrating peptide
DBU	1,8-diazabi-cyclo[5.4.0]undec-7-ene
DCM	Dichloromethane
DI(P)EA	*N*,*N*-Diisopropylethylamin*e* or Hünig's base
DLS	Dynamic light scattering
DMBA	*N*,*N*-dimethylbarbituric acid
DMF	*N*,*N*-dimethylformamide
2,2-DMP	2,2-Dimethoxypropane
DMSO	Dimethyl sulfoxide
DNA	Deoxyribonucleic acid
EDA	Ethylenediamine
ESI-MS	Electrospray ionization mass spectroscopy
FACS	Fluorescence-activated cell sorting
Fmoc	9-Fluorenylmethoxycarbonyl
FP	Fusion peptide
FWHM	Full width at half maximum
GIXD	Grazing incidence X-Ray diffraction
Gly	Glycine
Glu	Glutamic acid
HATU	1-[Bis(dimethylamino)methylene]-1*H*-1,2,3-triazolo[4,5-*b*]pyridinium 3-oxid hexafluorophosphate
HD50	Concentration required for the lysis of 50% of the red blood cells

HOBt	1-Hydroxybenzotriazole
IBC-Cl	Isobutylchloroformate
IRRAS	Infrared reflection-absorption spectroscopy
Leu	Leucine
Lys	Lysine
MALDI	Matrix-assisted laser desorption/ionization
MAP	Membrane active peptide
MeCN	Acetonitrile
MeOH	Methanol
MIC	Minimal inhibitory concentration
MsCl	Mesyl chloride
NMM	*N*-methylmorpholine
NMR	Nuclear magnetic resonance spectroscopy
NOESY	Nuclear Overhauser effect spectroscopy
OSu	Succinimide
PAA	Poly(amidoamine)
PC	Phosphatidylcholine
Pd/C	Palladium on carbon
PG	Phosphatidylglycerol
Phe	Phenylalanine
PIFA	Phenyliodine bis(trifluoroacetate) or bis(trifluoroacetoxy)iodobenzene
Pip	Piperidine
POPC	1-palmitoyl-2-oleoyl-sn-glycero-3-phosphocholine
POPG	1-palmitoyl-2-oleoyl-sn-glycero-3-phospho-(1'-rac-glycerol)
PPh_3	Tripheylphosphine
Py	Pyridine
PyBOP	Benzotriazol-1-yl-oxytripyrrolidinophosphonium hexafluorophosphate
RhB	Rhodamine B
RNA	Ribonucleic acid
ROESY	Rotating frame nuclear Overhauser effect spectroscopy
RP HPLC	Reverse phase high performance liquid chromatography
rt	Room temperature
SAR	Structure-activity relationship
Ser	Serine

siRNA	Small interfering ribonucleic acid
SPPS	Solid phase peptide synthesis
SPS	Solid phase synthesis
Suc	Succinic anhydride
*s*Xaa	Succinyl analogue of the amino acid residue Xaa
*t*Bu	*tert*-Butyl
TEA	Triethylamine
TFA	Trifluoroacetic acid
THF	Tetrahydrofuran
Thr	Threonine
TIS	Triisopropylsilane
TMSCl	Trimethylsilyl
Tr	Trityl ot tryphenylmethyl
Tris	Tris(hydroxymethyl)aminomethane
Val	Valine
*v*Xaa	Vicinal diaminoalkyl analogue of the amino acid residue Xaa
Xaa	Amino acid residue
XR	X-Ray reflectivity

References

(1) Channon, K.; Bromley, E. H. C.; Woolfson, D. N. *Curr. Opin. Struct. Biol.* **2008**, *18*, 491.
(2) Loughlin, W. A.; Tyndall, J. D. A.; Glenn, M. P.; Hill, T. A.; Fairlie, D. P. *Chem. Rev.* **2010**, *110*, PR32.
(3) Wadhwani, P.; Reichert, J.; Burck, J.; Ulrich, A. S. *European Biophysics Journal with Biophysics Letters* **2012**, *41*, 177.
(4) Mason, J. M. *Future Medicinal Chemistry* **2010**, *2*, 1813.
(5) Cui, H. G.; Webber, M. J.; Stupp, S. I. *Biopolymers* **2010**, *94*, 1.
(6) Goodman, C. M.; Choi, S.; Shandler, S.; DeGrado, W. F. *Nature Chemical Biology* **2007**, *3*, 252.
(7) Gellman, S. H. *Accounts Chem. Res.* **1998**, *31*, 173.
(8) Matson, J. B.; Stupp, S. I. *Chemical Communications* **2012**, *48*, 26.
(9) Cavalli, S.; Albericio, F.; Kros, A. *Chem. Soc. Rev.* **2010**, *39*, 241.
(10) Luo, Z. L.; Zhang, S. G. *Chem. Soc. Rev.* **2012**, *41*, 4736.
(11) Horne, W. S.; Gellman, S. H. *Accounts Chem. Res.* **2008**, *41*, 1399.
(12) Seebach, D.; Gardiner, J. *Accounts Chem. Res.* **2008**, *41*, 1366.
(13) Guichard, G.; Huc, I. *Chemical Communications* **2011**, *47*, 5933.
(14) Seebach, D.; Beck, A. K.; Bierbaum, D. J. *Chem. Biodivers.* **2004**, *1*, 1111.
(15) Seebach, D.; Overhand, M.; Kuhnle, F. N. M.; Martinoni, B.; Oberer, L.; Hommel, U.; Widmer, H. *Helv. Chim. Acta* **1996**, *79*, 913.
(16) Appella, D. H.; Christianson, L. A.; Karle, I. L.; Powell, D. R.; Gellman, S. H. *J. Am. Chem. Soc.* **1996**, *118*, 13071.
(17) Seebach, D.; Hook, D. F.; Glattli, A. *Biopolymers* **2006**, *84*, 23.
(18) Heck, T.; Limbach, M.; Geueke, B.; Zacharias, M.; Gardiner, J.; Kohler, H. P. E.; Seebach, D. *Chem. Biodivers.* **2006**, *3*, 1325.
(19) Porter, E. A.; Weisblum, B.; Gellman, S. H. *J. Am. Chem. Soc.* **2002**, *124*, 7324.
(20) Liu, D. H.; DeGrado, W. F. *J. Am. Chem. Soc.* **2001**, *123*, 7553.
(21) Hamuro, Y.; Schneider, J. P.; DeGrado, W. F. *J. Am. Chem. Soc.* **1999**, *121*, 12200.
(22) Raguse, T. L.; Porter, E. A.; Weisblum, B.; Gellman, S. H. *J. Am. Chem. Soc.* **2002**, *124*, 12774.
(23) Arvidsson, P. I.; Frackenpohl, J.; Ryder, N. S.; Liechty, B.; Petersen, F.; Zimmermann, H.; Camenisch, G. P.; Woessner, R.; Seebach, D. *Chembiochem* **2001**, *2*, 771.
(24) Werder, M.; Hauser, H.; Abele, S.; Seebach, D. *Helv. Chim. Acta* **1999**, *82*, 1774.
(25) Kritzer, J. A.; Lear, J. D.; Hodsdon, M. E.; Schepartz, A. *J. Am. Chem. Soc.* **2004**, *126*, 9468.
(26) Kritzer, J. A.; Hodsdon, M. E.; Schepartz, A. *J. Am. Chem. Soc.* **2005**, *127*, 4118.
(27) Stephens, O. M.; Kim, S.; Welch, B. D.; Hodsdon, M. E.; Kay, M. S.; Schepartz, A. *J. Am. Chem. Soc.* **2005**, *127*, 13126.
(28) Kritzer, J. A.; Stephens, O. M.; Guarracino, D. A.; Reznik, S. K.; Schepartz, A. *Bioorg. Med. Chem.* **2005**, *13*, 11.
(29) Daura, X.; Gademann, K.; Schafer, H.; Jaun, B.; Seebach, D.; van Gunsteren, W. F. *J. Am. Chem. Soc.* **2001**, *123*, 2393.
(30) Gademann, K.; Ernst, M.; Hoyer, D.; Seebach, D. *Angew. Chem.-Int. Edit.* **1999**, *38*, 1223.
(31) Gademann, K.; Ernst, M.; Seebach, D.; Hoyer, D. *Helv. Chim. Acta* **2000**, *83*, 16.
(32) D. L. Nelson, M. M. C. *Lehninger Principles of Biochemistry* **2008**, *5th ed.,*, 117.
(33) Martinek, T. A.; Toth, G. K.; Vass, E.; Hollosi, M.; Fulop, F. *Angew. Chem.-Int. Edit.* **2002**, *41*, 1718.
(34) Martinek, T. A.; Hetenyi, A.; Fulop, L.; Mandity, I. M.; Toth, G. K.; Dekany, I.; Fulop, F. *Angew. Chem.-Int. Edit.* **2006**, *45*, 2396.
(35) Seebach, D.; Abele, S.; Gademann, K.; Jaun, B. *Angew. Chem.-Int. Edit.* **1999**, *38*, 1595.

(36) Krauthauser, S.; Christianson, L. A.; Powell, D. R.; Gellman, S. H. *J. Am. Chem. Soc.* **1997**, *119*, 11719.
(37) Chung, Y. J.; Christianson, L. A.; Stanger, H. E.; Powell, D. R.; Gellman, S. H. *J. Am. Chem. Soc.* **1998**, *120*, 10555.
(38) Langenhan, J. M.; Guzei, I. A.; Gellman, S. H. *Angew. Chem.-Int. Edit.* **2003**, *42*, 2402.
(39) Langenhan, J. M.; Gellman, S. H. *Organic Letters* **2004**, *6*, 937.
(40) Rua, F.; Boussert, S.; Parella, T.; Diez-Perez, I.; Branchadell, V.; Giralt, E.; Ortuno, R. M. *Organic Letters* **2007**, *9*, 3643.
(41) Segman, S.; Lee, M. R.; Vaiser, V.; Gellman, S. H.; Rapaport, H. *Angew. Chem.-Int. Edit.* **2010**, *49*, 716.
(42) Segman-Magidovich, S.; Lee, M. R.; Vaiser, V.; Struth, B.; Gellman, S. H.; Rapaport, H. *Chemistry-a European Journal* **2011**, *17*, 14857.
(43) Fischer, L.; Guichard, G. *Organic & Biomolecular Chemistry* **2010**, *8*, 3101.
(44) Huc, I. *Eur. J. Org. Chem.* **2004**, 17.
(45) Fowler, S. A.; Blackwell, H. E. *Organic & Biomolecular Chemistry* **2009**, *7*, 1508.
(46) Kamena, F.; Monnanda, B.; Makou, D.; Capone, S.; Patora-Komisarska, K.; Seebach, D. *Chem. Biodivers.* **2011**, *8*, 1.
(47) Blumenthal, R.; Clague, M. J.; Durell, S. R.; Epand, R. M. *Chem. Rev.* **2003**, *103*, 53.
(48) Zheng, Z.; Yang, R.; Bodner, M. L.; Weliky, D. P. *Biochemistry* **2006**, *45*, 12960.
(49) Amblard, M.; Fehrentz, J. A.; Martinez, J.; Subra, G. *Molecular Biotechnology* **2006**, *33*, 239.
(50) Su, Y. C.; Li, S. H.; Hong, M. *Amino Acids* **2013**, *44*, 821.
(51) Henriques, S. T.; Melo, M. N.; Castanho, M. *Biochem. J.* **2006**, *399*, 1.
(52) Henriques, S. T.; Melo, M. N.; Castanho, M. *Molecular Membrane Biology* **2007**, *24*, 173.
(53) Jenssen, H.; Hamill, P.; Hancock, R. E. W. *Clinical Microbiology Reviews* **2006**, *19*, 491.
(54) Spellberg, B.; Powers, J. H.; Brass, E. P.; Miller, L. G.; Edwards, J. E. *Clin. Infect. Dis.* **2004**, *38*, 1279.
(55) Donadio, S.; Maffioli, S.; Monciardini, P.; Sosio, M.; Jabes, D. *Journal of Antibiotics* **2010**, *63*, 423.
(56) Eckert, R. *Future Microbiology* **2011**, *6*, 635.
(57) Hancock, R. E. W.; Sahl, H. G. *Nature Biotechnology* **2006**, *24*, 1551.
(58) Zasloff, M. *Nature* **2002**, *415*, 389.
(59) Giuliani, A.; Pirri, G.; Bozzi, A.; Di Giulio, A.; Aschi, M.; Rinaldi, A. C. *Cell. Mol. Life Sci.* **2008**, *65*, 2450.
(60) Fjell, C. D.; Hiss, J. A.; Hancock, R. E. W.; Schneider, G. *Nature Reviews Drug Discovery* **2012**, *11*, 37.
(61) Matsuzaki, K.; Murase, O.; Miyajima, K. *Biochemistry* **1995**, *34*, 12553.
(62) Chan, D. I.; Prenner, E. J.; Vogel, H. J. *Biochim. Biophys. Acta-Biomembr.* **2006**, *1758*, 1184.
(63) Rotem, S.; Mor, A. *Biochim. Biophys. Acta-Biomembr.* **2009**, *1788*, 1582.
(64) Yeaman, M. R.; Yount, N. Y. *Pharmacol. Rev.* **2003**, *55*, 27.
(65) Wang, G. S.; Li, X.; Wang, Z. *Nucleic Acids Research* **2009**, *37*, D933.
(66) Claudon, P.; Violette, A.; Lamour, K.; Decossas, M.; Fournel, S.; Heurtault, B.; Godet, J.; Mely, Y.; Jamart-Gregoire, B.; Averlant-Petit, M. C.; Briand, J. P.; Duportail, G.; Monteil, H.; Guichard, G. *Angew. Chem.-Int. Edit.* **2010**, *49*, 333.
(67) Mowery, B. P.; Lindner, A. H.; Weisblum, B.; Stahl, S. S.; Gellman, S. H. *J. Am. Chem. Soc.* **2009**, *131*, 9735.
(68) Mowery, B. P.; Lee, S. E.; Kissounko, D. A.; Epand, R. F.; Epand, R. M.; Weisblum, B.; Stahl, S. S.; Gellman, S. H. *J. Am. Chem. Soc.* **2007**, *129*, 15474.
(69) Epand, R. M.; Vogel, H. J. *Biochim. Biophys. Acta-Biomembr.* **1999**, *1462*, 11.

(70) Liu, D. H.; Choi, S.; Chen, B.; Doerksen, R. J.; Clements, D. J.; Winkler, J. D.; Klein, M. L.; DeGrado, W. F. *Angew. Chem.-Int. Edit.* **2004**, *43*, 1158.
(71) Bergsson, G.; Arnfinnsson, J.; Steingrimsson, O.; Thormar, H. *Apmis* **2001**, *109*, 670.
(72) Kelsey, J. A.; Bayles, K. W.; Shafii, B.; McGuire, M. A. *Lipids* **2006**, *41*, 951.
(73) Knapp, H. R.; Melly, M. A. *Journal of Infectious Diseases* **1986**, *154*, 84.
(74) Seo, M. D.; Won, H. S.; Kim, J. H.; Mishig-Ochir, T.; Lee, B. J. *Molecules* **2012**, *17*, 12276.
(75) Heitz, F.; Morris, M. C.; Divita, G. *British Journal of Pharmacology* **2009**, *157*, 195.
(76) Hassane, F. S.; Saleh, A. F.; Abes, R.; Gait, M. J.; Lebleu, B. *Cell. Mol. Life Sci.* **2010**, *67*, 715.
(77) Juliano, R.; Alam, M. R.; Dixit, V.; Kang, H. *Nucleic Acids Research* **2008**, *36*, 4158.
(78) Fischer, R.; Fotin-Mleczek, M.; Hufnagel, H.; Brock, R. *Chembiochem* **2005**, *6*, 2126.
(79) Magzoub, M.; Graslund, A. *Quarterly Reviews of Biophysics* **2004**, *37*, 147.
(80) Deshayes, S.; Morris, M. C.; Divita, G.; Heitz, F. *Cell. Mol. Life Sci.* **2005**, *62*, 1839.
(81) Deshayes, S.; Morris, M.; Heitz, F.; Divita, G. *Advanced Drug Delivery Reviews* **2008**, *60*, 537.
(82) Deshayes, S.; Heitz, A.; Morris, M. C.; Charnet, P.; Divita, G.; Heitz, F. *Biochemistry* **2004**, *43*, 1449.
(83) Deshayes, S.; Gerbal-Chaloin, S.; Morris, M. C.; Aldrian-Herrada, G.; Charnet, P.; Divita, G.; Heitz, F. *Biochim. Biophys. Acta-Biomembr.* **2004**, *1667*, 141.
(84) Nakase, I.; Takeuchi, T.; Tanaka, G.; Futaki, S. *Advanced Drug Delivery Reviews* **2008**, *60*, 598.
(85) Duchardt, F.; Fotin-Mleczek, M.; Schwarz, H.; Fischer, R.; Brock, R. *Traffic* **2007**, *8*, 848.
(86) Jones, A. T. *International journal of pharmaceutics* **2008**, *354*, 34.
(87) Varkouhi, A. K.; Scholte, M.; Storm, G.; Haisma, H. J. *J. Control. Release* **2011**, *151*, 220.
(88) Parton, R. G.; Simons, K. *Nat. Rev. Mol. Cell Biol.* **2007**, *8*, 185.
(89) Lajoie, P.; Nabi, I. R. In *International Review of Cell and Molecular Biology, Vol 282*; Jeon, K. W., Ed.; Elsevier Academic Press Inc: San Diego, 2010; Vol. 282, p 135.
(90) Conner, S. D.; Schmid, S. L. *Nature* **2003**, *422*, 37.
(91) Doherty, G. J.; McMahon, H. T. In *Annual Review of Biochemistry*; Annual Reviews: Palo Alto, 2009; Vol. 78, p 857.
(92) Wadia, J. S.; Stan, R. V.; Dowdy, S. F. *Nature Medicine* **2004**, *10*, 310.
(93) Kaplan, I. M.; Wadia, J. S.; Dowdy, S. F. *J. Control. Release* **2005**, *102*, 247.
(94) Nakase, I.; Niwa, M.; Takeuchi, T.; Sonomura, K.; Kawabata, N.; Koike, Y.; Takehashi, M.; Tanaka, S.; Ueda, K.; Simpson, J. C.; Jones, A. T.; Sugiura, Y.; Futaki, S. *Molecular Therapy* **2004**, *10*, 1011.
(95) Nakase, I.; Tadokoro, A.; Kawabata, N.; Takeuchi, T.; Katoh, H.; Hiramoto, K.; Negishi, M.; Nomizu, M.; Sugiura, Y.; Futaki, S. *Biochemistry* **2007**, *46*, 492.
(96) Nakase, I.; Hirose, H.; Tanaka, G.; Tadokoro, A.; Kobayashi, S.; Takeuchi, T.; Futaki, S. *Molecular Therapy* **2009**, *17*, 1868.
(97) Mercer, J.; Helenius, A. *Nature Cell Biology* **2009**, *11*, 510.
(98) Swanson, J. A. *Nat. Rev. Mol. Cell Biol.* **2008**, *9*, 639.
(99) Nakase, I.; Akita, H.; Kogure, K.; Graslund, A.; Langel, U.; Harashima, H.; Futaki, S. *Accounts Chem. Res.* **2012**, *45*, 1132.
(100) Richard, J. P.; Melikov, K.; Brooks, H.; Prevot, P.; Lebleu, B.; Chernomordik, L. V. *Journal of Biological Chemistry* **2005**, *280*, 15300.
(101) Ziegler, A.; Nervi, P.; Durrenberger, M.; Seelig, J. *Biochemistry* **2005**, *44*, 138.
(102) Pelkmans, L.; Burli, T.; Zerial, M.; Helenius, A. *Cell* **2004**, *118*, 767.
(103) Glover, D. J.; Lipps, H. J.; Jans, D. A. *Nature Reviews Genetics* **2005**, *6*, 299.
(104) Greenfield, N. J. *Anal. Biochem.* **1996**, *235*, 1.
(105) Johnson, W. C. *Proteins* **1990**, *7*, 205.
(106) Greenfield, N. J. *Nat. Protoc.* **2006**, *1*, 2876.

(107) DeGrado, W. F.; Schneider, J. P.; Hamuro, Y. *Journal of Peptide Research* **1999**, *54*, 206.
(108) Guichard, G.; Abele, S.; Seebach, D. *Helv. Chim. Acta* **1998**, *81*, 187.
(109) Glattli, A.; Daura, X.; Seebach, D.; van Gunsteren, W. F. *J. Am. Chem. Soc.* **2002**, *124*, 12972.
(110) Dannehl, C.; Travkova, O. G.; Brezesinski, G. *Chemistry Letters* **2012**, *41*, 1178.
(111) Duysens, L. N. M. *Biochimica Et Biophysica Acta* **1956**, *19*, 1.
(112) Wallace, B. A.; Mao, D. *Anal. Biochem.* **1984**, *142*, 317.
(113) Wuthrich, K. *Angew. Chem.-Int. Edit.* **2003**, *42*, 3340.
(114) Vaz, E.; Pomerantz, W. C.; Geyer, M.; Gellman, S. H.; Brunsveld, L. *ChemBioChem* **2008**, *9*, 2254.
(115) Kojic-Prodic, B.; Kroon, J. *Croat. Chem. Acta* **2001**, *74*, 1.
(116) Benedetti, E. *Biopolymers* **1996**, *40*, 3.
(117) Cherepanov, D. A.; Feniouk, B. A.; Junge, W.; Mulkidjanian, A. Y. *Biophysical Journal* **2003**, *85*, 1307.
(118) Teschke, O.; de Souza, E. F. *Chemical Physics Letters* **2005**, *403*, 95.
(119) Jiang, D. L.; Dinh, K. L.; Ruthenburg, T. C.; Zhang, Y.; Su, L.; Land, D. P.; Zhou, F. M. *J. Phys. Chem. B* **2009**, *113*, 3160.
(120) Olak, C.; Muenter, A.; Andrae, J.; Brezesinskia, G. *J. Pept. Sci.* **2008**, *14*, 510.
(121) Weiner, S.; Traub, W. *FEBS Lett.* **1980**, *111*, 311.
(122) Tu, R. S.; Tirrell, M. *Adv. Drug Deliv. Rev.* **2004**, *56*, 1537.
(123) Leon, L.; Logrippo, P.; Tu, R. *Biophys. J.* **2010**, *99*, 2888.
(124) Maltseva, E.; Kerth, A.; Blume, A.; Mohwald, H.; Brezesinski, G. *Chembiochem* **2005**, *6*, 1817.
(125) Wang, C. S.; Zheng, J. Y.; Zhao, L.; Rastogi, V. K.; Shah, S. S.; DeFrank, J. J.; Leblanc, R. M. *Journal of Physical Chemistry B* **2008**, *112*, 5250.
(126) Hoernke, M.; Koksch, B.; Brezesinski, G. *Biophysical Chemistry* **2010**, *150*, 64.
(127) Stefaniu, C.; Vilotijevic, I.; Santer, M.; Silva, D. V.; Brezesinski, G.; Seeberger, P. H. *Angew. Chem.-Int. Edit.* **2012**, *51*, 12874.
(128) Dluhy, R. A. *J. Phys. Chem.* **1986**, *90*, 1373.
(129) Jackson, M.; Mantsch, H. H. *Critical Reviews in Biochemistry and Molecular Biology* **1995**, *30*, 95.
(130) Tamm, L. K.; Tatulian, S. A. *Quarterly Reviews of Biophysics* **1997**, *30*, 365.
(131) Daniels, D. S.; Petersson, E. J.; Qiu, J. X.; Schepartz, A. *J. Am. Chem. Soc.* **2007**, *129*, 1532.
(132) Cheng, R. P.; Gellman, S. H.; DeGrado, W. F. *Chemical Reviews* **2001**, *101*, 3219.
(133) Hintermann, T.; Seebach, D. *Synlett* **1997**, 437.
(134) Pohl, G.; Beke-Somfai, T.; Csizmadia, I. G.; Perczel, A. *Amino Acids* **2012**, *43*, 735.
(135) Mosca, S.; Wojcik, F.; Hartmann, L. *Macromolecular Rapid Communications* **2011**, *32*, 197.
(136) Wojcik, F.; Mosca, S.; Hartmann, L. *J. Org. Chem.* **2012**, *77*, 4226.
(137) Ponader, D.; Wojcik, F.; Beceren-Braun, F.; Dernedde, J.; Hartmann, L. *Biomacromolecules* **2012**, *13*, 1845.
(138) Wojcik, F.; O'Brien, A. G.; Gotze, S.; Seeberger, P. H.; Hartmann, L. *Chemistry (Weinheim an der Bergstrasse, Germany)* **2013**, *19*, 3090.
(139) Chorev, M.; Goodman, M. *Accounts Chem. Res.* **1993**, *26*, 266.
(140) Boeijen, A.; van Ameijde, J.; Liskamp, R. M. J. *The Journal of Organic Chemistry* **2001**, *66*, 8454.
(141) Reetz, M. T.; Jaeger, R.; Drewlies, R.; Hubel, M. *Angew. Chem.-Int. Edit. Engl.* **1991**, *30*, 103.
(142) Mandal, P. K.; Ren, Z.; Chen, X.; Xiong, C.; McMurray, J. S. *Journal of Medicinal Chemistry* **2009**, *52*, 6126.
(143) Zhang, X. J.; Krishnamurthy, R. *Angew. Chem.-Int. Edit.* **2009**, *48*, 8124.

(144) Hartmann, L.; Krause, E.; Antonietti, M.; Borner, H. G. *Biomacromolecules* **2006**, *7*, 1239.
(145) Evans, D. A.; Wu, L. D.; Wiener, J. J. M.; Johnson, J. S.; Ripin, D. H. B.; Tedrow, J. S. *J. Org. Chem.* **1999**, *64*, 6411.
(146) Seebach, D.; Schaeffer, L.; Gessier, F.; Bindschadler, P.; Jager, C.; Josien, D.; Kopp, S.; Lelais, G.; Mahajan, Y. R.; Micuch, P.; Sebesta, R.; Schweizer, B. W. *Helv. Chim. Acta* **2003**, *86*, 1852.
(147) Hintermann, T.; Seebach, D. *Helv. Chim. Acta* **1998**, *81*, 2093.
(148) Micuch, P.; Seebach, D. *Helv. Chim. Acta* **2002**, *85*, 1567.
(149) Gaul, C.; Schweizer, B. W.; Seiler, P.; Seebach, D. *Helv. Chim. Acta* **2002**, *85*, 1546.
(150) Evans, D. A.; Britton, T. C.; Dorow, R. L.; Dellaria, J. F. *Tetrahedron* **1988**, *44*, 5525.
(151) Pounder, R. J.; Dove, A. P. *Biomacromolecules* **2010**, *11*, 1930.
(152) Arvidsson, P. I.; Frackenpohl, J.; Seebach, D. *Helv. Chim. Acta* **2003**, *86*, 1522.
(153) Joullie, M. M.; Lassen, K. M. *Arkivoc* **2010**, 189.
(154) Li, G.; Xue, H.; Cheng, G.; Chen, S.; Zhang, F.; Jiang, S. *J Phys Chem B* **2008**, *112*, 15269.
(155) Hartmann, L.; Krause, E.; Antonietti, M.; BÃ¶rner, H. G. *Biomacromolecules* **2006**, *7*, 1239.
(156) El-Faham, A.; Albericio, F. *Chem. Rev.* **2011**, *111*, 6557.
(157) Seebach, D.; Abele, S.; Gademann, K.; Guichard, G.; Hintermann, T.; Jaun, B.; Matthews, J. L.; Schreiber, J. V. *Helv. Chim. Acta* **1998**, *81*, 932.
(158) Seebach, D.; Namoto, K.; Mahajan, Y. R.; Bindschadler, P.; Sustmann, R.; Kirsch, M.; Ryder, N. S.; Weiss, M.; Sauer, M.; Roth, C.; Werner, S.; Beer, H. D.; Munding, C.; Walde, P.; Voser, M. *Chem. Biodivers.* **2004**, *1*, 65.
(159) Jiang, S. Y.; Cao, Z. Q. *Adv. Mater.* **2010**, *22*, 920.
(160) Andersen, O. S. *Annual Review of Physiology* **1984**, *46*, 531.
(161) Du, C. M.; Valko, K.; Bevan, C.; Reynolds, D.; Abraham, M. H. *Analytical Chemistry* **1998**, *70*, 4228.
(162) Blondelle, S. E.; Houghten, R. A. *Biochemistry* **1992**, *31*, 12688.
(163) Deshayes, S.; Morris, M. C.; Divita, G.; Heitz, F. *J. Pept. Sci.* **2006**, *12*, 758.
(164) Marsh, D. *Biochim. Biophys. Acta-Rev. Biomembr.* **1996**, *1286*, 183.
(165) Sahl, H. G.; Pag, U.; Bonness, S.; Wagner, S.; Antcheva, N.; Tossi, A. *Journal of Leukocyte Biology* **2005**, *77*, 466.
(166) Godballe, T.; Nilsson, L. L.; Petersen, P. D.; Jenssen, H. *Chemical Biology & Drug Design* **2011**, *77*, 107.
(167) Khandelia, H.; Langham, A. A.; Kaznessis, Y. N. *Biochim. Biophys. Acta-Biomembr.* **2006**, *1758*, 1224.
(168) Watson, P.; Jones, A. T.; Stephens, D. J. *Advanced Drug Delivery Reviews* **2005**, *57*, 43.
(169) Fretz, M. M.; Koning, G. A.; Mastrobattista, A.; Jiskoot, W.; Storm, G. *Biochim. Biophys. Acta-Biomembr.* **2004**, *1665*, 48.
(170) Frackenpohl, J.; Arvidsson, P. I.; Schreiber, J. V.; Seebach, D. *Chembiochem* **2001**, *2*, 445.